Faculty of Science and Engineering

# Augmentation and Optimisation of the Australian Desert Fireball Network to Enable New Planetary Science

Robert Michael Howie

This thesis is presented for the Degree of
Doctor of Philosophy
of
Curtin University

January 2019

## Declaration

To the best of my knowledge and belief this thesis contains no material previously published by any other person except where due acknowledgement has been made. This thesis contains no material which has been accepted for the award of any other degree or diploma in any university.

10 January 2019

# Abstract

The advancement of planetary science is constrained by the availability of extraterrestrial material with known origins. Without knowing the source of a sample, the conclusions that can be drawn from even the most careful physical and chemical analysis are limited. Conveniently, extraterrestrial samples are regularly delivered to the Earth's surface in the form of meteorites. Systematic fireball observations performed by fireball camera networks can provide this critical link between samples and the context required to interpret their analysis by supplying meteorite origins as heliocentric pre-atmospheric entry meteoroid orbits. Fireball trajectory data can also be used to estimate meteorite fall positions in order to facilitate the recovery of meteorites. As meteorite producing fireball events are relatively rare, fireball camera networks must cover vast areas if they wish to regularly recover meteorites.

The primary objective of this work was to develop a more cost effective fireball observatory with a long service interval without sacrificing performance to enable Desert Fireball Network's digital expansion. The Desert Fireball Network is a large fireball camera network purposefully situated within the excellent meteorite searching terrain of Australia's arid and desert regions.

A novel fireball timing technique using timecodes constructed from de Bruijn sequences was developed. This technique allows both relative and absolute timing to be recorded directly into long exposure fireball images and eliminates the need for a separate absolute timing subsystem. This simplification allows the development of more cost effective fireball observatories that are also compatible with automated data reduction techniques. The time encoding technique was

extended to more general applications where both very high spatial and temporal resolution are required and the traditional techniques (high frame rate video) are limited by data bandwidth.

New digital all-sky fireball observatories implementing the time encoding technique were developed around off-the-shelf consumer photographic cameras. The result was a low cost design with sufficient precision for meteorite recovery and orbit calculation. The low cost and ease of assembly, deployment and maintenance of the observatory design allowed the deployment of a network much larger than originally planned.

The Desert Fireball Network now consists of 49 these observatories covering over 2.5 million km$^2$, or one third of of Australia, which is large enough to observe several meteorite dropping fireballs per year. The new digital network has recovered two meteorites with orbits (Murrili and Dingle Dell), observed more than a dozen additional meteorite dropping fireballs and generated a dataset of more than 800 bright fireballs with orbits. The project is now expanding globally with a new observatory design revision focused on improving maintainability for collaborators. This latest iteration has a longer autonomy period of up to twenty months and a user friendly modular design.

As a regular source of extraterrestrial samples with known origins, the Desert Fireball Network has now cemented itself as a critical piece of planetary science infrastructure in the far-reaching quest to unravel the enigma that is Solar System formation and evolution.

# Acknowledgements

This research was supported by the Australian Government through an Australian Postgraduate Award (APA) scholarship, the Australian Research Council through the Australian Laureate Fellowships scheme and receives institutional support from Curtin University.

**Jonathan Paxman**—Thank you for your continued encouragement and guidance, without which I could not have made this exciting and rewarding journey. The optimism and interest with which you tackle problems inspires me to always improve my approach.

**Philip Bland**—Thank you for introducing me to the fascinating field of planetary science and for inspiring me to pursue a career in research. Thank you for sharing your knowledge with me and for making the DFN possible. Your unrelenting commitment to science is truly amazing.

**Martin Towner**—Thank you for your technical guidance over the course of this endeavour. Your pragmatic perspective is appreciated more than you know.

**My DFN colleagues**—Thank you for the camaraderie and support. Your endless patience for my incessant questioning is greatly appreciated.

**My friends**—Thank you for keeping me sane and enduring all my talk about space rocks.

**My family: Jan, Graeme and Peter**—Thank you for putting up with me over the years and for never losing faith.

**Kirsten**—Thank you for your generous love, unwavering support and sincere encouragement. I hope you enjoy never again having to hear the phrase "after my PhD is finished ..."!

# Contents

# List of Publications Included as Part of This Thesis

This thesis includes a number of first author publications that were created as a part of this work.

## First Author Peer Reviewed Articles

### Chapter 2 and Appendix A:

R. M. Howie, J. Paxman, P. A. Bland, M. C. Towner, E. K. Sansom, and H. A. R. Devillepoix, "Submillisecond fireball timing using de Bruijn timecodes," *Meteoritics & Planetary Science*, vol. 52, no. 8, pp. 1669–1682. 2017. DOI: 10.1111/maps.12878

### Chapter 3 and Appendix B:

R. M. Howie, J. Paxman, P. A. Bland, M. C. Towner, M. Cupak, E. K. Sansom, and H. A. R. Devillepoix, "How to build a continental scale fireball camera network," *Experimental Astronomy*, vol. 43, no. 3, pp. 237–266. 2017. DOI: 10.1007/s10686-017-9532-7).

### Chapter 4:

R. M. Howie, J. Paxman, P. A. Bland and M. C. Towner, "Absolute Time Encoding for Temporal Super-resolution Using de Bruijn Timecodes," *Machine Vision and Applications*, under review.

## First Author Conference Abstracts

### Appendix C.1:

R. M. Howie, J. Paxman, P. A. Bland, M. C. Towner, M. Cupak and E. K. Sansom, "Advanced Digital Fireball Observatories: Enabling the Expansion of the Desert Fireball Network," presented at the XXXIst URSI General Assembly and Scientific Symposium (URSIGASS 2014) in Beijing, China.

### Appendix C.2:

R. M. Howie, J. Paxman, P. A. Bland, M. C. Towner, M. Cupak, E. K. Sansom, "Development of the Automated Digital Fireball Observatory for the Desert Fireball Network," presented at the 14th Australian Space Research Conference (ASRC 2014) in Adelaide, Australia.

### Appendix C.3:

R. M. Howie, E. K. Sansom, P. A. Bland, J. Paxman and M. C. Towner, "Precise Fireball Trajectories Using Liquid Crystal Shutters and de Bruijn Sequences," presented at the 46th Lunar and Planetary Science Conference (LPSC 2015) in Houston, USA.

### Appendix C.4:

R. M. Howie, J. Paxman, P. A. Bland, M. C. Towner, E. K. Sansom and M. J. Galloway, "How to Turn a DSLR into a High End Fireball Observatory," presented at the 78th Annual Meeting of the Meteoritical Society (MetSoc 2015) in Berkeley, USA.

### Appendix C.5:

R. M. Howie, J. Paxman, P. A. Bland and M. C. Towner, "Deploy Your Own Desert Fireball Network Observatory," presented at the 15th Australian Space Research Conference (ASRC 2015) in Canberra, Australia.

## Patents

### Appendix D:

R. M. Howie, J. Paxman, P. A. Bland and M. C. Towner, "Spatial tracking of a moving object," Australian provisional patent application no. 2016900714.

# List of Coauthored Publications

Contributions were made to the following coauthored publications as a part of this work, but they are not included as parts of this thesis.

## Coauthored Peer Reviewed Articles

H. A. R. Devillepoix, P. A. Bland, E. K. Sansom, M. C. Towner, M. Cupak, R. M. Howie, B. A. D. Hartig, T. Jansen-Sturgeon, M. A. Cox, "Observation of metre-scale impactors by the Desert Fireball Network," *Monthly Notices of the Royal Astronomical Society.* Accepted 2018. DOI: 10.1093/mnras/sty3442

E. K. Sansom, T. Jansen-Sturgeon, M. G. Rutten, H. A. R. Devillepoix, P. A. Bland, R. M. Howie, M. A. Cox, M. C. Towner, M. C. Cupak and B. A. D. Hartig, "3D Meteoroid Trajectories," *Icarus.* Accepted 2018. DOI: 10.1016/j.icarus.2018.09.026

H. A. R. Devillepoix, E. K. Sansom, P. A. Bland, M. C. Towner, M. C. Cupak, R. M. Howie, T. Jansen-Sturgeon. M. A. Cox, B. A. D. Hartig, G. K. Benedix and J. P. Paxman,"The Dingle Dell meteorite: A Halloween treat from the Main Belt," *Meteoritics & Planetary Science*, vol. 53, no. 10, pp. 2212–2227. 2018. DOI: 10.1111/maps.13142

I. Andreoni, K. Ackley, J. Cooke, A. Acharyya, J. R. Allison, G. E. Anderson, M. C. B. Ashley et al. including R. M. Howie, "Follow Up of GW170817 and Its Electromagnetic Counterpart by Australian-Led Observing Programmes," *Publications of the Astronomical Society of Australia* , vol. 34, pp. L12. 2017. DOI: 10.1017/pasa.2017.65

B. P. Abbott, R. Abbott, T. D. Abbott, F. Acernese, K. Ackley, C. Adams, T. Adams et al. including R. M. Howie, "Multi-messenger observations of a binary neutron star merger," *Astrophysical Journal Letters*, vol. 848, no. 2, pp. L12. 2017. DOI:10.3847/2041-8213/aa91c9

J. P. Paxman, P. A. Bland, R. M. Howie, M. C. Towner, M. Cupak, H. A . R. Devillepoix, E. K. Sansom, "The Desert Fireball Network: A Sensor Network for Meteorite Tracking and Recovery," *2016 14th International Conference on Control, Automation, Robotics and Vision (ICARCV)*, 2016.

## Coauthored Conference Abstracts

P. A. Bland, M. C. Towner, E. K. Sansom, H. Devillepoix, R. M. Howie, J. P. Paxman, M. Cupak, G. K. Benedix, M. Cox, T. Jansen-Sturgeon, D. Stuart and D. Strangway, "Fall and Recovery of the Murrili Meteorite, and an Update on the Desert Fireball Network," presented at presented at the 79th Annual Meeting of the Meteoritical Society (MetSoc 2016) in Berlin Germany.

G. K. Benedix, L. V. Forman, L. Daly, R. C. Greenwood, I. A. Franchi, J. M. Friedrich, M. M. M. Meier, C. Maden, H. Busemann, K. C. Welten, M. W. Caffee, P. A. Bland, J. Paxman, M. Towner, M. Cupak, E. K. Sansom, R. M. Howie, H. A. R. Devillepoix, M. A. Cox, T. Jansen-Sturgeon, K. Merigot, D. Stuart, and D. Strangway, "Mineralogy and Petrology of the Murrili Meteorite," presented at the 79th Annual Meeting of the Meteoritical Society (MetSoc 2016) in Berlin Germany.

H. A. R. Devillepoix, P. A. Bland, M. C. Towner, E. K. Sansom, R. M. Howie, M. Cupak, G. K. Benedix, T. Jansen-Sturgeon, B. A. D. Hartig, M. A. Cox and J. P. Paxman, "Fall and Recovery of the Dingle Dell Meteorite," presented at the 80th Annual Meeting of The Meteoritical Society (MetSoc 2017) in Santa Fe, USA.

G. K. Benedix, L.V. Forman, L. Daly, B. Godel, L. Esteban, M. M. M. Meier, C. Maden, H. Busemann, Q. Z. Yin, M. Sanborn, K. Ziegler, J. M. Friedrich, J. W. Strasser, K. C. Welten, M. W. Caffee, D. P. Glavin, J. P. Dworkin, P. A. Bland, J. P. Paxman, M. C. Towner, M. Cupak, E. K. Sansom, R. M. Howie, H. A. R. Devillepoix, M. A. Cox, T. Jansen-Sturgeon, B. A. D. Hartig, and A. W. R. Bevan, "Mineralology, Petrology and Geochronology of the Dingle Dell Meteorite," presented at the 80th Annual Meeting of The Meteoritical Society (MetSoc 2017) in Santa Fe, USA.

# Chapter 1

# Introduction

This doctoral thesis primarily describes the development of a new fireball camera observatory design that has enabled the digital expansion of the Desert Fireball Network (DFN). The DFN is a fireball camera network covering a large portion of the Australian desert and arid regions with the goal of meteorite recovery and pre-atmospheric entry orbit calculation to provide samples of known origin to planetary science. Previous fireball observatories have been large, expensive and required frequent servicing. This new design is cost effective and practical for a large network spread across remote unpopulated locations but does not compromise on imaging performance to achieve these gains.

A new fireball timing technique based on de Bruijn sequences was developed to eliminate the separate timing method used on previous fireball observatories and embed all timing information within the long exposure image. The technique was also adapted to and demonstrated in industrial imaging applications where the high bandwidth associated with the traditional approach (high frame rate video) prohibits capture with both very high spatial and temporal resolution.

The new fireball observatories developed for the DFN are high performing, reliable, cost effective and have a long service interval, satisfying the design requirements. Cost and complexity were minimised through careful observatory design

keeping manufacture, assembly and maintenance in mind. The success of the design has allowed the DFN to expand to cover over 2.5 million km$^2$ (over 2.5 times the original coverage goal), recover two meteorites with orbits, observe over a dozen additional meteorite dropping fireballs, produce a dataset of more than 1000 bright fireballs (the biggest fireball dataset ever collected) with orbits, and now expand globally with a revised design. This latest iteration focuses on even better maintainability and extends the interval up to 20 months of autonomous operation.

The work described within this thesis has enabled the DFN to expand to become the largest fireball camera network in the world. The network currently covers over one third of Australia and is large enough to observe several meteorite producing fireball events per year and produce regular samples of known origin for the advancement of Solar System science.

## 1.1 Why Are Fireball Camera Networks Needed?

Despite decades of work, the formation and evolution of the Solar System are still open problems. One reason for this lack of certainty is the difficulty in obtaining planetary samples of known origin. There is no shortage of extraterrestrial samples (in the form of meteorites—nearly 60,000 in worldwide collections [1]); however samples with known origins are exceedingly rare. The only extraterrestrial samples available with known origins are—

- lunar samples from the Apollo missions 11,12 and 14-17[2] and Luna missions 16,20 and 24 [3]–[5],
- comet 81P/Wild 2 coma samples collected by the Stardust mission [6],
- solar wind samples collected by the Genesis mission [7], [8]
- dust particles from asteroid 25143 Itokawa returned by the Hayabusa mission [9],
- lunar meteorites (≈360 as of August 2017 [1]),
- Martian meteorites (≈198 as of August 2017 [1]),

- HED (howardite–eucrite–diogenite) meteorites thought to originate from minor planet 4 Vesta [10], [11] (≈1894 as of August 2017 [1]) and
- 32 recovered meteorites with orbits calculated from serendipitous or systematic photographic observations (as of December 2016) [12].

The value of these samples is evident by the investment made in sample return missions. These missions cost hundreds of millions of dollars each to visit a single target and often only return grams or milligrams of sample material. Fireball camera networks are not a replacement for sample return, which delivers pristine samples with their precise geological context, but the pre-atmospheric entry orbits they provide for meteorites are an extremely valuable constraint on origin.

## 1.2 What is a Fireball?

A meteoroid is "a 10-μm to 1-m-size natural solid object moving in interplanetary space"[13]. These small objects originate from larger Solar System bodies including asteroids, comets, minor planets, and planets as a result of collisions and breakups. These larger source objects are the very bodies that planetary scientists are interested in sampling in their quest to unravel the history of the Solar System. Meteoroids that arrive on Earth (as meteorites) provide a convenient way to obtain these samples.

When meteoroids collide with Earth they enter the atmosphere at high speed (tens of km/s) and generate significant heat during the ablation process as the body is decelerated by the atmosphere. This heating begins to sublimate the meteoroid material at the surface. Light is emitted via spontaneous emission as excited molecules in high energy states transition back to lower energy states [14], [15] and via blackbody emission[15], [16]. The emission of this light creates the visual phenomenon known as a meteor (or colloquially a shooting star).

Meteors brighter than magnitude -4 are known as fireballs [17], [18] and are often produced by larger asteroidal meteoroids which are more likely to partially survive ablation and produce a meteorite on the Earth's surface (although meteoroid ve-

locity, composition and structure—not just size—also greatly affect survivability and brightness).

The fast passage of a meteoroid during the phase where it is producing light and visible to human observers and photographic cameras is referred to as bright flight or luminous trajectory. Some meteoroids completely burn up in this ablation process, but some survive long enough to slow down to the point where ablation stops. The part of the trajectory from this point onwards is known as dark flight as there is no longer a visible meteor. Meteoroids that partially survive the ablation process usually slow to terminal velocity during dark flight and fall vertically to the surface of the Earth. Most meteorite impacts leave little or no trace on the surface of the Earth.

## 1.3 Why Are Orbits so Important?

Whilst new extraterrestrial samples are always appreciated, the conclusions that can be drawn from a sample of unknown origin within the Solar System are limited. Proper context is the key to interpreting the results of any sample analysis and meteorites are no exception. This geological context is provided for meteorites in the form of heliocentric pre-atmospheric orbits. In some cases these orbits can be linked to particular source regions, families or bodies and this is what makes meteorites with orbits so valuable to Solar System science. Systematic observations of meteoroid entries carried out by large fireball camera networks are the best method of recovering these conveniently delivered samples and, crucially, their orbits as meteorite dropping fireballs are relatively rare.

## 1.4 How are Meteorites Recovered with Orbits via Photographic Observations?

Fireball camera networks capture systematic optical observations of fireballs from multiple geographically distinct locations. The fireball trajectories derived from these observations allow the calculation of meteoroid orbits as well as meteorite

fall position estimates. A broad overview of the steps involved in the operation of a fireball camera network and recovery of a meteorite with an orbit is outlined below in order to provide a context to the contributions of this thesis.

### 1.4.1 Fireball Observation

As fireball light is radiated in the visible band, off-the-shelf cameras are well suited to record their trajectories. Video and photographic still cameras are both commonly used by fireball and meteor observation networks around the world. Video observations capture data at a temporal resolution of tens of frames per second, and photographic imaging captures long exposures (tens of seconds in length). As both path *and* timing data of the trajectory are important to trajectory analysis, photographic long exposure observatories must employ one or more methods of time determination. In order to determine the relative timing (to derive velocity after triangulation), photographic fireball cameras periodically interrupt the exposure using a periodic shutter. Rotating shutters, mechanical switching shutters and electro-optic modulators can be used for this purpose. The liquid crystal shutters used by the DFN are controlled in a unique way to embed both relative *and* absolute timing within the long exposure image (see sections 1.8.1 and 1.8.3 as well as the corresponding chapters 2 and 4). The visible parts of the trail that are created when these periodic shutters are open are referred to as dashes and the gaps between these dashes are referred to as breaks. The rate at which the periodic shutter interrupts the optical path is dependant on the configuration of the imaging system, but are usually in the range of 10-20 dashes per second for fireball camera networks with the aim of meteorite recovery [19]–[24]. Meteor camera networks often use higher dash rates than fireball camera networks as meteor events are often shorter and higher velocity than the meteorite dropping fireballs that fireball camera networks are primarily interested in.

It is important to recognise the distinction between meteor camera networks and fireball camera networks due to the difference in their approaches, methods and goals. Meteor camera networks are primarily focused on the detection and characterisation of meteors, which in general do not produce meteorites. The aim of these programs is to characterise meteor flux rates and to detect and study

meteor streams. As these streams are mostly composed of smaller dust grain sized cometary material, and because dust grain sized objects are much more abundant than larger fireball and meteorite producing meteoroids in general[25]–[27], meteor networks are designed to be as sensitive to dim meteors as possible. This allows the collection of data on as many meteors as possible and provides more flux data to those studying the near Earth environment, including those analysing impact risks to spacecraft [28]. Unfortunately, this focus on dim meteors forces compromises in other areas: usually field of view or geographical coverage area. Both amateur and professional meteor networks exist, and, with the advent of video imaging, the distinction between the two is mainly down to approach and funding (not observational capability) [29]. Recently, the line between professional and amateur networks has started to blur as some who started as amateurs have become professionals and professional networks have turned to interested amateurs in order to expand their coverage[29], [30].

Fireball networks on the other hand, have the primary objectives of meteorite recovery and orbit calculation. Fireballs are more likely to result in meteorite falls and usually associated with asteroidal debris, rather than the cometary dust which accounts for the majority of faint meteors. For fireball camera networks, coverage area and spatial precision are king. Maximising coverage area is critical because the occurrence of meteorite producing fireballs is so rare. As an example, the initial film camera based DFN covered 200,000 $km^2$, recovered two meteorites and observed five more meteorite (>100 g) dropping fireballs from 2007 to 2013[31]. High spatial precision is also vital to ensure that the fall distribution (the probability distribution of likely fall positions) is narrowed as much as possible in order to maximise the chances of meteorite recovery via a dedicated search. Much of the technical work described in this thesis is concerned with maximising coverage area by designing cost effective observatories without sacrificing precision (see section 1.8.2 and the corresponding chapter 3). Meteorites have been recovered regularly using fireball observatories with a spatial precision of approximately one arcminute and observatory spacings of 70-150 km[22], [32]–[36]. For a fireball network, it is acceptable to miss some dim meteors that will not result in (macro scale) meteorites in order to reach these coverage and precision goals. The peak brightness of meteorite dropping fireballs is typically the range of magnitude -7 to -15[37], and systems with a limiting magnitude of

-2.5 have successfully been used for orbit calculation and meteorite recovery in the past [38].

Fireball networks are mostly conducted by professionals due to the large scale of the networks and the increased cost and technical barriers associated with high spatial precision imaging. The remainder of this work will focus on fireball camera networks with the goal of meteorite recovery, not meteor camera networks.

### 1.4.2 Event Detection

Systematic observation programs require some sort of event detection to detect potential meteorite dropping fireballs when they occur and initiate the remaining steps in the data processing and meteorite recovery chain. Fireballs are able to be distinguished from most other bright night-time phenomena by their high and fairly well constrained initial velocities (tens of kilometres per second [15]). Some events such as low flying planes, nearby car headlights and other human activity can be difficult to filter on this criteria alone, as a single camera can only measure angular velocity and has no distance information. Corroboration with other observatory stations via attempted preliminary triangulations can be used to eliminate these false positives. Low altitude events such as low flying planes and local human activity will not appear on multiple stations which are separated by distances in the order of 100 km. The remaining bright, fast events above $\approx$10 kilometres altitude are likely fireballs caused by meteoroids.

In practice, it is not always possible to implement this last corroboration step in a timely manner as it requires feature detection and communication between observatory stations. Preliminary single station event detection is usually based on brightness, angular velocity or trajectory shape (in camera space, without range). Past detection implementations have utilised radiometers (measuring all-sky brightness) [20], [22], image analysis [39] and a particularly ingenious solution of a radiometer behind interleaved perforated cones combined with an electronic frequency filter circuit to detect bright events within a suitable angular velocity range [21]. Digital networks such as the DFN are able to use automated image analysis software in order to detect fireball events. This allows for more control

over the tuning of the detection thresholds and more flexibility than hardware based solutions.

### 1.4.3 Triangulation and Trajectory Analysis

Fireball observations are angular in nature and made from multiple geographically separated camera sites. These must be triangulated in order to determine trajectories in three dimensions. Spatial precision of the triangulated trajectories is determined by the optical performance of the observatories and the triangulation geometry for each event. Orthogonal observations provide ideal triangulation geometry; spatial precision decreases as the geometry moves away from this configuration [40].

Stations in fireball camera networks are typically separated by 70-200 km [19]–[22], [38], [41]. This separation is needed to achieve the required coverage without an impractically large number of stations, and provides favourable triangulation geometry for the initial high altitude parts of the trajectory used for orbit determination.

A number of different triangulation methods can be used (somewhat depending on the type of timing data available for the observations):

- intersection of planes,
- straight least-squares,
- multi-parameter fit,
- individual point wise, and
- recursive Bayesian estimation.

The intersection of planes method [40] calculates triangulated fireball trajectories from the intersection of the planes formed by each observatory station and the best fit trajectory line as viewed from that station. In the case of two stations, the intersection of the two planes defines the fireball trajectory; in the case of

observations from more than two stations the trajectory is computed as a weighted average of each two-station combination [40].

The straight least-squares method [42] finds the linear meteor trajectory that minimises the angular residuals to the observational lines of site from all cameras. Each line of sight (in 3D space) corresponds to a data point in 2D projective camera space.

Both of these methods can be used either with or without timing for the data points. The straight least-squares method [42] states that the time is "usually ... taken to be constant". (In this case the triangulation is performed assuming that all data points were recorded at one point in time, neglecting the effect of Earth's rotation during the event). However, if the timing of all data points *is* known, these straight line methods can be applied (more correctly) in an inertial reference frame which accounts for Earth's rotation. The impact of effects that cause deviations from a straight line trajectory (such as the Earth's rotation and gravity—in an Earth fixed reference frame) is minimal for short fireballs that are observed with limited spacial precision. However, when considering longer fireballs and observations of higher spatial precision, these effects can be significant and should be considered.

The multi-parameter fit approach [43] was developed to solve the trajectory determination problem in one step, instead of a two step process where the trajectory path is calculated first and the meteoroid position over time along that path is calculated as a second independent step. This method provides better results for suboptimal observation geometries [43] and better initial velocity estimates than the above two techniques [44].

Where absolute timing is known for each point in the trajectory observations and these observations are synchronised (by navigation satellites for example), it is possible to triangulate the meteoroid position over time for each synchronised observation using the correlated observational lines of sight (this is called individual point wise triangulation). This capability is currently unique to the DFN and made possible by the syncronised time encoding method described in this thesis (see sections 1.8.1 and 1.8.3 as well as the corresponding chapters 2 and 4). The

comparisons made in [45] indicate this individual point wise approach may be more suitable than methods that assume a linear trajectory.

Recursive Bayesian estimation, including particle filter [46], [47] (sequential Monte Carlo) methods are relatively new techniques for analysing fireball trajectories, and can be used as a separate step after the trajectory is triangulated using another method [46], [48] or can model the trajectory in three dimensions from the angular observations directly [45], [47]. The advantage of these trajectory analysis techniques is that they incorporate observational uncertainty and model the physical behaviour of the meteoroid to robustly quantify the uncertainty of results.

### 1.4.4 Mass Estimation

Mass estimation is part of the trajectory analysis and is critical to successfully recovering meteorites from photographic observations. A meteoroid's final mass (after ablation) greatly affects the distance travelled downrange (in the direction of the fireball's motion) once bright flight ceases. Accurate modelling of the behaviour during the dark flight is required as the meteoroid is not visible to photographic or human observers during this phase. (Although meteoroids can be observed in dark flight with radar if available [49].)

There are two methods used to determine meteoroid mass from fireball observations: the photometric method and the dynamic method. Both the dynamic and photometric methods depend on the single body theory of meteoroid mass loss and deceleration [50], [51] or more recent advanced models build upon the single body theory which attempt to account for meteoroid fragmentation [52]–[54]. Traditional dynamic techniques have been limited by the need to assume the drag coefficient, shape and density[15], but recent Bayesian modelling techniques in combination with higher precision fireball data are attempting to remove this limitation [47]. The photometric methods take the single body equations one step further and assume that the mass loss rate is directly related to brightness (with a particular luminous efficiency parameter). These methods depend on the theory of meteor radiation [55]–[57] and estimate mass by integrating fireball

light curves over time [54], [58], [59]. Unfortunately, much of this photometric approach is dependant upon empirical data from a limited number of fireballs, and automation and reproduction are difficult as light curves must be manually interpreted in order to create fragmentation time inputs [59], [60].

### 1.4.5 Dark Flight Modelling

As meteoroids cannot be observed by fireball camera networks during dark flight, this portion of the meteoroid's journey must be modelled. The inputs to this modelling are the results from the luminous trajectory analysis and an atmospheric weather model for the relevant volume at the time of the meteoroid's passage [15], [40]. Two important parameters from the luminous trajectory analysis are required from the dark flight modelling. One is the drag coefficient and the other incorporates the mass and cross-sectional area of the meteoroid [40]. Lift coefficient and spin rate could also be incorporated into dark flight modelling, but bright flight analysis rarely well constrains these additional parameters. In order to complete the dark flight modelling, some assumptions have to be made about the behaviour of these parameters over time.

In the case of the DFN, atmospheric data is generated from a regional numerical weather prediction model (the Weather Research and Forecasting model). This is performed at higher resolutions than is normally used for weather forecasting by national meteorological bodies. These models incorporate data from a number of publicly available sources, but wind data from high altitude balloon flights, in particular, is especially useful. The accuracy of the atmospheric model used for dark flight can be significantly influenced by the distance and time between balloon flight data and a meteoroid dropping fireball event.

The shape of the fall position probability distribution depends on the fireball event parameters, namely the results of mass estimation, entry angle, final velocity and wind conditions. A meteoroid with a steep fireball trajectory will penetrate deeper in to the atmosphere before slowing down and therefore will be less affected by winds than a meteoroid with a shallow entry (where bright flight terminates at a higher altitude) that spends more time falling at terminal velocity. This results in

a shorter fall line and a smaller, shorter fall distribution than the shallower event. Events with shallow entry angles can result in fall distributions tens of kilometres in length along the fall line. (A fall line plots the likely landing position of fragments of varying mass.) Larger fragments usually travel further along the fall line than smaller fragments that are decelerated by the atmosphere more quickly. Due to the varying wind conditions at different altitudes and mass uncertainty, fall lines are usually curved (especially so at the low mass end).

### 1.4.6 Search and Recovery

The approach to locating and recovering meteorites depends on the nature of the fall location. In populated areas, alerts can be disseminated to advise the population of a fall which sometimes results in a recovery without the need for a dedicated search. Sometimes, meteorite fragments are recovered by members of the public even before trajectory analysis and fall position estimation. In less populated areas (like the Australia Outback), a dedicated search is required to recover meteorites. It should be stated that despite all the effort that has gone into refining the above methods over the last half of a century, recovering meteorites is difficult, and never a certainty due to the number of unknowns.

Searches are usually conducted visually on foot. The terrain greatly influences the rate at which ground can be covered as it greatly affects the spacing between searchers, from ≈10 metres on salt lakes down to a couple of metres in dense bush. Logistical constraints limit most searches in the Outback to 4-12 $km^2$. This places an upper bound on the acceptable size of the fall distribution and informs the precision requirements of fireball networks in remote areas.

A challenging part of meteorite recovery is the decision of when to search at all. Searching in remote areas is costly in terms of time and monetary investment. Careful analysis of the fireball event and interpretation of the data is required in order to make a sound decision. Additional data sources (apart from photographic observations) including radar[61], human reports[62], infrasound and satellite observations[63] can all provide useful additional data to incorporate into this decision.

Fortunately meteorites remain recoverable for tens of thousands of years on the right terrain[64], so there is more than one opportunity to recover a meteorite (even if there will be increased terrestrial contamination). The recovery of the Benešov meteorite 20 years after its photographically recorded fall via careful reanalysis of the fireball observations from 1991 [36] prove the value of high quality photographic observations, importance of rigorous data analysis, and give hope for the recovery of more observed but not yet recovered falls.

### 1.4.7 Orbit Calculation

Orbits are calculated using the initial velocity vector from the trajectory analysis. Whilst the problem initially seems simple once the initial vector is known, it is complicated by the the effect of Earth's rotation and motion on the observations and the fact that meteoroids are already being influenced by the Earth's gravity and atmosphere when observations are made.

Orbit calculation is the primary driver for absolute timing precision as it determines the orientation of the Earth and therefore the fireball camera network when the observations are made. The timing precision requirement in the DFN is a little different as the absolute and relative timing (that gives velocity) are interlinked due to the time encoding method that is used for both.

Traditionally, an analytical method which compensates for the Earth's gravity has been employed for orbit calculation[40], but recent efforts have used numerical integration based techniques to account for more perturbations including atmospheric drag, Earth's flattening and the Moon's gravity [65], [66].

## 1.5 Fireball Camera Networks Around the World

The first meteor photograph was captured by Ladislaus Weinek from the Klementium Observatory in Prague in 1885 [67]. This commenced a long history of meteor and fireball observation that continues to this day in what is now the Czech Republic. The 1890's introduced rotating shutters for velocity determina-

tion[68] as well as the first meteor spectra [69]. The first half of the twentieth century brought about the first systematic photographic meteor observation programs [68], [70], [71] along with the single body theory of meteor motion, mass loss [50], [51] and radiation [55], [56].

### 1.5.1 The Big Three 20th Century Fireball Camera Networks

The fall of the Přibram chondrite which was recorded by the double station meteor cameras at Ondřejov observatory in 1961 [72] and was the first meteorite with a calculated orbit. This spurred the development of the first fireball camera network in Czechoslovakia which commenced operations in 1963 [19]. The US Prairie and Canadian MORP (meteorite observation and recovery project) networks closely followed in 1964 and 1971 respectively [20], [21]. These latter two networks recovered one meteorite each before ceasing operations[21], [73], but the network that started as the Czechoslovak network is still operating today as the larger European Fireball Network [22], [74], [75] and has recovered a number of meteorites[76]–[78]. These three networks were notable for their size and meteorite recoveries in the second half of the 20th century. An overview of these networks is presented in section 3.2. More recently, a number of new fireball networks have commenced operations with varying degrees of success.

### 1.5.2 Recent Networks

The Desert Fireball Network commenced routine operation in 2005 with a network of four autonomous large format film observatories based on the automated Czech design [31], [32]. This film network was conceived as a trial for a future larger network and covered around 200,000 $km^2$. Two meteorites were recovered from 2007 to 2013 [34], [79]. (See sections 1.6 and 3.2.5 for more on the film based DFN) This planned expansion has now occurred, and the DFN now covers 2.5 million $km^2$ with a new digital network; most of the technical work described in this thesis relates to the design of the digital observatories that enabled this expansion.

The Spanish Fireball Network (SPMN) also commenced operation with four initial stations in 2005[41] expanding up to 8 by 2009[80]. Meteorites from two daylight bolides were recovered during this time with an orbit for one of these calculated from casual video and photographic observations [81], [82]. Unfortunately these daylight events were not recorded by the camera network which operated only at night at this point. Recently, daytime monitoring has been added, but is only of limited spatial precision [83].

The French FRIPON network will consist of 100 1.2 megapixel all sky digital video cameras covering France with additional passive radar measurements with the aim of meteor and fireball observation as well as meteorite recovery [84]–[86]. The Doppler velocity measurements are aimed to compensate for the limited precision of the 1.2 MP optical observations [87]. The majority of the optical network had been rolled out as of June 2016 [88].

The Finnish Fireball Network is a mostly amateur network consisting of 24 stations; operations started in 2002 and fireball observations lead to the recovery of a meteorite in 2014[89].

The Polish Fireball Network started digital photographic observations around 2005[90] and currently consists of 36 stations with a mix of video and photographic cameras[91].

The Southern Ontario Meteor Network (SOMN) consists of seven all sky video stations and commenced operations in 2004 [92], [93]. The network is primarily used to image smaller meteoroids that are not expected to result in meteorites and as a trigger for other radar, infrasound and optical observations[92].

The NASA All Sky Fireball Network was established in 2008 and currently consists of 15 all sky video stations running the SOMN ASGARD software [94], [95]. The focus of the network, run by the NASA Meteoroid Environment Office, is to characterise meteoroid flux for the benefit of space operations.

Even though both the Southern Ontario and NASA networks have limited preci-

sion compared to other fireball networks (due to their use of low resolution video) their coverage area makes the observation of a meteorite dropping fireball likely at some point. Doppler weather radar coverage is good in the continental United States, so limited spatial precision may not be an obstacle to meteorite recovery [49].

The Tajikistan Fireball Network consists of five stations to observe fireballs and other optical transient phenomena with a mix of film and digital cameras and started routine operations in 2008 [96].

### 1.5.3 Two Notable Meteor Camera Networks

While meteor camera network without the primary goal of meteorite recovery are numerous (and not within the scope of this thesis) two particularly noteworthy systems should be mentioned.

Cameras for Allsky Meteor Surveillance (CAMS) uses 20 standard definition video cameras per station with narrow angle lenses to cover the entire sky[97]. Routine observations started from three stations in 2011. CAMS observations were used in the calculation of the Novato meteorite in 2012[98], and now has stations in nine different regions around the globe[99]. CAMS is notable for its GPS synchronised operation and spatial resolution achieved through many cameras which allows the calculation of more precise orbits than other meteor camera groups using standard definition video cameras to cover the entire sky. As a project mainly aimed at characterising meteoroid streams, its geographical coverage is limited compared to fireball camera networks with the primary goal of meteorite recovery.

The Canadian Automated Meteor Observatory (CAMO) provides high resolution intensified video imagery of meteors using a dual mirror optically scanned narrow field camera coupled with a wide field acquisition camera (the system also has an additional wide field camera for separate meteoroid flux measurements)[100]. This configuration provides extremely high spatial resolution imagery from its guided camera for accurate deceleration measurements, trajectory analysis and direct observation of fragmentation events. Better understanding of the ablation

process and fragmentation in particular from data like this will assist with the development of better trajectory analysis techniques in general. In time this could lead to more accurate fall position estimations for fireball camera networks.

## 1.6 The Desert Fireball Network

One of the factors that limited the success of the three large fireball networks of the 20th century was the difficulty in recovering meteorites. The terrain covered by these networks was not particularly conducive to meteorite recovery. The aim of the Desert Fireball Network was to significantly improve network productivity over previous attempts by locating the network within some of the best meteorite searching terrain in the world. The pale rock geology[101] of the Australian Nullarbor is ideal searching terrain for recovering meteorites as the (usually) black rocks stand out against the pale limestone and red dirt.

The network originally consisted of four film stations based on the automated Czech design [22] deployed in the Nullarbor (as shown in Fig. 1.1). The film network proved the rational behind the network; it was much more productive (in terms of recoveries per year) than prior efforts, recovering two meteorites between 2005 and 2013[31]. This success spurred the digital expansion beginning in 2012 with brand new observatories developed fully in house and with a focus on cost effective performance to maximise coverage area[102].

## 1.7 The Digital Expansion of Desert Fireball Network

Film based camera networks require regular attendance to replace and retrieve film even if the operation is automated for a number of nights. This personnel time requirement limits these networks to regions where film magazines can be swapped regularly (about monthly for the film based DFN observatories). Unfortunately some of the best meteorite searching terrain (such as the Australian Nullarbor) is remote with little to no population. A fireball observatory with a

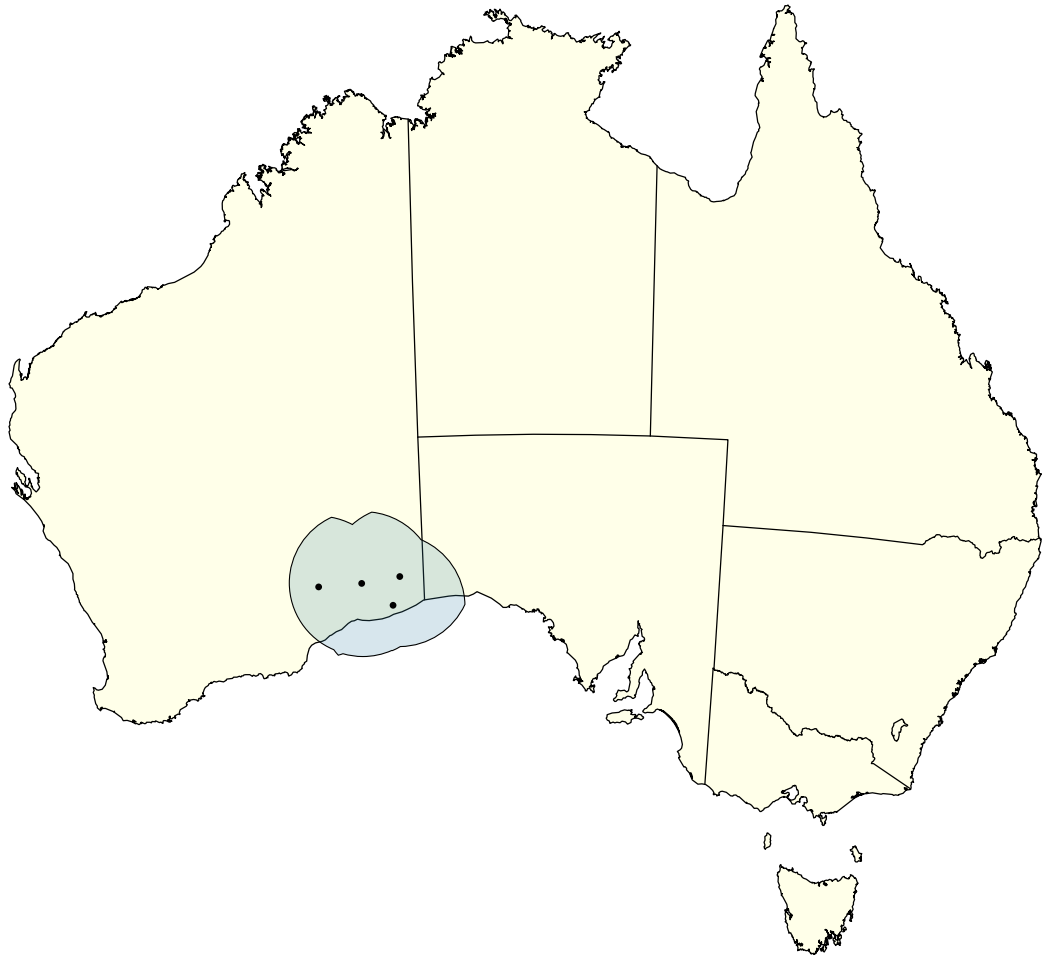

Figure 1.1: DFN four station film deployment covering ≈200,000 km$^2$ which recovered two meteorites with orbits from 2005 to 2013 and observed five more meteorite dropping fireballs

long service interval (several months at least) is required to cover these sorts of regions effectively. (For a more complete discussion on the need for a better fireball observatory and the operational requirements see sections 3.3 and 3.4.1.) Digital cameras with automated event detection and long term storage capabilities make this sort of network possible. The goal of the DFN's digital expansion was to cover one million square kilometres and become a regular source of planetary samples of known origin.

## 1.8 Overview of this Thesis

The contributions of this thesis are broken up into the four body chapters of this work, consisting of three journal articles and one additional chapter detailing development and engineering work not covered in the three articles.

### 1.8.1 Submillisecond fireball timing using de Bruijn time-codes

One of the previous obstacles to reducing the cost and complexity of fireball cameras was the use of multiple sensors for timing. Previous photographic fireball observatories used a periodic shutter to produce relative timing (velocity) in the camera system as well as a separate fireball detector for absolute (time of arrival) timing. This also complicates the data processing problem as the records must be correlated.

To enable the development of a smaller, more cost effective high performance fireball observatory, a novel timing technique for long exposure fireball photography was developed employing de Bruijn sequences to encode timing into the long exposure using a liquid crystal (LC) shutter. The operation is GNSS synchronised across the camera network and produces timing precision better than one millisecond.

This technique is described in chapter 2 which is an article published in the journal *Meteoritics and Planetary Science*.

### 1.8.2 How to build a continental scale fireball camera network

The design of the fireball observatory that enabled the digital expansion of the DFN is presented in chapter 3 which is an article published in the journal *Experimental Astronomy*.

The new design achieves similar spatial precision (around one arcminute) to the previous highest precision fireball observatories (the film based systems of the European Network and the DFN) at less than one tenth of the cost with an eight times longer service interval. This is achieved by building the observatory around off-the-shelf consumer components where possible and designing for ease of assembly and manufacture. The maintainability of the observatories was also considered during the design process, making the DFN observatories much more practical to use as part of a large remote fireball camera network than previous designs.

Using this design, the DFN has expanded to cover around 2.5 million square kilometres of good meteorite searching terrain in the Australian Outback (see Fig. 3.12). This coverage area makes the DFN the largest fireball camera network in the world and is sufficient to observe several meteorite producing fireballs each year.

### 1.8.3 Absolute Time Encoding for Temporal Super-resolution Using de Bruijn Timecodes

The time encoding technique created for fireball timing was further developed for other applications where high temporal and spatial precision trajectory data is required. A proof of concept prototype was developed and demonstrated for industrial imaging applications. This is described in chapter 4 which is an article that is currently under review after submission to the journal *Machine Vision and Applications*.

An overview of the general technique is presented including four different implementation configurations. A number of different possible encoding methods are discussed and the operation of the method in an industrial imaging application at 36 megapixels and 1000 Hz is demonstrated. Achieving temporal and spatial resolutions this high is not currently possible using traditional high frame rate video due to the high data bandwidth.

A provisional patent application was filed for this technique (Australian provi-

sional patent application no. 2016900714) and this is attached as appendix D.

### 1.8.4 Development of the Desert Fireball Observatories

A substantial amount of work involved in the component selection and design engineering of the observatories was not included in the above articles. Some of this is described in chapter 5 with a focus on the selection of the camera, lens and optical modulator. This chapter also presents the motivation behind the concept design of the digital fireball observatories and the evolution of the design over time. This chapter also describes the newest iteration of the digital DFN observatory design which is engineered to be more reliable, more usable and have a longer service interval than the previous versions. This is the observatory that is powering the global expansion, which is already underway.

### 1.8.5 Scope of This Thesis

It is important to note that the DFN as a project is much larger than the scope of this thesis. This thesis is concerned with the engineering design that enables the science of the DFN. The science performed by the DFN team is outside of the scope of this thesis, and for this reason these topics will not be covered in depth here. Some of these areas include trajectory modelling, sensitivity of orbital modelling to spatial and temporal precision and network efficiency as a function of time in order to determine impact rates. For this information the reader is encouraged to seek out the work of the author's DFN colleagues. The relevant works on which the author of this thesis is a coauthor and were produced during this work are listed on pages xix-xx.

### 1.8.6 Other Contributions

Whilst this dissertation covers most of the contributions of this work, there are two areas that will be discussed here but are not described at length elsewhere within this thesis.

An enormous amount of work goes into maintaining the software and hardware of a modern fireball camera network that stretches more than halfway across Australia. This is a team effort, but the component that can be attributed to this work is in the thousands of hours of mechanical and electronic design, firmware development and observatory maintenance. Thankfully, some of this time is spent in the beautiful remote locations of the Australian Outback.

The recovery of the Murrili and Dingle Dell meteorites would not have been possible without the observations made by the new digital fireball observatories. The current size of the network (significantly larger than the orignal scope for the digital expansion) is made possible by the cost effective and high performing observatory design and the effective DFN team behind it. The final result of this larger network brought about by good observatory engineering is the recovery of more planetary samples with known origins which will further the field of planetary science.

# References


[1] Meteoritical Society, *Meteoritical Bulletin*, 2017. [Online]. Available: `https://www.lpi.usra.edu/meteor` (visited on 11/21/2016).

[2] R. W. Oloff, *Apollo by the Numbers: A Statistical Reference, NASA SP-2000-4029*. NASA, 2000, ISBN: 0-16-050631-X.

[3] A. P. Vinogradov, "Preliminary data on lunar ground brought to Earth by automatic probe" Luna-16"," in *Lunar and Planetary Science Conference Proceedings*, vol. 2, 1971, p. 1.

[4] A. Vinogradov, "Preliminary data on lunar soil collected by the Luna 20 unmanned spacecraft," *Geochimica et Cosmochimica Acta*, vol. 37, no. 4, pp. 721–729, 1973.

[5] V. Barsukov, "Preliminary data for the regolith core brought to earth by the automatic lunar station Luna 24," in *Lunar and Planetary Science Conference Proceedings*, vol. 8, 1977, pp. 3303–3318.

[6] D. Brownlee, P. Tsou, J. Aléon, C. M. Alexander, T. Araki, S. Bajt, G. A. Baratta, R. Bastien, P. Bland, P. Bleuet, *et al.*, "Comet 81P/Wild 2 under a microscope," *science*, vol. 314, no. 5806, pp. 1711–1716, 2006.

[7] D. Burnett, B. Barraclough, R. Bennett, M. Neugebauer, L. Oldham, C. Sasaki, D. Sevilla, N. Smith, E. Stansbery, D. Sweetnam, *et al.*, "The Genesis Discovery Mission: return of solar matter to Earth," *Space Science Reviews*, vol. 105, no. 3-4, pp. 509–534, 2003.

[8] K. McKeegan, A. Kallio, V. Heber, G. Jarzebinski, P. Mao, C. Coath, T. Kunihiro, R. Wiens, J. Nordholt, R. Moses, *et al.*, "The oxygen isotopic composition of the Sun inferred from captured solar wind," *Science*, vol. 332, no. 6037, pp. 1528–1532, 2011.

[9] T. Nakamura, T. Noguchi, M. Tanaka, M. E. Zolensky, M. Kimura, A. Tsuchiyama, A. Nakato, T. Ogami, H. Ishida, M. Uesugi, *et al.*, "Itokawa dust particles: a direct link between S-type asteroids and ordinary chondrites," *Science*, vol. 333, no. 6046, pp. 1113–1116, 2011.

[10] H. Y. McSween, D. W. Mittlefehldt, A. W. Beck, R. G. Mayne, and T. J. McCoy, "HED Meteorites and Their Relationship to the Geology of Vesta and the Dawn Mission," *Space Science Reviews*, vol. 163, no. 1, pp. 141–174, Dec. 2011, ISSN: 1572-9672. DOI: 10.1007/s11214-010-9637-z. [Online]. Available: https://doi.org/10.1007/s11214-010-9637-z.

[11] T. B. McCord, J. B. Adams, and T. V. Johnson, "Asteroid Vesta: Spectral reflectivity and compositional implications," *Science*, vol. 168, no. 3938, pp. 1445–1447, 1970.

[12] M. Meier, "Meteoriteorbits. info-Tracking All Known Meteorites with Photographic Orbits," in *Lunar and Planetary Science Conference*, vol. 48, 2017.

[13] A. E. Rubin and J. N. Grossman, "Meteorite and meteoroid: New comprehensive definitions," *Meteoritics & Planetary Science*, vol. 45, no. 1, pp. 114–122, 2010.

[14] E. Milley, R. Hawkes, and J. Ehrman, "Meteor luminosity simulation through laser ablation of meteorites," *Monthly Notices of the Royal Astronomical Society: Letters*, vol. 382, no. 1, pp. L67–L71, 2007.

[15] Z. Ceplecha, J. Borovička, W. G. Elford, D. O. ReVelle, R. L. Hawkes, V. Porubčan, and M. Šimek, "Meteor phenomena and bodies," *Space Science Reviews*, vol. 84, no. 3-4, pp. 327–471, 1998.

[16] J. Borovička, P. Koten, P. Spurný, J. Boček, and R. Štork, "A survey of meteor spectra and orbits: evidence for three populations of Na-free meteoroids," *Icarus*, vol. 174, no. 1, pp. 15–30, 2005.

[17] M. J. Belton, *Mitigation of hazardous comets and asteroids*. Cambridge University Press, 2004.

[18] International Meteor Organization, "Glossary," Aug. 2017. [Online]. Available: `http://www.imo.net/resources/glossary`.

[19] Z. Ceplecha and J. Rajchl, "Programme of fireball photography in Czechoslovakia," *Bulletin of the Astronomical Institutes of Czechoslovakia*, vol. 16, p. 15, 1965.

[20] R. E. McCrosky and J. H. Boeschenstein, "The Prairie Meteorite Network," *Optical Engineering*, vol. 3, no. 4, pp. 304 127–304127–, 1965.

[21] I. Halliday, A. Blackwell, and A. Griffin, "The Innisfree meteorite and the Canadian camera network," *Journal of the Royal Astronomical Society of Canada*, vol. 72, pp. 15–39, 1978.

[22] P. Spurný, J. Borovička, and L. Shrbený, "Automation of the Czech part of the European fireball network: equipment, methods and first results," *Proceedings of the International Astronomical Union*, vol. 2, no. S236, pp. 121–130, 2006.

[23] P. Spurný, "Instrumentally documented meteorite falls: two recent cases and statistics from all falls," *Proceedings of the International Astronomical Union*, vol. 10, no. S318, pp. 69–79, 2015.

[24] R. M. Howie, J. Paxman, P. A. Bland, M. C. Towner, M. Cupak, E. K. Sansom, and H. A. R. Devillepoix, "How to build a continental scale fireball camera network," *Experimental Astronomy*, vol. 43, no. 3, pp. 237–266, 2017. DOI: `10.1007/s10686-017-9532-7`. [Online]. Available: `https://doi.org/10.1007%2Fs10686-017-9532-7`.

[25] B. Ivanov, G. Neukum, W. Bottke, and W. Hartmann, "The comparison of size-frequency distributions of impact craters and asteroids and the planetary cratering rate," *Asteroids III*, vol. 1, pp. 89–101, 2002.

[26] P. Bland and N. Artemieva, "Efficient disruption of small asteroids by Earth's atmosphere," *Nature*, vol. 424, no. 6946, p. 288, 2003.

[27] M. Zolensky, P. Bland, P. Brown, and I. Halliday, "Flux of extraterrestrial materials," *Meteorites and the early solar system II*, pp. 869–888, 2006.

[28] H. Dietzel, G. Eichhorn, H. Fechtig, E. Grun, H.-J. Hoffmann, and J. Kissel, "The HEOS 2 and HELIOS micrometeoroid experiments," *Journal of Physics E: Scientific Instruments*, vol. 6, no. 3, p. 209, 1973.

[29] J. Rendtel, "Review of amateur meteor research," *Planetary and Space Science*, 2017.

[30] P. Jenniskens, Q. Nénon, P. Gural, J. Albers, B. Haberman, B. Johnson, D. Holman, R. Morales, B. Grigsby, D. Samuels, *et al.*, "CAMS confirmation of previously reported meteor showers," *Icarus*, vol. 266, pp. 355–370, 2016.

[31] P. Bland, P. Spurný, A. Bevan, K. Howard, M. Towner, G. Benedix, R. Greenwood, L. Shrbený, I. Franchi, G. Deacon, *et al.*, "The Australian Desert Fireball Network: a new era for planetary science," *Australian Journal of Earth Sciences*, vol. 59, no. 2, pp. 177–187, 2012.

[32] P. A. Bland, "The desert fireball network," *Astronomy & Geophysics*, vol. 45, no. 5, pp. 5–20, 2004.

[33] P. Spurný, P. Bland, J. Borovička, M. Towner, L. Shrbený, A. W. Bevan, and D. Vaughan, "The Mason Gully meteorite fall in SW Australia: Fireball trajectory, luminosity, dynamics, orbit and impact position from photographic records (abstract 6369)," in *Proceedings, Asteroids, Comets, Meteors 2012*, 2012.

[34] P. A. Bland, P. Spurný, M. C. Towner, A. W. Bevan, A. T. Singleton, W. F. Bottke, R. C. Greenwood, S. R. Chesley, L. Shrbený, J. Borovička, Z. Ceplecha, T. P. McClafferty, V. David, G. K. Benedix, G. Deacon, K. T. Howard, I. A. Franchi, and R. M. Hough, "An anomalous basaltic meteorite from the innermost main belt," *Science*, vol. 325, no. 5947, pp. 1525–1527, 2009.

[35] P. Spurný, J. Oberst, and D. Heinlein, "Photographic observations of Neuschwanstein, a second meteorite from the orbit of the Příbram chondrite," *Nature*, vol. 423, no. 6936, pp. 151–153, 2003.

[36] P. Spurný, J. Haloda, J. Borovička, L. Shrbený, and P. Halodová, "Reanalysis of the Benešov bolide and recovery of polymict breccia meteorites–old mystery solved after 20 years," *Astronomy & Astrophysics*, vol. 570, A39, 2014.

[37] I. Halliday, A. T. Blackwell, and A. A. Griffin, "The typical meteorite event, based on photographic records of 44 fireballs," *Meteoritics*, vol. 24, no. 2, pp. 65–72, 1989.

[38] P. Spurný, P. A. Bland, L. Shrbený, J. Borovička, Z. Ceplecha, A. Singelton, A. W. Bevan, D. Vaughan, M. C. Towner, T. P. McClafferty, *et al.*, "The Bunburra Rockhole meteorite fall in SW Australia: fireball trajectory, luminosity, dynamics, orbit, and impact position from photographic and photoelectric records," *Meteoritics & Planetary Science*, vol. 47, no. 2, pp. 163–185, 2012.

[39] P. S. Gural, "Algorithms and software for meteor detection," *Earth, Moon, and Planets*, vol. 102, no. 1-4, pp. 269–275, 2008.

[40] Z. Ceplecha, "Geometric, dynamic, orbital and photometric data on meteoroids from photographic fireball networks," *Bulletin of the Astronomical Institutes of Czechoslovakia*, vol. 38, pp. 222–234, 1987.

[41] J. Trigo-Rodríguez, A. Castro-Tirado, J. Llorca, J. Fabregat, V. Martínez, V. Reglero, M. Jelínek, P. Kubánek, T. Mateo, and A. de Ugarte Postigo, "The development of the Spanish Fireball Network using a new all-sky CCD system," in *Modern Meteor Science An Interdisciplinary View*, Springer, 2005, pp. 553–567.

[42] J. Borovička, "The comparison of two methods of determining meteor trajectories from photographs," *Bulletin of the Astronomical Institutes of Czechoslovakia*, vol. 41, pp. 391–396, 1990.

[43] P. S. Gural, "A new method of meteor trajectory determination applied to multiple unsynchronized video cameras," *Meteoritics & Planetary Science*, vol. 47, no. 9, pp. 1405–1418, 2012.

[44] A. Egal, P. Gural, J. Vaubaillon, F. Colas, and W. Thuillot, "The challenge associated with the robust computation of meteor velocities from video and photographic records," *Icarus*, vol. 294, pp. 43–57, 2017.

[45] E. K. Sansom, T. Jansen-Sturgeon, M. G. Rutten, H. A. Devillepoix, P. A. Bland, R. M. Howie, M. A. Cox, M. C. Towner, M. Cupák, and B. A. Hartig, "3D Meteoroid Trajectories," *Icarus*, vol. 321, pp. 388–406, 2019, ISSN: 0019-1035. DOI: 10.1016/j.icarus.2018.09.026.

[46] E. K. Sansom, M. G. Rutten, and P. A. Bland, "Analyzing Meteoroid Flights Using Particle Filters," *The Astronomical Journal*, vol. 153, no. 2, p. 87, 2017. [Online]. Available: http://stacks.iop.org/1538-3881/153/i=2/a=87.

[47] E. Sansom, T. Jansen-Sturgeon, M. Rutten, P. Bland, H. Devillepoix, M. Towner, M. Cupak, R. Howie, M. Cox, J. Desayes, J. Paxman, and B. Hartig, "Modelling fireball network data in three dimensions," in *Proceedings, Asteroids, Comets, Meteors 2017*, 2017.

[48] E. Sansom, P. Bland, M. Rutten, J. Paxman, and M. Towner, "Filtering Meteoroid Flights Using Multiple Unscented Kalman Filters," *The Astronomical Journal*, vol. 152, no. 5, p. 148, 2016.

[49] M. Fries and J. Fries, "Doppler weather radar as a meteorite recovery tool," *Meteoritics & Planetary Science*, vol. 45, no. 9, pp. 1476–1487, 2010.

[50] J. Hoppe, "Die physikalischen Vorgänge beim Eindringen meteoritischer Körper in die Erdatmosphäre," *Astronomische Nachrichten*, vol. 262, no. 10, pp. 169–198, 1937.

[51] F. L. Whipple, "Photographic meteor studies, I," *Proceedings of the American Philosophical Society*, pp. 499–548, 1938.

[52] J. G. Hills and M. P. Goda, "The fragmentation of small asteroids in the atmosphere," *The Astronomical Journal*, vol. 105, pp. 1114–1144, 1993.

[53] Z. Ceplecha, P. Spurný, J. Borovička, and J. Keclikova, "Atmospheric fragmentation of meteoriods," *Astronomy and Astrophysics*, vol. 279, pp. 615–626, 1993.

[54] Z. Ceplecha and D. O. Revelle, "Fragmentation model of meteoroid motion, mass loss, and radiation in the atmosphere," *Meteoritics & Planetary Science*, vol. 40, no. 1, pp. 35–54, 2005.

[55] E. Öpik, *Atomic collisions and radiation of meteors*. Astronomical Observatory of Harvard College, 1933.

[56] E. Öpik, "Meteor radiation, ionization and atomic luminous efficiency," in *Proceedings of the Royal Society of London A: Mathematical, Physical and Engineering Sciences*, The Royal Society, vol. 230, 1955, pp. 463–501.

[57] E. Öpik, "Tables of meteor luminosities," *Irish Astronomical Journal*, vol. 6, p. 3, 1963.

[58] P. Spurný, J. Borovička, J. Kac, P. Kalenda, J. Atanackov, G. Kladnik, D. Heinlein, and T. Grau, "Analysis of instrumental observations of the Jesenice meteorite fall on April 9, 2009," *Meteoritics & Planetary Science*, vol. 45, no. 8, pp. 1392–1407, 2010.

[59] J. Borovička, J. Tóth, A. Igaz, P. Spurný, P. Kalenda, J. Haloda, J. Svoreň, L. Kornoš, E. Silber, P. Brown, *et al.*, "The Košice meteorite fall: Atmospheric trajectory, fragmentation, and orbit," *Meteoritics & Planetary Science*, vol. 48, no. 10, pp. 1757–1779, 2013.

[60] E. K. Sansom, P. Bland, J. Paxman, and M. Towner, "A novel approach to fireball modeling: The observable and the calculated," *Meteoritics & Planetary Science*, vol. 50, no. 8, pp. 1423–1435, 2015, ISSN: 1945-5100. DOI: 10.1111/maps.12478. [Online]. Available: http://dx.doi.org/10.1111/maps.12478.

[61] P. Jenniskens, M. D. Fries, Q.-Z. Yin, M. Zolensky, A. N. Krot, S. A. Sandford, D. Sears, R. Beauford, D. S. Ebel, J. M. Friedrich, *et al.*, "Radar-enabled recovery of the Sutter's Mill meteorite, a carbonaceous chondrite regolith breccia," *Science*, vol. 338, no. 6114, pp. 1583–1587, 2012.

[62] H. Devillepoix, P. Bland, M. Towner, E. Sansom, R. Howie, M. Cupak, G. Benedix, T. Jansen-Sturgeon, B. Hartig, M. Cox, and J. Paxman, "Fall and Recovery of the Dingle Dell Metorite," in *80th Annual Meeting of the Meteoritical Society 2017*, 2017. [Online]. Available: https://www.hou.usra.edu/meetings/metsoc2017/pdf/6211.pdf.

[63] P. Brown, D. Pack, W. Edwards, D. ReVelle, B. Yoo, R. Spalding, and E. Tagliaferri, "The orbit, atmospheric dynamics, and initial mass of the Park Forest meteorite," *Meteoritics & Planetary Science*, vol. 39, no. 11, pp. 1781–1796, 2004.

[64] A. T. Jull, "Terrestrial ages of meteorites," in *Accretion of extraterrestrial matter throughout Earth's history*, Springer, 2001, pp. 241–266.

[65] V. Dmitriev, V. Lupovka, and M. Gritsevich, "Orbit determination based on meteor observations using numerical integration of equations of motion," *Planetary and Space Science*, vol. 117, pp. 223–235, 2015.

[66] D. L. Clark and P. A. Wiegert, "A numerical comparison with the Ceplecha analytical meteoroid orbit determination method," *Meteoritics & Planetary Science*, vol. 46, no. 8, pp. 1217–1225, 2011.

[67] S. Hughes, *Catchers of the Light: The Forgotten Lives of the Men and Women Who First Photographed the Heavens*. Stefan Hughes, 2012, ISBN: 9781620509616. [Online]. Available: `https://books.google.com.au/books?id=iZk5OOf7fVYC`.

[68] V. Fedynsky, *Meteors*. The Minerva Group, Inc., 2002.

[69] E. C. Pickering, "Spectrum of a Meteor," *Astronomische Nachrichten*, vol. 145, no. 4-5, pp. 77–80, 1898.

[70] L. G. Jacchia and F. L. Whipple, "The Harvard photographic meteor programme," *Vistas in Astronomy*, vol. 2, pp. 982–994, 1956.

[71] Z. Ceplecha, "Statistical Observations of Meteors 1951.," *Bulletin of the Astronomical Institutes of Czechoslovakia*, vol. 3, p. 53, 1952.

[72] Z. Ceplecha, "Multiple fall of Přibram meteorites photographed. 1. Double-station photographs of the fireball and their relations to the found meteorites," *Bulletin of the Astronomical Institutes of Czechoslovakia*, vol. 12, p. 21, 1961.

[73] R. McCrosky, A. Posen, G. Schwartz, and C.-Y. Shao, "Lost City meteorite—Its recovery and a comparison with other fireballs," *Journal of Geophysical Research*, vol. 76, no. 17, pp. 4090–4108, 1971.

[74] J. Oberst, S. Molau, D. Heinlein, C. Gritzner, M. Schindler, P. Spurný, Z. Ceplecha, J. Rendtel, and H. Betlem, "The "European Fireball Network": current status and future prospects," *Meteoritics & Planetary Science*, vol. 33, no. 1, pp. 49–56, 1998.

[75] A. Bischoff, J.-A. Barrat, K. Bauer, C. Burkhardt, H. Busemann, S. Ebert, M. Gonsior, J. Hakenmüller, J. Haloda, D. Harries, *et al.*, "The Stubenberg meteorite—An LL6 chondrite fragmental breccia recovered soon after precise prediction of the strewn field," *Meteoritics & Planetary Science*, 2017.

[76] J. Borovička, P. Spurný, and P. Brown, "Small near-Earth asteroids as a source of meteorites," *et al., Asteroids IV, Univ. of Arizona, Tucson*, pp. 257–280, 2015.

[77] P. Spurný, J. Borovička, J. Haloda, L. Shrbený, and D. Heinlein, "Two Very Precisely Instrumentally Documented Meteorite Falls: Žďar nad Sázavou and Stubenberg–Prediction and Reality," *LPI Contributions*, vol. 1921, 2016.

[78] P. Spurný, J. Borovička, G. Baumgarten, H. Haack, D. Heinlein, and A. Sørensen, "Atmospheric trajectory and heliocentric orbit of the Ejby meteorite fall in Denmark on February 6, 2016," *Planetary and Space Science*, 2016.

[79] M. Towner, P. Bland, P. Spurný, G. Benedix, K. Dyl, R. Greenwood, J. Gibson, I. Franchi, L. Shrbený, A. Bevan, *et al.*, "Mason Gully: The second meteorite recovered by the Desert Fireball Network," vol. 74, 2011, p. 5124.

[80] J. M. Trigo-Rodríguez, J. Llorca, J. M. M. Gil, I. Williams, A. J. C. Tirado, J. L. O. Moreno, J. A. Azcárate, J. Zamorano, V. Lanchares, J. A. Docobo, *et al.*, "The impact of neos and their fragments recorded from the ground: ongoing research lines of the spanish fireball network," in *1st IAA Planetary Defense Conference: 27-30 April 2009, Granada, Spain*, 2009.

[81] J. M. Trigo-Rodríguez, J. Borovička, P. Spurný, J. L. Ortiz, J. A. Docobo, A. J. CASTRO-TIRADO, and J. Llorca, "The Villalbeto de la Peña meteorite fall: II. Determination of atmospheric trajectory and orbit," *Meteoritics & Planetary Science*, vol. 41, no. 4, pp. 505–517, 2006.

[82] J. M. Trigo-Rodríguez, J. Borovička, J. Llorca, J. M. Madiedo, J. Zamorano, and J. Izquierdo, "Puerto Lápice eucrite fall: Strewn field, physical description, probable fireball trajectory, and orbit," *Meteoritics & Planetary Science*, vol. 44, no. 2, pp. 175–186, 2009.

[83] E. Blanch, J. M. Trigo-Rodríguez, J. Madiedo, E. Lyytinen, M. Moreno-Ibáñez, M. Gritsevich, and D. Altadill, "Detection of nocturnal and daylight bolides from Ebre Observatory in the framework of the SPMN fireball network," in *Assessment and Mitigation of Asteroid Impact Hazards*, Springer, 2017, pp. 185–197.

[84] F. Colas, B. Zanda, S. Bouley, J. Vaubaillon, P. Vernazza, J. Gattacceca, C. Marmo, Y. Audureau, M. K. Kwon, L. Maquet, *et al.*, "The FRIPON and Vigie-Ciel networks," in *Proceedings of the International Meteor Conference, Giron, France, 18-21 September 2014*, vol. 1, 2014, pp. 34–38.

[85] F. Colas, B. Zanda, J. Vaubaillon, S. Bouley, C. Marmo, Y. Audureau, M. K. Kwon, J.-L. Rault, S. Caminade, P. Vernazza, *et al.*, "French fireball network FRIPON," in *International Meteor Conference Mistelbach, Austria*, 2015, pp. 37–40.

[86] J.-L. Rault, F. Colas, and J. Vaubaillon, "Radio set-up design for the FRIPON project," in *Proceedings of the International Meteor Conference, Giron, France, 18-21 September 2014*, vol. 1, 2014, pp. 185–186.

[87] FRIPON, *Radio network*, Sep. 2017. [Online]. Available: `https://www.fripon.org/spip.php?article42`.

[88] T. Watson, "France launches massive meteor-spotting network: tracking space rocks that reach earth will give insight into the early Solar System," *Nature*, vol. 534, no. 7607, pp. 304–306, 2016.

[89] M. Gritsevich, E. Lyytinen, J. Moilanen, T. Kohout, V. Dmitriev, V. Lupovka, S. Midtskogen, N. Kruglikov, A. Ischenko, G. Yakovlev, V. Grokhovsky, J. Haloda, P. Halodova, J. Peltoniem, A. Aikkila, A. Taavitsainen, J. Lauanne, M. Pekkola, P. Kokko, P. Lahtinen, and M. Larionov, "First meteorite recovery based on observations by the Finnish Fireball Network," in *Proceedings of the International Meteor Conference, Giron, France*, 2014, pp. 162–169.

[90] A. Olech, P. Zoladek, M. Wisniewski, Krasnowski M., M. Kwinta, T. Fajfer, K. Fietkiewicz, D. Dorosz, L. Kowalski, J. Olejnik, K. Mularczyk, and K. Zloczewski, "Polish Fireball Network," in *Proceedings of the International Meteor Conference, 24th IMC, Oostmalle, Belgium, 2005*, L. Bastiaens, J. Verbert, and V. C. J.-M. Wislez, Eds., Aug. 2006, pp. 53–62.

[91] M. Wiśniewski, P. Żołądek, A. Olech, Z. Tyminski, M. Maciejewski, K. Fietkiewicz, R. Rudawska, M. Gozdalski, M. Gawroński, T. Suchodolski, *et al.*, "Current status of Polish Fireball Network," *Planetary and Space Science*, 2017.

[92] R. Weryk, P. Brown, A. Domokos, W. Edwards, Z. Krzeminski, S. Nudds, and D. Welch, "The Southern Ontario all-sky meteor camera network," *Earth, Moon, and Planets*, vol. 102, no. 1-4, pp. 241–246, 2008.

[93] P. Brown, R. Weryk, S. Kohut, W. Edwards, and Z. Krzeminski, "Development of an all-sky video meteor network in Southern Ontario, Canada The ASGARD System," *WGN, Journal of the International Meteor Organization*, vol. 38, pp. 25–30, 2010.

[94] W. J. Cooke and D. E. Moser, "The status of the NASA all sky fireball network," in *Proceedings of the International Meteor Conference, 30th IMC, Sibiu, Romania, 2011*, 2012, pp. 9–12.

[95] NASA Meteoroid Environment Office, *NASA All Sky Fireball Network*, Sep. 2017. [Online]. Available: `https://www.nasa.gov/offices/meo/outreach/all_sky_fireball_network_detail.html`.

[96] G. Kokhirova, P. Babadzhanov, and U. K. Khamroev, "Tajikistan fireball network and results of photographic observations," *Solar System Research*, vol. 49, no. 4, pp. 275–283, 2015.

[97] P. Jenniskens, P. Gural, L. Dynneson, B. Grigsby, K. Newman, M. Borden, M. Koop, and D. Holman, "CAMS: Cameras for Allsky Meteor Surveillance to establish minor meteor showers," *Icarus*, vol. 216, no. 1, pp. 40–61, 2011, ISSN: 0019-1035. DOI: `10.1016/j.icarus.2011.08.012`. [Online]. Available: `http://www.sciencedirect.com/science/article/pii/S0019103511003290`.

[98] P. Jenniskens, A. E. Rubin, Q.-Z. Yin, D. W. Sears, S. A. Sandford, M. E. Zolensky, A. N. Krot, L. Blair, D. Kane, J. Utas, *et al.*, "Fall, recovery, and characterization of the Novato L6 chondrite breccia," *Meteoritics & Planetary Science*, vol. 49, no. 8, pp. 1388–1425, 2014.

[99] P. Jenniskens, *CAMS: Participate*, Sep. 2017. [Online]. Available: `http://cams.seti.org/easyCAMS.html`.

[100] R. Weryk, M. Campbell-Brown, P. Wiegert, P. Brown, Z. Krzeminski, and R. Musci, "The Canadian automated meteor observatory (CAMO): system overview," *Icarus*, vol. 225, no. 1, pp. 614–622, 2013.

[101] A. Bevan and R. Binns, "Meteorites from the Nullarbor Region, Western Australia: I. A review of past recoveries and a procedure for naming new finds," *Meteoritics*, vol. 24, no. 3, pp. 127–133, 1989.

[102] M. C. Towner, P. A. Bland, P. Spurný, G. K. Benedix, K. Dyl, A. W. R. Bevan, and D. Vaughan, "Towards a Digital Desert Fireball Network for Meteorite Recovery," vol. 75, Sep. 2012, p. 5123.

# Chapter 2

# Submillisecond fireball timing using de Bruijn timecodes

Robert M. Howie[1], Jonathan Paxman[1], Philip A. Bland[2], Martin C. Towner[2], Eleanor K. Sansom[2], and Hadrein A. R. Devillepoix[2]

[1]Department of Mechanical Engineering, Curtin University, Perth, Australia
[2]Department of Applied Geology, Curtin University, Perth, Australia

*This article is published in Meteoritics & Planetary Science (available at DOI: 10.1111/maps.12878),*  *The formatting and referencing style have been modified for presentation in this thesis. The original article is reprinted in its published form with permission in Appendix A.*

# Authorship Declaration

**Article Title:** Submillisecond fireball timing using de Bruijn timecodes

**Journal:** Meteoritics & Planetary Science

**Publication Status:** Published on 16 May 2017

## Author Contributions

### Robert Howie

Led the development, implementation and testing of the timing technique; conceived, drafted and revised manuscript; and handled the publication process

Manuscript contribution: 82%  22 September 2017

### Jonathan Paxman

Assisted with concept development, implementation and manuscript editing

Manuscript contribution: 5%  20 September 2017

**Philip Bland**

Led specification development and assisted with concept development and manuscript editing

Manuscript contribution: 5%  22 September 2017

**Martin Towner**

Assisted with concept implementation, specification development and manuscript editing

Manuscript contribution: 2%  19 September 2017

**Eleanor Sansom**

Performed trajectory modelling for manuscript example fireball and assisted with manuscript editing

Manuscript contribution: 3%  19 September 2017

**Hadrien Devillepoix**

Performed orbit calculation for manuscript example fireball and assisted with manuscript editing

Manuscript contribution: 3%  19 September 2017

**Abstract** Long-exposure fireball photographs have been used to systematically record meteoroid trajectories, calculate heliocentric orbits, and determine meteorite fall positions since the mid-20th century. Periodic shuttering is used to determine meteoroid velocity, but up until this point, a separate method of precisely determining the arrival time of a meteoroid was required. We show it is possible to encode precise arrival times directly into the meteor image by driving the periodic shutter according to a particular pattern—a de Bruijn sequence—and eliminate the need for a separate subsystem to record absolute fireball timing. The Desert Fireball Network has implemented this approach using a microcontroller driven electro-optic shutter synchronized with GNSS UTC time to create small, simple, and cost-effective high-precision fireball observatories with submillisecond timing accuracy.

## 2.1 Introduction

Meteorites provide valuable insight into the formation and history of the solar system and have remained relatively undisturbed since the formation of their parent bodies. There is no shortage of recovered meteorites available for study, but interpreting the results of the physical and chemical analysis is constrained by a lack of knowledge of the precise origins of the samples; this lack of context also limits the conclusions that can be drawn from a single meteorite. The solution is to study planetary materials of known origins. Sample return and rendezvous space missions to asteroids and comets are expensive and high-risk approaches to solving this problem; fireball camera networks which record atmospheric trajectories of bright meteors can provide a cost-effective alternative.

Fireball camera networks traditionally use long-exposure photography from multiple stations to produce a triangulated trajectory with sufficient precision to recover meteorites and calculate heliocentric orbits that can be compared to the orbits of potential parent bodies [103]. Long-exposure images are occulted by a periodic shutter in order to determine meteoroid velocity during the observable trajectory [70], [104]. Traditionally, these systems have required separate timing subsystems to record absolute arrival times for orbit calculation [20], [21]. We present a technique using timecodes constructed from de Bruijn sequences [105],

[106] to embed the arrival time into the fireball trail image using an electro-optic shutter with no moving parts. This approach enables much smaller, lower power, and more cost-effective fireball cameras than previously possible, and has allowed the rapid deployment of the Desert Fireball Network (DFN) [31] in the Australian Outback. The development is significant in that it allows off-the-shelf cameras to be turned into high-precision fireball observatories without the need for additional sensors. The design also significantly simplifies data reduction. The motivation and development will be outlined along with a demonstration of the results produced using the technique to gather all required trajectory data from a single long-exposure image per station.

Using this technique, the Desert Fireball Network has achieved spatial precision of approximately 1 arcminute and submillisecond timing precision at a fraction of the cost of previous observatories. The technique could also be applied to other areas where high-precision motion-time data are required, including spacecraft, particle image velocimetry, and tracking other objects or phenomena.

## 2.2 Fireball Camera Networks

Fireball camera networks continuously observe the night sky for rare bright meteors known as fireballs or bolides, which may result in single or multiple meteorite falls. The bright flight or observable luminous trajectory of the fireball (as the meteoroid ablates in the atmosphere) is recorded on a highly accurate imaging device from multiple geographically distinct stations. The meteoroid's trajectory through the Earth's atmosphere is triangulated from these multiple observations in order to determine the estimated fall location and the meteoroid's preatmospheric entry orbit. In addition to the path through the atmosphere, the distributed observatories must also accurately record timing of the trajectory. The relative timing is vital for determining meteoroid velocity and deceleration, which, in combination with the path geometry, allows the estimation of its mass and hence a fall position distribution. The absolute arrival time of the fireball is required to accurately determine the heliocentric orbit of the meteoroid due to the constant orbital motion and rotation of the Earth.

Three large fireball networks were developed in the 1960s and 1970s. The Czechoslovak Fireball Network (now the European Fireball Network) commenced operations with all-sky cameras in 1963 [19], shortly followed by the Prairie Meteorite Network in the Midwest United States in 1964 [20] and the Canadian Meteorite Observation and Recovery Project (MORP) in 1971 [21]. The Desert Fireball Network (DFN), located in the remote Australian Outback, commenced operation in 2003 with the testing of a large-format film-based observatory based on the recent European Network automated design [22] with modifications for the Australian climate [31]. The network became operational with three stations in 2005, and a fourth station was added in 2007 [38] . The trial network successfully recovered two meteorites: Bunburra Rockhole [34], [38] and Mason Gully [33], [107]. This success paved the way for the development and deployment of the first all digital fireball camera network designed for meteorite recovery.

Fireball trajectories must be recorded with high accuracy and precision to ensure meteorites can be located and meteoroid orbits can be meaningfully compared to the orbits of potential parent bodies. Due to the extremely low population density and remoteness of the region, meteorite searches in the Australian Outback are typically conducted by small teams (5–12 persons) on foot, for up to 2 weeks. This places an upper limit on the area of searchable terrain for each predicted meteorite fall (approximately 2–6 $km^2$), which informs the precision requirements for the network (DFN precision goals for bright flight observations: meteoroid trajectory: $<$50 m, triangulation final vector: $<0.05°$, mass: 1 order of magnitude). The relative timing along the bright flight trajectory provides the velocity information required to calculate a fall position probability distribution, while the precise absolute arrival time is required for the orbital calculation. Trajectory analysis and mass estimation are performed using the dynamic method detailed in [60], giving a robust analysis of the observational and modeling errors involved. After the mass distribution has been estimated, dark flight modeling simulates the meteoroid behavior as it falls to the ground after ablation ceases and it is no longer visible to the camera network; the atmospheric conditions are modeled in the relevant volume from a climate model based on the best available local meteorological data including ground- based measurements and balloon flight data.

Uncertainties in the observed position and velocity of the meteoroid during the trajectory increase the area of the ground search; for this reason, meteor camera networks have previously used large-format film-based cameras to achieve high spatial precision (approximately 1 arcminute, limited by film developing and scanning techniques [38]). The DFN uses high- resolution (36 megapixel), full-frame (24.9 $\times$ 36 mm) digital sensors with fisheye all-sky lenses to achieve similar spatial precision. The digital observatories are constructed from off-the-shelf components where possible to simplify manufacturing and reduce costs [24]. They are significantly smaller and easier to manufacture and install than previous designs and integrate with an automated data processing pipeline to greatly reduce the data reduction workload of a large network.

### 2.2.1 Relative Fireball Trajectory Timing

Relative fireball timing is determined by periodically occulting the sensor or film plane during a long-exposure fireball image. This chops the meteor trail (Fig. 2.1a) into small segments (Fig. 2.1b) at a known rate, allowing the calculation of meteoroid velocity throughout the luminous trajectory after triangulation from multiple stations. The first purpose-built fireball observatories in the Czechoslovak network used a mechanical rotating shutter to periodically obstruct the film plane similar to previous meteor camera designs [19], [108]. The rotational position of the shutter is tightly controlled with respect to time. As the shutter rotates throughout the exposure, the open sectors in the disk create the visible dashes, and the opaque sectors create blanks in the trail where the light path from the fireball to the film plane is obstructed. This relative timing data enables the estimation of fall site distributions but not heliocentric orbits. The Prairie Network replaced the rotating mechanical shutter with a solenoid-controlled switching shutter that moved a lightweight blade in and out of the optical path within the lens [20]. This switching shutter operated at 20 cycles per second to produce regular dashes in fireball trails for relative timing similar to the rotating approach. The Canadian MORP network used modified slow-rotating shutters with three different sectors producing four dashes per second, one transparent and two different neutral density filters to allow the imaging of very bright fireballs that would otherwise overexpose the film [21].

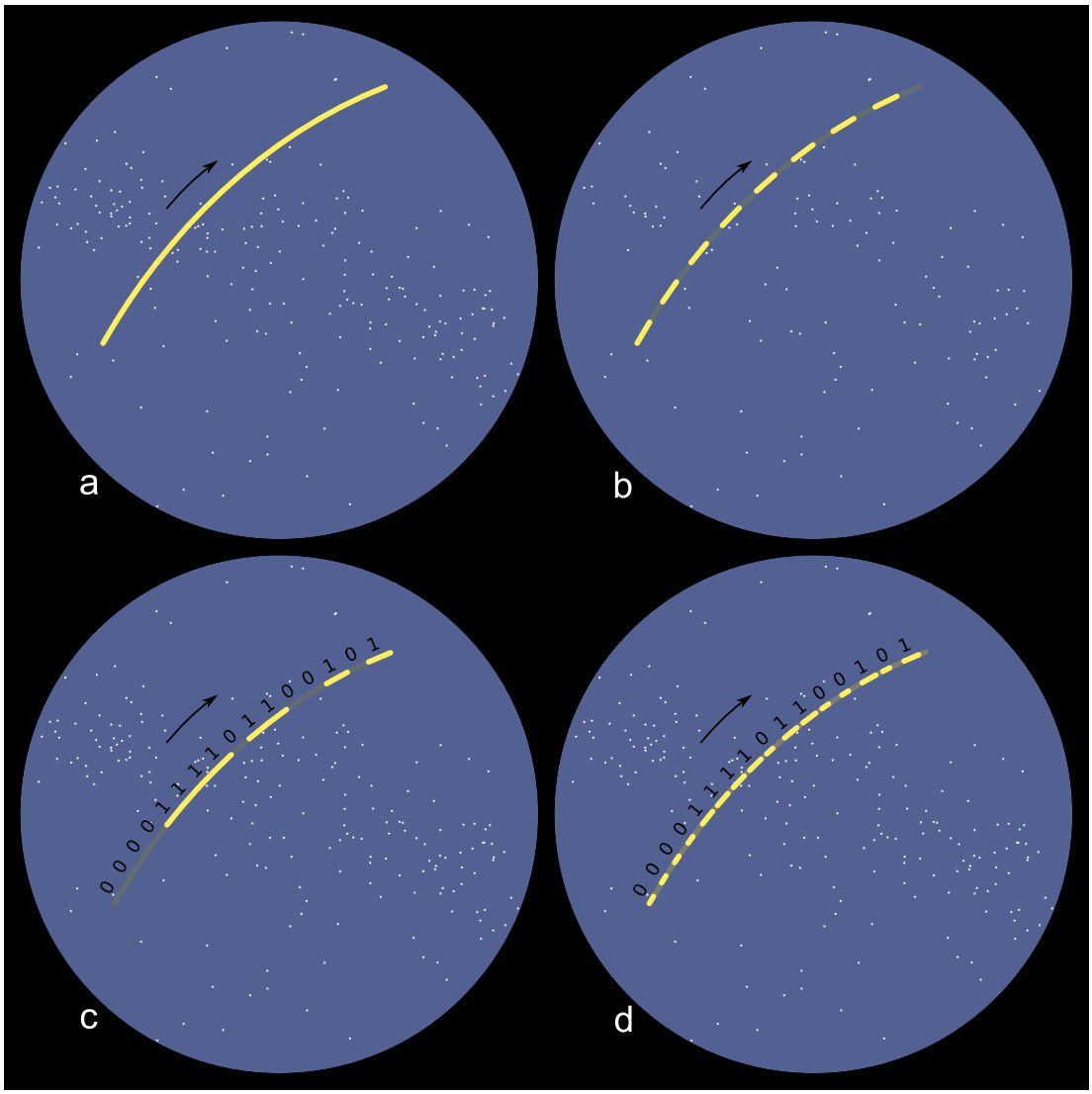


Figure 2.1: Long exposure fireball encoding using a light modulator
a) long exposure, no encoding
b) traditional periodic occultation for velocity determination
c) de Bruijn sequence encoded as shutter opacity (0: closed, 1:open)
d) de Bruijn sequence encoded as pulse width (0: short, 1:long)

### 2.2.2 Absolute Fireball Trajectory Timing (Arrival Time)

The absolute arrival time of a meteoroid is required in addition to the path and velocity of the meteor's luminous trajectory in order to calculate the meteoroid's preatmospheric orbit due to the constant orbital motion and rotation of the Earth. Because photographs in long-exposure fireball camera networks can be up to one night in length, a method of determining the arrival time of a fireball within the exposure is required. The three large networks took different approaches to the absolute timing problem. The Czechoslovak network initially relied on chance human observations for arrival times, but was then upgraded to determine absolute timing by comparing images from the fixed fireball cameras with rotating shutters to concurrent images from identical sidereal-guided cameras on equatorial mounts [108]. The difference in position of the meteor trail image between the two cameras is determined by the position of the guided camera when the meteor arrives. This allows the calculation of the arrival time due to the precise relationship between time of day and the guided camera's position. This method is theoretically simple but relies on very precise movement of the equatorial mount to achieve the specified timing precision of $\pm 5$ s [109]. The Prairie Network recorded absolute timing by modifying the switching shutter's pattern of operation. A break was extended to denote the beginning of a timing window. Different dashes were omitted in each window by holding the switching shutter closed to indicate which 10.4 s window in the 4 h exposure a fireball appeared [20]. A photomultiplier tube (PMT) was also used to timestamp arrivals, but only for meteors brighter than magnitude -4 (fireballs). The MORP observatories were also equipped with a PMT—this time behind interleaved perforated masks to detect motion in the appropriate (angular) velocity range for meteors via an electronic filter circuit. This meteor detector printed the arrival time on the current sheet of film in the camera and then advanced the film to the next frame. The Czechoslovak design (now operating within the European Fireball Network) was updated in the late 1990s with the addition of a PMT to record meteor light curves at a high sample rate and remove the need for guided cameras operating alongside the fixed cameras [74]; this Czech design was later automated to reduce the labor demand [22].

Standard video cameras are also used in some fireball networks (Finnish Fireball

Network [89], Spanish Fireball Network [41], Polish Fireball Network [90], the Croatian Meteor Network [110], and others). These video cameras can offer good timing precision, do not require data integration from multiple sensors, and are often used in amateur and collaborative networks where the low per station cost makes them an attractive option. However, the poor spatial resolution offered by systems built around commonly available video cameras paired with all-sky lenses produces significant uncertainty in the fall position and orbit, reducing the likelihood of successful meteorite recovery and the chance of matching an orbit to a potential parent body. Video systems based on expensive high-resolution industrial imaging cameras or using multiple video cameras with rectilinear lenses (such as Cameras for Allsky Meteor Surveillance [CAMS] [Jenniskens et al. 2011]) can achieve similar spatial precision to still cameras. However, the high data rates can make the overall solution complex.

The absolute timing precision required for accurate orbit determination depends on the spatial precision of the observatory. Absolute timing precision of 1 s is sufficient for orbit determination by networks similar to the DFN (high-resolution still cameras with all-sky lenses). More precise timing will not result in more precise orbits due to the spatial uncertainty. The submillisecond timing precision offered by this technique becomes more useful for orbit determination when higher spatial precision instruments such as traditional telescopes and fireball observatories incorporating narrow angle rectilinear lenses are used. The technique can be applied in these higher spatial precision instruments without additional difficulty.

High absolute timing precision is also useful for other purposes aside from orbit determination. The ability to precisely align camera network fireball observations with other timed data sources such as Doppler RADAR (which can provide meteoroid positions at lower altitudes than camera networks) can be beneficial for the recovery of meteorites in more difficult situations. Accurate absolute timing of the data points in fireball images also makes a wider range of triangulation techniques possible because the trajectory data points can be individually triangulated.

## 2.3 A New Approach

The primary objective during the development of a new fireball observatory for the DFN was to reduce the per station cost in order to deploy the largest network possible on a finite budget while maintaining the precision required for meteorite recovery. The expected number of meteorite dropping fireballs observed by the network per year depends primarily on the network coverage area, and the likelihood of recovery depends on the suitability of the meteorite searching terrain. The primary factors contributing to the high cost of previous designs were the custom large-format film-based imaging system, the precision manufacturing and assembly required to produce the mechanical shutter, and the expensive and complex photomultiplier tube subsystem. The new DFN observatories are based around off-the-shelf consumer digital cameras in order to significantly reduce the per station cost and utilize an automatic data pipeline for triangulation, fall position estimation, and orbit calculation. After testing a number of camera and lens options, the Nikon D810 (offering high resolution and good low-light noise performance) and Samyang 8 mm f/3.5 II (offering a favorable projection and good value) were selected. A mechanical shutter of the rotating or switching type presents an obstacle to reducing the per observatory cost; the tight manufacturing tolerances and difficult assembly required to implement a precisely controlled mechanical shutter between the lens and sensor plane would significantly contribute to the overall cost of each observatory.

An electro-optic shutter does not require such tight manufacturing tolerances and significantly reduces complexity with no moving parts, resulting in greatly reduced manufacturing and assembly costs. Liquid crystal, polymer-dispersed liquid crystal, and switchable liquid crystal mirror shutter technologies were tested; the liquid crystal (LC) shutter option was selected for its proven track record in long-lasting consumer products (liquid crystal displays), ease of implementation, low cost, and availability. The LC shutter also has the added advantage of global operation, where the transmittance changes across the whole frame with the same timing and hence timing is position independent. This is in contrast to a rotating shutter where the sweeping motion of the rotating shutter across the frame over time must be considered [40]. The drawback of LC shutters is the limited open state transmittance—approximately 36% for the LC-Tec X-FOS shutters

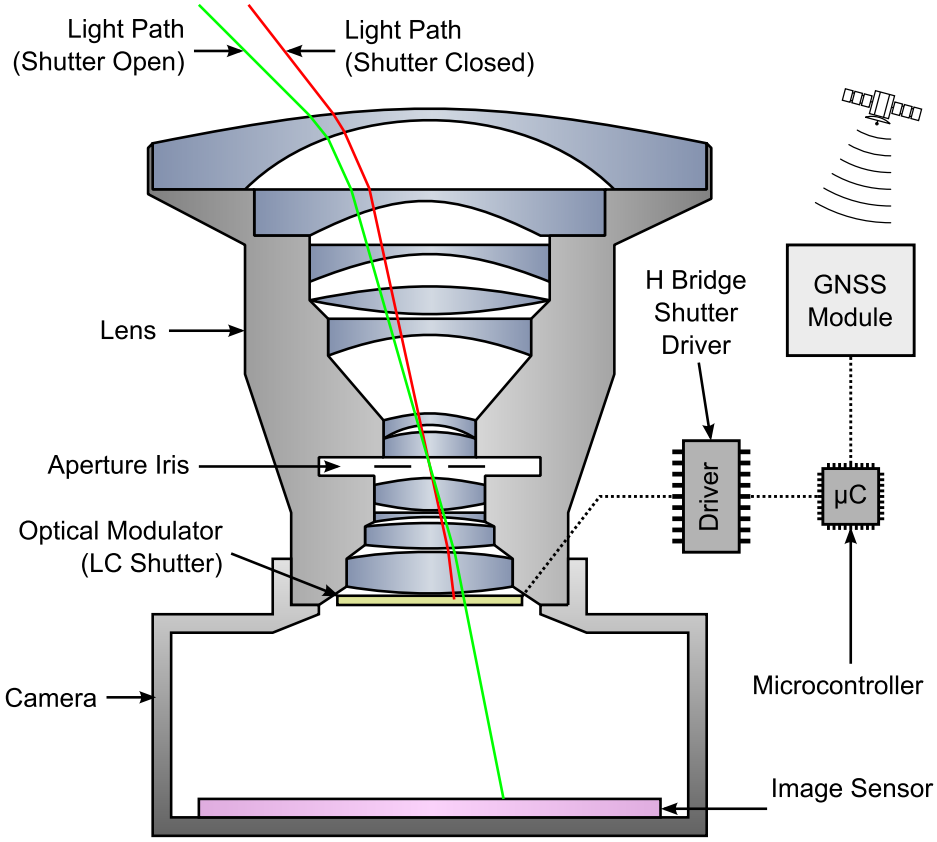


Figure 2.2: Imaging system showing all-sky lens, camera, LC shutter, shutter driver, microcontroller, and GNSS receiver.

used by the DFN [111]; this drives the need for good low-light performance from the camera. The LC shutter is mounted between the lens and the sensor plane to periodically obstruct the light path like the mechanical shutters of previous designs, but without moving parts. The shutter must be as thin as possible to minimize focus shift and optical aberrations. The LC shutter is simply mounted over the rear element of the all-sky lens (Fig. 2.2), and the thin drive wires are routed out through the side of the lens.

### 2.3.1 A new Technique for Absolute Timing

The previous techniques for determining arrival time in long-exposure fireball images are not ideal for a low-cost fireball camera network deployed in the Aus-

tralian Outback where the observatories must operate in harsh conditions without manual intervention for periods up to 1 yr. The dust and high winds prevalent in the outback make it difficult and expensive to design and construct precision mechanical systems that operate reliably without frequent maintenance; the dual guided and unguided camera configuration of the original Czechoslovak system was not considered for this reason. The photomultiplier tubes of the recent European network design provide fireball timing along with well-resolved brightness data but are expensive and require high voltage power supplies, complex supporting electronics, a separate optical window or cover, and constant drive voltage adjustments in order to capture a high dynamic range and prevent destruction of the PMT. Processing the brightness curve data is not simple due to the changing drive voltage (affecting gain) and the angle-dependent response of the PMT. Avoiding the added cost and complexity of a separate absolute timing subsystem enables a more cost-effective, smaller, and more power efficient fireball camera. The coded shutter approach of the Prairie Meteorite Network [20] partly achieves this as it records absolute timing in the fireball's trail as it travels across the frame of the long-exposure image, but the precision of the system is too low (within a 10.4 s window) to meet the DFN's objectives for high orbital accuracy.

### 2.3.2 Time Encoding

Electro-optic shutters make more advanced time encoding straightforward: the devices have fast response times compared to mechanical alternatives and are simple to drive electronically. The flexibility of a microcontroller-driven LC shutter makes it possible to encode absolute timing data (arrival time) by slightly varying the pattern used for relative timing data (velocity) according to a timecode without requiring any additional hardware. Higher precision than previous attempts at using timecodes—in absolute timing and therefore orbits—is achieved with a constantly changing sequence that does not repeat during the exposure and by synchronizing the operation with highly accurate GNSS time. GNSS or global navigation satellite systems use constellations of satellites (including GPS, GLONASS, QZSS, Galileo, and Compass/BeiDou) to provide users with precise positioning and timing data. When a meteor or fireball appears, the image of the meteor trail is embedded with a part of this timecode as the meteor moves across the frame, while the LC shutter modulates the light transmittance accord-

ing to the timecode sequence. The part of the timecode sequence visible in the meteor trail corresponds to the time within the long exposure where the fireball was visible. This records the absolute timing data including the arrival time, and makes the calculation of the heliocentric orbit possible. The recording of the relative and absolute timing data is inherent in the image and does not require the integration of data from multiple subsystems, therefore simplifying the data processing problem.

The ideal timecode should be as long as possible in order to maximize the possible exposure length, but require as few elements visible as possible for time decoding in order to capture the arrival times of short fireballs. While short fireballs are less likely to drop recoverable meteorites, they appear more frequently and are important for the statistical analysis of meteoroid orbits, a secondary goal of the DFN.

A number of different types of sequences were considered as timecodes. The characters in the sequence produce uniquely recognizable image features (e.g., brightness, or dash length—depending on the encoding used); the absolute timing of the trajectory can be determined when the pattern of features visible in the image can be matched with a section of the timecode sequence. The conceptually simplest is a counter sequence with each digit encoded as a different shutter opacity (the first approach in Table 2.1). This type of sequence is not optimal because the start of each subsequence is not defined and the number of elements that must be visible to decode the unique arrival time varies throughout the sequence. An alternate encoding with a character reserved to define the start of each subsequence could be used (the second approach in Table 1), but this is an inefficient usage of a character in the sequence alphabet that could otherwise be used to extend the sequence. A longer sequence allows a longer exposure on the fireball observatory; this extends the camera lifetime and reduces the amount of data collected per night resulting in longer periods between visits for maintenance and drive changes.

Table 2.1: A simplistic comparison of three timecode approaches using the three character alphabet 0,1,2. Each sequence requires three elements to be known for the unique position within the sequence (time within the timecode) to be discovered (for all positions in the sequence).

| **Approach** | **Resulting sequence** | **Sequence Length** |
|---|---|---|
| Counter sequence | 000102101112202122 | 18 |
| Counter sequence with reserved start character | 000102101112202122 | 12 |
| de Bruijn sequence | 000102101112202122 | 27 |

The optimal solution for this type of problem is a sequence that includes every subsequence exactly once for a given subsequence length (the third approach in Table 1). This type of sequence is known as a full length cycle or de Bruijn sequence [105], [106].

## 2.4 De Bruijn Sequences

De Bruijn sequences are the shortest cyclic sequences containing all possible subsequences for a given alphabet and subsequence length. Their existence was formally described by Flye Sainte-Marie [105] and then independently described again several times in the 20th century [112]. De Bruijn's paper [106] is the best known of these rediscoveries and the reason they are often referred to as de Bruijn sequences today. Interestingly, their use dates at least as far back as an ancient Sanskrit sutra for memorizing rhythms around 1000 AD [113], [114]. As an example, the de Bruijn sequence "00011101" contains all of the eight possible three element subsequences "000," "001," "011," "111," "110," "101," "010," and "100" for the binary alphabet $\mathbf{A}=\{0, 1\}$ when considered cyclically (the last three digit subsequence is formed by the last digit and the first two). As a window three elements in length is slid along the cyclical sequence, each subsequence is revealed. In the fireball camera application, the sequence is encoded by the electro-optic shutter over time and the window revealing a particular subsequence is the appearance of a fireball in the frame. The elements visible in the fireball's trail indicate the position in the timecode and therefore the fireball's time of arrival. Subsequences are also referred to as n-tuples, where n is the subsequence length; de Bruijn sequences are also known as full-length cycles because they contain all possible $n$-tuples.

Given an alphabet $\boldsymbol{A}$ with size $k$ (a k-ary alphabet) and a subsequence length of n, there are number of different particular de Bruijn sequences that satisfy the above criteria. The number $|\boldsymbol{B}|$ distinct sequences $\boldsymbol{B}_{\mathrm{i}}$ for the case $\boldsymbol{B}(k,\, n)$ can be calculated from de Bruijn's Theorem generalized for $k$-ary alphabets [115] (Equation 2.1).

$$|B(k,n)| = \frac{(k!)^{n-1}}{k^n}. \tag{2.1}$$

For many applications such as meteor trajectory encoding, it is not important to know all of these sequences, or even the number of distinct sequences. What is required, however, is the ability to procedurally generate at least one of these sequences for all relevant cases of $n$ and $k$. There are various algorithms for developing de Bruijn sequences, many of which are discussed in [116] and [117]. Memory usage and computation speed of these algorithms are of interest to users in the fields of communication and genetics where sequences can be billions of elements long [118]; these factors are unimportant for fireball cameras where only relatively short sequences (several hundred elements in length) are required for encoding meteor trajectory data. The length of the de Bruijn sequences $N$ depends on the subsequence length $n$ and the alphabet size $k$ (Equation 2.2).

$$N = k^n \tag{2.2}$$

This length refers to the size of the cyclic sequence where the subsequence beginning with the last element in the sequence is completed by the first $n$-1 elements. The number of possible sequences increases rapidly as the alphabet size or subsequence lengths increase. There are 24 possible distinct sequences of nine elements in length for $\boldsymbol{B}(k{=}3,\, n{=}2)$, but this increases to 373,248 distinct sequences of 27 elements in length for the case $\boldsymbol{B}(k{=}3,\, n{=}3)$.

### 2.4.1 De Bruijn Sequence Generation

A repeatable method of generating de Bruijn sequences is required to implement the encoding on the observatory and the decoding in the image processing pipeline; one of the simpler ways to construct a de Bruijn sequence is the prefer high method which is a generalization of the prefer one method for binary alphabets detailed in [116]. The construction starts with $n$ zeros. Then the highest number in the alphabet ($k$-1) is inserted unless this would produce an $n$-tuple already present in the sequence. In this case, the next highest element is tried and the process continues until the sequence is complete. An implementation of this algorithm is presented above in pseudocode.

This method is simple to implement, but there is no methodical way to know where a particular subsequence appears in the sequence without generating it and performing a search. This requirement can become quite computationally expensive for longer sequences. Others have focused on constructing decodable de Bruijn sequences that do not require this brute force approach [117], but this is unnecessary for meteor time encoding as the short sequences only take fractions of a second to generate and search.

## 2.5 Sequence Encoding

The sequence encoding defines the way in which the de Bruijn sequence is used to modulate the transmittance of the electro-optic shutter. The state of the shutter is changed over time according to the elements of the sequence; two options were tested on the DFN observatories. In the initial method, the sequence was encoded in shutter opacity. A "0" was encoded with a fully darkened shutter, a "1" was encoded with a partially opened shutter, and a "2" was encoded with a fully opened shutter. This encoding is simple to implement, even with an alphabet of arbitrary size, but has two main drawbacks for meteor trajectory timing. First, it can be difficult to distinguish between the fully and partially open shutter states for fireballs with rapidly changing brightness due to fragmentation. This is especially true when examining dim fireballs at the edges of all-sky images where resolution is decreased and optical aberrations are more prevalent. The

problem can be alleviated by only using a binary alphabet with the shutter open and closed, producing the encoding as in Fig. 2.1c. The second problem with the opacity encoding approach is the ambiguity when velocity is uncertain. If only a few sequence elements are visible, it can be impossible to decode the sequence because the dash length is unknown. For example, the subsequence "222000111," which would be encoded as a bright dash, a blank of equal length, and then a dim dash of equal length, appears identical to the subsequences "220011" and "201" if the velocity is completely unknown. A related problem is that the data points from the dash endpoints are not generated at a consistent rate. Areas of the de Bruijn sequence where elements are repeated have a lower data point density than locations where elements are not repeated. This is undesirable and can increase trajectory velocity uncertainty for fireballs arriving at certain times.

A more appropriate encoding method would eliminate this velocity ambiguity and provide data points at a constant rate. Encoding the sequence elements as pulse width instead of opacity (Fig. 2.1d) is simple with the flexible shutter driver and accomplishes this goal. The encoding has only been implemented for a binary alphabet for ease of decoding with high sequence rates, but could be generalized to larger alphabets. A "0" is encoded with a short dash length and a "1" is encoded with a longer dash length; there is no velocity ambiguity and data points have a consistent density throughout the sequence. Pulse width encoding also clearly shows the direction of a fireball even when only a couple of dashes are visible.

### 2.5.1 Sequence Parameters for Fireball Observation

The appropriate parameters of the de Bruijn sequence depend on the imaging configuration and target meteor characteristics. The appropriate sequence rate (in elements per second) depends on the expected velocity of the target meteor and the amount of halation or blurring caused by optical aberrations in the imaging system and meteor trail length. If the sequence rate is too high for a particular scenario, the elements (dashes) in the sequence will smear together making the decoding difficult or impossible. A sequence rate near the upper limit is desirable to provide as many trajectory timing data points as possible and therefore, a

more accurate meteoroid mass estimation—using the dynamic method [60]—and fall position distribution. Faster meteors can be imaged with a higher sequence rate than slower meteors because each dash and blank of the meteor trail is projected across more pixels on the sensor making it easier to discern between the individual segments. The DFN is currently optimized for slower fireballs operating at a rate of 10 sequence elements per second with 8 mm all-sky lenses and 36 megapixel full frame (36.9 × 24 mm) sensors. If the targets of interest are faster, dimmer meteors from a known shower instead of slower, brighter fireballs, the operating parameters could be tuned to produce as many trajectory data points as possible by increasing the sequence rate. The DFN plans to add this capability of switching into an alternate mode of operation during peak periods of known showers in the future.

The sequence duration ($t_S$) must be greater than the exposure time to avoid duplicating subsequences during the exposure, thereby ensuring a meteor's arrival time during the exposure is unambiguous. The sequence duration depends on the sequence length and the sequence rate (Equation 3); extending the exposure time with a longer sequence duration is desirable due to the corresponding reduction in data rate and storage requirements. If star trails are not a concern, the exposure length is limited by the long-exposure noise performance of the camera.

The minimum time a fireball must be visible for, in order to be decoded, $t_{\mathrm{Min}}$ is equal to the subsequence length divided by the sequence rate (Equation 3). $t_{\mathrm{Min}}$ has a large impact on ts and therefore the corresponding data rate of the observatories, all other parameters being equal (Equation 2.4).

$$t_S = \frac{N}{r_S} = \frac{k^n}{r_S} = \frac{k^{t_{\mathrm{Min}} r_S}}{r_S} \tag{2.3}$$

$$t_{\mathrm{Min}} = \frac{n}{r_S} \tag{2.4}$$

The alphabet size is determined by the number of distinguishable distinct patterns using the chosen encoding and sequence rate. A binary alphabet ($k = 2$) with

pulse width modulation at 10 elements per second is used by the DFN ($r_S$ = 10). The subsequence length currently used is nine elements (n = 9), and hence the minimum decodable meteor duration ($t_{Min}$) is 0.9 s. This limits the exposure length to 52.0 s. Zeros in the sequence are represented by a short dash where the LC shutter is open for 0.02 s, and ones are represented by a long 0.06 s dash. The starts of the dashes are aligned (every 0.1 s). The DFN observatories take 25 s exposures every 30 s during operation. However, work to extend the open time to 29.0-29.5 s out of 30 is underway. The approximate exposure start time is recorded in the image file by the camera. The de Bruijn sequence and the camera exposure start every 30 s at the top and bottom of the UTC minute and are precisely (better than 1 ms) synchronized with UTC time through a global navigation satellite system (GNSS) receiver.

### 2.5.2 Decoding Arrival Time

The DFN currently uses a semiautomated approach to de Bruijn sequence decoding. If the automated event processing routines detect a large fireball appearing simultaneously at multiple stations, the images are downloaded for analysis and decoding. The camera's sequences are synchronized (via the GNSS receivers) so points in the sequence from multiple cameras can be matched. Trajectory triangulation is possible without any knowledge of the de Bruijn sequence.

The search for the subsequence in the overall de Bruijn sequence revealed by each fireball can be performed in a few seconds, either manually or with the assistance of a DFN software tool designed for matching partially obscured de Bruijn sequences. The sequence of long and short dashes are manually translated into the corresponding sequence of "0"s and "1"s; this string is then either found manually within the sequence (usually using a text editor) or fed into the error tolerant search tool. The Hamming distance [119] provides a good metric for finding the location of the subsequence within the complete de Bruijn sequence in a fault tolerant manner. The fault tolerant search is possible because each additional element visible past the required n elements provides a degree of error checking. The current search tool also permits searching for partially obstructed sequences by entering unknown elements. In this situation, the Levenshtein distance [120]

is used because it also accounts for insertions and deletions unlike the Hamming distance. This is important if the number of elements obstructed is unknown.

Once the subsequence is located within the overall de Bruijn sequence, the absolute timing of the trajectory is simply calculated from the element length $t_{\mathrm{E}}$, location found in the sequence search, and the dash lengths. The propagation delay due to the operation of the microcontroller and the shutter driver as well as the time response of the LC shutter are also accounted for (these can be determined experimentally and should be less than a millisecond). The approximate time in the image metadata is examined to determine the precisely synchronized sequence start time (hh:mm:00.000 or hh:mm:30.000 UTC) and this is added to the time within the sequence to produce the absolute timing for the trajectory (including the arrival time).

## 2.6 Implementation

The first four prototype long-exposure fireball cameras using LC shutters with de Bruijn timecodes were deployed to The Nullarbor in December 2012. The design has since been revised to expand storage, increase computing power for image processing, and optimize power management. The network now consists of more than 49 observatories covering a double station triangulable area of over 2.5 million square kilometers—approximately one-third of Australia.

The operation of the de Bruijn timecode has been verified in the laboratory with a phototransistor (≈10 us time response) and a data logging digital oscilloscope. The precision—relative to the GNSS time source—is better than 1 ms, and the time response of the LC shutter is the limiting factor.

This technique, combined with the use of digital off-the-shelf hardware where possible, has enabled the development of smaller, lighter (10×), more cost- effective (20×) fireball observatories for the DFN (compared to the initial film systems) and enabled the rapid roll-out of the digital network. The initial digital DFN observatory for solar-powered operation in remote locations proved the viability

of the technique and core imaging system. The observatory hardware is presented in detail in [24]. Recently, an even smaller and lower cost mains powered rooftop variant of the autonomous digital fireball observatory has been developed for powered sites that can be attended more frequently (twice per year).

The LC shutters have proven reliable and long- lasting, and the de Bruijn sequence time encoding has been used to capture precise timing data for over 1,000 fireballs including at least one nine station event and one meteorite recovery with an orbit (Murrili) [121]. Approximately a dozen of the fireballs observed as of February 2016 have been classified as meteorite dropping by the data processing pipeline, and searches will be conducted for many of these in the future.

### 2.6.1 Limitations

The technique is validated by the large number of successfully imaged and processed fireballs with timing as well as the recovery of the Murrili meteorite but has a few limitations. Under some conditions, it can be hard to decode the sequence. Extremely bright fireballs pose problems for a few reasons. The all-sky lenses in the DFN's implementation perform best at the image center, but optical aberrations become more prevalent toward the edge of the image. These imperfections can cause the brighter dashes to smear together, becoming hard to distinguish. Extremely bright fireballs have the potential to saturate large areas of the sensor at the high sensitivity settings used to image as much of the fading fireball at the end of its luminous trajectory as possible. This obstacle is present in all imaging systems because of the limited dynamic range of digital sensors and film. This problem will be reduced as higher dynamic range sensors are developed and become available. The other limitation with respect to bright fireballs is the transmittance of the shutter in the closed state. The shutter still allows a small percentage of the incoming light (approximately 0.45%) [111] through in the closed state. This light bleed can complicate the time decoding of extremely bright fireballs. Fireball tails and fragmentation also present some problems for the implementation of timecodes in long-exposure images. Very long tails can be visible in the space where the image of the fireball head was darkened by the shutter. This is the downside of this sort of spatial-time encoding used for the de

Bruijn sequence time encoding and previous long-exposure meteor camera techniques (rotating and switching shutters). If the tail is long enough to completely cover the break between dashes, decoding timing can become difficult or impossible. Video networks solve this timing problem by eliminating the long exposures, but compromise on spatial precision. The precise positioning of the data points can be degraded by the tail effect in both video and photographic networks if a simple data point extraction algorithm (such as finding the centroid) is used. The tail has the effect of dragging the apparent data point away from the true point at the head of the fireball.

Another limitation inherent in any long exposure system employing a periodic shutter is that part of the fireball trail is obscured. Flares due to fragmentation and other variations in brightness during breaks where the shutter is closed can be missed. For this reason, radiometers such as PMTs are used where the mass estimation is performed using the photometric method [122]. The dynamic method used as part of the DFN's data pipeline [48] incorporates these fragmentation events by the corresponding observed deceleration, but most DFN observatories also employ a video camera so that data can be collected on these fragmentation events more directly.

Fragmentation performance of the de Bruijn sequence time encoding has been better than expected. While fragmentation of the fireball into multiple heads does make the (currently manual) point picking process take longer, it is possible to distinguish between the main mass and smaller fragments in almost every case. These fragments have been processed separately on a number of fireballs to produce separate fall position estimates for the fragments and main mass estimates.

These limitations are present in all long-exposure meteor camera systems that interrupt the meteor image for relative or absolute timing. In its current state, the approach is suitable for imaging the vast majority of meteorite dropping fireballs, but as lens designs and sensor technologies improve (with reduced optical aberrations and increased sensor dynamic range), the results for very faint and extremely bright fireballs will only improve.

## 2.7 Results in Practice: DN150417_01

On April 17, 2015, a fireball event in the upper atmosphere above the West Australian Nullarbor designated as DN150417_01 was recorded by five DFN observatories and is presented here to demonstrate the use of de Bruijn timecodes in long-exposure fireball photography; the object became visible to the camera network at UTC20:04:04.3270 ± 0.0006 s traveling eastwards and remained observable for 10.4590 ± 0.0007 s without visible flares or fragmentation until observable ablation ceased at UTC20:04:14.7864 ± 0.0001 s.

The best observations were made from the closest DFN cameras at Kybo (Fig. 2.3a) and Forrest (Fig. 2.3b), adjacent settlements located along the Trans-Australian Railway. The sites are separated by nearly 150 km and each have a permanent population of approximately two persons (giving an indication of the population density in the coverage area of the DFN). The trajectory triangulation was performed using four of the five observations (Kybo, Forrest, Deakin North, and Kanandah). Hughes was excluded because distant and low to the horizon observations result in reduced precision (compared to the closer cameras with better triangulation geometry).

Trajectory timing was recorded by the DFN observatories using the de Bruijn timecode approach. The timing embedded by the GNSS synchronized LC shutter into the Forrest observatory image is illustrated in Fig. 4. The trajectory was triangulated according to the straight least squares method [42] and analyzed using the dynamic method described previously [60], which uses the observations to estimate the position, mass, and velocity of a meteoroid while statistically constraining the uncertainties in these parameters introduced by observation and dynamic model errors. The object appeared at a height of 85.80 ± 0.05 km at 126.7166 ± 0.0003°E 31.02550 ± 0.00022°S (WSG 84) with an initial velocity of 17.98 ± 0.07 km $s^{-1}$ and an entry angle of 15.14 ± 0.05° from the horizontal. The object gradually decelerated over the 143.31 ± 0.01 km luminous trajectory, which ceased at a height of 45.70 ± 0.03 km at 128.23950 ± 0.00017°E 30.57766 ± 0.00015°S (WSG 84) and a final velocity of 4.4 ± 0.7 km $s^{-1}$ . The trajectory analysis indicates the fireball event was the result of a small meteoroid with an initial mass of 32 ± 4 kg entering the atmosphere at a shallow angle before

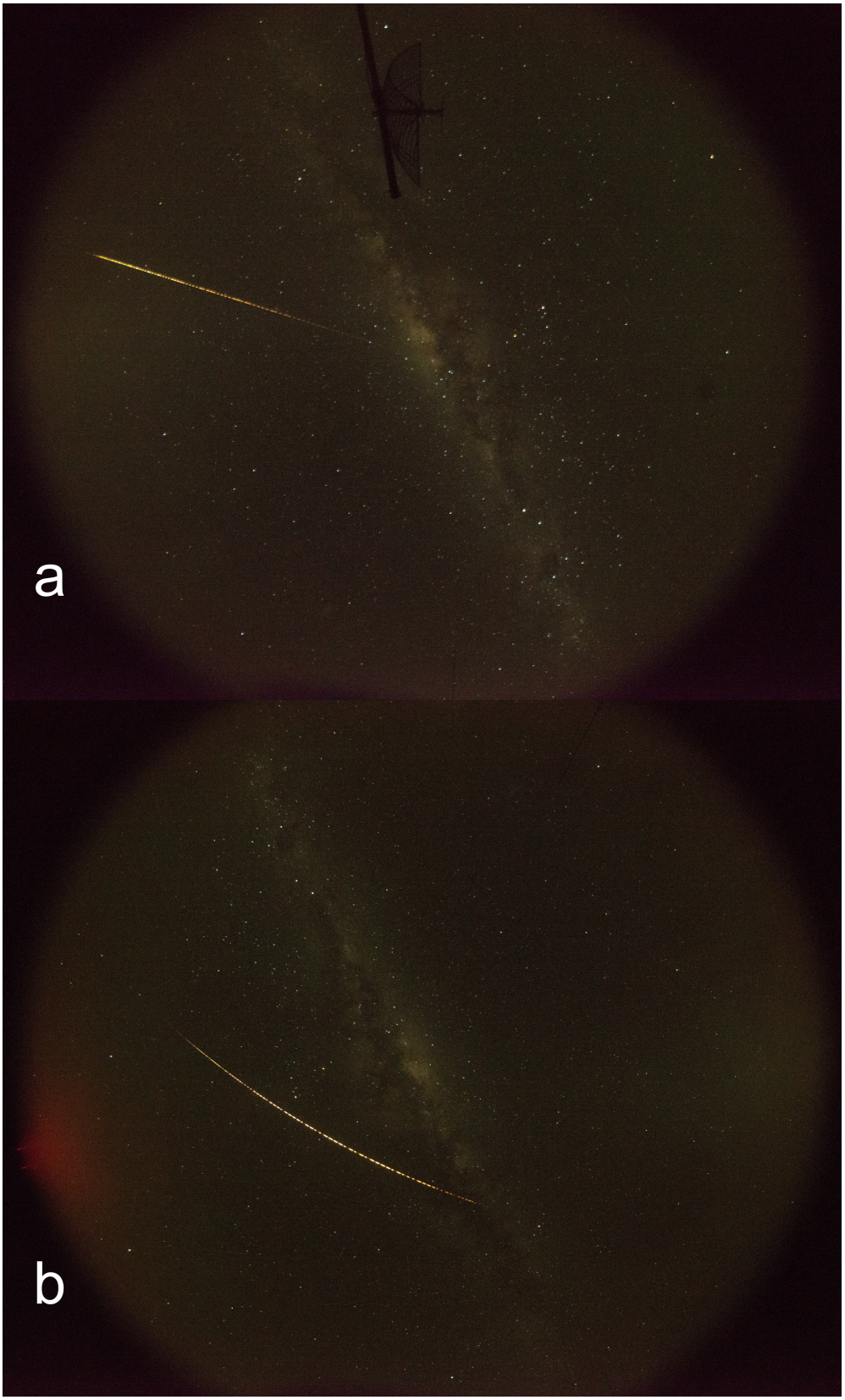


Figure 2.3: DN150417_01 Fireball seen from DFN observatories at Kybo (a) and Forrest (b).

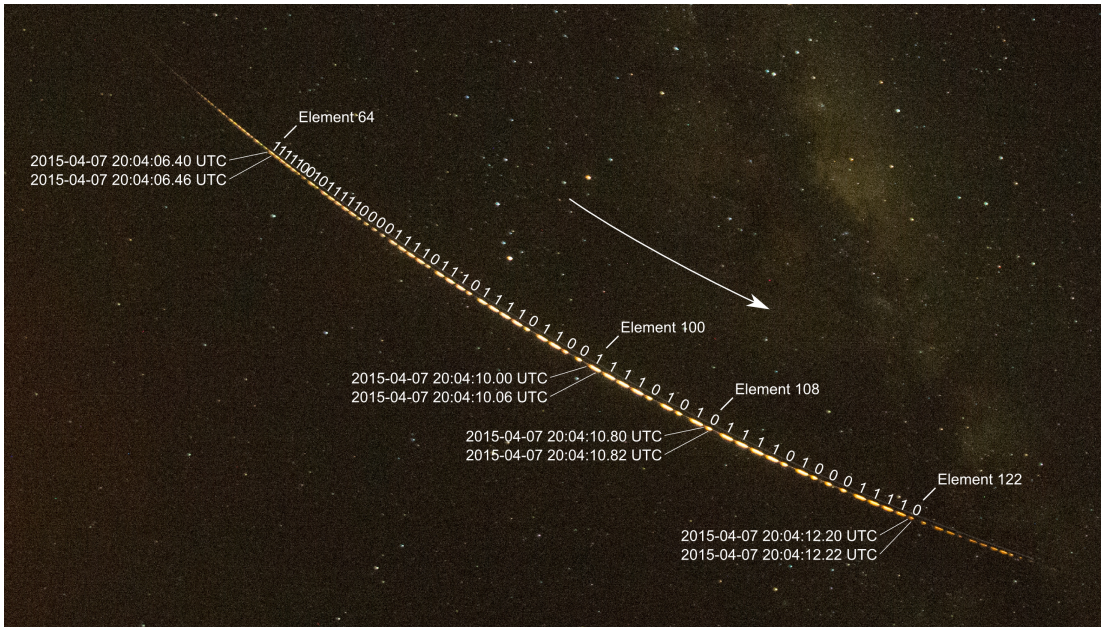


Figure 2.4: DN150417_01 fireball observed from Forrest observatory showing de Bruijn sequence encoded timing (alphabet size k = 2, subsequence length n = 9, rate rs = 10 elements per second, generated using the prefer high method). Element 0 is at 2015- 04-07 20:04.00 UTC. Sequence: 000000000111111111011111110011111101011111100011111011011111010011**11100101111100001111011101111011001111010101111010001111**0110111100100111100101111100001111011100111011011110101001110100101110100001110011001110010101110010001110001101110001001110000101110000000110110110100110110010110110000110101010101101010001101001001101000101101000000110011000110010100110010000110001010110001000110000100110000010110000000101010100101010000010100100010100000010010010000001000100001 (labeled elements in bold)

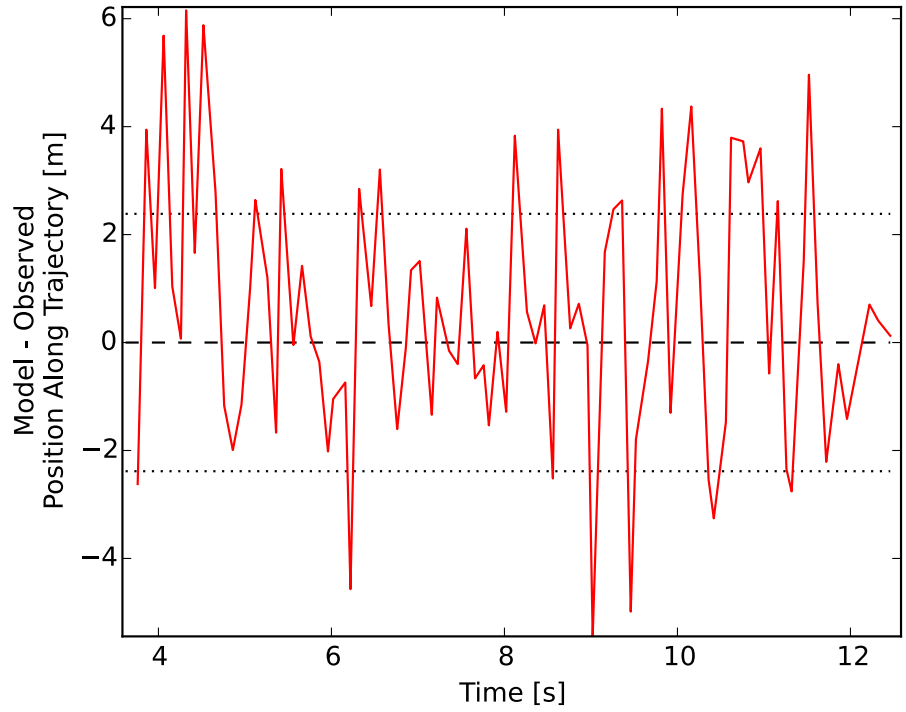


Figure 2.5: Observed versus modeled position residuals along the straight-line trajectory, dashed lines indicate $\pm 1\sigma$ range.

completely burning up. The position residuals from the trajectory analysis (Fig. 2.5) show a good fit between the observations and the dynamic model. The heliocentric orbit (Fig. 2.6) was calculated from the initial entry vector using a numerical propagation technique that accounts for perturbations caused by a number of small solar system bodies. The eccentric and slightly inclined orbit has its aphelion inside the Main Belt and its perihelion between the orbits of Earth and Venus ($e = 0.5992$, $a = 2.132$ AU, $i = 6.960°$, $\Omega$ =207.59011°, $\omega = 51.06°$ J2000). These data were entirely derived from the four images taken by the DFN observatories with the relative timing for trajectory analysis and the absolute timing for orbit calculation embedded by the de Briujn sequence timecode.

f

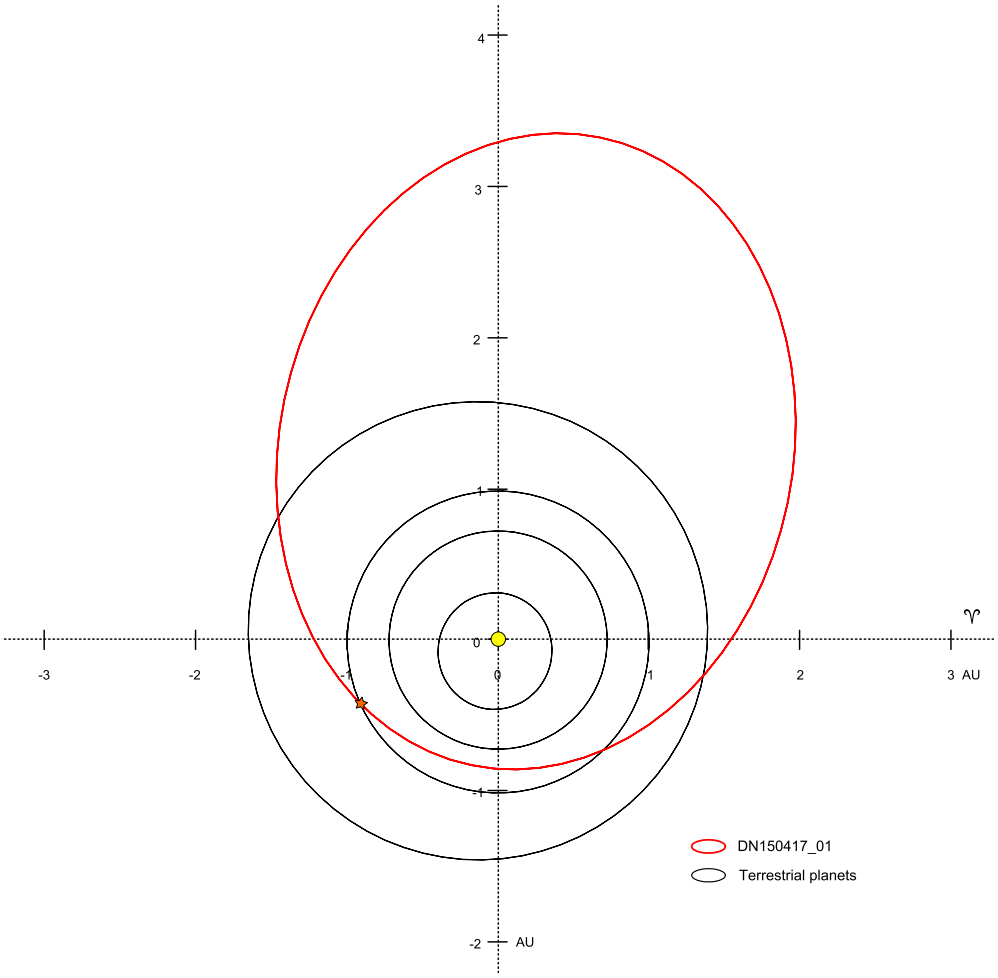


Figure 2.6: Heliocentric orbit for DN_15041701 meteoroid.

## 2.8 Future Work

Extraction of fireball data points from images with timing is currently performed manually with the assistance of a custom software tool. It is the only time consuming step remaining in the DFN's data pipeline that has not been automated. The development of image-processing software to handle this task is a priority. The problem is simple in the ideal case (a fast moving fireball in the center of the lens with no blown highlights and minimal fragmentation and tail), but significantly more difficult when the fireball is partially obstructed, close to the extreme edge of the image, or contains bright flares. Once the data points can be precisely located automatically in most conditions, the automatic decoding of de Bruijn sequence timing is simple. Newer trajectory triangulation techniques that take advantage of the fact that each data point along the trajectory can be independently triangulated are currently being developed and will be tested against more traditional techniques that make the straight line assumption. Other aspects warranting further study include the viability of larger ternary and quaternary alphabets (three or four different pulse lengths), higher sequence rates for imaging known meteor showers, real-time adjustment of the LC shutter in response to very bright fireballs to prevent sensor saturation, and the testing of other higher transmittance electro-optic shutter technologies. The method may also be useful in other fields where precise motion-time data are required such as spacecraft, fluid dynamics, and high speed tracking of other (nonmeteoroid) objects.

**Acknowledgments** The authors thank Robert Yuncken for discussions in the development of this work. This research was supported by the Australian Research Council through the Australian Laureate Fellowships scheme and receives institutional support from Curtin University. The authors also thank Maria Gritsevich and Lukáš Shrbený for their constructive feedback which has significantly improved the quality of this manuscript. The authors have no conflicts of interest to declare.

**Editorial Handling** Dr. Josep M. Trigo-Rodríguez

# References


[19] Z. Ceplecha and J. Rajchl, "Programme of fireball photography in Czechoslovakia," *Bulletin of the Astronomical Institutes of Czechoslovakia*, vol. 16, p. 15, 1965.

[20] R. E. McCrosky and J. H. Boeschenstein, "The Prairie Meteorite Network," *Optical Engineering*, vol. 3, no. 4, pp. 304 127–304127–, 1965.

[21] I. Halliday, A. Blackwell, and A. Griffin, "The Innisfree meteorite and the Canadian camera network," *Journal of the Royal Astronomical Society of Canada*, vol. 72, pp. 15–39, 1978.

[22] P. Spurný, J. Borovička, and L. Shrbený, "Automation of the Czech part of the European fireball network: equipment, methods and first results," *Proceedings of the International Astronomical Union*, vol. 2, no. S236, pp. 121–130, 2006.

[24] R. M. Howie, J. Paxman, P. A. Bland, M. C. Towner, M. Cupak, E. K. Sansom, and H. A. R. Devillepoix, "How to build a continental scale fireball camera network," *Experimental Astronomy*, vol. 43, no. 3, pp. 237–266, 2017. DOI: 10.1007/s10686-017-9532-7. [Online]. Available: https://doi.org/10.1007%2Fs10686-017-9532-7.

[31] P. Bland, P. Spurný, A. Bevan, K. Howard, M. Towner, G. Benedix, R. Greenwood, L. Shrbený, I. Franchi, G. Deacon, *et al.*, "The Australian Desert Fireball Network: a new era for planetary science," *Australian Journal of Earth Sciences*, vol. 59, no. 2, pp. 177–187, 2012.

[33] P. Spurný, P. Bland, J. Borovička, M. Towner, L. Shrbený, A. W. Bevan, and D. Vaughan, "The Mason Gully meteorite fall in SW Australia: Fireball trajectory, luminosity, dynamics, orbit and impact position from photographic records (abstract 6369)," in *Proceedings, Asteroids, Comets, Meteors 2012*, 2012.

[34] P. A. Bland, P. Spurný, M. C. Towner, A. W. Bevan, A. T. Singleton, W. F. Bottke, R. C. Greenwood, S. R. Chesley, L. Shrbený, J. Borovička, Z. Ceplecha, T. P. McClafferty, V. David, G. K. Benedix, G. Deacon, K. T. Howard, I. A. Franchi, and R. M. Hough, "An anomalous basaltic meteorite from the innermost main belt," *Science*, vol. 325, no. 5947, pp. 1525–1527, 2009.

[38] P. Spurný, P. A. Bland, L. Shrbený, J. Borovička, Z. Ceplecha, A. Singelton, A. W. Bevan, D. Vaughan, M. C. Towner, T. P. McClafferty, *et al.*, "The Bunburra Rockhole meteorite fall in SW Australia: fireball trajectory, luminosity, dynamics, orbit, and impact position from photographic and photoelectric records," *Meteoritics & Planetary Science*, vol. 47, no. 2, pp. 163–185, 2012.

[40] Z. Ceplecha, "Geometric, dynamic, orbital and photometric data on meteoroids from photographic fireball networks," *Bulletin of the Astronomical Institutes of Czechoslovakia*, vol. 38, pp. 222–234, 1987.

[41] J. Trigo-Rodríguez, A. Castro-Tirado, J. Llorca, J. Fabregat, V. Martínez, V. Reglero, M. Jelínek, P. Kubánek, T. Mateo, and A. de Ugarte Postigo, "The development of the Spanish Fireball Network using a new all-sky CCD system," in *Modern Meteor Science An Interdisciplinary View*, Springer, 2005, pp. 553–567.

[42] J. Borovička, "The comparison of two methods of determining meteor trajectories from photographs," *Bulletin of the Astronomical Institutes of Czechoslovakia*, vol. 41, pp. 391–396, 1990.

[48] E. Sansom, P. Bland, M. Rutten, J. Paxman, and M. Towner, "Filtering Meteoroid Flights Using Multiple Unscented Kalman Filters," *The Astronomical Journal*, vol. 152, no. 5, p. 148, 2016.

[60] E. K. Sansom, P. Bland, J. Paxman, and M. Towner, "A novel approach to fireball modeling: The observable and the calculated," *Meteoritics & Planetary Science*, vol. 50, no. 8, pp. 1423–1435, 2015, ISSN: 1945-5100. DOI: 10.1111/maps.12478. [Online]. Available: http://dx.doi.org/10.1111/maps.12478.

[70] L. G. Jacchia and F. L. Whipple, "The Harvard photographic meteor programme," *Vistas in Astronomy*, vol. 2, pp. 982–994, 1956.

[74] J. Oberst, S. Molau, D. Heinlein, C. Gritzner, M. Schindler, P. Spurný, Z. Ceplecha, J. Rendtel, and H. Betlem, "The "European Fireball Network": current status and future prospects," *Meteoritics & Planetary Science*, vol. 33, no. 1, pp. 49–56, 1998.

[89] M. Gritsevich, E. Lyytinen, J. Moilanen, T. Kohout, V. Dmitriev, V. Lupovka, S. Midtskogen, N. Kruglikov, A. Ischenko, G. Yakovlev, V. Grokhovsky, J. Haloda, P. Halodova, J. Peltoniem, A. Aikkila, A. Taavitsainen, J. Lauanne, M. Pekkola, P. Kokko, P. Lahtinen, and M. Larionov, "First meteorite recovery based on observations by the Finnish Fireball Network," in *Proceedings of the International Meteor Conference, Giron, France*, 2014, pp. 162–169.

[90] A. Olech, P. Zoladek, M. Wisniewski, Krasnowski M., M. Kwinta, T. Fajfer, K. Fietkiewicz, D. Dorosz, L. Kowalski, J. Olejnik, K. Mularczyk, and K. Zloczewski, "Polish Fireball Network," in *Proceedings of the International Meteor Conference, 24th IMC, Oostmalle, Belgium, 2005*, L. Bastiaens, J. Verbert, and V. C. J.-M. Wislez, Eds., Aug. 2006, pp. 53–62.

[103] I. Halliday, "Photographic Fireball Networks," in *Evolutionary and physical properties of meteoroids: the proceedings of the International Astronomical Union's colloquium # 13, held at the State University of New York, Albany, N.Y., on June 14-17, 1971*, ser. NASA Special Publications, C. Hemenway, P. Millman, A. Cook, and I. A. Union, Eds., Scientific, Technical Information Office, National Aeronautics, and Space Administration; [for sale by the Supt. of Docs., U.S. Govt. Print. Off.], 1973.

[104] Z. Ceplecha, "Photographic Geminids 1955," *Bulletin of the Astronomical Institutes of Czechoslovakia*, vol. 8, p. 51, 1957.

[105] C. Flye-Sainte Marie, "Solution to problem number 48," *L'Intermédiaire des Mathématiciens*, vol. 1, pp. 107–110, 1894.

[106] N. G. de Bruijn and P. Erdős, "A combinatorial problem," *Koninklijke Nederlandse Akademie v. Wetenschappen*, vol. 49, no. 49, pp. 758–764, 1946.

[107] K. A. Dyl, G. K. Benedix, P. A. Bland, J. M. Friedrich, P. Spurný, M. C. Towner, M. C. O'Keefe, K. Howard, R. Greenwood, R. J. Macke, *et al.*, "Characterization of Mason Gully (H5): The second recovered fall from the Desert Fireball Network," *Meteoritics & Planetary Science*, vol. 51, no. 3, pp. 596–613, 2016.

[108] Z. Ceplecha, J. Rajchl, and L. Sehnal, "Complete data on bright meteor 15761," *Bulletin of the Astronomical Institutes of Czechoslovakia*, vol. 10, p. 204, 1959.

[109] P. Spurný, "Photographic monitoring of fireballs in Central Europe," in *Optical Science, Engineering and Instrumentation'97*, International Society for Optics and Photonics, 1997, pp. 144–155.

[110] Z. Andreic and D. Segon, "The first year of Croatian Meteor Network," in *Proceedings of the International Meteor Conference, 27th IMC, Sachticka, Slovakia, 2008*, vol. 1, 2010, pp. 16–23.

[111] LC-Tec, *Fast Optical Shutter Series*. Jan. 2013. [Online]. Available: `http://www.lc-tec.se/products/fast-optical-shutters/`.

[112] N. G. de Bruijn, "Acknowledgement of priority to C. Flye Sainte-Marie on the counting of circular arrangements of 2n zeros and ones that show each n-letter word exactly once," 1975.

[113] S. Kak, "An interesting combinatoric sutra," *Indian Journal of History of Science*, vol. 35, pp. 123–127, 2000.

[114] S. K. Stein, *Mathematics: The Man-Made Universe (Dover Books on Mathematics)*. Dover Publications, 1994, ISBN: 0486404501.

[115] T. van Aardenne-Ehrenfest and N. G. de Bruijn, "Circuits and trees in oriented linear graphs," *Simon Stevin: Wis-en Natuurkundig Tijdschrift*, vol. 28, p. 203, 1951.

[116] H. Fredricksen, "A survey of full length nonlinear shift register cycle algorithms," *SIAM review*, vol. 24, no. 2, pp. 195–221, 1982.

[117] C. J. Mitchell, T. Etzion, and K. G. Paterson, "A method for constructing decodable de Bruijn sequences," *Information Theory, IEEE Transactions on*, vol. 42, no. 5, pp. 1472–1478, 1996.

[118] P. E. Compeau, P. A. Pevzner, and G. Tesler, "How to apply de Bruijn graphs to genome assembly," *Nature biotechnology*, vol. 29, no. 11, pp. 987–991, 2011.

[119] R. W. Hamming, "Error detecting and error correcting codes," *Bell System technical journal*, vol. 29, no. 2, pp. 147–160, 1950.

[120] V. I. Levenshtein, "Binary codes capable of correcting deletions, insertions, and reversals," in *Soviet physics doklady*, vol. 10, 1966, pp. 707–710.

[121] P. A. Bland, M. C. Towner, E. K. Sansom, H. A. R. Devillepoix, R. M. Howie, J. P. Paxman, M. Cupak, G. K. Benedix, M. A. Cox, T. Jansen-Sturgeon, D. Stuart, and D. Strangway, "Fall and Recovery of the Murrili Meteorite, and an Update on the Desert Fireball Network (abstract #6265)," *Meteoritics & Planetary Science*, vol. 51, no. S1, A144–A692, 2016, ISSN: 1945-5100. DOI: 10.1111/maps.12704. [Online]. Available: http://dx.doi.org/10.1111/maps.12704.

[122] M. Gritsevich and D. Koschny, "Constraining the luminous efficiency of meteors," *Icarus*, vol. 212, no. 2, pp. 877–884, 2011.

# Chapter 3

# How to build a continental scale fireball camera network

Robert M. Howie[1], Jonathan Paxman[1], Philip A. Bland[2], Martin C. Towner[2], Martin Cupak[2], Eleanor K. Sansom[2], and Hadrien A. R. Devillepoix[2]

[1]Department of Mechanical Engineering, Curtin University, Perth, Australia
[2]Department of Applied Geology, Curtin University, Perth, Australia

*This article is published in Experimental Astronomy (available at DOI: 10.1007/s10686-017-9532-7),* © *Springer Science+Business Media Dordrecht 2017, and used here with permission. The formatting and referencing style have been modified for presentation in this thesis. The original article is reprinted in its published form with permission in Appendix B.*

*Experimental Astronomy, How to build a continental scale fireball camera network, Volume 43, 2017, pp 237–266, Robert M. Howie, Jonathan Paxman, Philip A. Bland, Martin C. Towner, Eleanor K. Sansom, and Hadrien A. R. Devillepoix,* © *Springer Science+Business Media Dordrecht 2017 with permission of Springer*

# Authorship Declaration

**Article Title:** How to build a continental scale fireball camera network

**Journal:** Experimental Astronomy

**Publication Status:** Published on 11 May 2017

## Author Contributions

### Robert Howie

Led mechanical and electronic detailed design of the observatory; developed observatory firmware; contributed to observatory concept design; conceived, drafted and revised manuscript; participated in the Murrili meteorite recovery expedition; and handled the publication process

Manuscript contribution: 85%  22 September 2017

### Jonathan Paxman

Assisted with hardware design and manuscript editing, and participated in the Murrili meteorite recovery expedition

Manuscript contribution: 3%  20 September 2017

**Philip Bland**

Led Desert Fireball Network project, contributed to observatory concept design, led the expedition to recover the Murrili meteorite; and assisted with hardware design and manuscript editing

Manuscript contribution: 4%  22 September 2017

**Martin Towner**

Led observatory software development; led DFN deployment; contributed to concept design and hardware design; and assisted with manuscript editing

Manuscript contribution: 3%  20 September 2017

**Martin Cupak**

Configured observatory operating systems; developed network communications infrastructure; and assisted with Murrili meteorite recovery, hardware design and manuscript editing

Manuscript contribution: 3%  20 September 2017

**Eleanor Sansom**

Performed trajectory modelling for the Murrili meteorite recovery and assisted with manuscript editing

Manuscript contribution: 1% 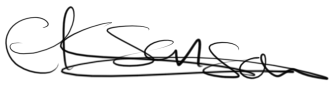 20 September 2017

**Hadrien Devillepoix**

Assisted with data reduction for the Murrili meteorite recovery and assisted with manuscript editing

Manuscript contribution: 1%  20 September 2017

**Abstract** The expansion of the Australian Desert Fireball Network has been enabled by the development of a new digital fireball observatory based around a consumer digital camera. The observatories are more practical and much more cost effective than previous solutions whilst retaining high imaging performance. This was made possible through a flexible concurrent design approach, a careful focus on design for manufacture and assembly, and by considering installation and maintenance early in the design process. A new timing technique for long exposure fireball observatories was also developed to remove the need for a separate timing subsystem and data integration from multiple instruments. A liquid crystal shutter is used to modulate light transmittance during the long exposure which embeds a timecode into the fireball images for determining fireball arrival times and velocities. Using these observatories, the Desert Fireball Network has expanded to cover approximately 2.5 million square kilometres (around one third of Australia). The observatory and network design has been validated via the recovery of the Murrili Meteorite in South Australia through a systematic search at the end of 2015 and the calculation of a pre-atmospheric entry orbit. This article presents an overview of the design, implementation and performance of the new fireball observatories.

## 3.1 Introduction

Meteorites provide insight into the formation and current state of the solar system, but the value of most of these (more than 50,000 worldwide) is limited because the origin of the sample, the heliocentric orbit, is unknown. The scientific value of samples with known origins is one of the motivations for sample return missions such as Stardust [6] and Hayabusa [123]. Meteorites with a known pre-atmospheric entry orbit determined by a fireball camera network allow us to constrain the origin of the rock in the main asteroid belt, and possibly in some cases, even the specific asteroid parent body. As of mid 2016, only about 29 [76]–[78], [121], [124], [125] recovered meteorites have orbits determined through fireball camera networks or other observational means.

Fireball camera networks continuously monitor the night sky for fireballs (meteors magnitude -4 or brighter) produced as larger meteoroids enter the Earth's

atmosphere at high speeds (tens of kilometres per second). These larger meteoroids are more likely to produce meteorites on the ground instead of completely burning up during the luminous trajectory (bright flight). The bright fireballs produced during the ablation process can be tracked as they move through the atmosphere using optical means. The observed trajectory (consisting of both position and timing data) allows the calculation of the heliocentric orbit of the meteoroid and a fall position estimate of the meteorite. The fall position must be known with sufficient certainty to recover the meteorite via a ground search, and orbital precision must allow meaningful comparison with the orbits of known Solar System bodies. These constraints inform the observational requirements of a fireball camera network.

The Australian Nullarbor plain is an exemplary site for a fireball camera network due to its dark skies, minimal cloud cover, low rainfall, lack of vegetation and pale geology [101]. The light coloured featureless terrain contrasts well with (usually) black recent meteorites for a visual search. The Australian Desert Fireball Network (DFN) aims to cover the Nullarbor and a significant fraction of the entire Australian Outback with fireball cameras in order to produce the first consistent source of meteorites with orbits (delivering multiple meteorites with orbits per year). The original goal was one million square kilometres of coverage [31], but that has since been revised upwards due to the performance of the new observatories exceeding initial expectations. The new goal is to cover as much good meteorite searching terrain as possible in Australia. The network recovered two meteorites with orbits during its initial phase using large format film cameras (see Section 3.2.5): Bunburra Rockhole, an anomalous basaltic meteorite [34] in 2008, and Mason Gully, an H5 ordinary chondrite [79], [107] in 2010. A third meteorite (Murrili) has now been recovered using the new digital observatories detailed in this work.

Meteorite recovery rates are determined by network coverage area which is limited by the per observatory cost relative to the imaging performance. Reducing this cost to expand the network is the driving motivation behind the development of a new cost effective fireball observatory for the DFN. The fully autonomous digital observatory (Fig. 3.1) is designed to record high resolution fireball trajectories in the harsh conditions of the remote Australian Outback and is based on commodity

Figure 3.1: Digtal DFN observatory installation at Mt Ive Station in South Australia

off-the-shelf digital imaging and computing hardware to minimise costs.

## 3.2 Fireball Camera Networks

The first meteor photograph was captured in 1885 [67], and systematic photographic meteor observations have taken place since 1936 [70]. Three large fireball camera networks with the aim of meteorite recovery were constructed in the latter half of the 20th century. The European Fireball Network (originally the Czechoslovak Fireball Network) and the US Prairie Meteorite Network started operations in the mid '60's, and the Canadian Meteorite Observation and Recovery Project (MORP) followed in the early '70's [103]. These networks used large format film based camera systems to achieve the required resolution and sensitivity to image fireballs for orbit determination and meteorite recovery. The observatories typically take one exposure per camera per night; an additional exposure is sometimes started after a bright fireball is detected (depending on network capability) [21].

Estimating fall positions of meteorites from fireball data requires camera networks to capture fireball trajectories with high spatial and temporal precision from multiple geographically distinct locations. The spatial precision of the cameras determines the accuracy of the trajectory path triangulation, and relative timing data is required to determine the velocity and deceleration of the meteoroid for mass estimation [46]. Absolute timing (time of appearance) is also required to calculate the pre-atmospheric entry orbit due to the constant orbital motion and rotation of the Earth. Previous networks have employed different approaches to determining absolute timing, ranging from relying on chance observations of the general public (no timing) to high precision sky brightness loggers [103].

### 3.2.1 Czechoslovak Fireball Network

Ondřejov Observatory has a long history of meteor observation, and commenced double station observations using multiple narrow angle meteor cameras in 1951 [71]. These employed a rotating shutter mounted in front of the objective lens to create periodic breaks (at 68 and 98 breaks per second [104]) in the meteor trails created as the shutter arms pass in front of the objective lens to indicate meteoroid velocity (once observations were triangulated with the secondary station). Since this technique only determines the relative timing (velocity) of the meteors and not the arrival times necessary for orbits, sidereal tracking cameras following the relative motion of the sky throughout the night were added alongside the fixed cameras by 1958 [108]. Meteor arrival times were determined by comparing the unguided (fixed pointing) and sidereal tracking guided images [109]. These meteor cameras captured the fireball that led to the recovery of the Příbram meteorite fragments in 1959, providing the first recovered meteorite with a known heliocentric orbit [72], [126].

The successful recovery of the Příbram chondrite spurred the creation of the Czechoslovak Fireball network—with the goal of meteorite recovery in addition to the previous objectives of meteor observation, trajectory analysis and orbit determination. This new network started operations with five stations in autumn 1963 [19]. These fireball cameras used a single all-sky camera per station instead of multiple narrow angle cameras used by the meteor photography stations; this

reduced the workload for the operators manually initiating the night long exposures. The camera and rotating shutter were mounted above a convex mirror to collect all sky imagery. The rotating shutter in the fireball cameras was driven to produce 12.5 breaks per second—slower than the rate used on the previous meteor cameras. The observatories gathered the data required for trajectory triangulation and fall position estimation (trajectory spatial and relative timing data) but employed no method of determining the arrival times of fireballs; the network originally relied on chance fireball observations by the public for arrival times and therefore orbits. Driven sidereal tracking cameras were added to three of the fireball camera sites at a later date to calculate arrival times in the same method used by the original meteor cameras with an accuracy usually within 5 seconds [109].

### 3.2.2 Prairie Meteorite Network

The US Prairie Meteorite Network was established in 1964 with sixteen stations in the Midwest [20]. Each station consisted of four cameras using repurposed rectilinear large format aerial imaging cameras integrated into small buildings with ancillary instrumentation. The Prairie Network observatories also periodically occulted the fireballs (20 times per second) to allow velocity measurement of triangulated events, but departed from the rotating shutter design of previous fireball and meteor cameras. The Prairie observatories utilised a switching shutter constructed from a bistable electromechanical relay attached to a lightweight blade which oscillated in and out of the optical path in the centre of the lens breaking meteor trail images according to a pre-programmed pattern. The pattern embedded into the fireball trail image recorded the fireball's arrival time. The system used repeating sequences which limited the timing precision to a 10.4 second window.

The Prairie systems were also equipped with sky photomultiplier tube (PMT) based photometers alongside each camera to extend the capabilities of the observatory. The photometer controlled the film exposure in response to sky brightness during normal operation, and during extremely bright fireball events, it could reduce the lens aperture and insert a neutral density filter to protect the exposure.

The photometer also stamped arrival times (more accurately than the switching shutter timecode) of bright meteors by re-illuminating the data chamber (containing the clock) when meteors brighter than magnitude -4 (fireballs) were detected [20]. The Prairie network recovered the Lost City meteorite with an orbit in 1971 [73] and ceased operation in 1975.

### 3.2.3 Meteorite Observation and Recovery Project

The Canadian Meteorite Observation and Recovery Project (MORP) was created after a number of Canadian meteorite falls were recovered in the 1960's, stimulating regional interest in the field. The network started routine operation in 1971 and took a similar approach in observatory design to the Prairie Network, with observatories consisting of five rectilinear cameras housed in a purpose built pentagonal building. The cameras used a rotating shutter with a unique three sector design, consisting of one transparent sector and two neutral density sectors (of densities 2.0 and 5.0) designed to image meteors across a large range of brightnesses [21]. Due their unique design, the rotating shutters in the MORP observatories were driven more slowly than previous designs to produce four dashes per second.

The MORP observatories used innovative PMT based meteor detectors for the precise recording of meteor arrival times. In order to detect fireballs, and reject other common bright transients, two concentric perforated cones were mounted over the PMT. A light source moving at typical fireball speeds would produce a signal in a particular frequency range as the light was periodically blocked and admitted through the holes in the interleaved cones. Signals in this frequency range were detected via electronic filtering, and this commanded the observatory to print the time of the meteor event and advance the film after an appropriate delay. The project operated from 1971 to 1985, recovering the Innisfree [21] meteorite with an orbit in 1977 and produced a sizeable fireball dataset [127]–[129].

### 3.2.4 European Fireball Network

The Czechoslovak network became the European Fireball Network in 1968 when a number of cameras were installed in southern Germany to work in conjunction with the Czechoslovak cameras. This coverage was again expanded in 1988 when the German cameras were redistributed to cover a larger area including Austria, Belgium and Switzerland [74]. The Czechoslovak part of the network has undergone considerable expansion and modernisation since its inception. The cameras have been upgraded multiple times, first, moving from the manual mirror based all sky cameras to manual large format fisheye lenses providing significantly better precision (angular resolution of approximately one arc minute) and sensitivity. Additional stations with guided cameras for absolute timing were added, and more recently (2003-2008) the manual observatories have been replaced with automated observatories [22]. These contain the same larger format film fisheye imaging configuration but are automated for 32 exposures providing five to seven weeks of autonomous observing, depending on conditions, by way of a magazine equipped film handling system [22]. The cameras monitor observing conditions using precipitation sensors and video camera based star counters. If conditions are favourable, the observatories commence night long exposures and continue to monitor the observing conditions throughout the night (pausing or ending observations as required). The automated observatories are also equipped with PMTs to measure sky brightness during fireball events. The brightness is logged at 500 Hz, (later upgraded to 5000 Hz [78]) producing detailed brightness curves for mass estimation via the photometric method [54]. The automated observatories are networked through a central server and can rapidly alert researchers of the occurrence of bright fireballs. The European Network has recovered a number of meteorites through systematic search campaigns (including Neuschwanstein [35], Košice [59], Žďár nad Sázavou [77] and Stubenberg [77]) and provided orbital or trajectory data for a number of other meteorites found by members of the public in Europe (including Jesenice [58] and Križevci [130]); the network continues to operate to this day. Recently the European Network has also started the transition to digital observatories [77].

### 3.2.5 Desert Fireball Network — Initial Phase

The excellent searching terrain in the Australian Nullarbor was the motivation for the development of the Australian Desert Fireball Network; the initial phase was conducted using four fireball observatories [31] based on the automated Czech design [22]. The design was modified to deal with the extreme heat of the Australian Outback with the addition of side panels and a retractable sunshield to shade the system during the day, a modified thermal management system, and special high reflectance paint to minimise solar heating. The solar powered observatories were installed on pastoral stations, network connectivity was provided by geostationary satellite data links, and the generous volunteer hosts changed the film magazines as required.

The initial DFN observatories track fireballs well, but are expensive, difficult to install and costly to run and maintain; the £60,000 120kg observatories (Fig: 3.2) required a truck and three days of work by a small team to install. The systems required monthly film magazine changes were powered by eighteen 80 Watt solar panels. Storage was provided by a small shed of flooded lead acid batteries. Maintenance was complicated by the size and weight of the observatory.

The initial phase of the DFN commenced routine operation in 2005 and produced two meteorites with orbits: Bunburra Rockhole [34], [38] in 2008 and Mason Gully [79], [107] in 2010. This proved the viability of a fireball camera network based in the Australian Outback and laid the groundwork for the expanded digital DFN. Operation of the initial film based observatories ceased in 2015 once the expanded digital network using the observatories described in this work commenced operations.

One aspect common to all of the custom engineered observatories used by these previous networks is their high cost and complexity. It would be cost prohibitive and impractical (due to the maintenance requirements) to cover an extremely large area like the Australian Outback with these designs. A substantial reduction in observatory cost and complexity whilst retaining high imaging performance was required to meet the DFN coverage goals.

## 3.3 The Need For a More Practical and Cost Effective Photographic Fireball Observatory

The meteorite recovery rate of a fireball camera network depends on the size of the coverage area and nature of the meteorite searching terrain. The southern half of the Australian Outback, and the Nullarbor in particular, is excellent terrain for meteorite recovery, so the primary factor influencing the number of meteorite recoveries is the observational capability of the DFN. With nearly ideal night time observing conditions in this region due to low light pollution and minimal cloud cover to interrupt observations, this capability is primarily dependant upon the double station (triangulable) coverage area.

Network coverage depends on the number and spacing of observatory stations which is constrained by observatory imaging capabilities and the logistics of installation and maintenance. The number of stations is directly determined by the costs and maintenance requirements of the fireball camera design. The ideal fireball observatory has a low upfront cost, low ongoing costs, simple installation, infrequent and minimal maintenance and high imaging performance.

Two types of fireball networks exist today: video networks and long exposure photographic networks. Video networks (such as the Southern Ontario All-sky Meteor Camera Network [92], the Slovak Video Meteor Network [131], the Finnish Fireball Network [89], and the French FRIPON network [85]) use analogue or digital video cameras to record meteor trajectories at a high frame rate (usually around 30 frames per second) but at low resolutions (0.3-1 megapixel (MP)). Photographic networks (such as those previously mentioned in Section 3.2 or the Tajikistan Fireball Network [96]) capture long exposure fireball photographs using high resolution (20+ MP digital or large format film) cameras to record meteor trajectories in a long exposure. The exposures can be up to a few hours in length, so these networks also utilise at least one method of determining meteor arrival times within the long exposure (see Section 3.4.3).

The video based approach has become popular in recent years due to the increased availability and affordability of sensitive video cameras. Observatories

can be constructed from widely available off-the-shelf hardware and software, and the per station cost is low, making them an attractive approach for amateur and collaborative networks. Sensitive video cameras are well suited for recording meteor trajectories to determine geophysical properties by examining ablation and fragmentation and for characterising meteoroid flux and orbital population distributions. However, low resolution cameras do not, generally, record trajectories with sufficient precision to refine fall position distributions to the point where meteorites can be reliably recovered through systematic search campaigns at specific locations (with the exception of more advanced multi camera systems such as [97]). All sky video networks do indicate the general region where meteorites may fall, and these are sometimes then recovered by the public (*cf.* [58], [98], [132]).Video networks also offer limited orbital precision (due to the spatial precision of trajectory observations) which can make matching sporadic fireballs (those not part of a known meteor stream) to parent bodies with high confidence more difficult.

Much higher resolution photographic cameras do offer the spatial precision required to determine fall positions with sufficient accuracy to reliably recover meteorites through systematic search campaigns. Large format film has been traditionally used to achieve spatial precision of approximately one arcminute (limited by film scanning techniques). Long exposure fireball observatories are more complex due to the need to periodically occult the exposure for velocity determination and—traditionally—the need for a separate absolute timing system. Digital photographic cameras now offer the necessary resolution, but are expensive and require custom camera control solutions to function as fireball cameras. For these reasons, the design and construction of high resolution long exposure fireball observatories have typically been out of reach for amateur and collaborative networks.

Reaching the DFN's original goals would be difficult using previous high precision fireball observatories. Modern digital still cameras present an opportunity to develop a smaller, lighter, more power efficient and less costly fireball observatory. This type of design, constructed around a high resolution consumer digital camera and off-the-shelf components, could satisfy the operational requirements and be constructed for a much lower cost than previously possible.

Figure 3.2: DFN large format film based observatory — used in initial phase, prototype digital observatory visible in background

## 3.4 The New Automated Digital Fireball Observatory

### 3.4.1 Requirements

The main design goals of the new Desert Fireball Network observatory are sufficient spatial and temporal precision to enable meteorite recovery by small teams on foot; the ability to operate reliably and unattended in the Australian Outback for long periods; compatibility with an automated data reduction pipeline; low per-system costs relative to the imaging performance; and simple, fast and inexpensive manufacture, assembly and deployment.

The observatories must be capable of withstanding the extremes of the Australian Outback including temperatures over 50°C, wind gusts carrying sand and dust in excess of 100 km/hr, thunderstorms bringing occasional torrential rain, and must operate unattended for long periods between servicing and data download

visits (ideally at least one year). This requires a robust design with the capability to recover from minor malfunctions such as software or subsystem crashes. Connectivity to enable remote access for administration, troubleshooting and fireball event data download is also desirable.

Small teams on foot in the Outback can cover 2-6 $km^2$ per week depending on the terrain; trips are usually limited to to around two weeks and 5-12 people due to logistical constraints. This drives the spatial and temporal precision requirements of the network. In order to reduce the uncertainty of the fall position estimate to the point where recovery within these constraints is probable, the trajectory triangulation should be accurate to $\pm$100 metres (triangulation final vector should be accurate to $\pm$ 0.05 degrees) and the mass estimation should be within one order of magnitude. Absolute temporal precision should be 0.01 seconds or better in order to obtain accurate pre-atmospheric entry orbits, enable independent point by point triangulation along the trajectory and allow straightforward alignment with measurements taken by any other instruments. Relative timing precision (for velocity determination and mass estimation) must be significantly more precise.

Camera spacing influences the choice of imaging system; around 100-150 km between sites is a good compromise between coverage density and servicing effort, and suits the spacing of availably installation sites (mostly pastoral stations) in the Outback. A high resolution imaging system is required in order to meet the trajectory precision requirements at this spacing; 36 MP image sensors are readily available in consumer digital cameras and exceed this requirement (even when used with all sky lenses).

In order to deploy a continental scale network, the upfront and ongoing per station costs must be minimised relative to the imaging performance. The upfront costs include materials, manufacturing, assembly and installation while the ongoing costs include maintenance and data connection costs. The move to digital imaging yields both cost reductions compared to film based systems and an automated data reduction capability. The cost and capability of digital imaging has greatly improved in the last decade to the point where commodity consumer cameras have the resolution and sensitivity required to capture fireball imagery with enough precision to produce orbits and recover meteorites. Basing the ob-

servatory around off-the-shelf components where possible enables significant cost reductions compared to the highly customised approach of previous observatories.

It is not possible to manually process the large volume of fireball events generated by a continental scale network. To process the huge amount of data generated, the new observatories must be compatible with an automated data reduction pipeline. Consumer digital cameras integrate well into this approach because they allow automatic data download to a computer in a readily accessiable format.

The size, weight and power draw of the observatories needed to be reduced compared to previous designs in order to make deployment and observatory maintenance fast and simple. On site maintenance is difficult in the Outback due to the dusty and sometimes harsh conditions. Ideally, the observatory would be small and light enough for spares to be carried on servicing trips. This would allow the observatories to be exchanged in the field and serviced in the lab (for more serious problems), allowing simpler and more time efficient network maintenance.

### 3.4.2 Concept Design

The proven approach of a long exposure fireball camera with an optical occulter was selected to satisfy the design requirements but implemented with a high resolution digital camera instead of large format film. The long exposures would be limited to around 30 seconds (instead of an entire night) to prevent star trails that hamper lens calibration and astrometry. These 30 second exposures would be collected continuously throughout the night during good observing conditions. A mechanical shutter, of the rotating or switching type, was eliminated early in the design process to reduce the number of expensive and failure prone precision mechanical components. A number of different electro-optic modulators, or shutters, were tested for suitability, and a LC-Tec X-FOS liquid crystal (LC) shutter was selected for it's ease of implementation, proven reliability and long lifetime (http://www.lc-tec.se/products/fast-optical-shutters/). (Liquid crystal displays have been operating in consumer devices for decades.) The LC shutter is driven via a microcontroller through an H-bridge driver. The microcontroller also triggers the camera exposures via the camera's remote release port. The operation

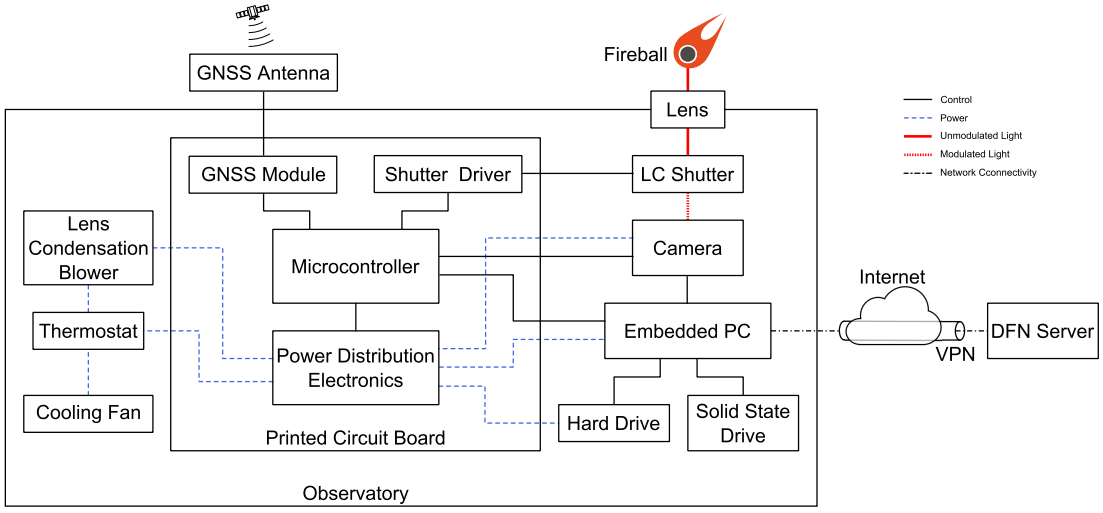


Figure 3.3: Digital Desert Fireball Network observatory block diagram showing data and power connections

of the microcontroller is tightly synchronised with highly precise global navigation satellite service (GNSS) time through a GNSS receiver module. The long exposure images captured by the camera throughout the night are downloaded via an embedded PC using the camera's USB connection; see Fig 3.3 for system topology. Images are then automatically analysed by the computer for fireball events before being moved from the solid state drive to the archival disk drives. As a part of the event detection, the observatories communicate with the network's central server via an Internet connection (where available) to corroborate potential fireball events with a preliminary approximate triangulation excluding single station false positives.

Rapid development of the fireball observatory was prioritised to get the digital network operational as quickly as possible. A number of cameras and all-sky lenses were tested for suitability. The Samyang 8mm f/3.5 UMC Fish-eye CS II was selected due to the favourable (stereographic) projection and acceptable image quality. The Nikon D800E (later replaced with the D810) digital single lens reflex camera (DSLR) was selected for its weather resistance, high resolution and good noise performance, as well as the ability to control it from a Linux computer via gPhoto2 (http://gphoto.sourceforge.net/). In order to determine the viability of a fireball observatory based around an off-the-shelf consumer camera, four prototypes were rapidly built and deployed for the 2012/13 summer to test the durability of the DSLRs in the hot Australian climate.

The decision to archive all images (instead of only fireball images) was made early in the concept design phase. This eliminated the chance of losing fireball images due to false negatives in the event detection algorithms and allows us to collect a complete wide field optical night sky dataset taken from multiple geographically distinct locations. This dataset is offered to interested researchers for investigation of optical counterparts to radio transients, meteorology, animal behaviour and other fields (contact the authors for access).

To keep the observatory cost low, the primary components (camera, lens, computer, data storage) are commercial off-the-shelf products with small modifications where necessary. The electronics to drive and synchronise the shutter with GNSS time and manage subsystem power are custom designed. The number of moving parts has been minimised to keep costs low and reduce the potential points of failure.

### 3.4.3 Fireball Timing

A photomultiplier tube is too large and expensive of a solution to fireball timing if the design goals were to be achieved (mostly due to the high voltage power supply required). The flexibility of the microcontroller controlled shutter driver makes it possible to drive the LC shutter to modulate the exposure according to a pattern or sequence. This can be used to embed a unique timecode into the fireball trail recorded by the camera as it travels across the frame during the (30 s) long exposure. This imprinted sequence shows the arrival time (absolute timing) and the velocity information (relative timing) of the meteoroid allowing the calculation of both a fall position and orbit. The ideal sequence is as long as possible while requiring the smallest part of the sequence to be known in order to identify a unique arrival time for the fireball. A longer sequence permits an extended exposure time, reducing the data rate of the camera and wear on the camera's shutter mechanism. This permits less frequent data download and maintenance visits, reducing operating demands and cost. It is desirable to be able to decode the timing from a short part of the sequence because short meteors are more abundant, and statistical analysis of meteoroid populations is another objective of the DFN.

The sequence that optimally satisfies these requirements is a De Bruijn sequence, defined as the shortest possible sequence containing all possible $n$-element subsequences [105], [106], [115]. The microcontroller is precisely synchronised with UTC time via a GNSS receiver to maintain timing precision. The technique eliminates the separate absolute timing subsystem required by most previous designs, reducing, size complexity, and cost. It is the main innovation allowing the new DFN digital fireball observatories to be so compact and cost effective; the approach is detailed in [133]. The Prairie Meteorite Network film cameras also used coded operation of the (mechanical) shutter to record fireball arrival times directly into the fireball image (on film), but this time was only known to within a 10.4 second window which doesn't meet the timing precision requirements of the DFN. For more accurate times the Prairie Network systems depended on the same complex and expensive PMT used in other designs, and this was limited to only bright meteors (fireballs, magnitude -4 and brighter).

The De Bruijn sequence technique used in the DFN observatories encodes absolute and relative timing for all meteors and fireballs that are clearly imaged by the cameras; The absolute timing precision is better than one millisecond and the relative timing is significantly more precise.

Fig 3.4 shows a good meteorite dropping fireball candidate (DN141129_01) with clearly visible time encoding as observed from the Perenjori DFN station.

The absolute timing precision allows independent triangulation of the fireball data points (two per dash, twenty per second) along the trajectory. This three dimensional point by point triangulation method eschews the straight line assumption used in the traditional methods (intersection of planes [40], least-squares [42] and multiparameter fit [43]).

### 3.4.4 Observatory Design

In order to rapidly develop the digital fireball observatory, we adopted a concurrent engineering design approach, prototyping early and often. This allowed us to quickly prove the viability of a digital fireball observatory based around

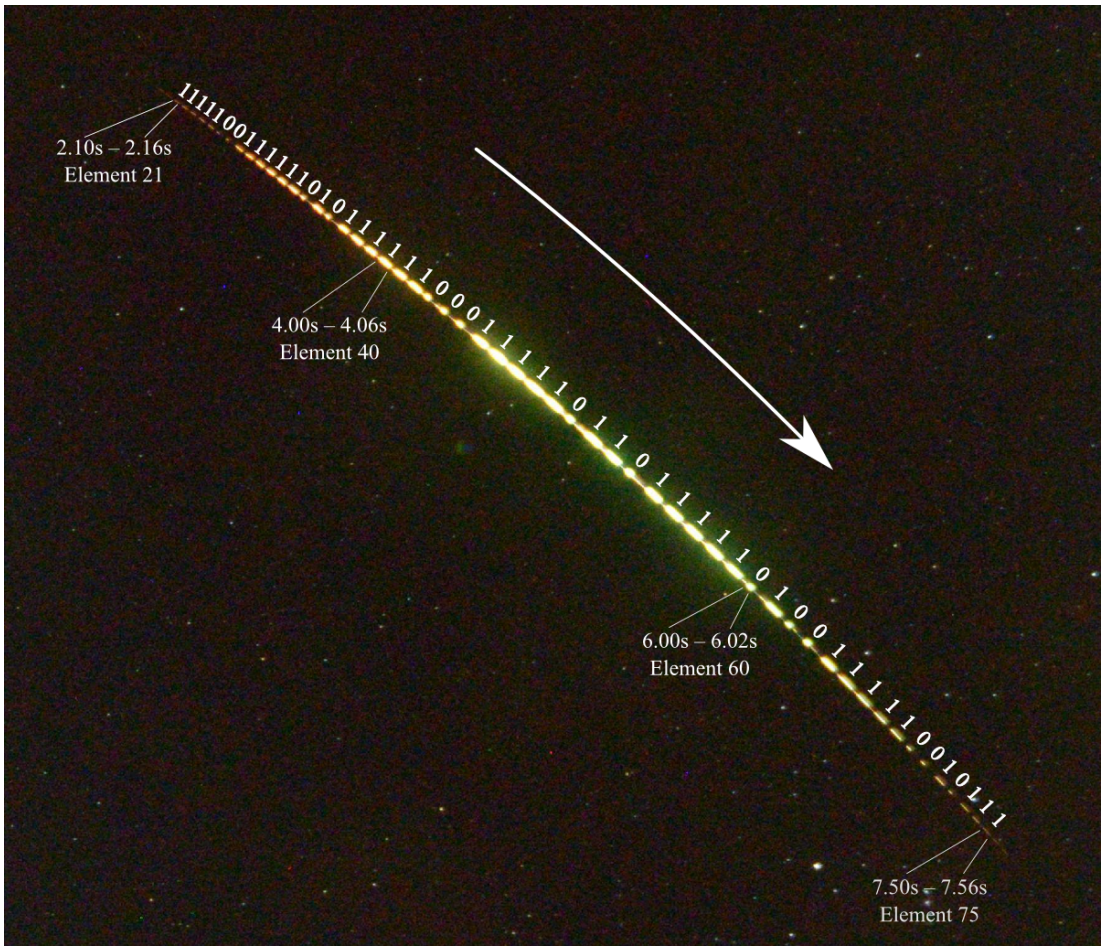


Figure 3.4: Enlarged view of DFN fireball event DN141129_01 with de Bruijn sequence time encoding clearly visible. Times relative to exposure start time at 14:31:30 UTC on 29 November 2014.

commodity imaging hardware and discover the key areas of difficulty early on in the design process.

Discovering these problems early on significantly accelerated the design process, and ensured design effort was targeted towards the aspects of the observatory that most required it. Areas where this additional effort was required included the lens environmental sealing and power supply reliability. Care was taken to devise and test simple and creative solutions to design challenges adding minimal cost and complexity before implementing more complex solutions. For example, instead of developing a mechanised lens cover, an inexpensive hydrophobic surface treatment was successfully tested on the prototypes to allow self cleaning of accumulated dust on the lenses during rainfall.

The observatory was designed with manufacture, assembly and maintenance in mind. The number of manual manufacturing steps had to be minimised to construct the significant number of observatories (more than 75) without contracting out the manufacture. This was achieved by modelling the design in a 3D computer aided design (CAD) package and then using affordable and flexible computer aided manufacturing (CAM) techniques including computer numeric control (CNC) laser cutting, CNC water jet cutting, 3D printing and CNC turning for the majority of the manufacturing operations. This computer aided approach allowed us to minimise the number of design revisions by examining the fit and alignment of components in the computer model without waiting for the manufacture of prototype components. Most of the (few) manufacturing steps were performed with these flexible and cost effective manufacturing processes (with minimal or no tooling cost) using the CAD model geometry directly resulting in short lead times. This made rapid design iterations and the short development time possible. Minimal manufacturing processes were performed in-house; the majority of in-house work was semi-skilled assembly performed by casual workers on an as needed basis. This flexibility allowed us to easily respond to design variations and respond to the changing demand as the network roll-out progressed.

Off-the-shelf components were used wherever possible, resulting in significant reductions in up front costs compared to previous fireball observatories (by a factor of about 12). Care was taken to keep the design modular to simplify

field and lab based maintenance. The various subassemblies are interconnected using pluggable connectors and, for the most part, can be removed and replaced without removing or disassembling the adjacent subassemblies.

The first observatory prototypes proved the reliability of the selected DSLR and LC shutter in the harsh conditions of the Australian summer as well as the operation of the De Bruijn encoding; the design was revised a number of times adding functionality and refining the existing systems. Care was taken whilst refining the design to ensure complexity was minimised.

The initial observatory prototypes contained a fisheye lens, LC shutter, camera, low powered PC with a system drive, power supplies and a basic circuit with the GNNS module, microcontroller, and shutter driver. The four prototypes were installed at the original film observatory sites (which were still operating at the time). Data was stored on a small dual 3.5 inch drive network attached storage (NAS) device located in the film camera's battery shed and connected via Ethernet. These prototypes successfully proved the concept, and underwent two major revisions to produce the final design: Fig 3.5 and Fig 3.6.

The first major revision added a video camera to provide additional imagery of the fireballs—especially of fragmentation events, increased computing power for image processing, moved the data storage inside the observatory enclosure and integrated more flexible power management.

Lens condensation blowers for the main and video lenses were added to prevent condensation obscuring the images when the temperature of the glass front elements dropped below the dewpoint at night. The design works particularly well because the airflow cools the internal components and then transfers heat to the lenses, reliably defogging them with minimal power usage (compared to lens heaters). Subsystem power management is controlled by the microcontroller and directed via the PC for a flexible system making fine grained power management possible. The subsystems can be powered on and off as required; allowing the solar powered observatory to achieve the desired low power usage. Fig 3.3 shows the power and control connections between the different observatory subsystems.

Figure 3.5: The exterior of the fireball observatory showing the door, lenses, outer blower ducting and sunshield mounting bolts with a 15 cm ruler for scale


Figure 3.6: Fireball observatory internals. Showing (clockwise from top left): video camera and lens, blower ducting, camera and lens (LC shutter inside), embedded PC, observatory management PCB (microcontroller, GNSS module), hard drive enclosure

The archival data storage consists of two 3.5 inch hard drives (WD Red models with an extended operating temperature range) in a dual drive enclosure connected via USB. Over time the total capacity has increased as larger drives (6 and 8 TB) have become available.

A small number of these second revision prototypes were constructed, and, after testing, the PCB was re-implemented with surface mount components to accelerate production and save board space. A serial level converter was added to allow the PC to also receive accurate time information from the GNSS module, and the self reset functionality was also slightly modified. The design as a whole has not changed since this revision, but minor changes have been made to the self reset circuitry and some modifications have been made for production reasons (eg: swapping IC packages for more reliable reflow soldering).

The other components in the observatory have evolved a little over the three years the design has been in use. The camera was upgraded to the Nikon D810 when it was released due to the slightly increased performance and lower cost compared to the D800E. The embedded PC was upgraded to a Commell LE-37D model equipped with USB 3.0 enabling faster image download from the camera, a wider input voltage range, more powerful CPU, additional expansion ports, and a more reliable power connector. The initial observatories had some reliability issues due to power supply problems, but these were eliminated by the PC upgrade, swapping to higher rated solar charge regulators and swapping the DC-DC converter regulating the power to the PC and hard disk drives (HDDs) to a more capable model with a wider input voltage range. The modular design of the observatory allowed most of these changes to be easily retrofitted to the existing systems in the field.

## 3.5 Notable Design Aspects

The observatory has a number of notable features and inventive solutions to problems encountered.

(a) (b)

Figure 3.7: Lens condensation blower and ducting. (a) The CAD design showing the complex ducting geometry. (b) The manufactured ducting assembly removed from the observatory with the blower.

### 3.5.1 3D Printed Blower Ducting

Directing airflow from the lens blower mounted inside the box over the lenses to remove condensation during the night was a significant challenge due to the tight space constraints. A two piece duct was designed in software from the geometry and layout of the box, blower and lenses. The duct is a complex organic shape designed to direct the airflow evenly over the two lenses without sharp turns and provide multiple drain locations for any accumulated water. The part was designed in CAD (see Fig 3.7a) and produced on two different 3D printers. This allowed the production of the complicated shape without the significant tooling expense of injection moulding. A simple coat of paint provides UV resistance to the printed plastic part. The final blower and ducting assembly is shown in Fig 3.7b.

### 3.5.2 Lasercut Interlocking Stand

Installation of the film observatories was a laborious, time consuming and expensive three day exercise requiring a truck, a large team and pouring of a concrete foundation. A faster and smaller scale installation procedure was required for the rapid deployment of the digital DFN; a semi-permanent support structure would

allow this faster deployment and uncomplicated camera relocations if required. The semi-permanent nature of the installation, leaving little to no trace after removal, allowed simpler negotiation of installation sites enabling rapid network deployment.

The stand (Fig 3.8) is constructed from interlocking laser cut steel plate which is cut to order with low lead times and machining costs. The interlocking plates fit together like a three dimensional jigsaw puzzle and are affixed with inexpensive steel wedges hammered into specially design slots in the interlocking tabs. This design packs flat and allows rapid installation in approximately thirty minutes. Torsional stability is provided by tensioned wire stays visible in Fig 3.1.

### 3.5.3 Weather sealed Lens Flanges and Hydrophobic Coating

To weatherproof the lenses against the infrequent but sometimes torrential rain, they are sealed into custom designed Aluminium flanges (clearly visible in Fig 3.5). The flanges also support the lenses and attached cameras. The flange meets the glass front element of the lens with a thin metal protrusion which is bonded to the glass with a small amount of precisely applied waterproof and flexible silicone sealant. The weather sealing on a few flanges failed initially; the sealant application procedure was modified and no further failures have occurred. The design is versatile and has been adapted to the Samyang 14mm f/2.8 rectilinear and Canon 8-15mm f/4 fisheye zoom lenses for testing and special purpose DFN observatories.

The open flange design does not protect the lens from dust which can lower the contrast and sensitivity of the imaging system. To minimise the accumulation of dirt and ensure water droplets run off the dome shaped front element (instead of evaporating in place leaving a precipitate) the lenses are coated with a consumer hydrophobic surface treatment. This is intended to make the lenses self cleaning; accumulated dust and dirt should be cleaned off when rain droplets bead up and run off the lens. The coating seems to perform as intended, as the lenses remain clean between servicing trips.

Image quality is not affected at all by the flanges making them preferred to protective domes. The weather sealed flanges are also much simpler and less costly than retractable lens covers. They are not susceptible to mechanical or electronic failure helping to increase reliability.

### 3.5.4 Flexible Network Connectivity

The observatories are networked via an Internet connection where available. This links them to the central server for status reporting and allows event detection to incorporate observations from multiple stations to increase reliability. The observatories support a wide variety of different connection types including: 3G mobile data from two different service providers, Ethernet, WiFi and satellite data. This versatility allows the installation of DFN observatories nearly anywhere, and allows the use of the lowest cost connection on a per-site basis. A virtual private network (VPN) is used to bridge the heterogeneous architecture creating a connection agnostic and seamless network. The majority of the network is connected through 3G mobile data. The connected observatories use a few hundred megabytes of data per month on logs and event detection notifications (which include small image tiles). The observatory is also capable of operating without a network connection; event detection is run on the data from these offline cameras when the hard drives are collected and ingested into the central data store. This mode of operation is used at some remote sites where satellite connections are currently prohibitively expensive.

### 3.5.5 Other Notable Aspects

Some other notable design aspects include the ability to power cycle all of the subsystems including the cameras, PC, HDD's and microcontroller. This allows recovery from occasional software glitches including frozen cameras or dropped USB connections. The observatory enclosure is an off-the-shelf steel hinged enclosure CNC water jet cut to accommodate the observatory fittings. This provides a high quality durable enclosure that meets the requirements without the expense and complication of designing and manufacturing a custom enclosure. CNC cut-

ting makes improvements and new prototypes simple to implement by modifying the CAD software design. Enclosure temperature is regulated by a thermostat controlled cooling fan. (Heating is not necessary at the current observatory sites.) A fixed sunshield mounted on top of the observatory reduces solar heating during the day. The shield is mounted below the protruding lenses and does not obscure the field of view.

### 3.5.6 Design for Manufacture and Assembly

Considerable design effort was focused on the ease of assembly of the observatory to make it possible to produce the design quickly and easily in-house. The manufacturing steps are automated from the CAD design, including the laser cutting of the backplane, HDD support, stand and sunshield; the water jet cutting of the enclosure, gasket, and flange rings; the CNC turning of the lens flanges; and the 3d printing of the blower ducting. The observatory is modular and easy to assemble; the in-house assembly is performed in small batches and takes approximately six hours per observatory.

## 3.6 Observatory Operation

The observatory is controlled by the embedded PC (Commell LE-37D); flexible scripting allows it to adapt to the operational conditions as required including: position, date, time of day, weather and remaining drive capacity. Online observatories regularly file status reports with the central server and relay fireball event detections, so potentially meteorite dropping fireballs can be analysed before HDD collection. Full size images can be downloaded from online cameras for analysis if required. This is only performed for significant potentially meteorite dropping fireball events due to the high data transfer costs of downloading large raw image files.

The PC is connected to the Atmel ATmega32U4 microcontroller via a USB virtual serial connection (using the LUFA library—http://www.fourwalledcubicle.com/LUFA.php) which controls the observatory

Figure 3.8: Stand made from interlocking lasercut steel plates which packs flat and can be assembled on site with steel wedges in about 30 minutes

subsystems. The PC directs operations with high level commands (eg: start camera triggering) that are sent to the microcontroller and then implemented at a low level (eg: triggering the DSLR every 30 seconds through the remote release port). This approach avoids tying the observatory to a specific embedded PC; any PC with USB connections for the microcontroller, camera and hard drives would be compatible. Subsystems are only powered by the power distribution electronics when required. This results in substantial power savings for the solar powered observatory as many subsystems are only required for a portion of the day or night (eg: camera and video camera at night during good observing conditions, hard drives for 30-60 minutes in the morning while data is archived). The operational and exposure parameters are listed in Table 3.1.

Observations are automatically controlled by local sunset and sunrise times at each site depending on season and location; observations start and stop when the Sun is six degrees below the horizon. Each exposure is modulated by the LC shutter between the lens and the image sensor to encode the arrival time of any fireballs. The microcontroller precisely synchronises the start and end of the exposure as well as the modulation of the LC shutter with GNSS time to ensure sub-millisecond timing precision. Images are captured in the Nikon raw format. Every fifteen minutes, an image is analysed to determine the quality of observing conditions which are quantified using a star counting algorithm comparing the count to a dynamically adjusted threshold that compensates for the presence of the Moon and other bright light sources within the image. Observations are paused in poor conditions to save storage space and shutter actuations (wear on the camera). Analysis of the observing conditions continues at 15 minute intervals, and normal operation is resumed if conditions improve.

The video camera operates at night in parallel with the still camera. One minute segments are saved to the SSD throughout the night and retained on the HDDs where a corresponding event is detected in the still images. The operational parameters for the video camera are shown in Table 3.2. The video camera observations are not currently incorporated into the automated data pipeline. Expanded video capabilities, including photometry, will be incorporated into the data pipeline in the future.

Table 3.1: Nominal DFN Operational Parameters

| **Parameter** | **Value** | **Note:** |
|---|---|---|
| Exposure Period | 30 s | time between exposure starts |
| Exposure Duration | 29 s | shutter open time |
| Deadtime | 1 s (out of every 30 s) | time where shutter is not open |
| Observing Time | 8-14 hours per night | depending on latitude and season |
| Camera | Nikon D810 | older systems use D800/D800E |
| Sensor Size | 35.9 x 24.0 mm | 35 mm "full frame" |
| Image Resolution | 36 MP (7360 x 4912) | 69% pixel utilisation, see Fig 3.14 |
| Bit Depth | 14 bits | |
| Colour Filter | RGGB Bayer array | |
| Image Size | 45 MB | ≈45-75 GB per cloudless night |
| Image Format | Nikon lossless compressed raw | (.NEF) |
| Embedded PC | Commell LE-37D | Intel Bay Trail based single board computer |
| Operating System | Debian GNU/Linux | |
| Camera Control Library | gPhoto2 | |
| ISO Speed | 6400 | most stations |
| Lens Aperture Setting | f/4 | most stations |
| Lens | Samyang 8mm F3.5 Fish-eye CS II | Nikon F mount |
| Lens Projection | stereographic fisheye | |
| Image Circle | ≈28.7 mm | slight crop at top and bottom of image circle |
| Field of view | 180 degrees | 5% of hemisphere area cropped |
| Limiting Magnitude, Fireballs | ≈0.5 stellar magnitude | |
| Limiting Magnitude, Stars | ≈7.5 stellar magnitude | |
| Optical Modulator | LC-Tec X-FOS LC Shutter | twisted nematic type liquid crystal shutter |
| Open state transmittance | 36% | |
| Closed state transmittance | 0.1% | |
| Shutter Operation | de Bruijn time-code | |
| Shutter Rate | 10 dashes per second, $t_e = 100$ ms | 10 elements per second sequence rate |
| Data Point Rate | 20 data points per second | dash starts and ends |
| Particular Sequence | prefer high de Bruijn sequence | $k = 2$ (binary), $n = 9$ (subsequence length) |
| Encoding | pulse width | $t_0 = 20$ ms, $t_1 = 60$ ms (dash length) |

Table 3.2: Nominal DFN Video Camera Operational Parameters

| **Parameter** | **Value** | **Note:** |
|---|---|---|
| Video Camera | Watec WAT-902H2 CCIR ULTIMATE | some older systems using EIA equivalent |
| Video Camera Resolution | 795 x 582 | |
| Colour Filter | none | panchromatic camera |
| Bit Depth | 8 bit, YUV colourspace | |
| Frame Rate | 25 fps, interlaced | |
| Exposure Time | 1/50 s | |
| Gain control | auto gain | |
| Capture Card | Commell MPX-885 | |
| Compression | H264 variable bit rate | FFmpeg "ultrafast" preset |
| Nominal Bit Rate | $\approx$ 27 Mbps | |
| Lens | Fujinon FE185C046HA-1 | 1/2" format 5 MP 185 degree fisheye |
| Lens Aperture Setting | f/1.4 | |
| Limiting Magnitude | $\approx$2 stellar magnitude | (fireballs and stars) |

In the morning, still images are downloaded from the camera's CF card over the USB connection using gPhoto2 and stored on a solid state drive (SSD). Custom automated event detection software then searches the sequence of images for meteor events which are then relayed back to the central server (for online cameras). The server attempts to corroborate the events across multiple observatories by performing a rough triangulation which eliminates most false positives: satellites, aircraft, stray lights. Data is periodically archived from the SSD to the larger HDDs to be collected during servicing and then ingested into the central data store.

When a significant fireball event is detected, the images are processed through the centralised data pipeline—Fig 3.9.

## 3.7 Data Pipeline

When a promising fireball event is flagged by the event detection, the relevant images are downloaded from the cameras or recalled from the data store. Event metadata is tracked throughout the entire pipeline. First, pixel coordinates are

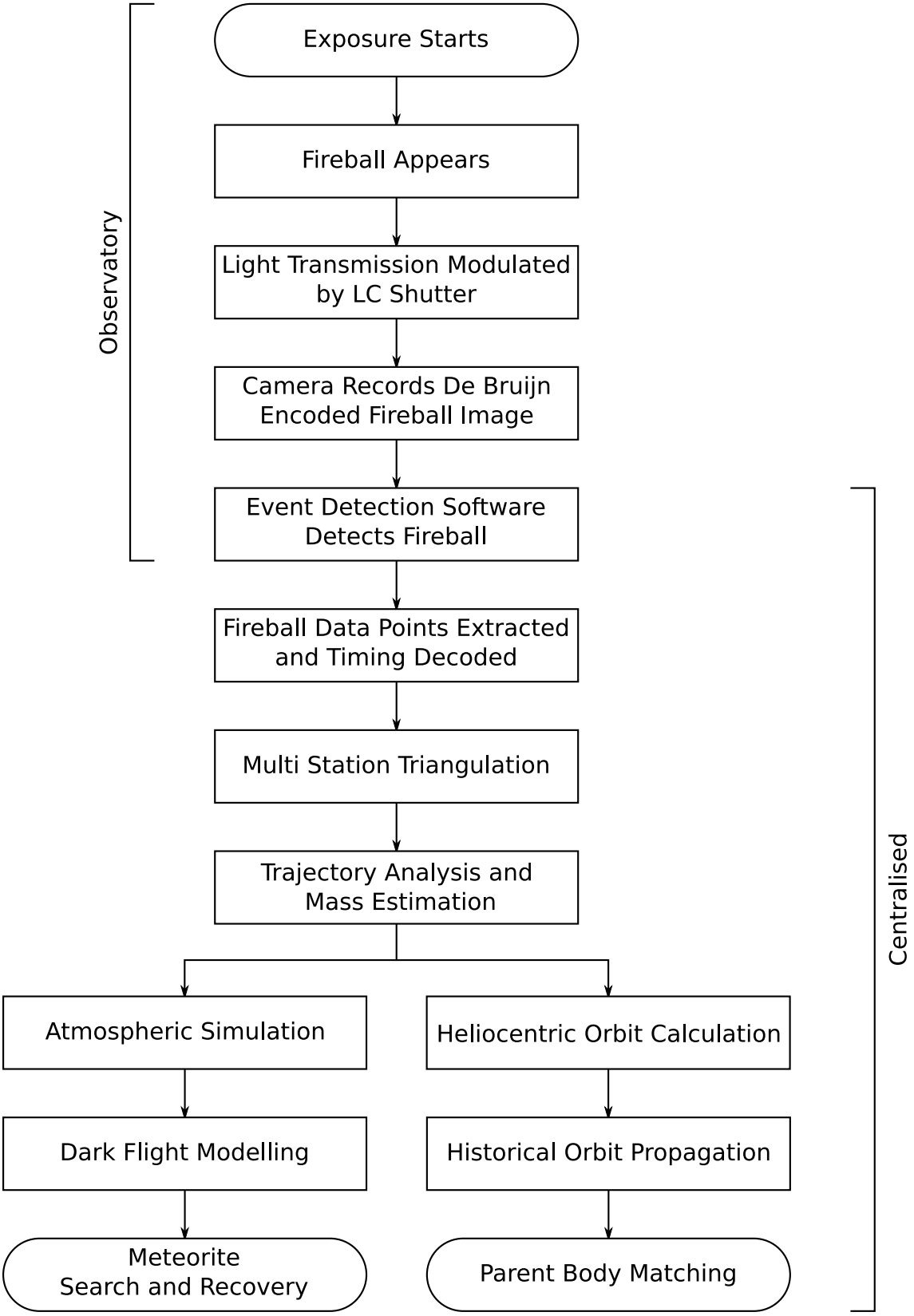


Figure 3.9: Stages in the data processing pipeline for a fireball event

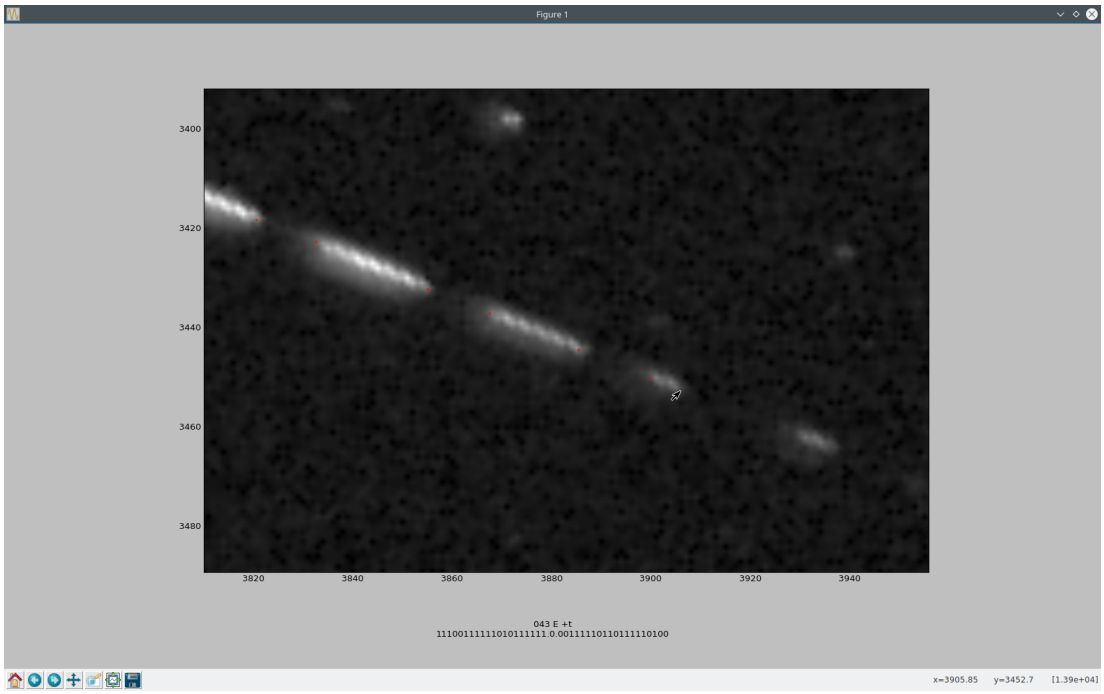


Figure 3.10: Fireball data point extraction tool. Times for the data points (in red) are automatically calculated from the corresponding de Bruijn sequence element. A partial preview of the sequence, as well as the currently selected element, is displayed to the user at the bottom of the window.

selected with timing from the fireball dashes; this is performed manually with a workflow optimised custom software tool (Fig 3.10) allowing the points to be selected quickly and reviewed or edited if required. This process takes approximately five minutes per image on average. The luminous trajectory is triangulated using these points and the camera calibration data which characterises the relationship between each observatory's pixel coordinates and the corresponding altitude and azimuth coordinates from each site. This relationship is dependant on the all-sky lens projection, atmospheric refraction, lens distortion (intrinsic parameters) and camera orientation (extrinsic parameters). Calibration is determined by analysing the starfield as imaged by the DLSR. Visible stars are matched to a catalogue iteratively from the centre of the image until the entire field of view is described by a polynomial fit.

Triangulation is currently performed using the least-squares method [42] which makes a straight line assumption, but we are currently developing a independent point by point three dimensional triangulation method that doesn't rely on this assumption. This is only possible due to the absolute timing precision of the

observations that is maintained by the GNSS synchronised operation.

The triangulated trajectory is analysed using the dynamic method as described by [46], which uses the observations to estimate meteoroid position, velocity and mass. This method calculates the likely errors based on the uncertainties of the observations and the single body dynamic model. This approach is advantageous because these uncertainties, and in particular the uncertainty of the final mass, can then be factored into the dark flight modelling and incorporated into search and recovery decisions.

The final vector and mass distribution is used to model the dark flight of the meteoroid once it has decelerated to the point where ablation ceases and it is no longer visible to the camera network. The first step of this process is high resolution (3km grid) WRF ARW (http://www.wrf-model.org/index.php) atmospheric modelling of the relevant volume initialised from a regional model incorporating local ground and weather balloon flight data. The fall position distribution is determined by simulation of meteoroid motion through this volume (dark flight) using the Monte Carlo method to incorporate uncertainties (mostly in the mass, final velocity, and the atmospheric model). This fall position distribution is then used to plan the search and recovery of the single meteorite or multiple meteorite fragments. The ideal fireball has a long visible trajectory at a steep angle, a slow final velocity at a low altitude, a final mass estimate of one kilogram or more and a search area in accessible featureless terrain with a stable hard surface [37], [134], [135].

The heliocentric meteoroid orbit is calculated from the initial atmospheric entry vector refined in the trajectory analysis using an numerical propagation technique, which can then be back propagated (in time) and possibly matched to a parent body or asteroid family. Where a link can be made and a meteorite recovered, the sample—now of known origin—can be analysed with the proper context; which may, in turn, contribute to new understanding about the formation and current state of the Solar System.

The data processing pipeline, in it's current state, is semi-automated; the individual steps (apart from fireball coordinate extraction) are automated but, for

now, the process is manually coordinated. Automation of the image analysis for coordinate extraction is a priority. While the problem is not difficult for the ideal case (a fast, unsaturated fireball in the higher resolution central area of the fisheye lens), it is challenging in many real world cases where the fireball is obstructed, slow or toward the edge of the lens. In the long term, all of the steps and the coordination of the pipeline will be fully automated to produce masses, fall positions and orbits from detected events without manual intervention.

## 3.8 Performance

The digital fireball observatory has satisfied the design requirements and enabled the rapid deployment of the digital Australian Desert Fireball Network. The observatories are so cost effective and easy to deploy that the coverage goal has been revised upwards to cover as much good searching terrain as possible within Australia—and this is well under way.

The system has proven to be reliable, suitable for harsh Australian conditions, compatible with a (semi-)automated data pipeline, and easy to install and maintain. The observatories successfully operate for long periods between data download and maintenance trips, but the desired goal of one year between download intervals has not been met yet. The cameras fill two 6TB drives after 8-10 months, but some configuration changes are planned to reduce the filesize of the images, by cropping them to just the region of the sensor used by the fisheye lens. This should extend the download interval to approximately one year when combined with drive upgrades (8 TB drives with suitable temperature ratings are now available and in use at some stations).

The spatial precision of the observatories is approximately one arcminute (down to 5 degrees above the horizon) which is similar to the precision of the previous film based observatories. This allows trajectory triangulation to within several tens of metres. Improvements past this point would do little to refine search areas on the ground due to the dark flight (wind profile) and mass uncertainties. The de Bruijn timecode has performed well: absolute timing precision on the trajectory is better than one millisecond and the techniques has even produced good results

for visibly fragmented meteors. The spatial and timing precision achieved more than satisfy the requirements for orbits and ground searches.

The observatories can be fully deployed and commissioned in four hours by two people. The observatories are are small (370x300x150 mm) and light (12 kg). This makes it simple to bring spare observatories on maintenance trips; for more serious problems, they can be exchanged in the field and serviced back in the clean laboratory with more capable equipment. Maintenance in the field and in the lab is made easier by the modular construction. Routine maintenance includes inspection, exchanging hard drives, cleaning the lenses, examining the power systems and connections, operations testing, replacement of the outer blower ducting if required and extracting the occasional spider. The periodic replacement of some parts is planned: the DSLR's mechanical focal plane shutter has a limited lifetime; the outer blower ducting usually lasts for one to two years, and lenses are predicted to degrade at some point from UV exposure and dust storms. Nikon rates the D800/D810 as tested to 200,000 shutter actuations; in practise, the cameras seem to last significantly longer than this: very few have failed to date. One D800 has taken more than 890,000 exposures to date and is still operating, but more time is required to determine the average shutter lifetime under observatory conditions. The cameras can be returned to the manufacturer for a focal plane shutter replacement when required.

A graphical summary of the performance and characteristics of the new digital fireball observatory compared to the previous large format film observatories is presented in Fig 3.11.

### 3.8.1 Network Deployment

The first four production observatories were installed in December 2012, and, as of December 2016, the Desert Fireball Network has expanded to 49 stations in three main regions: Western Australia (Wheatbelt and Mid-west), The Nullarbor and South Australia. A new southern Queensland region is also being established. Nominal camera spacing is about 130 km, and the current network coverage (Fig 3.12) is $\approx$2.5 million km$^2$ (approximate double station coverage — where fireball

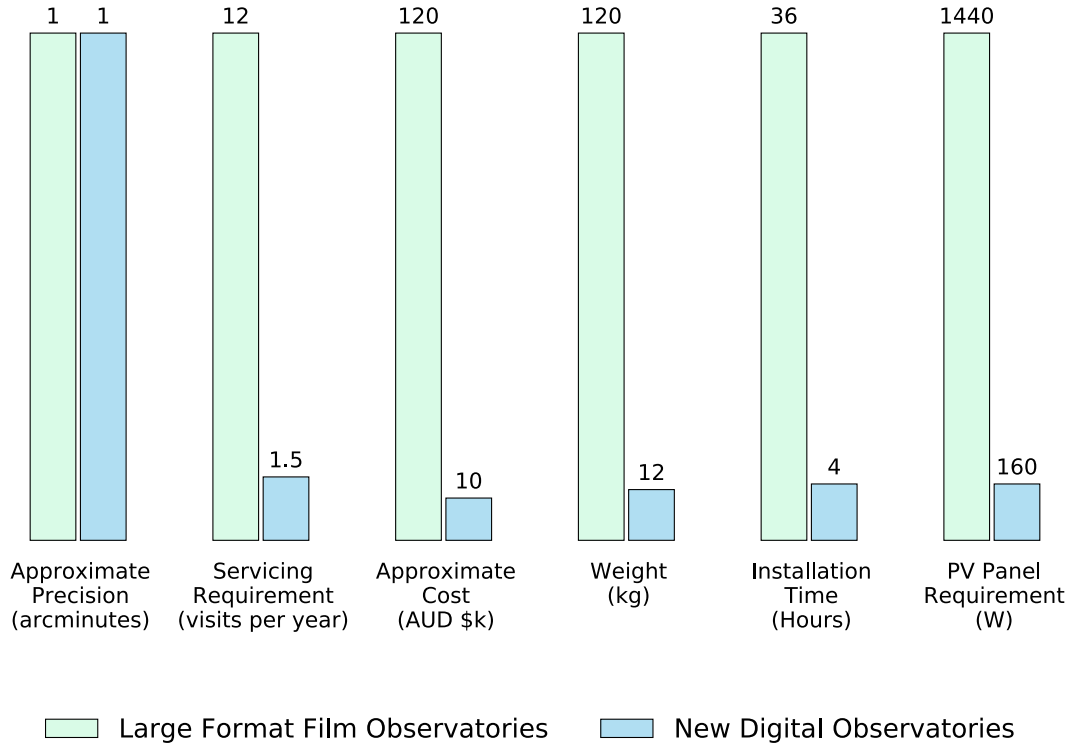


Figure 3.11: A comparison of the new digital DFN observatories and the previous film based observatories used in the initial phase

triangulation is possible), which is roughly one third of Australia.

### 3.8.2 First Recovery — Murrili Meteorite

The DFN recovered the Murrili Meteorite at the end of 2015 (Fig 3.13) using observations from four of the new digital observatories. This is the third meteorite recovered by the DFN and the first using the new digital network. The 6.1 second fireball (Fig: 3.14) appeared on 27 November 2015 on a steep trajectory into Kati Thanda—Lake Eyre South in South Australia. The heliocentric orbit has also been calculated, and will be presented in a future publication. The 1.7 kg meteorite was located through a systematic search by a small team of three researchers and excavated from the thick salt lake mud by hand from a depth of 42 cm. The Arabana People, the local indigenous people, assisted with the recovery and naming of the meteorite. This result demonstrates the success of the digital DFN and the viability of the new observatory design.

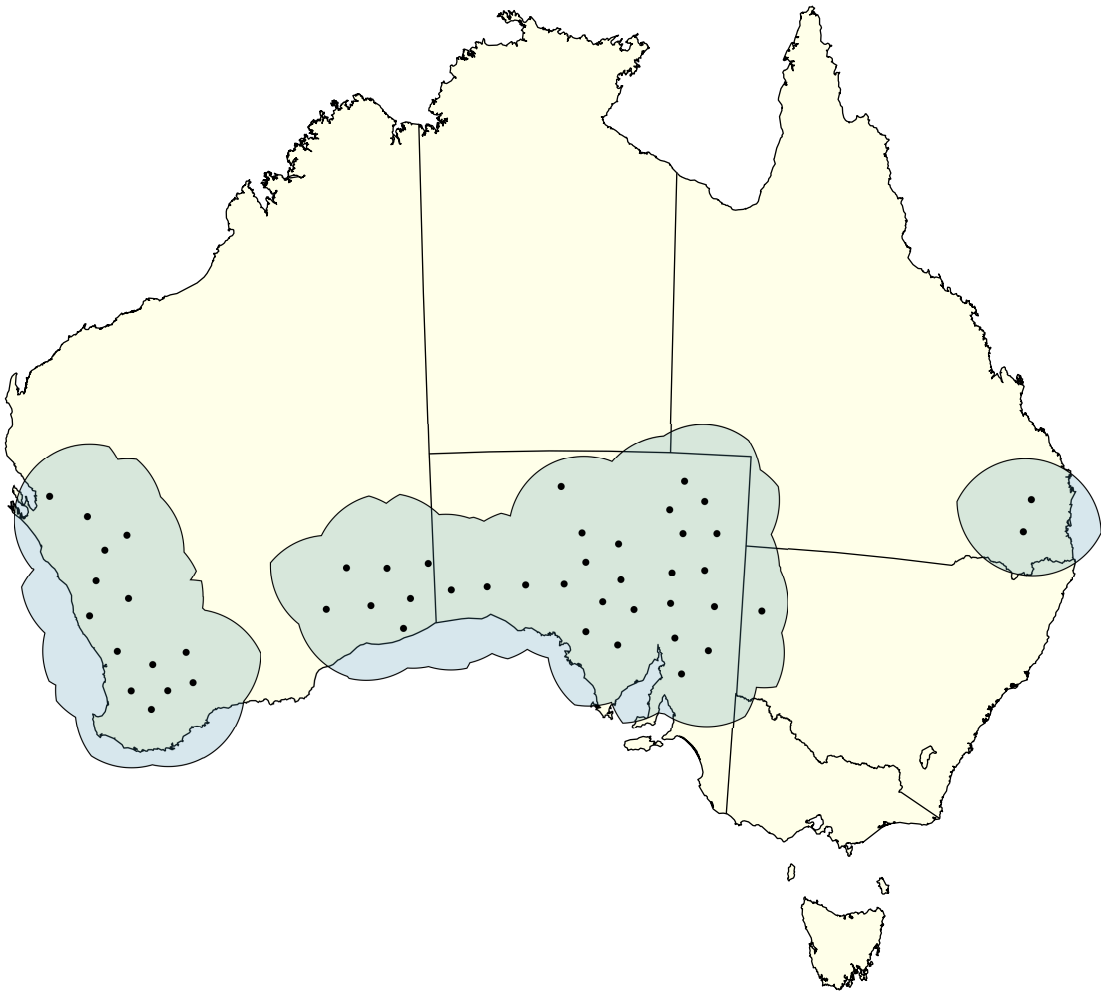

Figure 3.12: Current DFN deployment of 49 stations showing approximate double-station coverage (triangulable area)

Figure 3.13: The Murrilli Meteorite — the first recovered using the new digital DFN observatories

Figure 3.14: The 6.2 second Murrili Meteorite Fireball, 27 November 2015 10:43:44.50 UTC as observed by the Billa Kalina DFN observatory

## 3.9 Future Work

Network expansion is ongoing in Australia and internationally through partner networks managed by collaborators. A new version of the camera designed for simple rooftop installation at mains powered sites is under development.

The extreme dynamic range of fireball events pose a problem for all imaging systems. The DFN observatories are well suited for imaging the vast majority of meteorite dropping fireballs, but extremely bright superbolides can saturate large areas of the image sensor, obscuring the trajectory and timing. While events like this are rare (a couple per year at the current network size), they are particularly interesting. Work to improve the dynamic range at both ends of the spectrum is currently under way.

The current (dynamic) mass estimation method [46] does not require brightness, so fireball photometry is not regularly performed. As the data processing pipeline is further developed, fireball photometry will be automatically derived from video

camera data using local brightness reference stars to be incorporated in future models.

More than a dozen good meteorite dropping fireball candidates have been observed to date. Fieldwork to recover some of these will be conducted in the future.

# References


[6] D. Brownlee, P. Tsou, J. Aléon, C. M. Alexander, T. Araki, S. Bajt, G. A. Baratta, R. Bastien, P. Bland, P. Bleuet, *et al.*, "Comet 81P/Wild 2 under a microscope," *science*, vol. 314, no. 5806, pp. 1711–1716, 2006.

[19] Z. Ceplecha and J. Rajchl, "Programme of fireball photography in Czechoslovakia," *Bulletin of the Astronomical Institutes of Czechoslovakia*, vol. 16, p. 15, 1965.

[20] R. E. McCrosky and J. H. Boeschenstein, "The Prairie Meteorite Network," *Optical Engineering*, vol. 3, no. 4, pp. 304 127–304127–, 1965.

[21] I. Halliday, A. Blackwell, and A. Griffin, "The Innisfree meteorite and the Canadian camera network," *Journal of the Royal Astronomical Society of Canada*, vol. 72, pp. 15–39, 1978.

[22] P. Spurný, J. Borovička, and L. Shrbený, "Automation of the Czech part of the European fireball network: equipment, methods and first results," *Proceedings of the International Astronomical Union*, vol. 2, no. S236, pp. 121–130, 2006.

[31] P. Bland, P. Spurný, A. Bevan, K. Howard, M. Towner, G. Benedix, R. Greenwood, L. Shrbený, I. Franchi, G. Deacon, *et al.*, "The Australian Desert Fireball Network: a new era for planetary science," *Australian Journal of Earth Sciences*, vol. 59, no. 2, pp. 177–187, 2012.

[34] P. A. Bland, P. Spurný, M. C. Towner, A. W. Bevan, A. T. Singleton, W. F. Bottke, R. C. Greenwood, S. R. Chesley, L. Shrbený, J. Borovička, Z. Ceplecha, T. P. McClafferty, V. David, G. K. Benedix, G. Deacon, K. T. Howard, I. A. Franchi, and R. M. Hough, "An anomalous basaltic meteorite from the innermost main belt," *Science*, vol. 325, no. 5947, pp. 1525–1527, 2009.

[35] P. Spurný, J. Oberst, and D. Heinlein, "Photographic observations of Neuschwanstein, a second meteorite from the orbit of the Příbram chondrite," *Nature*, vol. 423, no. 6936, pp. 151–153, 2003.

[37] I. Halliday, A. T. Blackwell, and A. A. Griffin, "The typical meteorite event, based on photographic records of 44 fireballs," *Meteoritics*, vol. 24, no. 2, pp. 65–72, 1989.

[38] P. Spurný, P. A. Bland, L. Shrbený, J. Borovička, Z. Ceplecha, A. Singelton, A. W. Bevan, D. Vaughan, M. C. Towner, T. P. McClafferty, *et al.*, "The Bunburra Rockhole meteorite fall in SW Australia: fireball trajectory, luminosity, dynamics, orbit, and impact position from photographic and photoelectric records," *Meteoritics & Planetary Science*, vol. 47, no. 2, pp. 163–185, 2012.

[40] Z. Ceplecha, "Geometric, dynamic, orbital and photometric data on meteoroids from photographic fireball networks," *Bulletin of the Astronomical Institutes of Czechoslovakia*, vol. 38, pp. 222–234, 1987.

[42] J. Borovička, "The comparison of two methods of determining meteor trajectories from photographs," *Bulletin of the Astronomical Institutes of Czechoslovakia*, vol. 41, pp. 391–396, 1990.

[43] P. S. Gural, "A new method of meteor trajectory determination applied to multiple unsynchronized video cameras," *Meteoritics & Planetary Science*, vol. 47, no. 9, pp. 1405–1418, 2012.

[46] E. K. Sansom, M. G. Rutten, and P. A. Bland, "Analyzing Meteoroid Flights Using Particle Filters," *The Astronomical Journal*, vol. 153, no. 2, p. 87, 2017. [Online]. Available: `http://stacks.iop.org/1538-3881/153/i=2/a=87`.

[54] Z. Ceplecha and D. O. Revelle, "Fragmentation model of meteoroid motion, mass loss, and radiation in the atmosphere," *Meteoritics & Planetary Science*, vol. 40, no. 1, pp. 35–54, 2005.

[58] P. Spurný, J. Borovička, J. Kac, P. Kalenda, J. Atanackov, G. Kladnik, D. Heinlein, and T. Grau, "Analysis of instrumental observations of the Jesenice meteorite fall on April 9, 2009," *Meteoritics & Planetary Science*, vol. 45, no. 8, pp. 1392–1407, 2010.

[59] J. Borovička, J. Tóth, A. Igaz, P. Spurný, P. Kalenda, J. Haloda, J. Svoreň, L. Kornoš, E. Silber, P. Brown, *et al.*, "The Košice meteorite fall: Atmospheric trajectory, fragmentation, and orbit," *Meteoritics & Planetary Science*, vol. 48, no. 10, pp. 1757–1779, 2013.

[67] S. Hughes, *Catchers of the Light: The Forgotten Lives of the Men and Women Who First Photographed the Heavens*. Stefan Hughes, 2012, ISBN: 9781620509616. [Online]. Available: `https://books.google.com.au/books?id=iZk5OOf7fVYC`.

[70] L. G. Jacchia and F. L. Whipple, "The Harvard photographic meteor programme," *Vistas in Astronomy*, vol. 2, pp. 982–994, 1956.

[71] Z. Ceplecha, "Statistical Observations of Meteors 1951.," *Bulletin of the Astronomical Institutes of Czechoslovakia*, vol. 3, p. 53, 1952.

[72] Z. Ceplecha, "Multiple fall of Přibram meteorites photographed. 1. Double-station photographs of the fireball and their relations to the found meteorites," *Bulletin of the Astronomical Institutes of Czechoslovakia*, vol. 12, p. 21, 1961.

[73] R. McCrosky, A. Posen, G. Schwartz, and C.-Y. Shao, "Lost City meteorite—Its recovery and a comparison with other fireballs," *Journal of Geophysical Research*, vol. 76, no. 17, pp. 4090–4108, 1971.

[74] J. Oberst, S. Molau, D. Heinlein, C. Gritzner, M. Schindler, P. Spurný, Z. Ceplecha, J. Rendtel, and H. Betlem, "The "European Fireball Network": current status and future prospects," *Meteoritics & Planetary Science*, vol. 33, no. 1, pp. 49–56, 1998.

[76] J. Borovička, P. Spurný, and P. Brown, "Small near-Earth asteroids as a source of meteorites," *et al., Asteroids IV, Univ. of Arizona, Tucson*, pp. 257–280, 2015.

[77] P. Spurný, J. Borovička, J. Haloda, L. Shrbený, and D. Heinlein, "Two Very Precisely Instrumentally Documented Meteorite Falls: Žďar nad Sázavou and Stubenberg–Prediction and Reality," *LPI Contributions*, vol. 1921, 2016.

[78] P. Spurný, J. Borovička, G. Baumgarten, H. Haack, D. Heinlein, and A. Sørensen, "Atmospheric trajectory and heliocentric orbit of the Ejby meteorite fall in Denmark on February 6, 2016," *Planetary and Space Science*, 2016.

[79] M. Towner, P. Bland, P. Spurný, G. Benedix, K. Dyl, R. Greenwood, J. Gibson, I. Franchi, L. Shrbený, A. Bevan, *et al.*, "Mason Gully: The second meteorite recovered by the Desert Fireball Network," vol. 74, 2011, p. 5124.

[85] F. Colas, B. Zanda, J. Vaubaillon, S. Bouley, C. Marmo, Y. Audureau, M. K. Kwon, J.-L. Rault, S. Caminade, P. Vernazza, *et al.*, "French fireball network FRIPON," in *International Meteor Conference Mistelbach, Austria*, 2015, pp. 37–40.

[89] M. Gritsevich, E. Lyytinen, J. Moilanen, T. Kohout, V. Dmitriev, V. Lupovka, S. Midtskogen, N. Kruglikov, A. Ischenko, G. Yakovlev, V. Grokhovsky, J. Haloda, P. Halodova, J. Peltoniem, A. Aikkila, A. Taavitsainen, J. Lauanne, M. Pekkola, P. Kokko, P. Lahtinen, and M. Larionov, "First meteorite recovery based on observations by the Finnish Fireball Network," in *Proceedings of the International Meteor Conference, Giron, France*, 2014, pp. 162–169.

[92] R. Weryk, P. Brown, A. Domokos, W. Edwards, Z. Krzeminski, S. Nudds, and D. Welch, "The Southern Ontario all-sky meteor camera network," *Earth, Moon, and Planets*, vol. 102, no. 1-4, pp. 241–246, 2008.

[96] G. Kokhirova, P. Babadzhanov, and U. K. Khamroev, "Tajikistan fireball network and results of photographic observations," *Solar System Research*, vol. 49, no. 4, pp. 275–283, 2015.

[97] P. Jenniskens, P. Gural, L. Dynneson, B. Grigsby, K. Newman, M. Borden, M. Koop, and D. Holman, "CAMS: Cameras for Allsky Meteor Surveillance to establish minor meteor showers," *Icarus*, vol. 216, no. 1, pp. 40–61, 2011, ISSN: 0019-1035. DOI: 10.1016/j.icarus.2011.08.012. [Online]. Available: http://www.sciencedirect.com/science/article/pii/S0019103511003290.

[98] P. Jenniskens, A. E. Rubin, Q.-Z. Yin, D. W. Sears, S. A. Sandford, M. E. Zolensky, A. N. Krot, L. Blair, D. Kane, J. Utas, *et al.*, "Fall, recovery, and characterization of the Novato L6 chondrite breccia," *Meteoritics & Planetary Science*, vol. 49, no. 8, pp. 1388–1425, 2014.

[101] A. Bevan and R. Binns, "Meteorites from the Nullarbor Region, Western Australia: I. A review of past recoveries and a procedure for naming new finds," *Meteoritics*, vol. 24, no. 3, pp. 127–133, 1989.

[103] I. Halliday, "Photographic Fireball Networks," in *Evolutionary and physical properties of meteoroids: the proceedings of the International Astronomical Union's colloquium # 13, held at the State University of New York, Albany, N.Y., on June 14-17, 1971*, ser. NASA Special Publications, C. Hemenway, P. Millman, A. Cook, and I. A. Union, Eds., Scientific, Technical Information Office, National Aeronautics, and Space Administration; [for sale by the Supt. of Docs., U.S. Govt. Print. Off.], 1973.

[104] Z. Ceplecha, "Photographic Geminids 1955," *Bulletin of the Astronomical Institutes of Czechoslovakia*, vol. 8, p. 51, 1957.

[105] C. Flye-Sainte Marie, "Solution to problem number 48," *L'Intermédiaire des Mathématiciens*, vol. 1, pp. 107–110, 1894.

[106] N. G. de Bruijn and P. Erdős, "A combinatorial problem," *Koninklijke Nederlandse Akademie v. Wetenschappen*, vol. 49, no. 49, pp. 758–764, 1946.

[107] K. A. Dyl, G. K. Benedix, P. A. Bland, J. M. Friedrich, P. Spurný, M. C. Towner, M. C. O'Keefe, K. Howard, R. Greenwood, R. J. Macke, *et al.*, "Characterization of Mason Gully (H5): The second recovered fall from the Desert Fireball Network," *Meteoritics & Planetary Science*, vol. 51, no. 3, pp. 596–613, 2016.

[108] Z. Ceplecha, J. Rajchl, and L. Sehnal, "Complete data on bright meteor 15761," *Bulletin of the Astronomical Institutes of Czechoslovakia*, vol. 10, p. 204, 1959.

[109] P. Spurný, "Photographic monitoring of fireballs in Central Europe," in *Optical Science, Engineering and Instrumentation'97*, International Society for Optics and Photonics, 1997, pp. 144–155.

[115] T. van Aardenne-Ehrenfest and N. G. de Bruijn, "Circuits and trees in oriented linear graphs," *Simon Stevin: Wis-en Natuurkundig Tijdschrift*, vol. 28, p. 203, 1951.

[121] P. A. Bland, M. C. Towner, E. K. Sansom, H. A. R. Devillepoix, R. M. Howie, J. P. Paxman, M. Cupak, G. K. Benedix, M. A. Cox, T. Jansen-Sturgeon, D. Stuart, and D. Strangway, "Fall and Recovery of the Murrili Meteorite, and an Update on the Desert Fireball Network (abstract #6265)," *Meteoritics & Planetary Science*, vol. 51, no. S1, A144–A692, 2016, ISSN: 1945-5100. DOI: 10.1111/maps.12704. [Online]. Available: http://dx.doi.org/10.1111/maps.12704.

[123] M. Yoshikawa, A. Fujiwara, and J. Kawaguchi, "Hayabusa and its adventure around the tiny asteroid Itokawa," *Highlights of Astronomy*, vol. 14, pp. 323–324, 2007.

[124] J. M. Trigo-Rodriguez, E. Lyytinen, M. Gritsevich, M. Moreno-Ibáñez, W. F. Bottke, I. Williams, V. Lupovka, V. Dmitriev, T. Kohout, and V. Grokhovsky, "Orbit and dynamic origin of the recently recovered Annama's H5 chondrite," *Monthly Notices of the Royal Astronomical Society*, vol. 449, no. 2, pp. 2119–2127, 2015.

[125] Meteoritical Society, "Creston," vol. 104, 2015. [Online]. Available: `http://www.lpi.usra.edu/meteor/metbull.php?code=62546` (visited on 11/21/2016).

[126] Z. Ceplecha, J. Rajchl, and L. Sehnal, "New Czechoslovak meteorite "Luhy"," *Bulletin of the Astronomical Institutes of Czechoslovakia*, vol. 10, p. 147, 1959.

[127] I. Halliday, A. A. Griffin, and A. T. Blackwell, "Detailed data for 259 fireballs from the Canadian camera network and inferences concerning the influx of large meteoroids," *Meteoritics & Planetary Science*, vol. 31, no. 2, pp. 185–217, 1996.

[128] I. Halliday, "Geminid fireballs and the peculiar asteroid 3200 Phaethon," *Icarus*, vol. 76, no. 2, pp. 279–294, 1988.

[129] M. Campbell-Brown and A. Hildebrand, "A New Analysis of Data from the Meteorite Observation and Recovery Project," in *Bulletin of the American Astronomical Society*, vol. 36, 2004, p. 1142.

[130] J. Borovička, P. Spurný, D. Šegon, Ž. Andreić, J. Kac, K. Korlević, J. Atanackov, G. Kladnik, H. Mucke, D. Vida, *et al.*, "The instrumentally recorded fall of the Križevci meteorite, Croatia, February 4, 2011," *Meteoritics & Planetary Science*, vol. 50, no. 7, pp. 1244–1259, 2015.

[131] J. Toth, L. Kornos, R. Piffl, J. Koukal, S. Gajdos, M. Popek, I. Majchrovic, M. Zima, J. Vilagi, D. Kalmancok, *et al.*, "Slovak Video Meteor Network-status and results: Lyrids 2009, Geminids 2010, Quadrantids 2011," in *Proceedings of the International Meteor Conference, 30th IMC, Sibiu, Romania, 2011*, 2012, pp. 82–84.

[132] P. Brown, P. McCausland, M. Fries, E. Silber, W. Edwards, D. Wong, R. Weryk, J. Fries, and Z. Krzeminski, "The fall of the Grimsby meteorite—I: Fireball dynamics and orbit from radar, video, and infrasound records," *Meteoritics & Planetary Science*, vol. 46, no. 3, pp. 339–363, 2011.

[133] R. M. Howie, J. Paxman, P. A. Bland, M. C. Towner, E. K. Sansom, and H. A. R. Devillepoix, "Submillisecond fireball timing using de Bruijn timecodes," *Meteoritics & Planetary Science*, vol. 52, no. 8, pp. 1669–1682, 2017, ISSN: 1945-5100. DOI: 10.1111/maps.12878. [Online]. Available: http://dx.doi.org/10.1111/maps.12878.

[134] G. Wetherill and D. ReVelle, "Which fireballs are meteorites? A study of the Prairie Network photographic meteor data," *Icarus*, vol. 48, no. 2, pp. 308–328, 1981.

[135] P. Brown, V. Marchenko, D. E. Moser, R. Weryk, and W. Cooke, "Meteorites from meteor showers: A case study of the Taurids," *Meteoritics & Planetary Science*, vol. 48, no. 2, pp. 270–288, 2013.

# Chapter 4

# Absolute Time Encoding for Temporal Super-resolution Using de Bruijn Timecodes

Robert M. Howie[1], Jonathan Paxman[1], Philip A. Bland[2], Martin C. Towner[2]

[1]Department of Mechanical Engineering, Curtin University, Perth, Australia
[2]Department of Applied Geology, Curtin University, Perth, Australia

*This article is undergoing peer review after submission to Machine Vision and Applications. The formatting and referencing style have been modified for presentation in this thesis.*

# Authorship Declaration

**Article Title:** Absolute Time Encoding for Temporal Super-resolution Using de Bruijn Timecodes

**Journal:** Machine Vision and Applications

**Publication Status:** undergoing peer review

## Author Contributions

### Robert Howie

Led development, implementation and testing of the timing method; conceived, drafted and revised manuscript; and handled the publication process

Manuscript contribution: 88%  22 September 2017

### Jonathan Paxman

Assisted with concept development, implementation and manuscript editing

Manuscript contribution: 6%  20 September 2017

**Philip Bland**

Assisted with concept development and manuscript editing

Manuscript contribution: 3%  22 September 2017

**Martin Towner**

Assisted with concept development and manuscript editing

Manuscript contribution: 3%  20 September 2017

**Abstract** Many target tracking tasks require high spatial and temporal precision. High frame rate imaging at high spatial resolution is commonly used, but this approach is expensive and generates large amounts of data which can complicate implementation. When tracking a single object in motion, almost all of this data is unused. A technique has been developed to exploit this sparsity and track motion with a long exposure where absolute timing is encoded by modulating the exposure over time according to a de Bruijn sequence. This technique has been implemented in the Desert Fireball Network to track bright meteors entering the Earth's atmosphere for orbit determination and successful meteorite recovery. An alternate proof of concept implementation was also developed demonstrating tracking at 36 megapixels and 1000 Hz using a consumer camera with an inexpensive modulated light source and retroreflective target. The technique could be applied to other tracking problems requiring high temporal and spatial precision such as particle image velocimetry and space surveillance and tracking.

## 4.1 Introduction

Imaging systems are exercises in compromise. Competing resolution, speed and sensitivity objectives force designers to sacrifice one for the advancement of another. The perfect camera does not exist; the next best thing is a camera ideally matched for its application, which leads to the differentiation of solutions into distinct categories: astronomy cameras, photographic stills cameras, video cameras, industrial cameras and high speed cameras.

Frequently in scientific and general imaging the trade-off between spatial resolution and temporal resolution must be made. The position along this spectrum is what defines most of the aforementioned categories. Photographic stills cameras posses the highest (spatial) resolution but low temporal resolution, and high speed (high temporal resolution) cameras and photodiode arrays are positioned at the other end of the spectrum with low spatial resolution. Solutions at either of these endpoints are affordable due to high demand, commoditisation and a low technical barrier. However, many imaging tasks would benefit from high spatial *and* high temporal resolution. These imaging systems are significantly more costly. This is primarily due to greatly increased data bandwidth which makes

these imaging systems significantly more complex to design and manufacture. The data bandwidth of a camera system is roughly correlated with cost. Data bandwidth is proportional to the product of the spatial resolution and temporal resolution (framerate) of a camera; Fig. 4.1 shows how this bandwidth can be allocated between spatial and temporal precision and the rough correlation with cost.

Some imaging tasks that require high spatial and temporal resolution do not actually require the full data bandwidth of the image sensor to accomplish the imaging objective. One such task is image-based object tracking. The goal of recording the position of a target over time with high spatial and temporal precision is accomplished by recording the scene with a high (spatial) resolution high speed (temporal resolution) camera. This high bandwidth capture is processed to reveal the target position over time. The data rate of the final processed (position) result is orders of magnitude less than the original capture, yet the imaging system must still be designed to handle the high throughput, most of which does not contribute to the final result.

If the imaging system could be redesigned in some way to capture only the data required to produce the final result, it could be less complex and avoid some of the drawbacks of high bandwidth systems. The goal is to move into the upper right of Fig. 4.1 without the associated increase in cost. This is the objective of compressed sensing (a nascent field of signal processing) and some implementations of computational imaging (where the problem is approached from an image processing and computer graphics perspective).

The computational imaging technique presented here uses coded exposures to track targets in motion with high spatial and temporal precision. The sparse nature of image based tracking data is exploited to circumvent the data bandwidth limit and avoid the trade-off between spatial and temporal resolution. This temporal super-resolution technique is well suited to capture fleeting events using off-the-shelf photographic still frame cameras enabling significant cost reductions as well as higher spatial and temporal precision than would be possible with conventional imaging techniques.

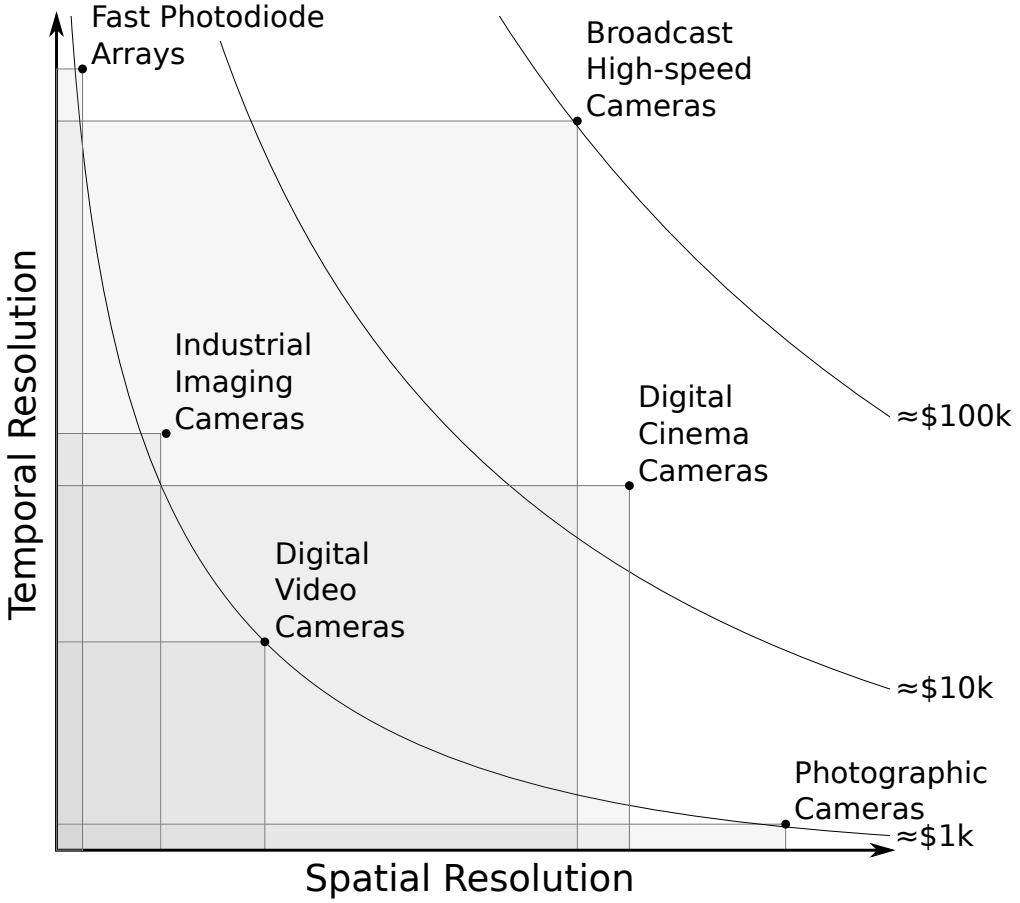


Figure 4.1: Approximate spatial and temporal resolutions of different camera types. Reciprocal curves show equal data bandwidth. Data bandwidth for camera categories is proportional to area within boxes and is strongly correlated with camera cost. Inspired by [136], Fig. 1 (a).

Sect. 4.2 presents a number of related techniques and Sect. 4.3 provides a brief overview of de Bruijn sequences. The proposed de Bruijn coded exposure technique is described in Sect. 4.4 and is followed by results (Sect. 4.5) and discussion (Sect. 4.6).

## 4.2 Related Techniques

A number of other techniques also aim to exploit sparsity in imaging for temporal super-resolution. These include both traditional and computational imaging techniques.

**Long Exposure** If object tracking only required trajectory path data and no timing, long exposure photography is a simple solution provided that the contrast between target and background is sufficient to allow trajectory features to be extracted from the final image. The required contrast depends on the duration of exposure This approach can also be applied to tasks where trajectory path *and* timing is required where the target is observable for substantially longer than the duration of the exposure and the acceleration of the target is well constrained (as is the case with satellite tracking). In this case the timing at the start and end of the streak are known from the timing of the exposure and the timing in between can be reliably interpolated.

**Periodic Shutter** If velocity data on events shorter than the exposure time is required (but not absolute timing within the exposure) it is possible to add a periodic shutter to long exposures. This approach has been used for meteor and fireball observations with rotating [19], [21], [104], mechanical switching [20], liquid crystal [137] and electronic [138] shutters. The shutter modulation here is global, or equal across the frame—ignoring mechanical motion effects of rotating and switching shutters. Stroboscopic photography is an equivalent technique where the exposure is modulated by the periodic operation of the lighting instead of a shutter.

**Flutter Shutter** [139] proposes using a "fluttered" global liquid crystal shutter to retain high frequency information in a long exposure that can be reconstructed later via deblurring algorithms. The technique allows a camera to clearly capture still images of fast events without the same degree of light loss as short exposures. Whilst the aim here is not temporal super-resolution, the technique is related in

that it uses a globally coded exposure to derive additional information from a long exposure.

**Per-pixel Coded Exposure** As opposed to the above techniques which modulate the exposure globally, some techniques code the exposure on a per-pixel basis to achieve temporal super-resolution. [140] used mechanical translation of coded aperture masks to encode sub-frames within a 30 fps standard definition video stream. A coded aperture was moved using a piezoelectric stage generating periodic triangular motion and synchronised with the camera's operation to take one frame per up or down stroke. The imaging system was configured to capture 14 or 148 sub-frames per video frame—a significant increase in temporal resolution.

Another notable per-pixel temporal super-resolution technique is described in [136]. A liquid crystal on silicon mirror device was used to simulate a CMOS sensor with per pixel shutter control. The pixels were individually triggered at random (with some constraints) producing a 9-18 times increase in temporal resolution. Notably, the pixel sampling function was restricted to be implementable on current CMOS sensors ("single bump"), and reconstruction was performed using learned dictionaries, yielding greater detail than other reconstruction techniques.

## 4.3 De Bruijn Sequences

This section presents an overview of de Bruijn sequences which are the type of cyclical sequence used to modulate the exposure in the proposed technique. The de Bruijn coded exposure technique itself is described in Sect. 4.4.

A de Bruijn sequence $\boldsymbol{B}$ is the shortest possible sequence containing all possible subsequences given an alphabet $\boldsymbol{A}$ of size $k$ and subsequence length $n$ [105], [106], [115]. De Bruijn sequences are cyclic, so the last subsequence (or $n$-tuple) is formed by the last element and the first $n-1$ elements. Calculation of the length $N$ of a de Bruijn sequence is simple because every subsequence is present

(4.1); for this reason, they are also known as full length cycles.

$$N = k^n \tag{4.1}$$

Van Aardenne-Ehrenfest and de Bruijn [115] demonstrated the calculation of the number of distinct de Bruijn sequences for a particular case ($k$ and $n$) (4.2).

$$|\boldsymbol{B}(k,n)| = \frac{(k!)^{n-1}}{k^n}. \tag{4.2}$$

Of the many possible generation methods, we have used the "prefer high" method for simplicity, which is a generalisation of the "prefer one" method [116] to $k$-ary alphabets.

As an example, the de Bruijn sequence constructed using the "prefer high" method for the case $\boldsymbol{B}(k = 2, n = 3)$ is 00011101. The subsequences {000, 001, 011, 111, 110, 101} are immediately visible as the three element "viewing window" is slid along the sequence, and the remaining subsequences {010, 100} become evident when considering the sequence as a cycle.

The utility of de Bruijn sequences can be demonstrated by the PIN code problem described in [116]. A four digit alarm without an enter key is disarmed when the last four digits entered match the valid PIN. The conventional method of attack is to try all four digit codes in some sort of order (e.g. 0000, 0001, 0002, 0003, ...); this would require 40,000 key presses. However, this approach is inefficient; it is possible to test two PINs with only five key presses, not eight. By typing in 00009 the attacker has tested the PINs 0000 and 0009. A more efficient method than the conventional method of attack is to use a de Bruijn sequence $\boldsymbol{B}(k = 10, n = 4)$ which is the shortest sequence containing all the possible decimal 4-tuples (four element subsequences of base ten). The de Bruijn sequence is 10,000 elements long and only 10,003 key presses are required to test all possible alarm PINs. (The first three elements are repeated because of the non cyclical nature of the alarm.)

This efficiency can be exploited to create optimal codes for a number of applications including position sensing encoders, and, in our technique, timecodes to record fleeting sporadic events within a coded long exposure.

## 4.4 De Bruijn Coded Exposures

In a de Bruijn coded exposure, a long exposure image of a target in motion is captured while the exposure is modulated globally over time according to a de Bruijn sequence. The result of this type of exposure is similar to the results of periodic shutter or stroboscopic photography, except the absolute timing of the features within the image are known as they can be uniquely matched to a section of the de Bruijn sequence. This timing is known even for events that only become visible after the start of the exposure and cease to be visible before the end of the exposure as long as $n$ sequence elements can be recognised. This makes the technique ideal for observing rare and fleeting events such as fireballs or sporadic meteors. Fig. 4.2 shows a de Bruijn coded exposure image of a fireball using pulse width encoding captured by the Desert Fireball Network (DFN).

De Bruijn sequences are specifically used because they are, by definition, the shortest sequence containing all possible subsequences, making them optimal for this application. These sequences allow the shortest events to be encoded and the longest possible exposure duration compared to other types of sequences.

Once the de Bruijn encoded image has been captured, the features corresponding to the elements in the sequence are recognised and matched to a particular subsequence within the de Bruijn sequence which gives the timing of the trajectory data relative to the start of the de Bruijn sequence. Where $n$ or more elements of the sequence are matched, the subsequence match is unique. If fewer elements are visible, there will be more than one possible position within the sequence. There are $k$ possibilities for events of only $n-1$ visible elements, $k^2$ for events $n-2$ elements in length and so on. Each additional visible element over the required $n$ provides a degree of error checking or additional certainty. To ensure that $n$ elements are visible, the encoding parameters should be adjusted to fit the imaging scenario. Once the sequence has been matched the timing of the

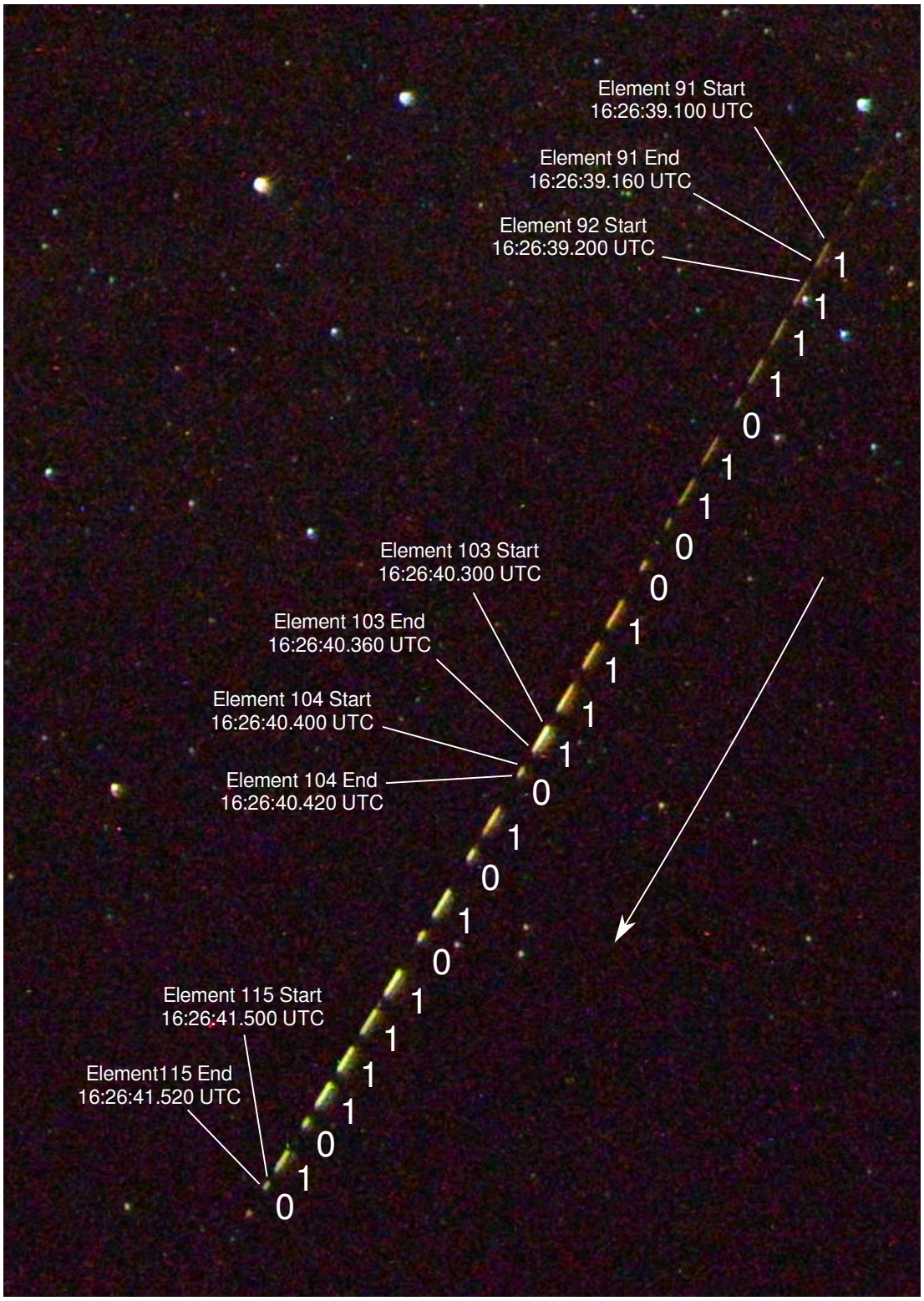


Figure 4.2: DN170305_01 fireball observed by the Kanandah station with pulse width encoding on 5 March 2017

features is known and the trajectory can be reconstructed (in camera space, over

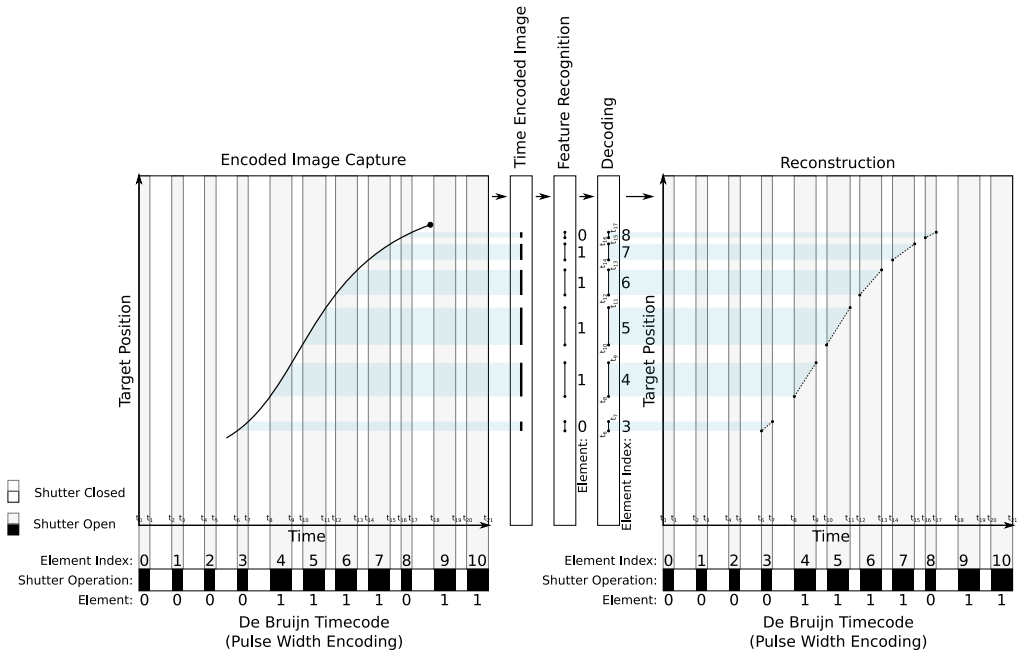


Figure 4.3: Visual representation of the process of de Bruijn coded exposure imaging and reconstruction for one dimensional motion over time. Steps are shown in order from left to right.

time). In order to provide absolute timing for the trajectory, the start of the de Bruijn sequence is tightly controlled with respect to time. This is achieved by synchronising the operation of the modulator drive hardware with a precision time source, or where the start of the sequence is triggered by some event, precisely recording the sequence start time.

The steps involved in the process from image capture to reconstruction are shown from left to right in Fig. 4.3.

### 4.4.1 Modulation

The exposure can be modulated in a number of ways depending on the imaging scenario and system constraints. Some possible modulation options are:

- transmittance (fully transmitting or blocking),

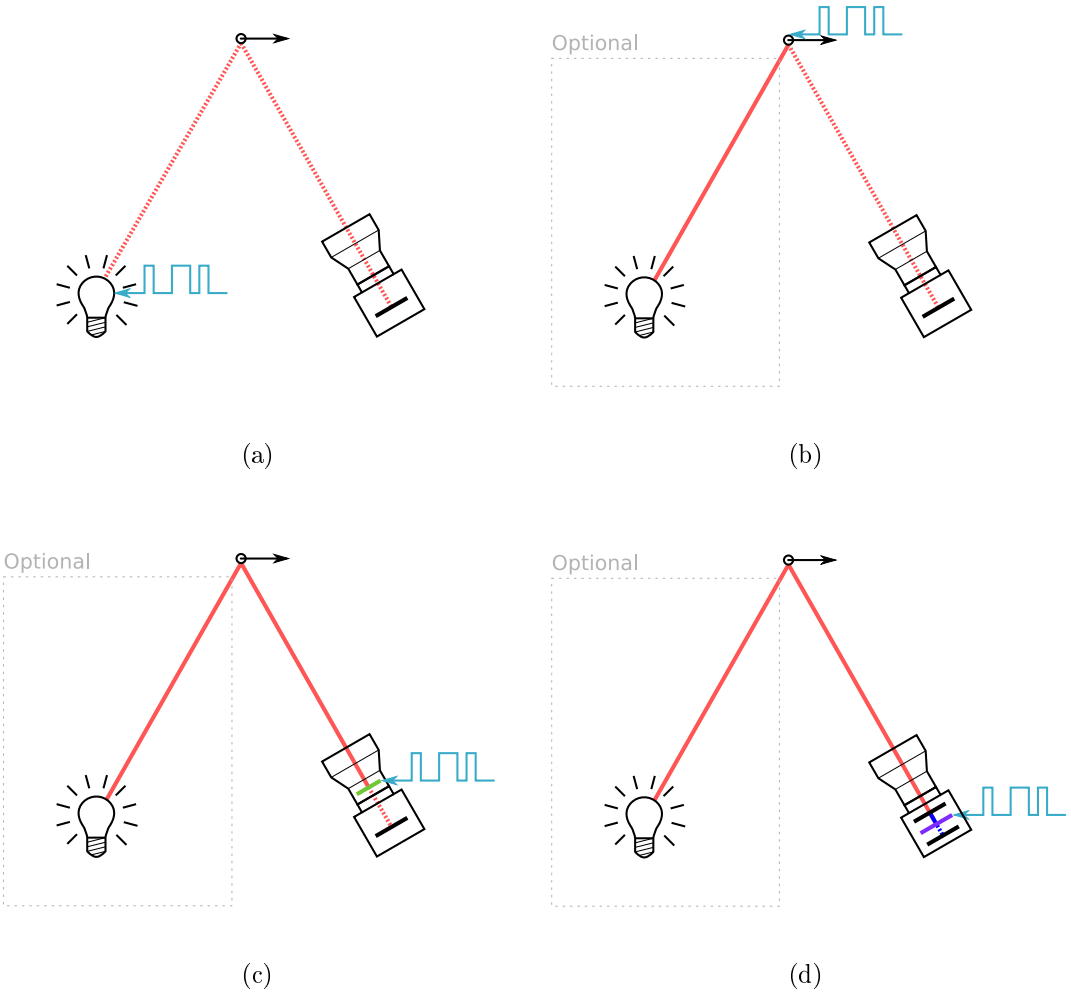


Figure 4.4: Possible system topologies: 4.4a) illumination modulation, 4.4b) target modulation, 4.4c) optical modulation, 4.4d) sensor modulation. Unmodulated light shown in solid red, modulated light shown in broken red, modulated point indicated in light blue, optical modulator indicated in green, unmodulated electrical signal in solid blue, modulated electrical signal in broken blue, electronic modulator in purple. A dedicated light source is required only for illumination modulation.

- opacity (with multiple transmittance levels),
- colour, and
- polarisation.

Note that whilst we refer to transmittance and opacity which imply that the modulation is occurring in the imaging optics, we are actually referring to controlling

the integration of the exposure. This can be implemented at different points in the imaging chain (see Sect. 4.4.2). For example, it is possible to implement transmittance modulation by controlling the illumination, target reflectance, a shutter in the imaging optics or the charge accumulation in the image sensor. Additionally, whilst transmittance modulation is only a specific implementation of opacity modulation (where the imaging system is either fully transmitting or fully blocking) identifying this modulation separately is useful as a number of encodings (see Sect. 4.4.3) are specifically suited to this modulation approach.

### 4.4.2 Topologies

Implementations can also be classified based on the point in the imaging chain where the modulation is performed. The four topologies that have been considered are:

- illumination modulation,
- target modulation,
- optical modulation, and
- sensor modulation.

In illumination modulation (Fig 4.4a) the exposure is modulated through the controlled operation of the light source. This topology is suited for use under more controlled conditions, but allows the technique to be implemented with unmodified off-the-shelf cameras and optics.

Target modulation is implemented by modulating the optical behaviour of the target (Fig. 4.4b). As an example this could be implemented with a controlled light source attached to a target, or a modulatable retroreflector. This topology can also be used with unmodified off-the-shelf cameras and optics.

Where the modulation is performed within the imaging optics (Fig. 4.4c), we refer to this as optical modulation. This topology could be implemented with a number of different optical modulators including mechanical shutters, liquid crystal shutters, polarisation modulators and electronically gated image intensifiers. Modification of the optics may be necessary in this case, but the implementation could be as simple as mounting a large format liquid crystal shutter at the front of the lens.

Sensor modulation where the accumulation or integration of the electrical charge throughout the exposure is modulated is also possible (Fig. 4.4d). This feature is implemented on some industrial imaging cameras where it is referred to as multi integration mode or multi exposure pulse width trigger mode.

### 4.4.3 Encoding

Encoding is the way in which the sequence is translated into recognisable features in the image by the exposure modulation. The choice of encoding for a particular scenario can have a large impact on the quality of results, and it is important to ensure that it will be possible to decode the $n$ sequence elements under all relevant conditions. The choice of system topology and modulator dictate the available encoding options.

The simplest encoding is an on/off encoding; for binary sequences and bright targets on dark backgrounds, '1's are encoded as a dashes where the shutter is open and '0's are encoded as blanks where the shutter is closed. This approach can be generalised to non-binary sequences if the modulator used is capable of intermediate transmission or integration values (opacity modulation). This type of encoding is shown in the first line of Fig. 4.5. The more basic on/off encoding is not shown as this type of encoding cannot be used with non-binary sequences such as the ternary example sequence.

While opacity encoding is simple to implement and easily extended to larger alphabets, it has two main flaws. Firstly, the rate of encoded points in the image is not constant. Repeated elements in the sequence are indistinguishable as the

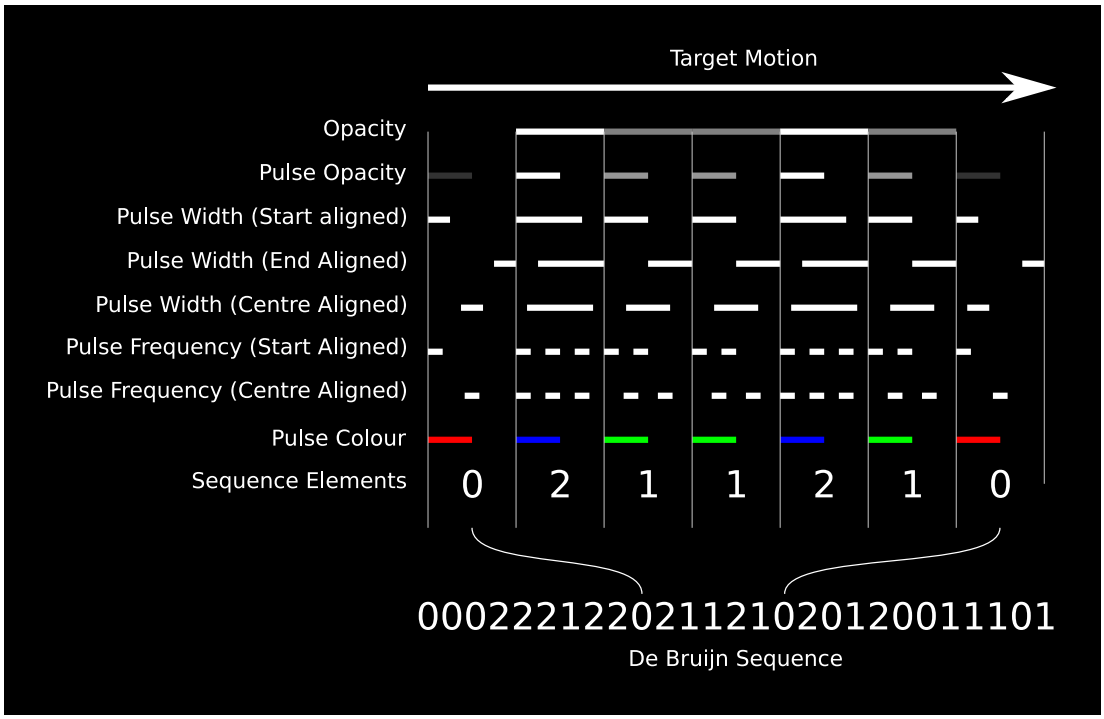


Figure 4.5: Examples of various possible encoding methods

shutter does not change state. This inconsistency can reduce the effective sampling rate for events that appear at certain times. The second problem is velocity ambiguity. If the target velocity is completely unknown, it can be impossible to distinguish the subsequences "101", "110011" and "111000111" without other visible elements or prior knowledge of target velocity because the encoded result appears identical [133].

Pulse encodings that use a dash (shutter open) and a blank (shutter closed) for every element do not suffer from these problems as features can be recognised even in the case of repeated elements. If opacity is varied this produces pulse opacity encoding (Fig. 4.5 line 2), and if pulse length is varied, this produces pulse width encoding (Fig. 4.5 lines 3–5). The pulses can be start aligned, end aligned or centre aligned depending on scenario requirements. One advantage of asymmetric pulse based encodings is that the target direction is immediately known, but periodic datapoints can also be beneficial in some cases, such as when optimising some Kalman filter implementations. Another pulse encoding option is pulse frequency, where the number of pulses per element is varied (Fig. 4.5 lines 6 & 7). Both pulse width and pulse frequency are expected provide more robust encoding than opacity based options under most conditions as varying shades of

brightness do not need to be distinguished. For applications where calculation of target brightness is desirable (such as fireball and satellite tracking) the constant integration time of the pulses in pulse frequency encoding can simplify the calculation of relative brightness over time (lightcurves).

Colour encoding (Fig. 4.5 line 8) encoding is particularly suited for encoding larger sequence alphabets which can allow longer exposures or shorter events to be recorded (see Sect. 4.4.4)—as long as a colour image sensor can be used. As with opacity encoding, pulse colour encoding should be used to avoid velocity ambiguity and inconsistent data point distribution. Illumination modulation using RGB (red green blue) or RGBW (red green blue white) LEDs (light emitting diodes) is a simple and inexpensive way to produce colour encoding. Each colour channel is driven from a separately modulated driver channel to produce the varying colours. Producing the primary colours (red, green, blue), secondary colours (cyan, magenta, yellow) and white is achieved through channel combinations, but the number of colours is only limited by the ability to distinguish them in the final image if analogue channel mixing is used.

### 4.4.4 Implementation

In order to implement de Bruijn coded exposures for a particular imaging task, the modulator operation, sequence parameters and exposure parameters should be matched to the scenario to ensure that an exposure of sufficient duration can be fully encoded and that the target motion can be decoded under all expected conditions.

The main considerations for implementation are to ensure:

- that the sequence rate $r_S$ and encoding provide trajectory data points at a sufficient rate,

- the sequence is long enough to fully encode the exposure at the chosen sequence rate,

- that $n$ is small enough that even the shortest events can be unambiguously decoded,

- the chosen modulation and encoding are able to encode $k$ different recognisable features which can be decoded under all required conditions, and

- that the timing precision is sufficient and well characterised.

### Sequence Parameters

The sequence rate $r_S$ (in elements per second) is determined by the data requirements as it is the effective sampling rate or temporal resolution. Depending on the encoding, each element will produce one or two data points (possibly more for some forms of pulse frequency encoding). These data points may or may not be periodic (depending on the encoding) but the timing of these data points is precisely known. If there is a strict requirement for periodic data, the user may choose to only use the periodic points or to use an encoding method where all data points are periodic.

In order to ensure a unique match to the observed subsequence, the de Bruijn sequence must be of sufficient length to allow the full exposure to be encoded at the required sequence rate. If the sequence is any shorter it would either end before the end of the exposure, resulting in some duration of uncoded exposure or have to be repeated which would introduce timing ambiguity as some subsequence matches would not be unique.

The maximum length of a fully encoded exposure ($t_S$) is calculated according to (4.3).

$$t_S = \frac{k^n}{r_S} \tag{4.3}$$

The minimum decodable event duration impacts the exposure length as it de-

termines $n$ for a given sequence rate $r_S$ as shown by (4.4). This parameter is often determined by the application however, so it usually cannot be arbitrarily lengthened to enable longer coded exposures.

$$t_{Min} = \frac{n}{r_S} \tag{4.4}$$

The most effective way to extend the exposure duration or reduce $t_{Min}$ is to increase $k$. This is the number of different distinguishable features that can be encoded with the chosen modulation and encoding. Colour encoding is particularly suitable where a high $k$ value is required.

Whilst the simple "prefer high" (or any other) sequence generation method should suffice for the vast majority of coded exposure applications, if extremely long sequences are used it may be beneficial to use specially constructed decodable sequences [117] which allow the position within the overall de Bruijn sequence to be determined from the observed subsequence without having to search the entire sequence.

### Imaging Scene Requirements

In traditional high frame rate imaging, high intensity lighting is required due to the short exposure lengths. As with stroboscopic photography, de Bruijn coded exposure imaging works best on a dark background with a bright target. This is because the background image is integrated onto the same pixels throughout the exposure whereas the integration of the target image is spread across a number of pixels due to the target's motion (for scenes with stationary backgrounds and moving targets). Depending on the modulation and encoding used, high intensity lighting may also be required. For example, if pulse frequency encoding was used with a liquid crystal shutter for modulation, and the pulses where the shutter is open were extremely short (e.g. millisecond order) high intensity continuous lighting would be required. A more efficient approach in this case would be to use illumination modulation. In this case the instantaneous lighting level during the short pulses would be high, but the average lighting level could be much lower.

At high frequencies this pulsing will be invisible to human observers under most conditions and only the lower average light level will be perceived.

### Hardware Implementation

Modern digital electronics are well suited to generating the control signals to drive a modulator for coded exposures. Microcontrollers (small, low power computers integrated into a single chip) excel at real time tasks and usually include peripheral subsystems to communicate with time sources and other computers (such as an embedded computer controlling the camera). For extremely high speed modulations, FPGAs (field programmable gate arrays) can also be considered, but come with increased complexity and development time.

Standard or timing specific GNSS (global navigation satellite system) modules that provide a PPS (pulse per second) or programmable frequency reference are ideally suited to provide an absolute timing source that is easily interfaced with microcontrollers or FPGAs. Standard GNSS modules are inexpensive (<\$50) and offer timing precision of approximately 20 ns on their PPS (pulse per second) output. Slightly more expensive (<\$100) specialised timing models offer lower jitter, can time stamp events and offer more flexible time pulse outputs.

Commercial-off-the-shelf cameras, lenses and computers are suitable for the remainder of the imaging system, although some modification may be required to integrate the modulation depending on the topology. Fig. 4.6 shows a block diagram of a typical implementation.

### Timing Precision

The main benefit of de Bruijn coded exposure imaging over traditional techniques such stroboscopic is the absolute timing of trajectory data. The two factors that influence absolute timing precision are the precision with which the modulator drive signals can be generated and the time response of the modulator.

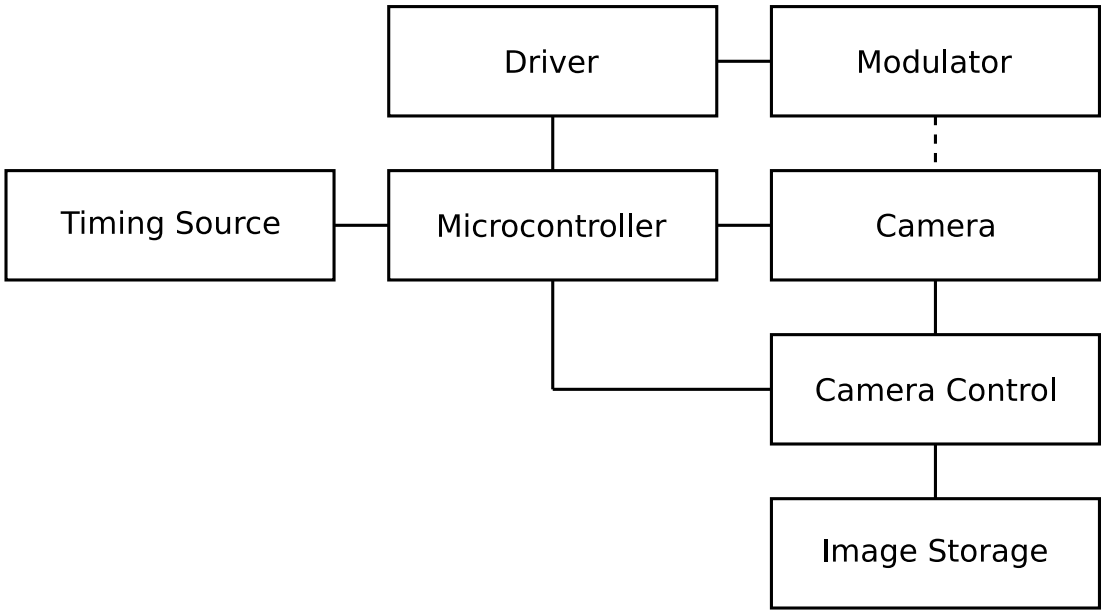


Figure 4.6: Block diagram showing the layout of a typical implementation. Optical connection between modulator and camera shown as dashed line. Camera optics and target are not shown.

Generating modulator drive signals with a jitter on the order of 100 ns can be achieved relatively easily with common 8 bit micro controllers (e.g. Atmel ATMega32U4) progammed in C by taking advantage of the built in hardware timers and interrupts. This For higher precision operation, 32 bit microcontrollers with higher clock speeds of several hundred MHz should be able to improve upon this by more than an order of magnitude.

The limiting factor in the absolute timing precision of most implementations will be the switching speed of the modulator itself. For example, the switching speeds of liquid crystal shutters can range from tens of milliseconds to tens of microseconds depending on the construction [111]. Optical modulators commonly have different switching speeds for different transitions, so—depending on the encoding method used—data points may vary in timing precision. Another factor to consider is that the timing precision will be better than the switching speed as the uncertainty is dependant on how reliably the transition can be detected in the final image not the length of time the transition takes.

## 4.5 Results

De Bruijn coded exposure imaging was implemented in two configurations. The first was using optical modulation to encode absolute timing for triangulated 3D fireball trajectories for the Desert Fireball Network observatories and the second was a proof of concept implementation to show the high spatial and temporal precision that could be achieved using inexpensive hardware and an unmodified camera under more controlled conditions. This proof of concept implementation used illumination modulation and pulse colour encoding to record target motion at 36 megapixels (MP) and 1000 samples per second.

Both configurations were implemented with an Atmel ATMega32U4 microcontroller running at 16 MHz. This 8 bit microcontroller is equipped with USB connectivity in addition to the usual array of hardware subsystems (analogue to digital converter, hardware timers, interrupts, etc.). USB connectivity is ideal in this case, as it allows the modulation controller to talk to any modern computer, from small low power embedded computers such as the Raspberry Pi all the way up to a high performance workstation. This capability is advantageous for systems that will be deployed on an ongoing basis, as the embedded computer can control the camera as well as transfer, store and analyse the resulting images.

### 4.5.1 Desert Fireball Network

The Desert Fireball Network (DFN) is a fireball camera network based in Southern Australia with the primary goals of orbit determination and meteorite recovery. The arid regions of Australia provide excellent meteorite searching terrain which allows the network to be more productive than previous networks which have not been situated in such ideal terrain. The initial phase of the DFN was conducted using four large format film based cameras before the digital expansion commenced in 2012. The de Bruijn coded exposure technique was developed in order to reduce complexity and cost of the digital fireball observatories as it removed the need for a separate absolute timing subsystem. Instead of using a rotating or switching shutter for relative timing and a radiometer for absolute timing as in previous designs [19]–[21], [31], the de Bruijn coded exposure allowed

all of the fireball data from each station to be collected in one image with a single instrument. The DFN now consists of ≈50 digital observatories covering ≈2.5 million km$^2$ (about one third of Australia—making it the largest fireball camera network) all using de Bruijn coded exposure imaging.

The DFN observatories use a stereographic fisheye lens (Samyang 8mm F3.5 Fish-eye CS II) to image nearly the entire sky in one frame with a high resolution (36 MP) Nikon D810 camera. This provides a pixel size of ≈2 arcminutes and results in astrometric precision of ≈1 arcminute (for elevations >5°). With a spacing of around 130 km between stations, this allows fireball trajectories to be triangulated to within several tens of metres [141].

The astrometric precision of the new digital observatories is similar to the four previously used film based observatories that were used during the initial phase of the DFN (also around one arcminute). The new de Bruijn coded exposure digital observatories are around one twelfth the cost of the film observatories. They are also much smaller, have much lower power requirements and a much longer service interval. More detail on the observatory hardware and the DFN in general can be found in [24].

25 second de Bruijn coded exposures are captured every 30 seconds for the entire night. The start of each image and the start of the de Bruijn sequence is aligned with the top and bottom of the UTC minute (hh:mm:00 and hh:mm:30). The fireball observatories implement optical encoding with a liquid crystal shutter (LC-Tec X-FOS LC Shutter) driven by an H-bridge (STMicroelectronics L293DD). The control signals are generated using software interrupts on the Atmel ATMega32U4 microcontroller which is syncronised with UTC time (network wide) via the GNSS modules (Telit SL869v2) with PPS outputs.

A number of encoding methods have been tested throughout the development of the digital fireball observatories. Initial results with ternary ($n = 3$) sequences and opacity encoding were unsuitable as the differing opacities were difficult to distinguish. The implementation could have been improved by adjusting the encoded opacities, but instead the move was made to binary ($n = 2$) pulse width encoding where the sequence elements are encoded as short and long dashes.

Table 4.1: DFN de Bruijn Coded Exposure Parameters—Pulse Width Encoding

| **Parameter** | **value or description** |
|---|---|
| Layout | optical modulation, between lens and sensor |
| Modulator | LC-Tec X-FOS TN type LC shutter |
| Sequence Construction | "prefer high" de Bruijn sequence |
| Sequence Rate $r_S$ | 10 elements per second |
| Alphabet Size $k$ | 2, binary {0, 1} |
| Subsequence Length $n$ | 9 |
| $t_{Min}$ | 0.9 s |
| $t_S$ | 52.0 linear (51.2 circular + $0.1 \times 8$) |
| Exposure Length | 25 s |
| Exposure Timing | every 30 s, xx:xx:00 and xx:xx:30 UTC |
| Deadtime | 5 s out of 30 s |
| Encoding Type | start aligned pulse width |
| $\tau_0$ | 20 ms ("0" : short dash length) |
| $\tau_1$ | 60 ms ("1" : long dash length) |

The encoding uses 20 and 60 ms pulses (for "0" and "1" elements respectively) where the starts are aligned with the tenths of each second (xx.x0 s). Pulse width encoding produced acceptable results and has been used for two successful meteorite recoveries using digital observatory data to date. Table 4.1 shows the sequence and encoding parameters of the DFN pulse width encoding. The top trace in Fig. 4.8 shows the operation of the LC shutter over time with pulse width encoding.

Extracting the start and end datapoints from dashes in pulse width encoded fireball images (see Fig. 4.2) was difficult due to optical aberrations introduced by substandard optics, and this impacted the quality (spatial precision) of the ob-

servations. In particular, this affected the velocity data which is critical to the accuracy of the orbit and mass estimation (which is required to find resulting meteorites. Another drawback of the pulse width encoding was that the integration time of each dash was unequal which made the calculation of fireball lightcurves more complicated.

As a solution to these problems, pulse frequency encoding with a constant integration time per-pulse was trialled. Instead of using long and short pulses to encode sequence, the pulse frequency encoding used single and double pulses. The implementation encodes a "0" as a single 10 ms pulse, and a "1" as two 10 ms pulses. The first pulse of each element is centre aligned on every tenth of a second (xx.x0 s) and the second pulse (if present) appears halfway between the first pulse of that element and the next element (centre aligned at xx.x5 s). The pulses used are significantly shorter than those used in pulse width encoding, so only one data point is extracted per pulse (instead of two); however, this midpoint can be determined with better spatial precision than the end points. A pulse frequency encoded fireball image is shown in Fig. 4.7, and the operation of the LC shutter over time with pulse frequency encoding is shown in the second trace of Fig. 4.8. Fireball observations have shown that this encoding method produces significantly improved velocity data over the pulse width encoding; recently, all online fireball observatories have been moved over to pulse frequency encoding.

**Timing Precison**

To verify correct operation of the exposure coding, the transmittance of the shutter over time was recorded with a 100 MHz digital oscilloscope. The times listed above in the encoding parameters are nominal, some amount of delay is added systematically to these times by the operation of the microcontroller, shutter driver and wiring and some random jitter is also introduced (mostly by the operation of the microcontroller). These delays and jitter were measured electrically using the oscilloscope and optically using a phototransistor with a time response of $\approx$10 $\mu$s. The measurements were taken relative to the PPS signal syncronsising the operation of the microcontroller which is specified to be accurate to within 20 ns.

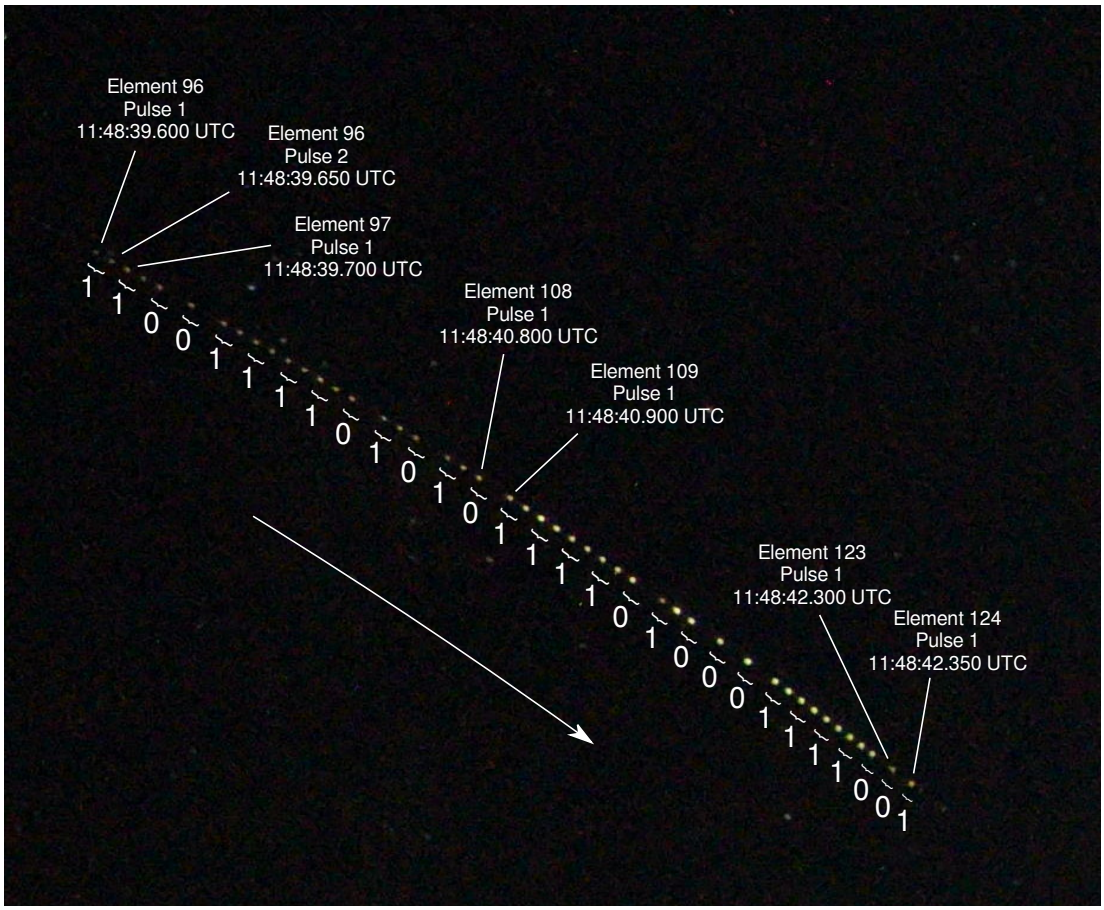


Figure 4.7: DN161103_01 fireball observed by the Yealering station with pulse frequency encoding on 3 November 2016

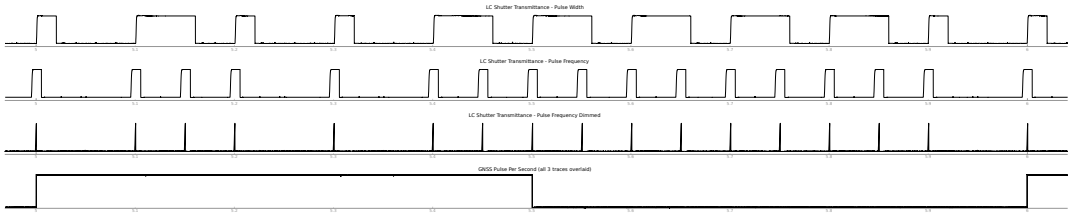

Figure 4.8: Timing verification data for DFN observatories showing shutter opacity timing and alignment with the GNSS PPS timing signal. Row 1: standard DFN pulse with modulation at 10 elements per second. Row 2: newer pulse frequency encoding (deployed on a smaller scale). Row 3: experimental dimmed pulse frequency mode operation for extremely bright fireballs. Row 4: GNNS Pulse Per Second output, rising on the second (overlaid for all three of the above modes). The standard DFN "prefer high" de Bruijn sequence $B(k = 2, n = 9)$ was used. The elements from 5.0-6.0 s (inclusive) shown above are "01001111100".

The delay from the PPS signal to start of the optical transition of the LC shutter was 9±3 microseconds (measured with the phototransistor). Due to the time response of the LC shutter and phototransistor, the inflection point was difficult

to observe, so measurements of the LC shutter drive waveforms were also taken. These account for the delay due to the microcontroller, firmware, drive circuit and wiring, but not the time response of the liquid crystal's phase transition. This delay was 6.3±0.1 $\mu$s. The jitter or variability in this delay is 0.1 $\mu$s and equates to around 2 clock cycles of the microcontroller (exceeding the DFN's timing precision requirements by orders of magnitude).

The transitions of the LC shutter were also examined. The shutter's closing time (95%-05%) is 46±2 microseconds as the electric field is applied; the opening time as the liquid crystal relaxes into its low energy state is slower at around 980±50 $\mu$s. (Measurements were taken at 12V, 22°C.)

More conservative switching times specified by the manufacturer (100 and 1300 $\mu$s closing and opening times respectively) are used when factoring the impact of switching speed into the DFN's data processing pipeline. The DFN records fireball tajectory data with sub-millisecond timing precision [24], [133].

### Evolution of the Implementation

The dead time between exposures of five seconds is due to the limited shutter speed options available in the Nikon DSLR. A 25 second exposure is used to make the 30 second exposure cadence possible. DSLRs do also offer a shutter speed of custom length (referred to as "bulb mode") that can be controlled through the shutter button or remote port (which is wired to the microcontroller in our implementation). The DFN attempted to move to bulb mode which required modification of the camera settings, microcontroller firmware and gphoto capture control code. Whilst the changes did allow the deadtime to be reduced, the new configuration did not prove to be reliable and the operation had to be reverted to 25 second exposures.

The DFN revised the observatory hardware design in late 2016 to improve the service interval and reliability, as part of this redesign the LC shutter supply voltage was changed from the battery supply voltage to the regulated output of a small boost converter. This increased the contrast between the on and off states

and also made the operation of the LC shutter independent of the battery's state of charge. The main benefit of the increased contrast is seen in observations of extremely bright fireballs; bright fireballs can be as bright or even brighter than the sun. Minimising light leakage in the off state is important in these cases to ensure that the encoding does not break down as the trail of dashes or dots turns into one big streak. A firmware change was also made to allow the microcontroller to drive the LC shutter in a dimmed mode where the pulse duration in the pulse frequency mode is reduced from 10 ms to around 1 ms to reduce the total exposure. Testing with light sources in the laboratory indicates that this will improve observations of bright events significantly, but more work on real time event detection based on the built in low resolution digital video camera is required in order to use this feature in practice. The shutter transmittance waveform of this experimental "dimmed mode" operation is visible as the third trace in Fig. 4.8.

### Meteorite Recoveries

De Bruijn coded exposures have been used to record over 1000 DFN fireball events triangulated from two or more cameras with spatial precision of ≈1 arcminute and submillisecond timing precision. The Australian network covers about 2.5 million square kilometres consisting of approximately 50 camera observatories.

The DFN's first recovery using the new digital network (and third recovery with an orbit overall) was the Murrili meteorite [121] in December 2015. The second digital recovery, the Dingle Dell meteorite [142], was recovered in November 2016 within a week of its fall. The relative timing for trajectory analysis and the absolute timing for orbit determination were recorded using de Bruijn coded exposure imaging for both events.

This result is significant due to the rarity of meteorites with known orbits; out of the ≈60,000 meteorites in collections worldwide, only 32 have known pre-atmospheric entry orbits (as of December 2016)[12].

### 4.5.2 Proof of Concept Pulse Colour Encoding

An alternate proof of concept implementation using colour illumination modulation was developed to demonstrate the potential of the de Bruijn coded exposure technique under more controlled conditions. The configuration was designed to replicate an industrial imaging task where a target would be tracked at high speed with high spatial and temporal resolution and precision.

Colour illumination modulation was selected as it would allow a higher $k$ value to be achieved easily, a simple implementation and for the camera and optics to remain unmodified. To increase the signal to noise ratio in the resulting images and therefore allow very short duration pulses for the colour encoding, retroreflective tape was used as the target. Short duration pulses were used to achieve a high sampling rate (increasing the temporal resolution) and reduce blurring (enhancing spatial precision). A custom multichannel LED (light emitting diode) ring light source was constructed and placed around the imaging lens to maximise the target signal, and a matte black background was used to minimise the background level.

The same Atmel ATMega32U4 microcontroller as used in the DFN observatories was used to produce the encoding for the high spatial and temporal resolution proof of concept implementation. This drove four channel CREE XLamp XM-L RGBW LEDs using four Recom Power RCD-24-1.0 constant current drivers. This simple and inexpensive combination was able to produce pulse encoding reliably up to about 1000 Hz. The imaging system was a 36 MP Sony A7R combined with a Canon 100mm f/2.8L IS USM lens. This gave the system a temporal resolution of 1 ms and pixel size of approximately 0.16 arcminutes per pixel (although this can easily be varied by changing imaging lens). A crop of one of the resulting images at 36 MP and 1000 Hz is shown in Fig. 4.9.

As this system was built only to demonstrate the high spatial and temporal resolution that could be achieved with a few hundred dollars worth of electronic components and an off the shelf imaging system and not to produce actual science data, the operation of the system was not extensively characterised, but the sequence rate of 1000 elements per second and the correct de Bruijn sequence op-

eration of the illumination modulation were verified. Testing was conducted using other encoding methods including pulse width encoding (Fig. 4.10); but pulse colour produced far superior results (in terms of minimising $t_{\min}$ and maximising $t_{\mathrm{S}}$) as $k$ can be much higher with pulse colour encoding. White, red, green, blue, yellow, cyan and magenta ($k = 7$) illumination was produced with combinations of the four (red, green, blue and white) drive channels of the RGBW LEDs. The short pulses used for the colour encoding also give better results here where the target is resolved; pulse width encoding is more suitable for unresolved distant point sources such as fireballs or small retroreflectors at a distance.

Recording trajectory data with similar temporal and spatial resolution using traditional imaging techniques would require multiple high speed 4k cameras costing on the order of $100,000 each (e.g. Phantom Flex4k) and producing over ten gigabytes of data per second. The cost of the de Bruijn coded exposure solution is a few hundred dollars in electronic components plus the cost of an off the shelf imaging solution (≈$3000 in this case). To implement 3D tracking with this configuration an additional camera and illumination module could be added. The same controller could be used to control the LEDs for short triangulation baselines, or separate but synchronised controllers could be used for longer baselines (as in the DFN).

## 4.6 Discussion

De Bruijn coded exposures can solve the high data bandwidth problem for some tracking tasks and avoid the associated complexity and expense that comes with it. The technique has been proven in production usage collecting science data for the DFN, and a proof of concept implementation showing the high temporal and spatial precision that can be achieved under more controlled conditions.

It has already been shown that encoding trajectory data with absolute timing data in one image can be beneficial for some applications. However, another use of of de Bruijn coded exposure imaging is the ability to get relative timing even in the case where moving targets stop (or slow dramatically) before resuming motion. If stroboscopic photography were used, it would not be possible to determine the

duration of the stop as the pulses would overlap for this duration making counting them difficult or impossible. In this case where motion stops and resumes, the timing of both moving segments (and therefore the intervening pause) can be determined as long as each moving segment (where the encoded features can be clearly read) is at least as long as the minimum event time $t_{\mathrm{Min}}$. An example of this is shown as a target changes direction in Fig. 4.10.

The timing precision of the DFN fireball observatories exceeds the precision required for accurate orbit determination, but enables two other unique capabilities. Firstly, the operation of the timecode is not only precise, but it is also synchronised across the network by the GNSS receiver modules. This means that the data points visible in images are aligned in time. Making independent triangulation of each point from all observing cameras possible. This is in contrast to the traditional meteor triangulation techniques [40], [42], [43] used by others which assume a straight line trajectory. This may allow better fitting of long fireballs where trajectory curvature may become observable. Secondly, multi sensor integration is greatly simplified with accurate absolute timing encoded directly into the photographic data. (Additional data sources including meteor radar, radiometers [54], video imagery and Doppler radar [49], [61] can assist with orbit calculation, confirmation of a meteoroid surviving the ablation process and meteorite recovery.)

**Limitations** The two main limitations of this temporal super-resolution technique are the need for substantial target motion relative to the target or marker size and the need for a dark background relative to the target. Other long exposure and stroboscopic techniques also have these limitations in common. In the case where it is not possible to darken the background relative to the target through optical techniques (e.g. controlled lighting or narrow band filters) or multiple modulation points a high speed video based solution may be more appropriate. Video observations are also more appropriate if trajectory data is required for targets without sufficient motion where the sequence rate would have to be lowered unacceptably to generate visible motion in the resulting images.

**Future Work** Going forward, effort will be focussed on optimising the encoding used for the Desert Fireball Network data and quantifying the improvement in velocity data realised by the move to pulse frequency modulation.

Currently fireball data points are extracted manually from images with a custom software tool that allows fast entry and automates the recording of times. Automation of this step through is planned in the future. Extremely bright and obscured fireball events are unlikely to ever be decoded automatically, and potential meteorite droppers will always be manually checked before searching expeditions are organised, but automated image processing should be able to handle the majority of fireball events detected.

Further investigations could also include application to more complicated targets, multiple targets and targets undergoing more complex motion. Real time adjustment of the sequence parameters and encoding could improve results for targets that vary their velocities greatly. This could be tackled using a low resolution real time video system in conjunction with a high resolution coded exposure photographic system. Different encodings built upon more advanced modulation techniques could also be tested including continuous analogue control of the optical modulation. De Bruijn time encoding may also be useful in other sensing applications such as RADAR and time-of-flight imaging.

**Other Possible Applications** Outside of planetary science, de Bruijn coded exposure imaging could be useful in a few areas. The first of these possible applications is particle image velocimetry (PIV). PIV is used to measure and visualise fluid flows using suspended particles. This normally uses one double exposure or two images captured in quick succession. De Bruijn coded exposures could allow longer captures without increasing the data bandwidth. This may allow higher temporal and spatial resolution observations of longer time scale effects such as oscillating airfoil wakes than would be possible using traditional PIV approaches. The method may also be useful for tracking objects moving at high speed in high speed automated production lines. In these situations the technique is probably better suited to passive data collection for applications such as preventative maintenance data collection or performance characterisation than

real time control. Another possible application could be in space surveillance and tracking; although long exposure imaging is usually used as the accelerations of objects and debris can be well modelled, there could be some use to have longer exposures with periodic breaks and absolute timing.

## 4.7 Summary

De Bruijn coded exposure imaging provides a temporal super resolution method circumventing traditional data bandwidth requirements when tracking targets in motion. This is achieved by modulating a single exposure over time according to a de Bruijn sequence and a chosen encoding method. Once the $n$ features in the long exposure image are recognised they can be uniquely matched to a particular point in the de Bruin sequence providing absolute timing for the trajectory data. The use of de Bruijn sequences ensures that the subsequence that can be matched is optimally short which allows fleeting and sporadic events to be observed with absolute timing. The technique can be implemented using common electronic components and is capable of high timing precision even with inexpensive components.

The method has been demonstrated in two implementations. The Desert Fireball Network uses de Bruijn coded imaging to observe fireballs with sub-millisecond timing precision without the use of a separate timing subsystem. The technique has been used to record over 1000 fireball trajectories and calculate the corresponding orbits as well as the recovery of two meteorites with orbits. The second implementation was a proof of concept demonstration of high temporal and spatial resolution tracking capabilities (36 MP at 1000 Hz) that are possible at a very low cost in a more controlled environment. This implementation used illumination modulation and only cost a few hundred dollars in addition to a standard off-the-shelf camera and optics.

The technique has proven its worth through the extremely valuable scientific data that has been collected by the Desert Fireball Network. It could possibly be applied to other problems including particle image velocimetry, object tracking in automated production lines and space surveillance and tracking. Further exten-

sions of the technique could focus on real time adjustment of the sequence rate and encoding to allow more consistent tracking of targets with greatly varying velocities or application of de Bruijn coding to non imaging instruments.

# References


[12] M. Meier, "Meteoriteorbits. info-Tracking All Known Meteorites with Photographic Orbits," in *Lunar and Planetary Science Conference*, vol. 48, 2017.

[19] Z. Ceplecha and J. Rajchl, "Programme of fireball photography in Czechoslovakia," *Bulletin of the Astronomical Institutes of Czechoslovakia*, vol. 16, p. 15, 1965.

[20] R. E. McCrosky and J. H. Boeschenstein, "The Prairie Meteorite Network," *Optical Engineering*, vol. 3, no. 4, pp. 304 127–304127–, 1965.

[21] I. Halliday, A. Blackwell, and A. Griffin, "The Innisfree meteorite and the Canadian camera network," *Journal of the Royal Astronomical Society of Canada*, vol. 72, pp. 15–39, 1978.

[24] R. M. Howie, J. Paxman, P. A. Bland, M. C. Towner, M. Cupak, E. K. Sansom, and H. A. R. Devillepoix, "How to build a continental scale fireball camera network," *Experimental Astronomy*, vol. 43, no. 3, pp. 237–266, 2017. DOI: 10.1007/s10686-017-9532-7. [Online]. Available: https://doi.org/10.1007%2Fs10686-017-9532-7.

[31] P. Bland, P. Spurný, A. Bevan, K. Howard, M. Towner, G. Benedix, R. Greenwood, L. Shrbený, I. Franchi, G. Deacon, *et al.*, "The Australian Desert Fireball Network: a new era for planetary science," *Australian Journal of Earth Sciences*, vol. 59, no. 2, pp. 177–187, 2012.

[40] Z. Ceplecha, "Geometric, dynamic, orbital and photometric data on meteoroids from photographic fireball networks," *Bulletin of the Astronomical Institutes of Czechoslovakia*, vol. 38, pp. 222–234, 1987.

[42] J. Borovička, "The comparison of two methods of determining meteor trajectories from photographs," *Bulletin of the Astronomical Institutes of Czechoslovakia*, vol. 41, pp. 391–396, 1990.

[43] P. S. Gural, "A new method of meteor trajectory determination applied to multiple unsynchronized video cameras," *Meteoritics & Planetary Science*, vol. 47, no. 9, pp. 1405–1418, 2012.

[49] M. Fries and J. Fries, "Doppler weather radar as a meteorite recovery tool," *Meteoritics & Planetary Science*, vol. 45, no. 9, pp. 1476–1487, 2010.

[54] Z. Ceplecha and D. O. Revelle, "Fragmentation model of meteoroid motion, mass loss, and radiation in the atmosphere," *Meteoritics & Planetary Science*, vol. 40, no. 1, pp. 35–54, 2005.

[61] P. Jenniskens, M. D. Fries, Q.-Z. Yin, M. Zolensky, A. N. Krot, S. A. Sandford, D. Sears, R. Beauford, D. S. Ebel, J. M. Friedrich, *et al.*, "Radar-enabled recovery of the Sutter's Mill meteorite, a carbonaceous chondrite regolith breccia," *Science*, vol. 338, no. 6114, pp. 1583–1587, 2012.

[104] Z. Ceplecha, "Photographic Geminids 1955," *Bulletin of the Astronomical Institutes of Czechoslovakia*, vol. 8, p. 51, 1957.

[105] C. Flye-Sainte Marie, "Solution to problem number 48," *L'Intermédiaire des Mathématiciens*, vol. 1, pp. 107–110, 1894.

[106] N. G. de Bruijn and P. Erdős, "A combinatorial problem," *Koninklijke Nederlandse Akademie v. Wetenschappen*, vol. 49, no. 49, pp. 758–764, 1946.

[111] LC-Tec, *Fast Optical Shutter Series*. Jan. 2013. [Online]. Available: `http://www.lc-tec.se/products/fast-optical-shutters/`.

[115] T. van Aardenne-Ehrenfest and N. G. de Bruijn, "Circuits and trees in oriented linear graphs," *Simon Stevin: Wis-en Natuurkundig Tijdschrift*, vol. 28, p. 203, 1951.

[116] H. Fredricksen, "A survey of full length nonlinear shift register cycle algorithms," *SIAM review*, vol. 24, no. 2, pp. 195–221, 1982.

[117] C. J. Mitchell, T. Etzion, and K. G. Paterson, "A method for constructing decodable de Bruijn sequences," *Information Theory, IEEE Transactions on*, vol. 42, no. 5, pp. 1472–1478, 1996.

[121] P. A. Bland, M. C. Towner, E. K. Sansom, H. A. R. Devillepoix, R. M. Howie, J. P. Paxman, M. Cupak, G. K. Benedix, M. A. Cox, T. Jansen-Sturgeon, D. Stuart, and D. Strangway, "Fall and Recovery of the Murrili Meteorite, and an Update on the Desert Fireball Network (abstract #6265)," *Meteoritics & Planetary Science*, vol. 51, no. S1, A144–A692, 2016, ISSN: 1945-5100. DOI: `10.1111/maps.12704`. [Online]. Available: `http://dx.doi.org/10.1111/maps.12704`.

[133] R. M. Howie, J. Paxman, P. A. Bland, M. C. Towner, E. K. Sansom, and H. A. R. Devillepoix, "Submillisecond fireball timing using de Bruijn timecodes," *Meteoritics & Planetary Science*, vol. 52, no. 8, pp. 1669–1682, 2017, ISSN: 1945-5100. DOI: 10.1111/maps.12878. [Online]. Available: http://dx.doi.org/10.1111/maps.12878.

[136] Y. Hitomi, J. Gu, M. Gupta, T. Mitsunaga, and S. K. Nayar, "Video from a single coded exposure photograph using a learned over-complete dictionary," in *Computer Vision (ICCV), 2011 IEEE International Conference on*, IEEE, 2011, pp. 287–294.

[137] F. C. Bettonvil, "Remote and automatic small-scale observatories: experience with an all-sky fireball patrol camera," in *SPIE Astronomical Telescopes+ Instrumentation*, International Society for Optics and Photonics, 2014, 91473U–91473U.

[138] F. Rigaud, I. Jegouzo, J. Gaudemard, and J. Vaubaillon, "Control and protection of outdoor embedded camera for astronomy," in *SPIE Astronomical Telescopes+ Instrumentation*, International Society for Optics and Photonics, 2012, 84462S–84462S.

[139] R. Raskar, A. Agrawal, and J. Tumblin, "Coded Exposure Photography: Motion Deblurring Using Fluttered Shutter," *ACM Trans. Graph.*, vol. 25, no. 3, pp. 795–804, Jul. 2006, ISSN: 0730-0301. DOI: 10.1145/1141911.1141957. [Online]. Available: http://doi.acm.org/10.1145/1141911.1141957.

[140] P. Llull, X. Liao, X. Yuan, J. Yang, D. Kittle, L. Carin, G. Sapiro, and D. J. Brady, "Coded aperture compressive temporal imaging," *Optics express*, vol. 21, no. 9, pp. 10 526–10 545, 2013.

[141] H. A. Devillepoix, E. K. Sansom, P. A. Bland, M. C. Towner, M. Cupák, R. M. Howie, T. Jansen-Sturgeon, M. A. Cox, B. A. Hartig, G. K. Benedix, *et al.*, "The Dingle Dell meteorite: A Halloween treat from the Main Belt," *Meteoritics & Planetary Science*, vol. 53, no. 10, pp. 2212–2227, DOI: 10.1111/maps.13142. eprint: https://onlinelibrary.wiley.com/doi/pdf/10.1111/maps.13142. [Online]. Available: https://onlinelibrary.wiley.com/doi/abs/10.1111/maps.13142.

[142] Meteoritical Society, *Dingle Dell*, 2017. [Online]. Available: http://www.lpi.usra.edu/meteor/metbull.php?code=62546 (visited on 11/21/2016).

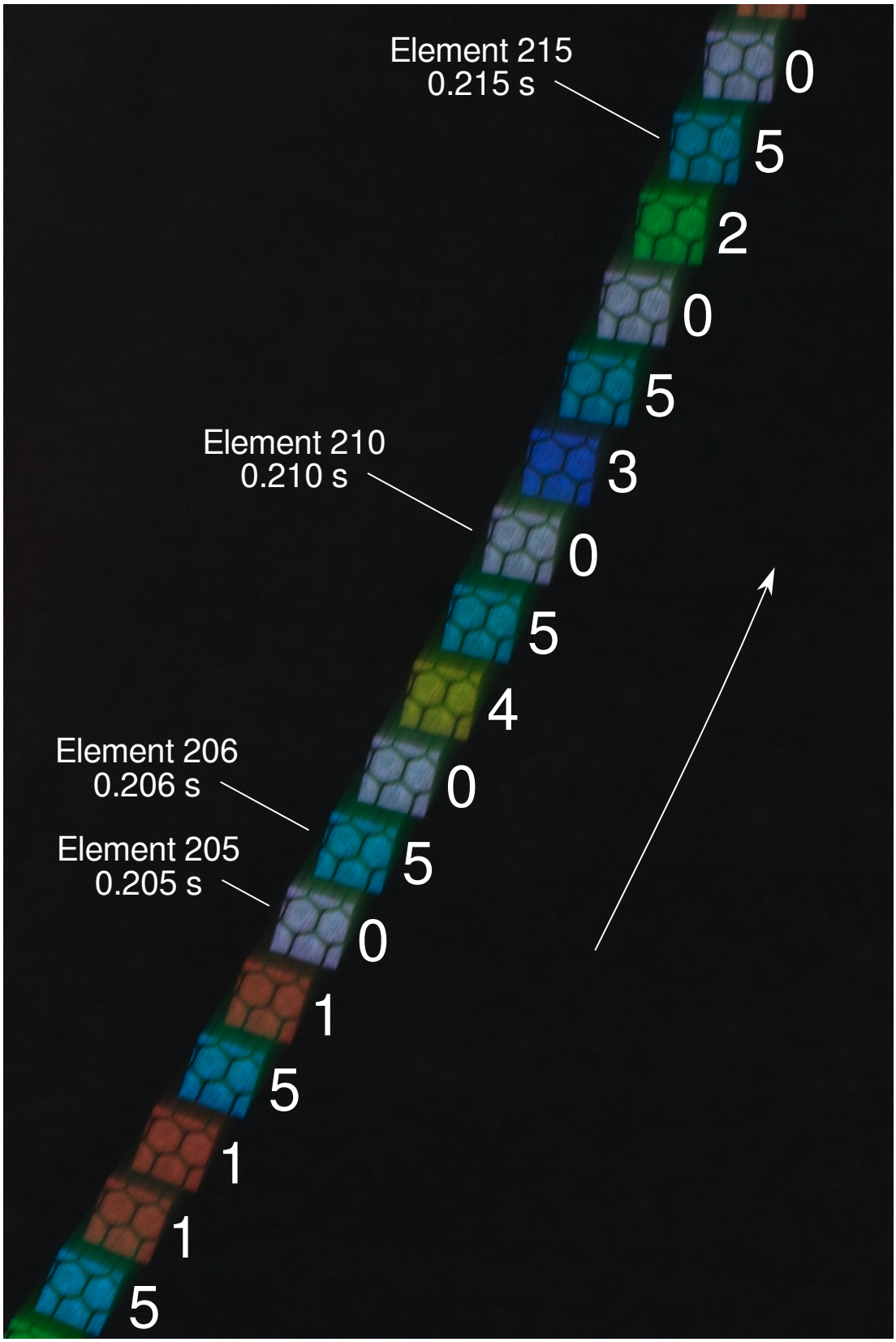


Figure 4.9: Proof of concept pulse colour operation at 1000 Hz using on-axis RGBW LEDs to illuminate retro reflective target. The hexagonal pattern of the retroreflective tape is clearly visible.

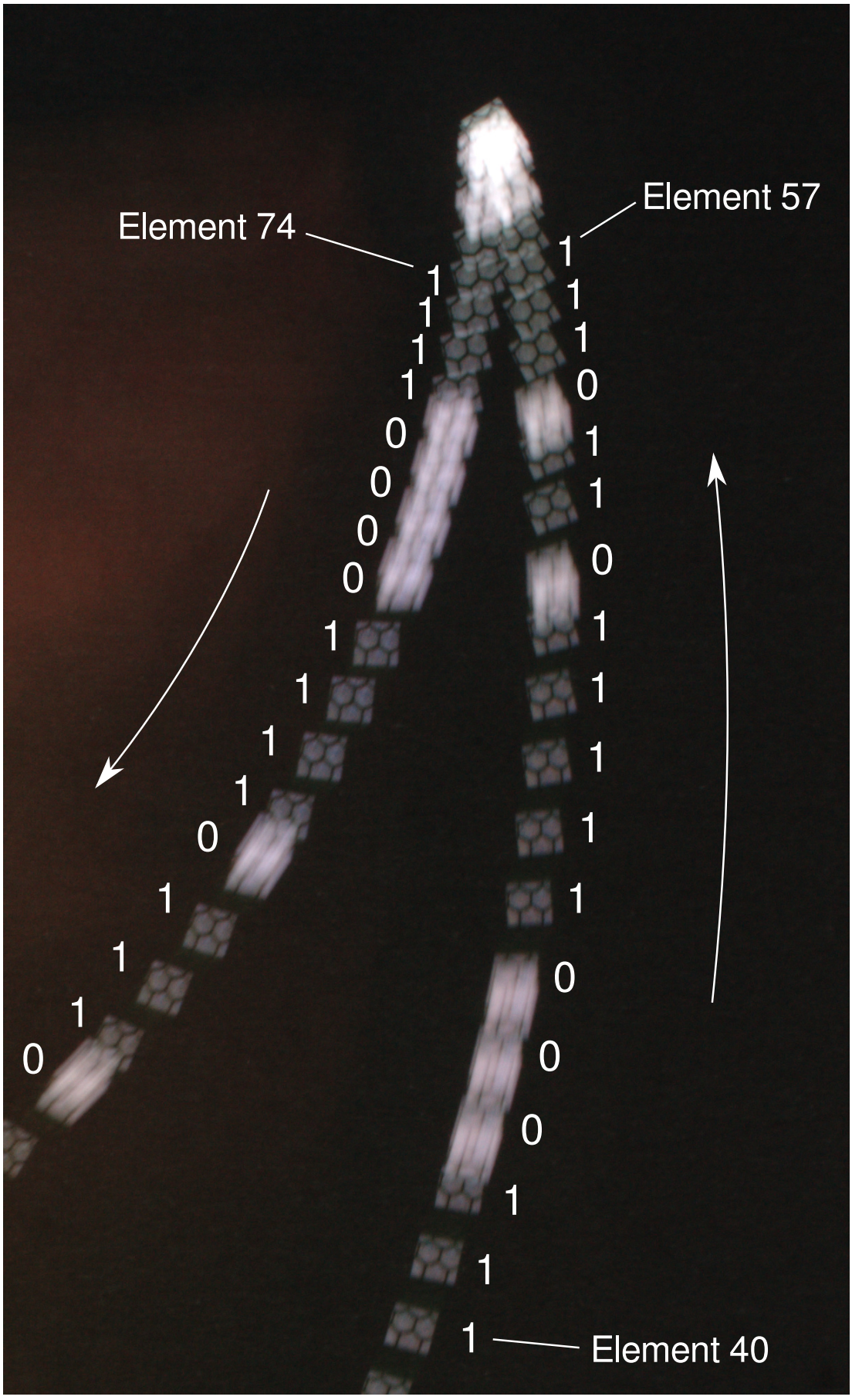


Figure 4.10: Pulse width modulated illumination modulation showing how separate segments can be independently decoded between pauses in motion or changes in direction. Pulse width encoding at 500 Hz, 0:long pulse, 1:short pulse.

# Chapter 5

# Development of the Desert Fireball Observatories

An iterative design approach was used to develop the DFN's new digital observatories which are now operating at 49 sites across Australia and being deployed to the United States, United Kingdom, Morocco, Canada, France, and Saudi Arabia. The concept was refined via early and frequent prototyping to produce the first production design which resulted in the manufacture of ≈60 observatories. These systems enabled the DFN's digital expansion to more than 2.5 million km$^2$ of triangulable area within Australia alone (around one third of Australia and 1.7 percent of the Earth's land surface area). This chapter covers the development and evolution of the observatory design.

## 5.1 Motivation

The core goal of the DFN's expansion was to increase the meteorite recovery rate by expanding the network coverage area using more affordable digital fireball observatories in place of the existing large format film observatories. The initial coverage goal for the DFN's digital expansion was 1 million km$^2$[31].

## 5.2 Concept Design

The decision to build the digital Desert Fireball Network around consumer off-the-shelf hardware was made once it became clear that it was possible to reach similar spatial precision as the previous film cameras (≈1 arcminute) using a consumer camera coupled with a fish-eye lens.

Whilst the resolution of the digital camera would be significantly lower than that of the large format 6 by 9 cm Ilford FP4 film used in the film cameras [22], the astrometric precision of digital cameras is not limited by film scanning, development and scanning techniques (film is not dimensionally stable due to the polymer film base) and the night long star trails. As digital camera sensors are dimensionally stable and shorter exposures can be used used, it is able to reach similar spatial precision with digital cameras even though they have much lower spatial resolution than large format film.

During the concept design phase, chopped long exposure operation (similar to the film cameras) was selected instead of triggered high frame rate imaging to eliminate the risk of missing fireballs due to problems detecting fireball events and shutter wear issues. Electro-optic modulation was selected instead of mechanical modulation due to the high cost and potential reliability problems associated with the latter option.

The concept design for the digital fireball observatory was a computer controlled long exposure fireball camera using a consumer digital camera and consumer fish-eye lens for all sky coverage. An electro-optic modulator was to be used to chop the exposure for velocity determination, and commodity hard disk drives were to be used for image storage. In order to keep costs low, the observatory would be constructed using as many consumer off-the-shelf components as possible.

## 5.3 Design Influence from the Previous Film-based Observatories

The DFN film cameras were modified versions of the Czech automated design[22], [38] used as part of the European network. These were developed from the manual Czechoslovak designs developed over the latter half of the twentieth century and retained the same imaging components. The observatories built and refined throughout this long legacy captured fireball trajectories with sufficient spatial precision for multiple meteorite recoveries in Europe and Australia. The strengths and weaknesses of these observatories informed the design of the DFN's own digital observatories. The aspects retained from the previous designs include—

- high spatial precision (≈1 arcminute),
- limiting magnitude of -2.5,
- an all-sky imaging configuration,
- untriggered long exposure operation,
- "chopped" exposures for meteoroid velocity determination,
- solar photo-voltaic (PV) power system with lead-acid battery storage,
- fireball event detection capability and
- network connectivity allowing real time updates and maintenance.

Spatial precision of approximately one arcminute is sufficient to triangulate fireballs during bright flight to within tens of metres (150 km station spacing, 30 km fireball height, favourable geometry). This precision in bright flight is sufficient for meteorite recovery as shown by the Bunburra Rockhole [34], [38] and Mason Gulley [79] meteorites. Exceeding this precision has little benefit in terms of search area size due to the uncertainty in mass estimations and wind data used for dark flight modelling. This spatial precision can be achieved with a single all-sky fisheye lens on a modern consumer digital camera and ≈150 km station spacing. A single all sky lens with a high resolution sensor was selected for the digital systems instead of a multi camera systems to reduce system complexity

and maintenance demands.

Similar spatial precision can also be achieved at lower altitudes (≈20 km where meteorite dropping fireballs often terminate) with more numerous and closely spaced lower resolution cameras; this approach may be useful in areas where localised inclement weather is likely to obstruct observations regularly, and is the approach taken by the French video network FRIPON with numerous 1.2 megapixel video cameras[85]. However, it is not possible to achieve the same precision at higher altitudes (for orbit determination) with this approach due to the increased (vertical) distance between the fireball and observatory. This type of network is also impractical for the DFN due to the huge coverage goals; too much time would be spent servicing (or more accurately, driving to) the hundreds of cameras required. Conveniently, observatory spacing of ≈130-150 aligns well with the spacing of pastoral stations throughout much of the Australian Outback (many of which have generously volunteered to host observatories).

The film systems recorded one long exposure per night under clear conditions and had a limiting magnitude of -2.5 [38]. Untriggered operation which retains all images whether or not they contain events is inherently less risky than triggered operation which relies on working fireball event detection to recognise fireballs quickly and reliably before initiating image capture. Triggered operation of the new digital observatories using consumer sports cameras was briefly investigated, but quickly abandoned due to the aforementioned risk and the difficulty in capturing the beginning of the fireball's trajectory. Triggered operation is better suited to continuously operating video based systems, where the decision is made to retain or delete the data once it has been fully analysed, not whether to capture it or not. Untriggered long exposure operation also allows the collection of a long term night sky dataset from multiple geographically distinct locations for astronomy and atmospheric science, and permits the use of higher spatial resolution (but slower) consumer studio and landscape oriented cameras. As the low light performance of modern digital cameras is superior to film, there were no sensitivity concerns given that film based observatories had produced successful recoveries in the past with a limiting magnitude of -2.5.

Long exposure operation where images are tens of seconds in length requires some

method to determine relative and absolute timing. Relative timing to derive velocity is essential for determining orbits, constraining final masses through trajectory analysis and calculating probably dark flight trajectories after meteoroids cease ablation and are no longer visible to the camera network, and absolute timing is required to account for the Earth's orbital motion and rotation. The film systems used a mechanical rotating shutter to regularly break the recorded fireball trail. A similar system was selected for the DFN's digital observatories, but was to be implemented with a solid state electro-optic modulator (along with some changes to also encode absolute timing as described in chapter 2).

Many remote sites in the Australian outback do not have grid power available. As the DFN sites are inland, solar photovoltaic (PV) power is more consistent than wind generation. The film observatories used solar PV with lead acid batteries and this approach was retained for the digital observatories. For future installations outside of Australia in places such as Northern Canada and the Antarctic, wind generation may be more appropriate.

Fireball camera networks present the opportunity to recover meteorites with reduced terrestrial contamination as samples can be recovered more quickly than casually observed falls (and much faster than finds which could have been lying on the Earth's surface for tens of thousands of years [64]). This opportunity is wasted if events are not detected until regularly scheduled data collection (film or hard disk drive exchanges) which could result in delays of several months. The film observatories used radiometer based event detection [22] to detect bright fireball events and email notifications were made via the camera's internet connection (Ethernet or mobile data in Europe and satellite in Australia). The plan for the digital observatories was to retain the capability of event detection, but to implement it via automated analysis of the digital images.

The same network connectivity used for event notifications on the film cameras also permitted the camera status to be monitored remotely as well as permitting some limited remote maintenance. This allowed some problems to be rectified remotely reducing maintenance costs as well as increasing network uptime. Even where problems cannot be resolved remotely, maintenance trips can be planned more effectively with the available diagnostic information. The digital observa-

tories would retain this remote maintenance functionality for the same reasons.

Despite the overall success of the film based observatories, they had a number of shortcomings. These were the—

- high per observatory cost,
- high ongoing costs (film processing and satellite connections),
- precision mechanical components (rotating shutter, film handling system),
- high power usage of the camera and satellite modem,
- complexity associated with the 240 V inverter and
- dependence on external suppliers for maintenance and repairs.

The film observatories were costly (approximately £100,000 in the early 2000's), which limited size of the network. A significantly lower per station cost was one of the major goals of the digital design. The ongoing costs of the film based systems were also high (several thousands of dollars per month for four systems) due to the costs of film processing and the satellite data connections. No film processing would be required for the new digital camera systems, and the continued rollout of the Telstra 3G mobile network in regional areas meant that the previous sites could now be serviced with inexpensive mobile data connections. Specifically, the installation of mobile service along the India Pacific rail route was key, as the Nullarbor was the first (and most remote) region of the digital DFN deployed. This is the reason that many of the new cameras are situated close to the Trans-Australian Railway (see Fig. 3.12).

The film cameras possessed a number of precision mechanical components that were integral to the operation of the observatory. These types of components are expensive to manufacture due to the tight tolerances and are prone to failure when exposed to dust, dirt and sand—which are abundant in the Australian Outback. The internal components of the film cameras were not vulnerable during normal operation due to the well sealed exterior housing, but many maintenance tasks could not be carried out in *in situ* as the risk of contaminating the internal mechanisms was too high. The task of transporting the 120 kg observatory

to a suitable location for servicing at these remote sites was difficult and time consuming.

The weather sealing of the film observatories relied on retractable lens covers which added two points of complexity. The observatories had to be equipped with rain sensors so the covers could be retracted in inclement weather, and a built in uninterrupted power supply (UPS) was required to ensure that the covers and heat shield could be returned to their storage positions in case of a power failure. Both of these subsystems were potential points of failure in the previous design, if either were to fail the system could be rendered inoperable or possibly damaged if the lens covers failed in the open position. In order to reduce the probability of failure in the new digital systems, the aim was to eliminate moving parts from the design wherever possible.

The film systems consumed a considerable amount of power, requiring eighteen 80 W PV panels. A large portion of this power was required by the the satellite modem, but the system was originally designed for mains powered operation (hence the built in UPS), so power consumption was probably not as high a priority as it would have been if the system had been designed for off grid use from the start. Low power consumption was another design objective of the new digital system, and they would be designed for off grid DC power from the start, so no inverter would be required for solar powered operation.

The Australian film based DFN depended on the Czech manufactures of the film systems for some maintenance tasks. After the DFN team relocated to Western Australia from the UK, this dependence increased the costs of servicing significantly as personnel still had to be flown from Europe. By developing the new digital observatories in-house, this expensive dependence was eliminated and servicing could occur with less delay. The move to in-house development would also reduce the per observatory cost, allow the design to be tailored more exactly to the requirements of the DFN, and accelerate development by allowing potential improvements to be prototyped and tested more quickly.

## 5.4 Design Approach

Since the design of the digital fireball camera was starting from a blank slate, the "release early, release often" approach was used. This approach, commonly used in the open source software community, allow the basic functionality to be tested immediately and then the polish to be added later. The strategy allows the most difficult aspects of the problem to be identified quickly and focuses design effort on the parts of the design that actually need improvement. By iteratively refining the design and re-testing often, unexpected problems or incompatibilities can be discovered before too much design effort is expended down an avenue that turns out to be unworkable.

## 5.5 Core Component Selection

Core component selection began with the optical system once the concept design was complete, as these components directly inform the science capabilities of the network. The optical modulator and timing control system were trialled before the first field prototypes were deployed for a longer term trial.

### 5.5.1 Camera Selection

A number of consumer cameras were tested to determine their suitability for use in the digital fireball network. The requirements were—

- low cost (for the image quality);
- sufficient spatial resolution;
- compatibility with appropriate all-sky fisheye lenses;
- good low light performance (signal to noise ratio at higher sensitivities);
- durability, weather resistance and long shutter lifetime; and
- computer interface for capture control and image download.

Cameras of 18MP and greater were considered to ensure adequate spatial precision with an all-sky fisheye lens. Consumer DSLRs and interchangeable lens mirrorless cameras were considered as these both offer sufficient spatial resolution and the ability to mount appropriate all-sky fisheye lenses. 35 mm full frame and APS-C format cameras were considered to ensure good noise performance (compared to smaller sensors) at low light levels and good availability of a number of different all-sky fisheye lenses. Full frame and APS-C refer to sensor dimensions of approximately $36 \times 24$ mm and $24 \times 16$ mm respectively. These are the largest sensors found in mass market consumer cameras and generally perform better at lower light levels than smaller sensors when using optics with similar fields of view and relative aperture sizes (f-number). This difference can sometimes be mitigated by using "faster" lenses possessing larger relative apertures with the smaller sensor, but fast small-format fisheye lenses are not common. Medium format digital cameras with sensors larger than $36 \times 24$ mm are available, but these cameras are significantly more expensive due to the smaller and less price sensitive market for these options (though prices have started to reduce in the last few years). The selection of all-sky fisheye lenses for medium format cameras is also very limited.

Specialised full frame and APS-C sized monochrome astronomy cameras were not considered due to their high cost compared to commodity consumer cameras. (Full frame monochrome astronomy cameras cost in excess of $10,000.) It should be noted however that the Bayer matrix colour filter array in consumer colour cameras does result in some light and resolution loss (in colour interpolation). If a mass market full frame monochrome CMOS camera was available it would be a strong contender for the preferred camera. There is no technical reason why a monochrome CMOS sensor could not be made at a comparable price to current colour sensors, but without the mass market demand of consumer photography prices will remain prohibitively high.

The Canon EOS-5D Mark II, Canon EOS-1D X, Canon EOS 550D, Canon EOS-7D, Sony Alpha NEX-7, and Nikon D800 were evaluated with respect to spatial resolution, sensor size, noise performance, computer interface, ruggedness and cost.

Camera spatial resolution determines the spatial precision of trajectory triangulations. A 36 MP (megapixel) camera with an all-sky lens reaches a spatial precision of approximately one arcminute (depending on lens projection, see section 5.5.2). With the planned station spacing of 120-150 km this allows triangulation to within tens of metres for an average event. Exceeding this precision is of little benefit with regards to fall position estimation due to the uncertainties in stratospheric winds and final mass.

Good low light performance is required to image the last moments of the luminous trajectory (bright flight) where the fireball is visible. These last moments are crucial for calculating the final vector used to model the dark flight of the meteoroid which produces the fall position distribution for meteorite recovery.

Apart from imaging capabilities, practical considerations also need to be taken into account. Computer compatibility is required to use the camera in an autonomous observatory, where the camera control and image download must be automated. The ruggedness (a combination of durability and weather resistance) of the cameras was also evaluated. Although housed inside an enclosure, the cameras still must be weather resistant to some degree to remain operational in the hot temperatures with some exposure to dust (as the enclosures are ventilated for cooling).

Cost must also be considered as the objective is to maximise the coverage area (and therefore the meteorite recovery rate) on a fixed budget. However, it is important to remember that the camera is only part of the cost of a complete digital observatory.

The qualitative camera evaluations are shown in Table 5.1.

Table 5.1: Evaluation of cameras for use in digital DFN observatories

| **Camera** | **Spatial resolution** | **Sensor size** | **Noise performance** | **Computer interface** | **Ruggedness** | **Cost (USD MSRP)** |
|---|---|---|---|---|---|---|
| Canon EOS-5D Mark II | good (21 MP) | good (36 × 24 mm) | fair | download, control & format | good | fair ($2700) |
| Canon EOS-1D X | fair (18 MP) | good (36 × 24 mm) | excellent | download, control & format | excellent | poor ($6800) |
| Canon EOS-550d | fair (18MP) | fair (22 × 15 mm) | fair | download, control & format | fair | excellent ($800) |
| Canon EOS-7d | fair (18MP) | fair (22 × 15 mm) | fair | download, control & format | excellent | good ($1700) |
| Sony Alpha NEX-7 | good (24 MP) | fair (24 × 16 mm) | good | download | fair | good ($1200) |
| Nikon D800 | excellent (36 MP) | good (36 × 24 mm) | good | download & control | good | fair ($3000) |

The spatial resolution and sensor size evaluations are straight forward, and can be completed from the cameras' specifications sheets. Noise performance was evaluated by visually analysing night sky images. The cameras from Sony and Nikon using Sony manufactured image sensors out performed the Canon sensors in terms of noise performance. The noise performance ratings in Table 5.1 are independent of sensor size; the final performance of a full frame Sony sensor rated "good" would exceed the final performance of an APS-C "good" rated Sony sensor when used with similarly specified lenses. The capabilities of the computer interface were also compared; all cameras allowed images to be downloaded using gPhoto2[143]; control of the capture settings was also possible with the Canons and Nikons, and the Canons also allowed memory card formatting. (Remote formatting can be extremely useful as a corrupt memory card will completely halt observatory operation.)

The Nikon D800 was the most appropriate camera for the digital fireball camera network. Its good noise performance and excellent spatial resolution offered the most attractive imaging package. The weather resistant and durable construction was also complemented by a long shutter lifetime ("tested to 200,000 cycles" as stated by the Manufacturer[144]—enough for around one year of operation before shutter replacement). The usability over the gphoto2 computer interface was also sufficient for fireball camera operation. The final selection of the camera also depended on lens selection, however; as not all lenses are compatible with all cameras.

### 5.5.2 Lens Selection

Lens selection is at least equally important as camera selection in fireball camera design. There is a wider variation in performance across relevant lenses than cameras, and performance can be hard to evaluate due to the difficulty in measuring and interpreting lens performance as well as the number of factors that have to be considered. In addition to image quality (which is notoriously hard to quantify), a lens's field of view, image circle diameter, projection, mount, flange distance, mechanics and build must be considered.

Table 5.2: Common fisheye projections

| **Projection** | **Radial Mapping** | **Note** |
|---|---|---|
| Stereographic | $r = 2f\tan(\frac{\theta}{2})$ | local angles are preserved |
| Equidistant | $r = f\theta$ | angular distances are preserved |
| Equisolid | $r = 2f\sin(\frac{\theta}{2})$ | constant solid angular area across field of view |
| Orthographic | $r = f\sin(\theta)$ | parallel projection of a hemisphere onto a plane |

Lenses are only available in certain mounts and can only sometimes be adapted depending on the flange distances (lens mount to sensor distance) and lens control scheme (differing mechanical and electronic options). The selection of fisheye lenses that offer all-sky views is somewhat limited. Many fisheye lenses are designed so that the image circle circumscribes the frame, leaving no unused pixels; these lenses are known as diagonal fisheyes and do not provide all-sky coverage; they only provide 180° coverage along the diagonals from corner to opposite corner. In circular fisheyes, the image circle is inscribed within the image frame so an entire hemisphere is visible, but there are a large number of unused pixels. Fisheye lenses are available in a number of projections with different mappings from the radial angle $\theta$ off the optical axis (the zenith for fisheye all-sky fireball cameras) to the distance $r$ from the centre of the image circle. Spatial resolution varies across the field of view depending on the projection, and the region where fireballs will appear most frequently must be accounted for when comparing lens projections.

The commonly available stereographic, equidistant, equisolid and orthographic fisheye projections are summarised in Table 5.2.

The radial mappings of these fisheye projections are shown in the top half of Fig. 5.1. The bottom half of Fig. 5.1 shows the radial (elevation) spatial resolution of the different projections.

Fireballs are visible at altitudes ranging from approximately 20 to 90 km. The maximum range at 20 km altitude is about 500 km due to the curvature of the Earth (with a perfectly unobstructed horizon). Therefore, fireballs are more likely

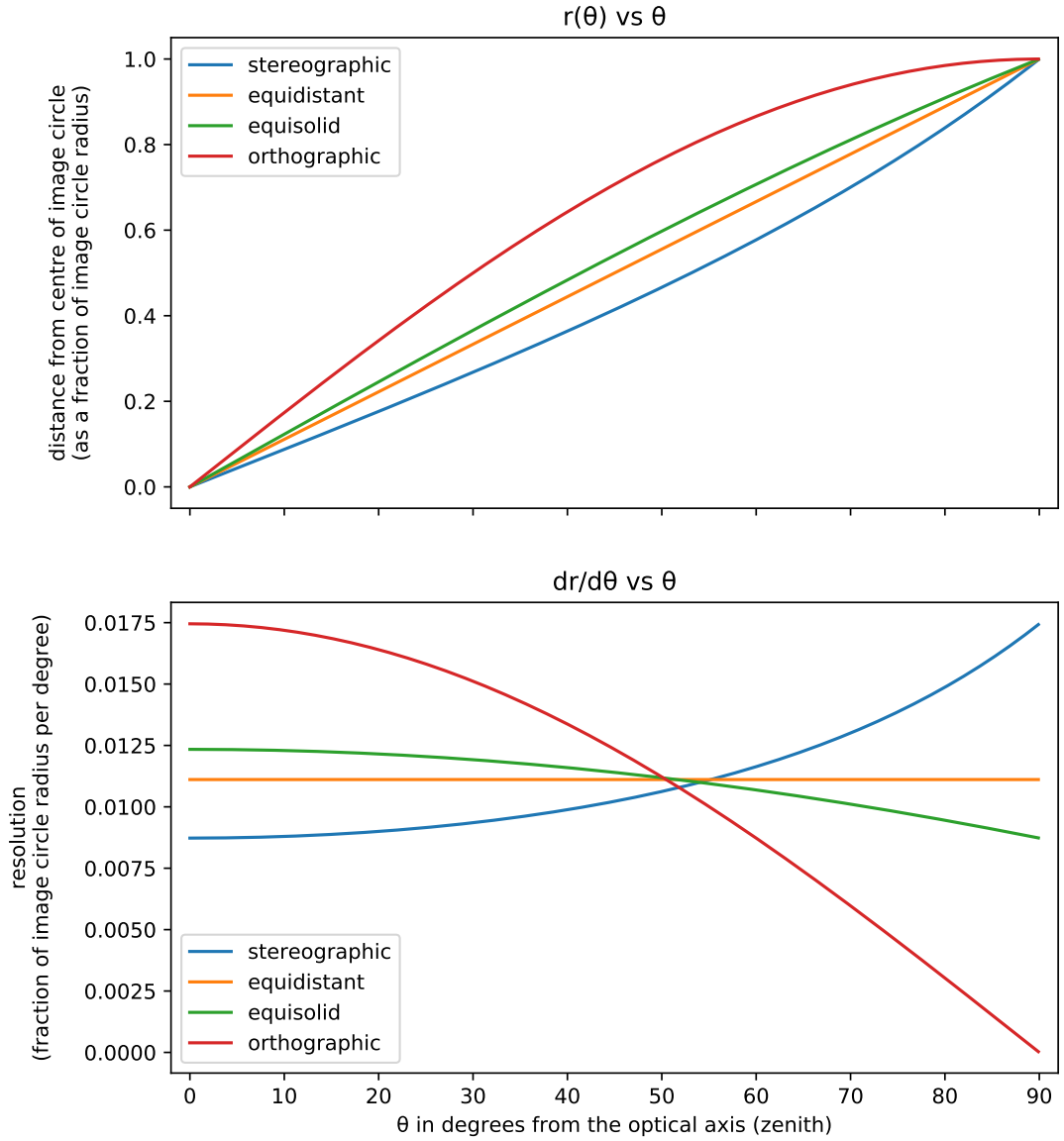


Figure 5.1: Radial mapping $r(\theta)$ and radial resolution $\frac{dr}{d\theta}$ vs $\theta$ from zenith ($\theta = 0°$) to horizon ($\theta = 90°$). The top plot shows the mapping from angular object space (from 0-90°) to image space (from 0 at the centre of the image circle to 1 at the edge) as $\theta$ varies. The bottom plot shows is is the derivative of the mapping and is displayed as fractions of the image circle radius per degree $\theta$. This is directly proportional to the radial (elevation direction) spatial resolution of the camera observations. In an all-sky fireball camera, the optical axis is aligned with the Zenith ($\theta$ is the complement of the elevation).

to appear low to the horizon than directly overhead from any camera site, as most of the monitored volume is far from the camera at a low elevation.

For fireballs below 30 degrees from the horizon, the stereographic projection provides higher spatial resolution than the alternatives in the elevation direction. With the DFN's camera spacing (130-150 km), most fireballs will appear below this elevation, making stereographic fish-eye lenses the preferred option.

Azimuthal resolution at different elevation angles depends on the distance from the centre of the image circle, and is proportional to $r(\theta)$. The projections with unfavourable radial (elevation) resolution at average fireball elevations (less than 30 degrees) actually have slightly higher azimuthal resolution at these low elevations because the fireball falls closer to the edge of the image circle. However, this slight increase in azimuthal resolution is not worth the much larger penalty in radial resolution.

The a number of possible fisheye lenses were considered for use in the digital DFN. They were evaluated by visual inspection of the images as the differences in performance were clearly visible. The results of this evaluation are summarised in Table 5.3.

Table 5.3: Lenses considered for use in the digital DFN observatories

| Lens | Format and Image Circle | Mount | Optical Performance | Projection |
|---|---|---|---|---|
| Sunex 5.6mm f/5.6 SuperFisheye | APS-C circular | Canon EF & Nikon F | fair | non-standard |
| Sigma 8mm f/3.5 EX DG Circular Fisheye | 35 mm full frame circular | Canon EF, Nikon F & Sigma SA | good | equisolid |
| Canon EF 8-15mm f/4L Fisheye USM | 35 mm full frame, zoom allows adjustment from diagonal to circular | Canon EF | excellent | equidistant |
| Samyang 8mm F/3.5 AS MC Fisheye CSII | APS-C diagonal or 35 mm nearly circular (≈5% of hemisphere area cropped) | Canon EF & Nikon F | good [1] | stereographic |
| Nikon AF DX Fisheye-Nikkor 10.5mm f/2.8G ED | APS-C diagonal, 35 mm nearly circular (with lens hood shaving) | Nikon F | fair [2] | non-standard |
| Peleng 8mm f3.5 Fisheye | 35 mm full frame circular | Canon EF, Nikon F & others | poor | equidistant |
| Yasuhara Madoka 180E Fisheye | APS-C circular | Sony E & Fuji X | not tested | orthographic |

1 some manufacturing variability was discovered upon further testing, see section 5.7.1

2 especially low edge performance

The Samyang 8mm f/3.5 was selected as the most suitable lens for use in the digital DFN due to its superior stereographic projection combined with its good optical performance. If there were multiple suitable lenses in consideration, the performance would have been compared by examining the shape of the point spread function across the image plane (with a focus on low to medium elevations). Unfortunately stereographic fisheye lens designs are uncommon, and this was not the case. Part of the image circle does fall outside of the sensor resulting in a crop at the top and bottom. This has the advantage of better pixel utilisation (69% vs 52%) at the cost of lost coverage at the top and bottom. Although the loss in terms of hemisphere area is small (around 5% total), the coverage holes reach up to around 15° elevation in the sensor top and bottom directions; fireballs are expected to regularly appear at this elevation, but in this case additional higher elevation observations should be available from closer DFN stations, unless the fireball appears at the perimeter of the network coverage area.

The Samyang 8mm f/3.5 performs significantly better than the Nikon 10.5mm f/2.8 at the edge of the image circle, and has a much more favourable projection than the Sigma 8mm f/3.5. The Canon 8-15mm f/4 performs very well in terms of image quality. When paired with a low noise full frame sensor could be a good choice for more densely spaced networks where the projection (with increased centre resolution) would be favourable, but was not selected for use in the DFN due to its unfavourable projection for the DFN's spacing and incompatibility with the well performing Nikon D800.

The Nikon D800 and Samyang 8mm F/3.5 AS MC Fisheye CSII were selected for the digital DFN observatories. The Nikon D800E is identical to the D800 except for the removal of the optical low pass filter, and was used in preference to the D800 when available. In 2014 the D810 was released and replaced the D800E as the camera of choice for the DFN observatories.

### 5.5.3 Optical Modulator

A number of electro-optic modulators were considered to periodically interrupt the long exposure fireball images image for velocity determination. The most

important considerations in the selection of an optical modulator for a fireball camera are contrast between the open and closed states, switching speed, open state transmittance and optical quality. The secondary considerations are the cost and availability of the modulator in suitable sizes, proven lifetime, environmental specifications and ease of implementation.

Only solid-state devices with no moving parts were considered to reduce cost and complexity of assembly and ensure high reliability with minimal maintenance. There are a number of different types of transmissive solid-state modulators available which vary different aspects of the light travelling through them including amplitude, wavelength spectrum, phase and polarisation. Reflective modulators are also available, but were not considered due to the limited back focal distance of the available all-sky lenses.

To provide high contrast between the on and off states as well as compatibility with as many colour and panchromatic imagers with differing spectral responses as possible, only amplitude modulators were tested for use in the fireball cameras. These modulators allow control of the amount of broadband visible spectrum light transmitted by varying the amount of light absorbed, scattered or reflected.

Three types of modulators were tested for use: twisted nematic liquid crystal shutters, polymer dispersed liquid crystal films, and chiral liquid crystal switchable mirrors.

### LC Shutters

Twisted nematic (TN) type liquid crystal (LC) shutters consist of a nematic phase liquid crystal surrounded by electrodes and sandwiched between two linear polarisers which are offset by 90 degrees (for a normally open shutter).

In the relaxed light transmitting state, unpolarised light entering the LC shutter is polarised with the orientation of the first polarising film. It then passes through the first transparent electrode (usually made of indium tin oxide—ITO) and then into the liquid crystal. Special surface treatments on the substrates align the

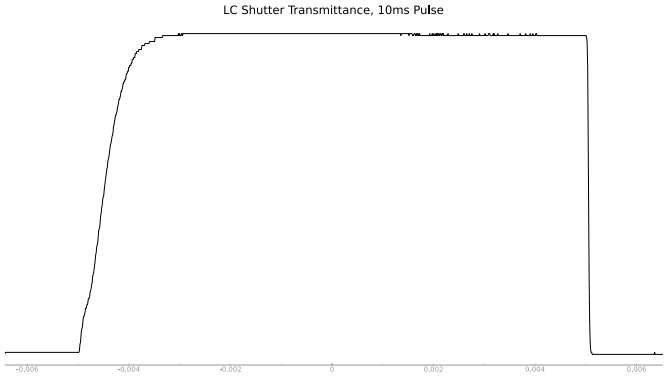


Figure 5.2: A 10ms pulse showing the slow opening and fast closing speeds of the TN-type LC shutter. Transmittance in arbitrary units on the vertical axis is and time in seconds on the horizontal axis.

liquid crystal molecules within the LC cell so that their orientations naturally twist 90 degrees throughout the thickness of the cell. The polarised light from the first polariser is then rotated 90 degrees as it passes through the liquid crystal before exiting through the second transparent ITO electrode. This aligns the polarised light with the second polariser (which is rotated 90 degrees to the first), allowing the transmission of the light that makes it through the first polariser.

In the powered light blocking state, an electrical potential is applied to the electrodes which reorients the LC molecules to align them in one direction. Without the twist, the light's polarisation is no longer rotated as it travels through the LC cell, and nearly all light is blocked by the two crossed polarisers.

The transition from the unpowered transmitting state to the powered blocking state is relatively fast (as low as tens of microseconds) as the electric field orients the LC molecules. This transition can even be accelerated by higher drive voltages and special drive waveforms. The slower (milliseconds) transition back to the relaxed transmitting state is reliant on the physical properties of the liquid crystal as the electric potential is removed and the liquid crystal relaxes back to its twisted state and cannot be accelerated with changes to the drive voltages. (Although it is somewhat controlled by temperature.) The asymmetry of the switching speeds is shown in Fig. 5.2.

LC shutters can operate at low voltages (≈3.3-18 V AC) and do not draw large

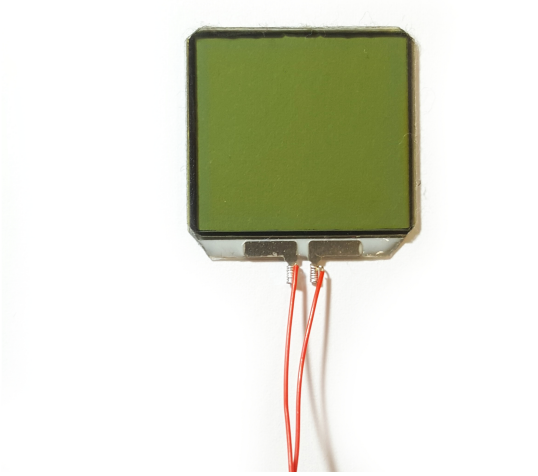

Figure 5.3: LC Shutter

amounts of current, making them ideal for integration into the DFN cameras. The only difficulty in driving LC devices is that alternating current (AC) waveforms with zero DC (direct current) bias must be used to prevent damage to the shutter due to ion migration in the liquid crystal layer [111]. (Although this is the case for all of the modulators considered for use.) These waveforms can be produced using a simple H-bridge driver which can be connected to a microcontroller. The downside to LC shutters is the limited open state transmittance due to the use of polarisers. Fig. 5.3 shows an LC shutter manufactured by LC-Tec Displays AB (Tunavägen, Sweden http://www.lc-tec.se) that was tested for use in the observatories. The open state transmittance is ≈36% and the closed state is <0.2% (at 18V AC)[111].

The peer reviewed literature does not indicate that meteors are polarised (although the question is not directly addressed), so no problems were anticipated from the use of a polarised modulator apart from the aformentioned loss of light. (The eventual observations from the DFN did not show any indication that visible fireball emissions are polarised, at least to the degree that would disrupt observations with polarised cameras.)

### PDLC Films

Polymer dispersed liquid crystal (PDLC) films consist of micrometer sized liquid crystal droplets suspended in a polymer matrix[145]. In the unpowered state, the LC axes are oriented randomly from droplet to droplet and the refractive index of the droplets does not match the refractive index of the matrix[145]. The changes in refractive index as light passes through the film cause a strong scattering effect[145]; in this state, the film appears dense and milky.

To enter the transmitting state, an electrical field is applied to the film (usually with transparent ITO electrodes) to align the axes of the LC droplets. This unifies the refractive index of the droplets and polymer matrix, eliminating most of the light scattering[145]; in this state, the film is transparent with a slightly cloudy appearance.

PDLC films are slower to switch than TN type LC shutters, but also exhibit a slow transition and a fast transition. The transition from the unpowered scattering state to the powered clear state is on the order of milliseconds, and the reverse transition can take several tens to hundreds of milliseconds depending on the construction of the film [146]. The drive voltage of PDLC films depends on the thickness and construction, but is generally higher than that of LC shutters (≈40-70V AC).

Open state transmittance for PDLC films is higher than that of LC shutters as no polarisers are used, but some scattering remains which can lead to a loss of contrast in imaging applications. The contrast is also lower than LC shutters as transmission in the blocking state is significantly higher (as inevitably some light is scattered forward).

For testing, a PDLC shutter (Fig. 5.4) was manufactured from commercial PDLC switchable privacy film from Switch Glass (O'Connor, Australia, switchglass.com.au). The transmittance is ≈80%[147] in the open state and ≈4%[148] in the light blocking state. The switching time is stated as approximately 100 ms at room temperature[149].

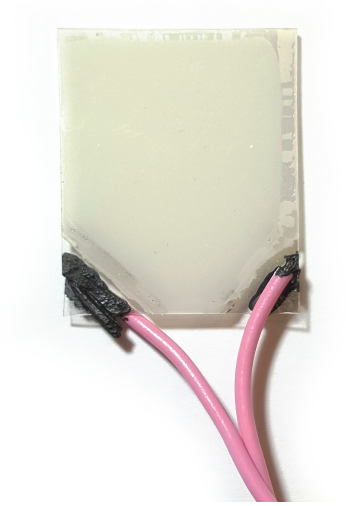

Figure 5.4: PDLC Film Shutter

### Chiral Liquid Crystal Switchable Mirrors

Chiral liquid crystal switchable mirrors (also known as cholesteric liquid crystal switchable mirrors) can be electronically switched between reflective and non-reflective transmitting states with the application of an AC electric potential. The chiral liquid crystal (CLC) phase is formed by asymmetric LC molecules that organise into a helical structure[150]. This structure reflects light with circular polarisation of the same handedness as the liquid crystal. For unpolarised light applications a left hand circularly polarised reflecting mirror is combined with a right hand reflecting mirror.

The transmitting state is achieved when an electric field is applied across the LC using transparent electrodes to align the LC axes in a similar fashion to LC shutters. The return to the helix arrangement (within a useful timeframe) is facilitated by a lightly crosslinked polymer network [150], [151] which forms a liquid crystal gel.

The response time of CLC switchable mirrors depends on construction (as is the case with all LC devices) but they are are longer than those of LC shutters and in the 20-100 ms range for commercially available products[152], [153]. The powered

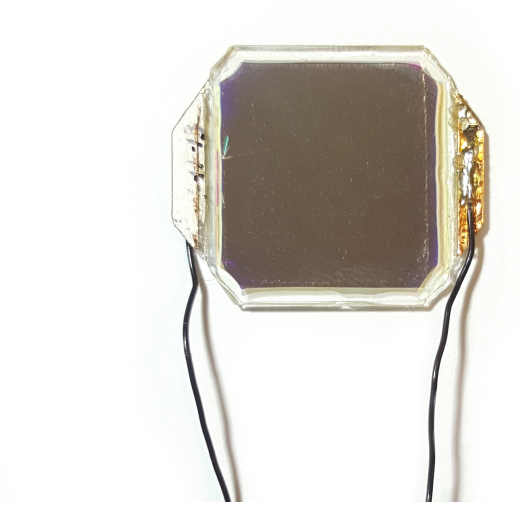

Figure 5.5: Mirror Shutter

and unpowered transitions are also likely to occur at different rates as with other LC technologies. The drive voltages of CLC mirrors are higher than LC shutters and PDLC films at ≈100-300 V AC.

The prime advantage of CLC switchable mirrors compared to LC shutters, is the lack of a polariser in the open state. This results in much higher open state light transmittance (≈87% vs ≈37%). The transmittance in the blocking (reflecting) state is ≈0.7%. The downsides are the higher switching voltages making driver implementation more complex and the slower switching times.

Fig. 5.5 shows the Kent Optronics Inc. (Hopewell Junction, USA, kentoptronics.com) switchable mirror that was tested.

### Modulator Evaluation

The three optical modulators discussed above and pictures in Figs. 5.3–5.5 were tested for use in the fireball cameras. The manufacturer supplied specifications of the three different optical modulators are presented below in Table 5.4.

Table 5.4: Specifications of exposure modulators tested for use in DFN observatories

| **Modulator** | **Drive Voltage** | **Open Transmittance** | **Blocking Transmittance** | **Contrast** | **Opening Time** | **Closing Time** | **Notes** |
|---|---|---|---|---|---|---|---|
| LC Shutter (18 V) | 18 V AC RMS square wave | 36% | <0.2% | >300:1 | 1.3 ms | 0.1 ms | [1] |
| LC Shutter (12 V) | 12 V AC RMS square wave | 36% | <0.5% | >100:1 | 1.3 ms | 0.1 ms | [1] |
| PDLC Shutter | 65 V AC RMS square wave | 80% | 4% | 20:1 | 100 ms | 100 ms | [2,3] |
| CLC Switchable Mirror | 260 V AC RMS square wave | 87% | 0.7% | 124:1 | 10-100 ms | 0.1 ms | [1,4] |

1 Designed for use in optical systems

2 Not designed for use in optical systems

3 Low contrast images in practice due to scattering (see Fig. 5.6)

4 Contrast seemed lower than 12V LC shutter in practice, could be due to angle dependence or manufacturing variability

The LC shutter was the first modulator considered. They are available from a number of manufacturers for use in optical systems and therefore are of high optical quality and well documented. The switching times are acceptable for operation above 10 Hz (which was the desired minimum frequency based on the success of previous networks). They also provide higher contrast than most of the alternatives, and are simple to drive due to their low voltage requirements.

The other major advantage of TN type LC devices is their proven track record. TN type liquid crystal displays (LCDs) have been used in consumer devices since the early 1970s. Some of these devices, such as digital watches with LCDs, show that simple LC devices can operate continuously for decades.

Due to the bulbous front element of all-sky lenses the optical modulator cannot be positioned in front of the objective. The simplest alternative is to place the it between the lens and the camera. It is also possible to mount the modulator within the lens (possibly in place of the controllable aperture iris), but this increases the assembly complexity and the optical quality of the lens could be degraded due to poor group alignment after reassembly if great care is not taken. Thin wires (30 AWG) are routed out through the lens in order to drive the modulator.

The LC proved to be suitable for use in a fireball camera. The primary drawback was the limited open state transmittance. This is a fundamental limitation in TN type LC cells due to the use of polarisers. Significant increases in transmittance require the use of a different modulator technology. In addition to the light loss, there was also some focus shift as a result of inserting the LC shutter with a higher refractive index (relative to air) into the optical path and a small amount of image degradation likely due a combination of dispersion within the shutter and small variations in thickness across the cell. The focus shift is compensated for by refocussing the lens which may require the removal of the normal focus limits. These effects can be minimised by using the thinnest shutter possible. The low open state transmittance was the motivation to examine PDLC films and CLC mirrors.

PDLC films were tested and found entirely unsuitable for use in a fireball observatory to modulate the exposure. Their scattering nature reduced the contrast

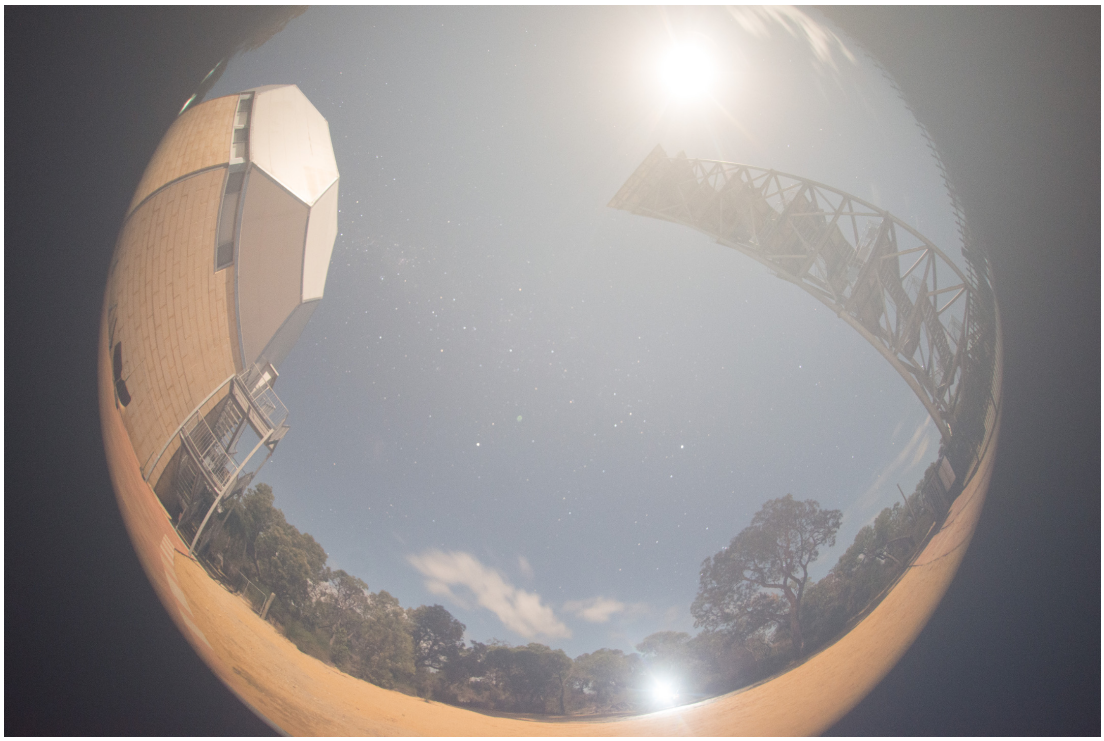

Figure 5.6: Nigh sky with moon and LED lamp visible showing low contrast with PDLC shutter. Nikon D800E, Nikon 10.5mm f/2.8, 30 s, ISO 3200, f/3.2

across the whole image to the point where the image was entirely unusable if any bright light sources such as the moon were present; this is shown in Fig. 5.6. Fireballs can be many orders of magnitude brighter than the moon making this option entirely unusable. If the optical tests had been successful, an alternate PDLC film would have been required due to the low switching speed (≈100 ms [149]) of the tested product. It is possible that future alternate (non scattering) dispersed liquid crystal devices could be suitable.

Tests were also conducted on the CLC mirrors, but the performance was not an improvement over the LC shutters. The transmittance in the open state was significantly higher than the LC shutter, but the transmittance in the light blocking state was also higher. The specified contrast ratio was similar to the LC shutters at 12 V but cannot be increased with drive voltage. In practice however, the contrast of the mirrors was lower than the LC shutter at 12 V, this is speculated to be due to manufacturing variability or angle dependence of the mirror. The switchable mirrors are also significantly more expensive than the LC shutters (by a factor of ≈10); the driving circuitry is also considerably more

complex and expensive due to the higher voltages involved.

The LC-Tec X-FOS thinned (0.8 mm) shutters were selected for use in the DFN observatories due to their good optical quality and high contrast between the open and blocking states. In the initial production designs these were used at 12 V AC RMS, but in the latest design (see section 5.6.2 the shutters have been used at 18 V AC RMS to significantly increase the contrast by reducing the transmittance in the blocking state.

An STMicroelectronics L293D H-bridge driver was used to drive the LC shutter. This driver is rated up to 36 V at up to 5 kHz[154], exceeding the LC shutter's requirements. In the more recent observatory revisions this has been swapped to the L293DD which is the same device in a surface mount package.

Fig. 5.7 is an excerpt of the schematic from the most recent revision of the DFN observatory showing the LC shutter driver; the other components and net labels have been omitted for clarity. In this most recent iteration the *LC Drive Supply* is 18 V DC. This is produced by a DC-DC switching regulator (not shown for clarity) to provide higher and more consistent shutter contrast than if the driver were supplied with the unregulated 12 V battery voltage as it was in previous versions. The GNSS (global navigation satellite system) input header is shown on the left, followed by the ATMega32U4 microcontroller (on and Arduino Micro develpment board), L293DD H bridge driver and, finally, the LC shutter header. As the LC shutter is driven with AC and 0 V DC bias, the polarity of the connection between the driver and shutter does not matter.

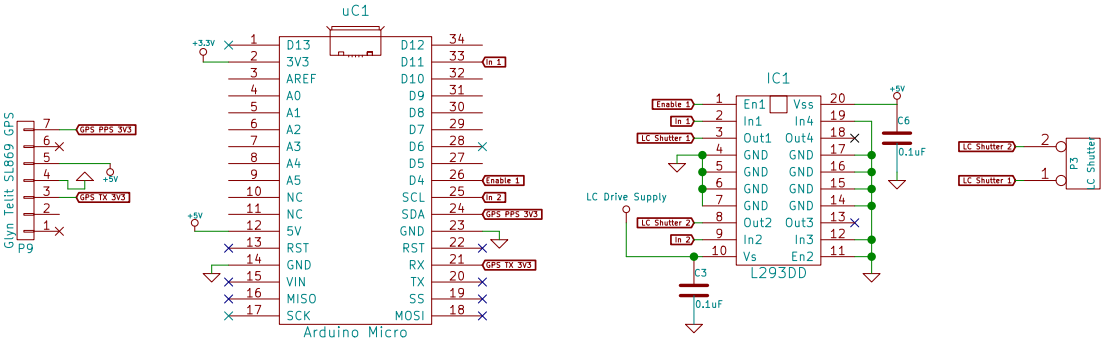


Figure 5.7: LC shutter driver schematic

## 5.6 Design Evolution

Initial testing of the camera shutter triggering and LC shutter driver was conducted on solderless breadboard during firmware development. Once the first version of the firmware was developed to trigger the camera and operate the LC shutter, four test systems were constructed on stripboard for overnight multi-station testing. These overnight test systems consisted of the LC shutter driver (Fig. 5.7), an ATMega328P microcontroller, GPS module and an optocoupler (Sharp PC123XNNSZ0F series) for triggering the camera (Fig. 5.8) via the remote release port. A 2.5mm TRS (tip ring sleeve) jack allowed wide camera compatibility via commonly available adaptor cables. Whilst the reliable and well packaged observatories used by the DFN today would be unrecognisable sitting next to these initial test systems from 2012, the design of today's observatories is the product of these initial test systems and years of revisions and improvements.

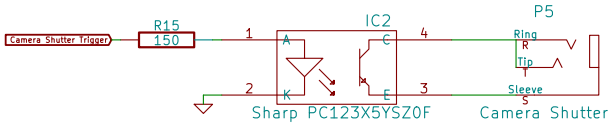


Figure 5.8: DSLR shutter release schematic

For longer term testing, four fully enclosed prototype observatories with embedded computes and long term image storage were constructed. The microcontroller

previously only controlling the LC shutter was now also tasked with managing the power to the various subsystems. An ATMega32U4 with USB connectivity was used instead of the ATMega328P to simplify communication between the PC and microcontroller.

The LUFA open source USB stack (fourwalledcubicle.com/LUFA.php) was (and still is) used on the microcontroller to implement a serial connection over USB. The ubiquity of serial over USB makes the arrangement compatible with virtually all major computer platforms and operating systems. The communication protocol is a simple single byte message for most commands with single or multi byte responses. Some commands are implemented with two sequential single byte commands to prevent accidental activation when interfacing with the device manually. Due to the simple nature of the protocol, it is possible to direct the operation of the microcontroller and attached observatory hardware subsystems using the keyboard via a serial terminal.

A small low powered x86 SoC (system on a chip) based computer (eBox-3300) was used in these prototype observatories for its low cost, low power usage and small size. A 2.5 inch hard disk drive (HDD) was used to give the systems a few months of autonomy before drive swaps would be required. These systems were installed at the four Outback film camera sites (Mundrabilla Station, Forrest, Kybo Station and Kanandah Station) to test the implementation of the basic electronics and the durability of the core components over the 2012/2013 Australian summer.

The prototype systems operated throughout the summer without significant hardware problems and allowed testing of the time encoding method. They shared power supplies and connectivity with the film cameras at these sites to simplify installation. This test deployment also allowed longer term testing of the time encoding method. A ternary sequence alphabet with opacity encoding of three different opacities was used initially, but this was then refined to binary pulse width encoding to increase the ease of fireball decoding.

### 5.6.1 DFNSMALL

The first production design of the digital DFN observatory was codenamed DFNSMALL. The ancillary systems were significantly upgraded over the four deployed prototype systems. The DFN is primarily composed of this iteration (as of mid 2017) which is documented in [24] (chapter 3). The internals of this design are shown in Fig. 5.9.

A video camera was added to provide more detail on fragmentation events (due to the higher sample rate), the possibility of independent event detection and backup absolute timing until the de Bruijn time encoding technique was proven. The embedded computer had to be upgraded to a significantly faster dual core x86_64 based model (Advantech MIO-5250) to handle the video data. In order to increase the service interval (while retaining all images), the storage capabilities were considerably expanded to dual 4 terabyte (TB) 3.5 inch HDDs making it possible to retain all captured images over an 8 month period. A larger enclosure was required to accommodate the video camera and expanded storage, and a blower was added to keep the lenses free from condensation overnight during observations. While a lens heater can provide better reliability as there are no moving parts, they consume significantly more power.

The PCB (printed circuit board) was redesigned to power the additional systems and to allow more granular power management of the subsystems. Linear regulators were used to power the camera and microcontroller which require ≈8 V and 5 V respectively. This simple approach minimised design complexity and part count. The low efficiency (compared to switching regulators) was acceptable for the low powered microcontroller, and tolerable for the camera which is only powered at night, and only consumes moderate amounts of power. Solid state relays connected to the microcontroller were used to switch the subsystems on and off. A monolithic 12 V output switching DC-DC regulator was used to supply the regulated 12 V for the hard disk drives.

The weather sealing of the lenses was upgraded to the current flange solution as shown in Fig. 5.10. In this design, the lenses are placed into tight fitting CNC (computer numeric control) machined aluminium flanges and sealed in using

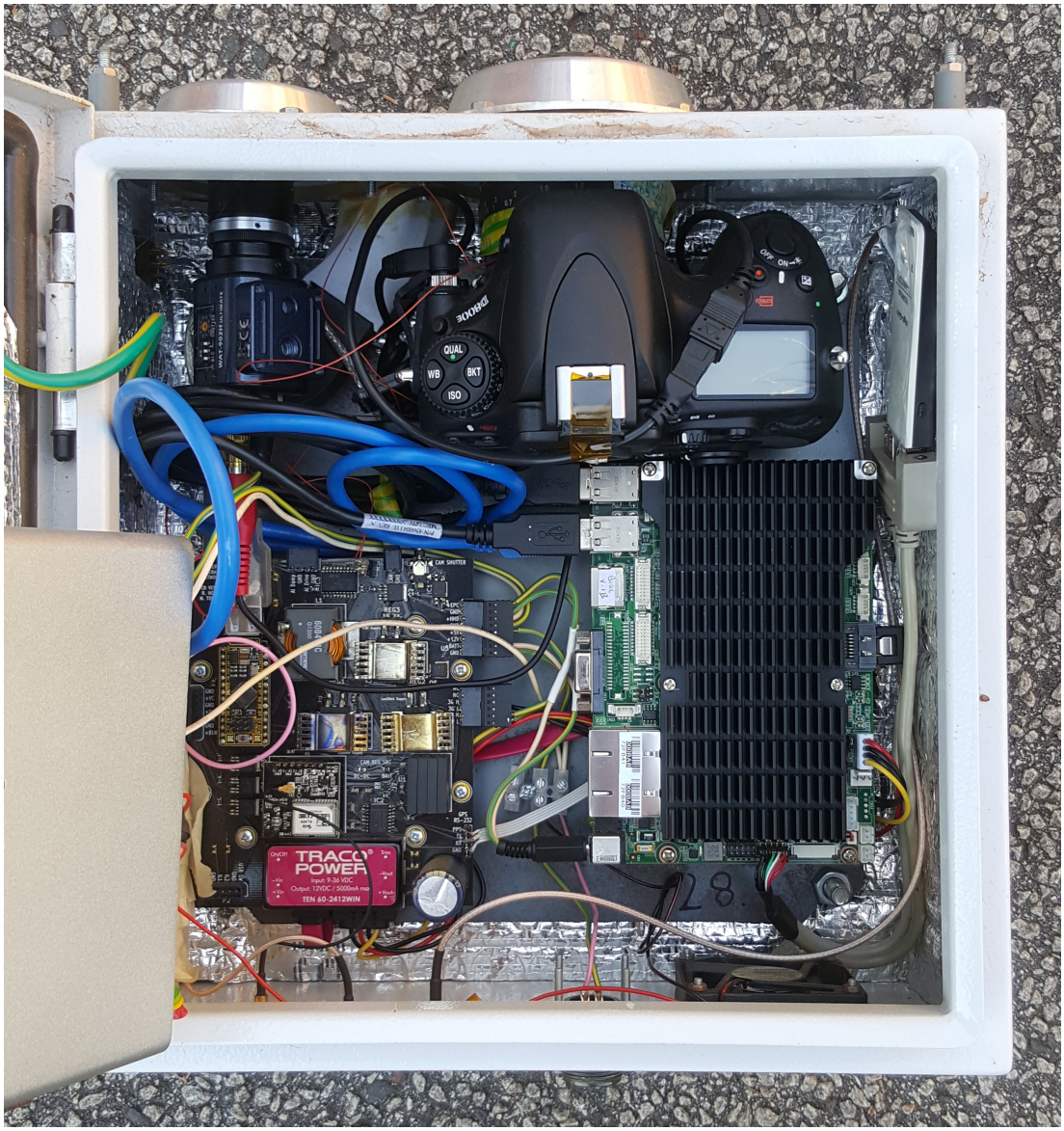


Figure 5.9: DFNSMALL: the DFN's first production digital observatory (revised SMD PCB in this particular observatory)

consumer weatherproof sealant. Two sealant beads are critical to the design. One small bead between the sharp and thin internal protrusion of the flange and the glass of the front element seals out water and dust, and one much larger bead between the inside midsection of the flange and the lens body secure the lens in the flange. The groove inside the flange helps secure this second bead, even in the presence of residual machining oils.

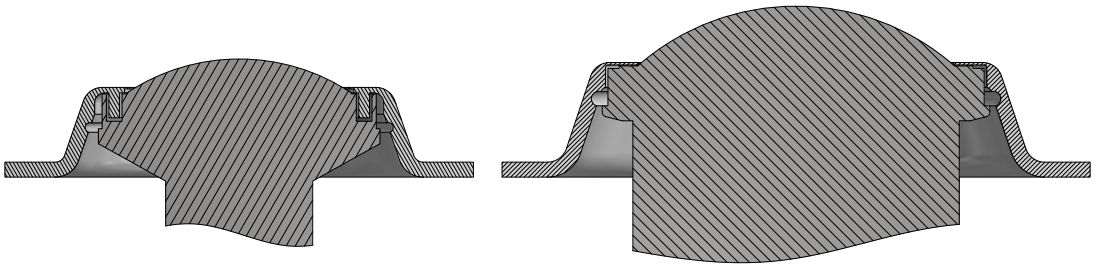

Figure 5.10: Lens flange cross section showing the video (left) and still (right) lenses and Aluminium weatherproofing flanges

### Revisions

As the DFNSMALL design has been in production for a number of years (2013-2015), the design has seen a number of revisions over time. The original through hole PCB design (Fig. 5.11)was reimplemented with a majority of SMD (surface mount device) components (Fig. 5.12). This streamlines the PCB assembly process as individual device by device throughole hand soldering is replaced by SMD reflow batch soldering and saves board space. The reflow process is commonly used to solder SMD PCBs on industrial scales (often as a continuous process) but can it can also be implemented effectively for small batches (tens to hundreds of PCBs) with careful board design. Through hole connectors were retained primarily for strength, and some other through hole devices were retained due to availability. The single sided design was reflow soldered using a hotplate before the connectors and few remaining through hole components were hand soldered.

Apart from the move to mostly surface mount components, the DC-DC converter was also upgraded to a higher current model so the PC could also be powered from this regulated output. This eliminated some reliability problems caused by

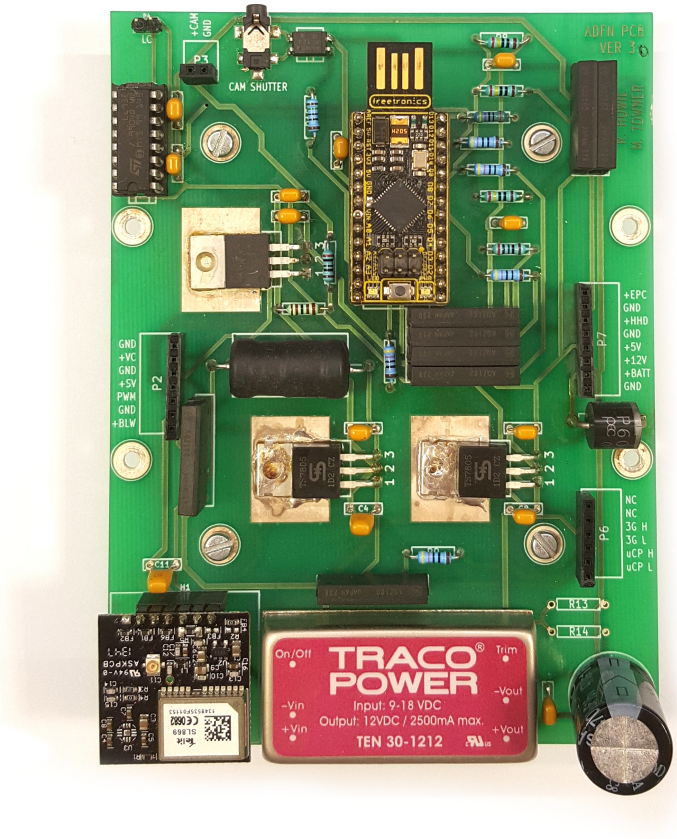


Figure 5.11: Original through hole DFNSMALL PCB, non-standard connectors are present on this particular example as it was used in an undeployed test system

the limited input voltage range of the PC and low battery voltages in winter. Small revisions were also made to the PCB throughout the time this design was in production: one IC (integrated circuit) package was exchanged for easier reflow soldering, and the reset circuitry was modified to fix some problems with the cold reset functionality.

During this iteration, the embedded computer was also changed to the Commell LE-37D which offers higher performance at a lower price. The Commell also had a number of other advantages: the Molex Mini-Fit Jr. power connector was more reliable than the previous barrel jack, and it possessed a wider input voltage range operating correctly down to 9 V. This wider range was useful on the models with the older PCB where the PC power supply was unregulated. As magnetic storage technology advanced, the drives were installed were upgraded from dual 4 to 6 and then finally 8 terabyte drives. These upgrades were performed as required

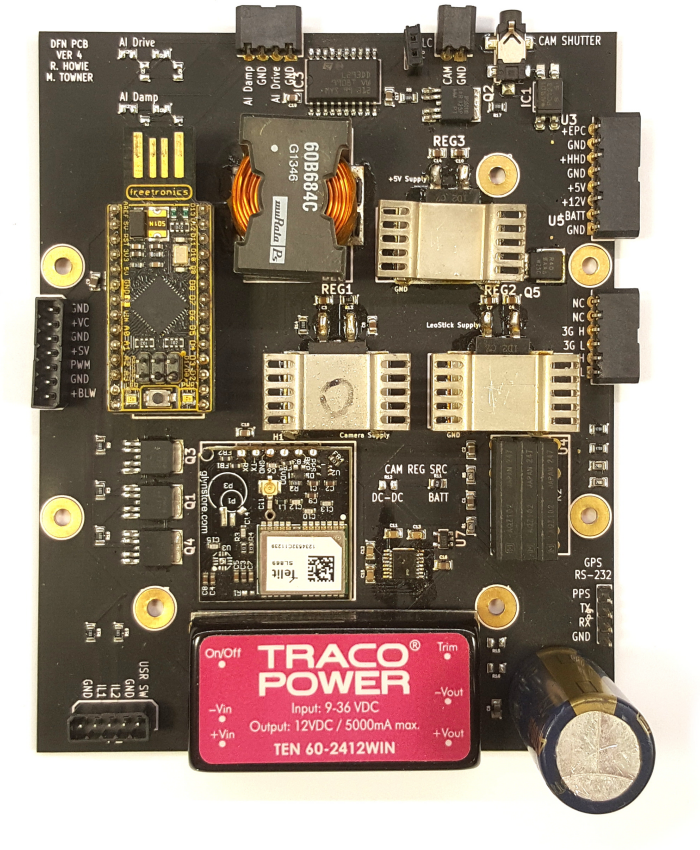


Figure 5.12: Revised SMD version of the the DFNSMALL PCB

with priority given to the least accessible stations at the edge of the network. The USB dual drive enclosure originally used in the DFNSMALL design was discontinued during the production lifetime. The replacement had a different physical layout, and complicated the mechanical design and usability of the the observatory. The discontinuation of this core component motivated some of the changes in the next iteration of the DFN observatory design.

### 5.6.2 DFNEXT

The success of the DFN within Australia spurred the decision to expand the network globally which motivated the development of a second generation digital fireball observatory—codenamed DFNEXT—in late 2016. The objectives of this design were to improve the DFNSMALL design in a number of key areas. The proven concept design and core imaging hardware were retained; the

improvements centred around improving the manufacturability, maintainability and usability of the observatories. The latter two aspects were of particular importance because these observatories were destined to be installed and maintained by overseas collaborators, not the core DFN team. The internals of the DFNEXT design are shown in Fig. 5.13.

The goals of this revision were—

- to improve the reliability of the connectors and wiring,
- to significantly extend the service interval,
- to improve the modularity of the design allowing components to be swapped more easily—even in the field,
- to make the video subsystem more useful,
- to improve temperature management,
- to improve the efficiency of the onboard power management, and
- to simplify observatory assembly, and
- to reduce the reliance on off-the-shelf components without a reliable supply.

### Mechanical Design and Wiring

Initially the DFNSMALL systems had some wiring reliability problems that can be traced back to three root causes: the use of spring clip wire retention in the pluggable terminal blocks, the use of solid cored wire and the ease of accidentally damaging one of the many exposed wires during maintenance of the observatories. The spring clip retention pluggable terminal blocks with solid cored wire were chosen for ease of assembly, but the difficulty stripping the precise length required, the inflexibility of the solid cored wire and the low pullout force (compared to other methods such as crimping or screw terminals) made them unreliable overall. This could have been partially mitigated by using stranded wire, but the difficulty of inserting the stranded wire into the spring clips made this approach unfeasible. Over time, the problems were minimised by fastening down most of the failure

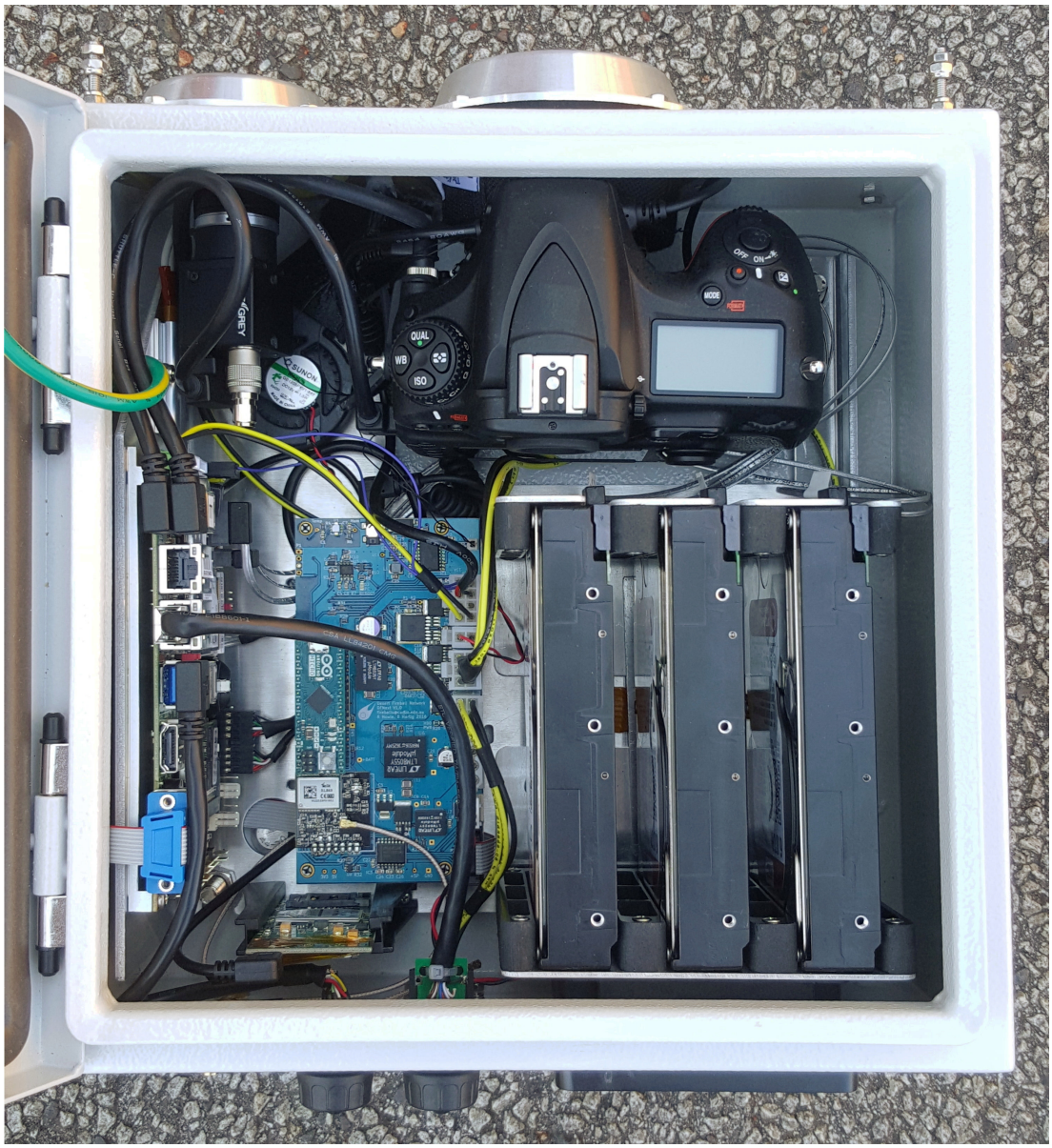


Figure 5.13: Revised DFNEXT observatory with an extended service interval

prone cable runs and taking additional care during servicing and assembly. Some of the connectors in the DFNSMALL design were also failure prone as well. The PC power barrel jacks had to be replaced with some frequency and the lack of space adjacent to the HDD enclosure's USB 3.0 connector meant that this cable was sometimes damaged.

A few changes were required in order to avoid similar problems on the DFNEXT generation. The pluggable terminal blocks with spring clip wire retention were replaced with Molex Mini-Fit Jr. crimped wire to board connectors for the general power connections (Fig. 5.14). The crimped connection should be significantly more reliable than the spring clips (when crimped correctly) and the connectors as well as the required tools are widely available due to their use in automotive applications and in standard ATX computer power supplies. These connectors do retain the option to remove single wires after assembly through a pin removal tool, making them more maintainable than soldered connections. The swap to these connectors did make component selection slightly more complex, as the wire gauges had to be matched to the available crimp contacts.

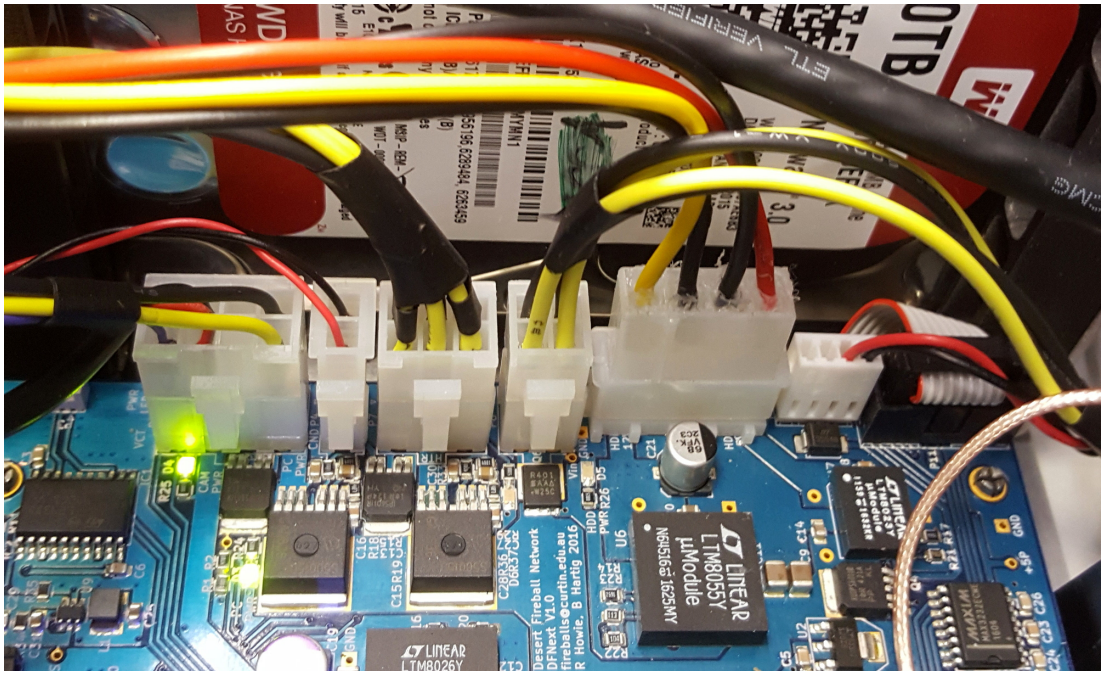


Figure 5.14: DFNEXT wire to board connectors

The new wiring was also significantly more modular than the previous wiring. The custom wiring in the DFNEXT observatories consists mainly of two wiring harness components (Fig. 5.15). This simplification was made possible by moving

the functionality of components that were previously integrated into the wiring (thermostats and diodes) onto the PCB. This modular wiring is simpler to produce in large batches separately from the observatory subsystems, and is suitable to be contracted out to an external manufacturer if required in the future.

Figure 5.15: Modular DFNEXT wiring harness

Standard connectors were used wherever possible so that off-the-shelf or semi-custom cables (using standard connectors, but of custom length) could be used to minimise assembly time. The use of mass produced overmoulded cables also helps increase the reliability (when compared to in-house hand assembled cables). Throughout this design the shortest cables possible are used to keep the observatory cabling as short and tidy as possible even when this required additional expense or assembly time. As these observatories are going to be maintained by

collaborators, it is important that the chances of inadvertently disconnecting or damaging a cable during routine drive swaps or servicing is minimised. When sourcing the cables, great care was taken to use angled plugs where necessary to avoid placing cables under strain which had led to the failure of the USB HDD data cables in the past.

Another change made to reduce cable strain was the elimination of all door mounted components. On the DFNSMALL observatories the door mounted hard drives were susceptible to failure due to the repetitive cable movements. This meant that the HDD operation had to be rechecked once servicing was finished and the door re-closed. The weight distribution was also problematic when assembling and maintaining the systems in the laboratory. This change was combined with the elimination of the USB dual drive enclosure to end the reliance on off-the-shelf components with a significant supply risk. The enclosures are hard to purchase in volume as the cost effective versions are commonly sold by small volume retailers, and particular models are liable to be discontinued without notice. This is problematic as the replacement models may not be mechanically compatible. To replace the USB to SATA bridge provided by the drive enclosure, a dual port mPCIe (mini PCI Express) SATA was added to the PC. Compatible cards are available from numerous manufacturers, and so have a low supply risk. This change required a new 3.5 inch HDD mounting and power delivery solution as this was previously provided by the drive enclosure. The advantage here was that it provided an opportunity to use the space within the observatory enclosure more efficiently and expand the storage capability to three 3.5 inch HDDs. With 10 TB drives now commonly available, 30 TB of storage extends the service interval of the observatories to over 20 months of normal operation. (This extended service interval is the origin of this generation's codename.) A number of different hard drive mounting solutions were modelled, prototyped and tested. The focuses were drive cooling, ease of drive replacement and manufacturability. The final design used lasercut and CNC bent brackets combined with lasercut HDPE (high-density polyethylene) rails. A foam block is affixed to the door and secures the drives when the observatory is closed. The orientation prevents the drives from sliding out accidentally when the observatory is installed or being serviced on the bench.

### Electrical Design

Two switching regulators were added to the PCB in order to supply the HDD's 5 and 12 V rails. The 5 V rail is supplied by a Linear Technology LTM8023 step-down regulator and the 12 V rail is supplied by a Linear Technology LTM8055 buck-boost regulator. These system-in-package regulators integrate the controller, switching components and inductor to save design effort, part count and board space relative to discrete component switching regulator circuits. The HDD power delivery circuitry is shown in Fig. 5.16.

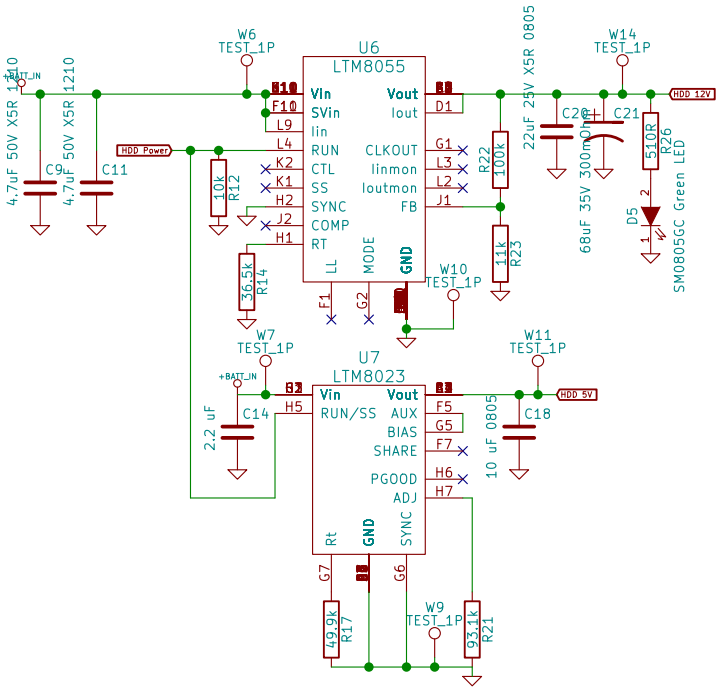


Figure 5.16: HDD 5 V and 12 V supply with enable

The DSLR power supply was also replaced with a switching regulator (Linear Technology LTM8026). Switching regulators are more efficient which reduces power draw (important due to solar powered operation) and minimises internal heat production. They are also necessary where the output voltage might have to be a close to or higher than the input voltage (such as in the case of the HDD 12 V rail). As these regulators also have an enable pin to turn the output on and off, they further help reduce the part count by eliminating separate switches. To change the output voltage of the regulator only two resistors need to be ex-

changed, making the design simple to customise to different cameras if required. The power supply to the camera is shown in Fig. 5.17.

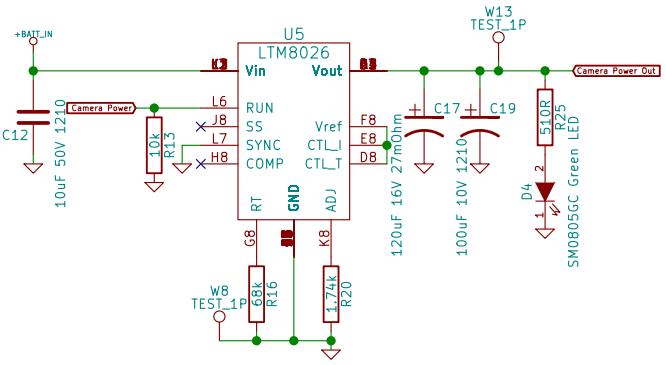


Figure 5.17: Camera power supply with enable

Nearly all the changes made in the DFNEXT revision are usability changes that do not affect the science data. The exception is the move from an unregulated 12 battery voltage LC supply to a regulated 18 V LC shutter supply. This increases the contrast of the LC shutter between the open and closed states from >100:1 to >300:1. This improves the imaging of bright fireballs and makes a new dimming function in the firmware more useful. The dimming function reduces the exposure of fireballs by reducing the pulse time in pulse frequency encoding when commanded (see section 4.5.1). The other advantage of the regulated supply is the independence from battery voltage; the contrast is now consistent throughout the night as the battery discharges and day to day as the weather changes. The 18 V supply is implemented with a Linear Technology LT3461 semi-integrated step-up DC-DC switching regulator. The device incorporates the switch and diode, but an external inductance is required. (No monolithic solution was available in the desired performance envelope.) The switched mode LC shutter supply is shown in Fig. 5.18.

In order to simplify the wiring, as much functionality was moved onto the PCB as possible. The thermostat that was previously was mounted to the HDDs was replaced with a digital temperature and humidity sensor on the PCB. The cooling fan was replaced with a larger slower model to increase the ventilation and reduce the noise level as these models are more likely to be installed in populated

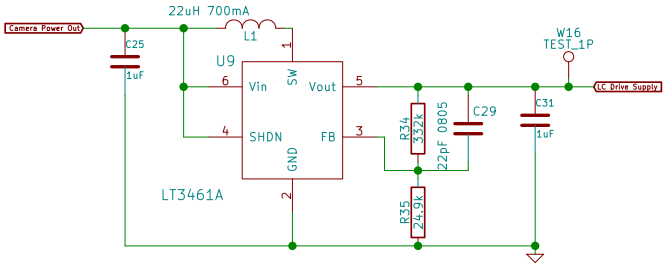


Figure 5.18: LC supply

locations. A heater control switch and plug were also added to the PCB to allow heating for cold locations in the USA and Canada. Heater and fan control was implemented in the microcontroller firmware. This greatly simplifies the wiring and assembly compared to the previous design which incorporated the thermostat and a diode into the wiring harness and allows more flexible temperature management. The firmware defaults to automatic management and attempts to keep the observatory temperature between ≈5-45 °C, but the computer has the option to take control of the heating and cooling if more advanced environmental control is required in the future.

Another aspect of the electronics that was improved in the DFNEXT design was the reboot circuitry. Previous designs allowed the PC to cold reboot (a reboot where the power is completely disconnected) the microcontroller and the microcontroller to cold reboot the PC. This design was overly complex and was not the ideal solution as it used the PC's GPIO (general purpose input/output [pins]) and depended on correct operation of the microcontroller. GPIO is not normally standardised between embedded PCs from different manufactures so the implementation might have to be modified if the PC model was changed. There is also a chance of microcontroller firmware corruption that could make it impossible to cold reboot the PC. The new design uses a 555 timer to disconnect the system power for a set period automatically after the PC is shut down. The shutdown is detected through the power LED pin on the Intel standard front panel header, and the PC is configured to power on automatically when power is connected. This system is more reliable as all devices are powered off with one switch and the 555 timer has no firmware that can be corrupted. The only vulnerable part

of the system is the wire between the front panel header and the PCB. If this were removed, the shutdown would not be detected and the PC would not be powered back on by the action of the 555. In this case, the automatic power on setting in the BIOS should wake the PC up at a predetermined time of day. If this situation were to occur the PC could then be configured to perform warm reboots (without power disconnection) instead of cold reboots in the future.

The 555 reboot and power switch circuitry is shown below in Fig. 5.19. Some of the passive components shown are required to delay the rising transition on the power switch's control input to guarantee normal operation due to some particularities of the Infineon BTS50015-1TAD smart high-side power switch.

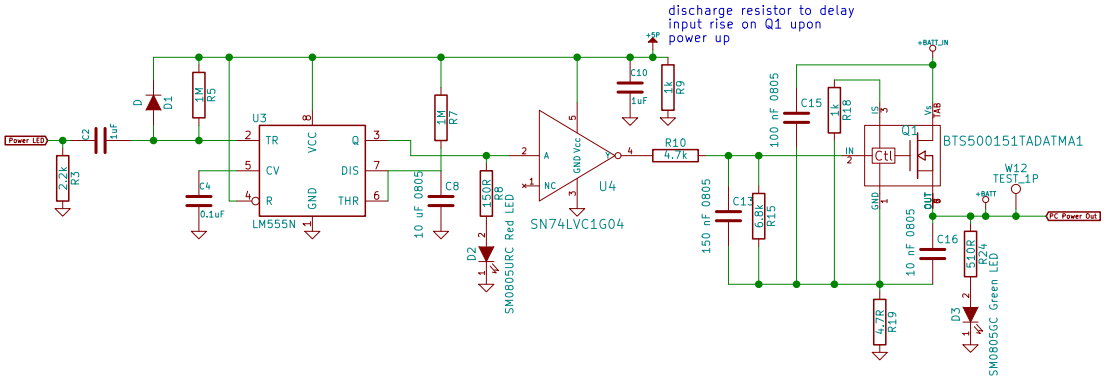


Figure 5.19: DFNEXT 555 timer based automatic cold reboot circuit

Indicator LEDs were added to the PCB to show the hardware status at a glance. A red LED shows when the system is powered off due to the operation of the 555 reboot circuit to help debug general power issues if they were to occur. Once the 555 reboot finishes and the PC is powered, this is indicated with a labelled green LED. Indicator LEDs also indicate when the DSLR, HDDs and heater are powered.

### PCB Layout and Process Changes

More care had to be taken with the DFNEXT PCB layout than previous versions due to the increase in part count, the need to accommodate the high frequency

switching DC-DC regulators and the high current demands of the enclosure heating required in cold weather installations. To ensure good performances of the switching regulators, the data-sheet reference implementations were followed as closely as possible. The layouts of these systems are key to performance due to the high switching frequencies involved. The input capacitor, output capacitor and inductor traces must be as short with as low an impedance as possible to minimise losses and electrical noise. The SMD heatsinks were used on the previous design with the linear regulators. Due to the more efficient operation of the switching converters, there was an opportunity to remove them with careful thermal design of the PCB. In order to minimise heat production and impedance, 4 oz copper layers were used with large area (zone) traces for the primary high current traces on the PCB, and the bottom layer of the two layer PCB was mostly reserved for a large ground plane (although there are numerous breaks for signal routing). Some parts of the layout were slightly complicated by the large trace clearance and minimum width due to the use of 4 oz copper layers (instead of thinner 1 or 2 oz copper). The monolithic DC-DC converters selected are well designed for use on one or two layer PCBs, and large planes or zones can be used to connect the power pins. These planes also allow the heat from the converters to be dissipated. A significant number of thermal vias are used to conduct heat from the converters on the top side to the additional planes (especially the ground plane) on the back. The DFNEXT PCB is shown in Fig. 5.20.

The high lead count (121 on the LTM8055) BGA (ball grid array) packages of the DC-DC converters required some refinements of the PCB soldering process. The reflow temperatures must be tightly controlled to avoid reflowing the internal solder joints inside the system-in-package converters. The hotplate reflow technique was reused from previous production runs, but the hotplate was upgraded to a purpose built soldering reflow hotplate to allow more precise temperature control. The assembly process was also factored into the board design; not only do the thermal vias beneath the converters conduct heat away during operation, they also conduct heat to converters and other large components during the reflow process. Some trial and error was required to determine the ideal reflow procedure, but once the temperatures and times had been determined, the process is surprisingly reliable considering its simplicity and low cost. Once the reflow soldering of the SMD components is complete, the through hole connectors are

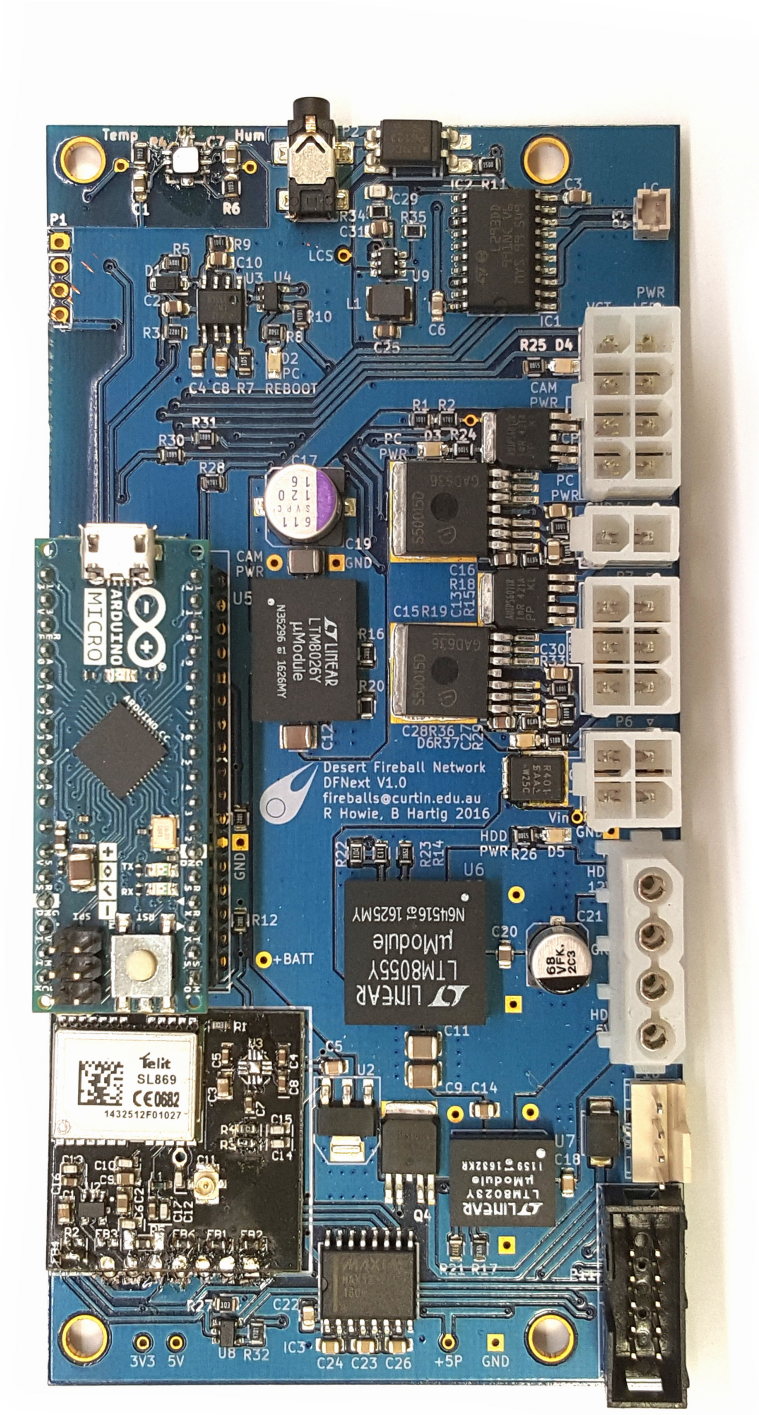


Figure 5.20: DFNEXT PCB with additional functionality and higher efficiency switching regulators

hand soldered. Thermal relief is used to reduce the amount of heat required for the through hole soldering (as otherwise the large copper zones would conduct the heat away too effectively).

### System Component Changes

To improve the video functionality of the observatories the analogue Watec WAT-902H2 was replaced with a FLIR BFLY-U3-23S6M-C USB 3.0 industrial imaging camera. This global shutter CMOS camera captures 2.3 MP at up to 40 frames per second. This should allow the collection of better fireball video imagery at higher resolution and less saturation due to the ability to quickly change the gain via software control. The camera also offers sequential HDR imaging modes where alternating frames can be captured with different exposure settings (up to four different exposures). To handle the increased video bandwidth and provide more compute power generally the embedded PC was upgraded from the Intel Celeron J1900 based Commell LE-37DNIP to the Intel Core i7-6600 based Commell LE-37GXIP7. In order to make the USB and Ethernet ports accessible the orientation of the PC was changed so that these ports are facing outwards when the door is open. The previous flat laser cut steel backplate to which the main components were attached was replaced with a CNC bent laser cut aluminium backplate as shown in Fig. 5.21.

Where the old backplate used holes with threaded fasteners on both sides to anchor the main components down, the new design used self clinching fasteners that are punched into the backplate. Whilst threaded machine screws are still used to mount most of the components, assembly time is greatly reduced as this can be done with access only to the top side. This makes assembly faster, but the main benefit is in the field where components such as the HDD rails or blower can now be exchanged without removing the backplate (a major exercise in the field). Snap fit PCB standoffs are used to make exchanging the PCBs as simple as possible. This makes it possible to for collaborators to fix even major hardware problems by swapping over a replacement PCB that can easily be posted to them.

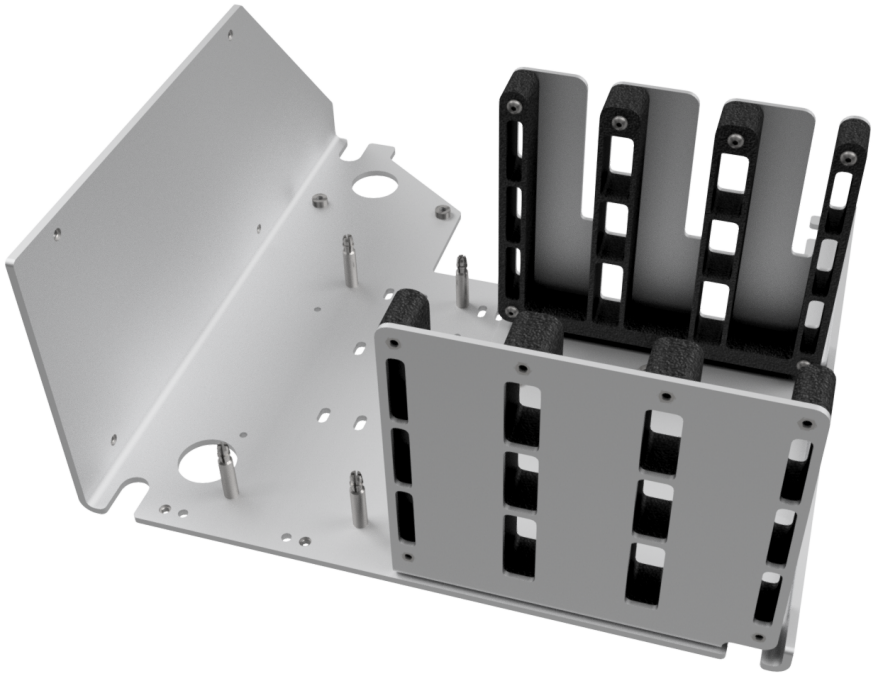

Figure 5.21: DFNEXT backplate and drive brackets

### Firmware Improvements

The downside of the new pulse frequency encoding (section 4.4.3) is the low average transmittance due to the reduced open time. This reduces the number of stars visible for calibration, especially in the important close to the horizon region. To overcome this, the operation of the observatory has been modified to take a dedicated calibration image every half an hour where the LC shutter is left open for an entire exposure. This is implemented by a microcontroller firmware command which turns the LC shutter off for the next exposure when commanded to do so by the PC.

A reoccurring objective during DFN hardware and software revisions is to reduce the network deadtime. The DFNSMALL cameras originally captured a 25 second image every 30 seconds. In order to extend this, the DSLRs were put in to bulb mode (where the shutter stays open for the length of time the shutter button is depressed) and the microcontroller firmware was modified to keep the shutter line low for 29 seconds. However, this change had to be rolled back as the Nikon DSLR firmware prevents downloading images while the shutter is open. The one second gap does not give enough time for the image download so the image files

start to accumulate on the memory cards which eventually fill and the camera ceases to operate (before the scheduled end of observations in the morning). After additional testing, a 27 second exposure is the longest that can be captured reliably every 30 seconds while still downloading images throughout the night.

The way in which gPhoto is used to download the images was also modified. Where the software previously frequently polled the camera and downloaded new images when they are discovered, the new software passively waits for new images (this is referred to as tethered capture). As part of this change, a way to trigger the exposure of a single image was required for cloudy operation where the camera needs to capture one image every five minutes to see if conditions are still cloudy or have improved. This was implemented with a firmware command to take one image and then stop when directed by the PC.

The new digital video cameras also allow the captured frames to be triggered by an external source. The microcontroller is wired up to this trigger pin the DFNEXT cameras so that the absolute frame timing is known and synchronised across the network using GNSS time. This is implemented in the microcontroller firmware by a small addition to the timer interrupt service routine that is used to generate the encoding and drive the LC shutter.

### 5.6.3 Satellites and Astronomical Transient Observations

The DFNEXT design is a flexible platform for autonomous imaging in general, and can be applied beyond fireball observation. Using the base design, some small changes were made to create a variant for observing satellites and astronomical transients (Fig. 5.22).

The Nikon D810 was retained, but the lens was swapped for a Sigma 85mm f/1.4 DG HSM Art which has an field of view of 24 by 16 degrees. As satellites are visible for longer durations than fireballs (tens of seconds to minutes for low earth orbit sattelites compared to fractions of a second to a few tens of seconds for fireballs), velocity can be measured by the movement from one frame to another, and an LC shutter is not required.

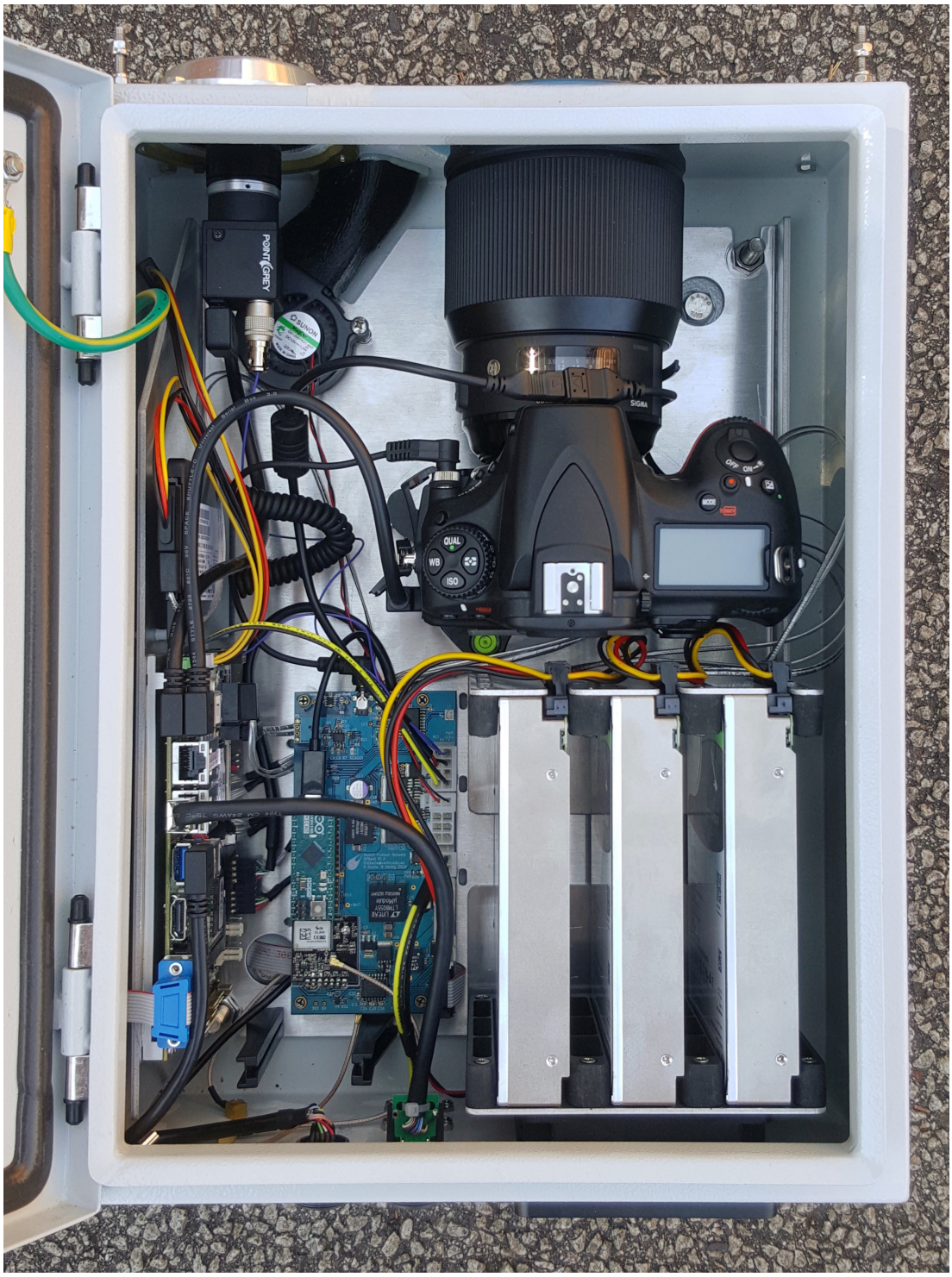


Figure 5.22: DFN satellite and astronomical observatory

Few changes were required to accommodate the new lenses. A 100 mm longer enclosure (400×300×150 mm) was used, and the flange was swapped for a 1 mm thick glass window due to the design of the lens which would have required significant mechanical modifications to fit a flange without pooling full of water. The outer blower duct was modified to fit and evenly direct air across the window. The video camera was retained to provide a wide field of view camera, but is not currently used. The cameras were mounted on modified stands allowing them to be pointed at varying elevations.

The observatories use three 10 TB drives and currently capture four images per minute with an exposure time of five seconds per image (these operational parameters can be adjusted as required). Preliminary results show the detection of ≈800 satellites per night, and triangulations have been performed to compare the performance of triangulated wide field observations to traditional single station satellite observations.

## 5.7 Results

The original production observatory design was significantly more cost effective than originally envisioned and allowed the DFN to expand to cover over 2.5 million $km^2$ (2.5 times the original goal). The observatories also met the other design requirements for a practical and reliable observatory with a long service interval (as detailed in chapter 3). The observatories met or exceeded the design goals, with spatial precision of ≈1 arcminute[24], [141], timing precision better than one millisecond and a limiting magnitude of 0.5. Now that the observatory design and deployment is mostly complete the network is producing high quality scientific data and also the analysis of the network performance has started. For some initial results from the network see [141] and [45] which discuss the astrometry, trajectory residuals and the problem with the straight line assumption.

The recovery of the Murrili and Dingle Dell meteorites with orbits prove the utility and viability of the network. The success of the Australian network in the Weatbelt, Nullarbor and South Australia spurred the global expansion, and as this would require a number of new observatories to be manufactured the decision

was made to revise the design to improve the maintainability and manufacturability from the experience with the initial version.

The DFNEXT systems are significantly easier to assemble than the previous generation observatories. This is mainly due to the use of the CNC bent backplate with preinstalled self clinching fasteners, improved wiring design and the modularity of the new design which allows components to be assembled in large batches and to be easily swapped in the field. The service interval of the observatory has also been extended to approximately 20 months (using three 10 TB drives). These changes will make these observatories more maintainable for collaborators, which was the main objective of this revision. The other design changes were successful too. The swap to switching regulators reduced overall power consumption even with the move to a more capable but slightly more power hungry PC. The new digital video cameras should allow better observations than the previous analogue cameras due to the increased resolution, image metadata detailing the exposure settings at all times, the ability to change exposure settings on the fly and the new GNSS synchronised capture capability. More time will be required to determine if the objective of better reliability was achieved, but the usability improvements are already paying dividends; manufacture and servicing are noticeably easier. The improved temperature management has been implemented, but testing in colder climates is required to assess performance. (Canadian systems are being deployed shortly.)

### 5.7.1 Lessons Learned

Overall, the design process of the observatories evolved as expected from the outset. The revisions made along the way were expected with the "release early, release often" approach. The fact that the same team is designing, building, maintaining and processing the data from the observatories has had a large impact on the evolution of the design over time. The tight feedback loop from this arrangement has resulted in a significantly improved final product. Whilst the performance of the observatories has already been discussed chapter 3, the implications of a few design decisions are particularly notable and will be discussed here.

The Samyang 8mm f/3.5 fisheye lens was chosen for its favourable projection when considering that most fireballs will appear at low elevations due to the distances between cameras. In hindsight, the decision to use a lens with a stereographic projection was correct, as the median elevation for fireball observations with the current network is only 22.1 degrees above the horizon. The spatial precision of stereographic lenses (in the elvation direction) is noticeably better than the alternatives at these elevations.

The choice of the particular Samyang 8mm f/3.5 fish-eye lens did have some downsides, however. This lens suffers from noticeable manufacturing variability, meaning that a significant number of lenses ordered are unusable (approximately half in one particularly bad shipment). This issue seems to vary over time, but this may be due to more stringent testing once the issue was detected. Some attempts have been made to have the performance of the lenses improved by optical adjustment by a third party, but this has not resulted in notable improvement. Despite these problems, there are currently no plans to move away from the Samyang 8mm f/3.5 fisheye, as it is the only stereographic fisheye lens widely available.

During the concept design phase, the focus was on open state transmittance of the modulator and low light sensitivity of the camera. As more data is collected on infrequent very bright (magnitude -15 and brighter) fireballs (which are likely to produce meteorites), it has become evident that modulator contrast and sensor dynamic range is more important than originally thought, and that these characteristics are more important than the open state transmittance of the modulator and low light sensitivity of the camera. Some work is currently ongoing to determine if it is practical to modify the camera or lens to allow the aperture iris to be manipulated during an exposure. This would make it possible to stop down the lens during a bright fireball event and avoid sensor saturation that can obscure position and timing.

## 5.8 Future Evolution

The exact cause of the slight image degradation due to to the insertion of the LC shutter in the optical path is currently unclear. Work is currently under way to determine this, as, once the source is known, there may be an opportunity to rectify the issue. The newest hypothesis is that the degradation could be caused by wavefront errors due to slight variations in thickness across the shutter, not by the thickness of the shutter itself. If this is the case, it might be possible to reduce these wavefront errors by using a thicker but flatter shutter substrate; if this works well it might even be possible to move to a thicker but much higher contrast dual cell LC shutter to improve results for very bright fireballs. Even if the performance of the shutter cannot be improved, it may also be possible to improve the spatial precision by stopping the lens down slightly more (reducing the operating aperture). The reduction in transmitted light has to be compared to the improvement in image quality to make this decision.

As the quality of the optical observations are generally good enough for the triangulation of fireball trajectories, and improvements in precision would not result in appreciably smaller ground search areas, new developments will focus on adding new capabilities to complement the long exposure optical observations. Some options that are being investigated include the addition of a radiometer and microbarometer to record high temporal resolution light curves and any meteoroid generated infrasound. High sample rate (kHz range) light curves should allow better mass estimations by either allowing the incorporation of brightness data into the dynamic method or allowing the comparison of dynamic and photometric masses. Infrasound can help measure meteoroid energy deposition into the atmosphere which may provide some additional insight into meteoroid mass.

Whilst the observatory hardware is at a relatively stable point, there are still software improvements that can be made. A significant amount of work has been expended to reduce the dead time between exposures. Due to the particularities of the Nikon camera's firmware, solving this problem has not been straightforward. The solution to reduce this delay as much as possible is nearly ready for deployment onto the observatory PCs, but some longer term testing is required before it is implemented across the network. Once this change is deployed, there

will be a move from observing software improvements to maintenance software improvements. Better automatic monitoring and automatic problem reporting will help increase observatory uptime and allow for better planning of maintenance in the future.

## 5.9 Conclusions

The latest DFN observatory design has met all the requirements for a reliable, practical and precise fireball observatory with a long service interval. Future work will focus on making incremental improvements to the observatory software and imaging hardware (as improved off-the-shelf hardware becomes available). The revisions made between the DFNSMALL and DFNEXT iterations have improved manufacturability and serviceability and extended the service interval. Future directions for DFN hardware development will explore new types of instrumentation to complement the proven stills based observatories and expand the science capabilities of this successful network.

# References


[22] P. Spurný, J. Borovička, and L. Shrbený, "Automation of the Czech part of the European fireball network: equipment, methods and first results," *Proceedings of the International Astronomical Union*, vol. 2, no. S236, pp. 121–130, 2006.

[24] R. M. Howie, J. Paxman, P. A. Bland, M. C. Towner, M. Cupak, E. K. Sansom, and H. A. R. Devillepoix, "How to build a continental scale fireball camera network," *Experimental Astronomy*, vol. 43, no. 3, pp. 237–266, 2017. DOI: 10.1007/s10686-017-9532-7. [Online]. Available: https://doi.org/10.1007%2Fs10686-017-9532-7.

[31] P. Bland, P. Spurný, A. Bevan, K. Howard, M. Towner, G. Benedix, R. Greenwood, L. Shrbený, I. Franchi, G. Deacon, *et al.*, "The Australian Desert Fireball Network: a new era for planetary science," *Australian Journal of Earth Sciences*, vol. 59, no. 2, pp. 177–187, 2012.

[34] P. A. Bland, P. Spurný, M. C. Towner, A. W. Bevan, A. T. Singleton, W. F. Bottke, R. C. Greenwood, S. R. Chesley, L. Shrbený, J. Borovička, Z. Ceplecha, T. P. McClafferty, V. David, G. K. Benedix, G. Deacon, K. T. Howard, I. A. Franchi, and R. M. Hough, "An anomalous basaltic meteorite from the innermost main belt," *Science*, vol. 325, no. 5947, pp. 1525–1527, 2009.

[38] P. Spurný, P. A. Bland, L. Shrbený, J. Borovička, Z. Ceplecha, A. Singelton, A. W. Bevan, D. Vaughan, M. C. Towner, T. P. McClafferty, *et al.*, "The Bunburra Rockhole meteorite fall in SW Australia: fireball trajectory, luminosity, dynamics, orbit, and impact position from photographic and photoelectric records," *Meteoritics & Planetary Science*, vol. 47, no. 2, pp. 163–185, 2012.

[45] E. K. Sansom, T. Jansen-Sturgeon, M. G. Rutten, H. A. Devillepoix, P. A. Bland, R. M. Howie, M. A. Cox, M. C. Towner, M. Cupák, and B. A. Hartig, "3D Meteoroid Trajectories," *Icarus*, vol. 321, pp. 388–406, 2019, ISSN: 0019-1035. DOI: 10.1016/j.icarus.2018.09.026.

[64] A. T. Jull, "Terrestrial ages of meteorites," in *Accretion of extraterrestrial matter throughout Earth's history*, Springer, 2001, pp. 241–266.

[79] M. Towner, P. Bland, P. Spurný, G. Benedix, K. Dyl, R. Greenwood, J. Gibson, I. Franchi, L. Shrbený, A. Bevan, *et al.*, "Mason Gully: The second meteorite recovered by the Desert Fireball Network," vol. 74, 2011, p. 5124.

[85] F. Colas, B. Zanda, J. Vaubaillon, S. Bouley, C. Marmo, Y. Audureau, M. K. Kwon, J.-L. Rault, S. Caminade, P. Vernazza, *et al.*, "French fireball network FRIPON," in *International Meteor Conference Mistelbach, Austria*, 2015, pp. 37–40.

[111] LC-Tec, *Fast Optical Shutter Series*. Jan. 2013. [Online]. Available: `http://www.lc-tec.se/products/fast-optical-shutters/`.

[141] H. A. Devillepoix, E. K. Sansom, P. A. Bland, M. C. Towner, M. Cupák, R. M. Howie, T. Jansen-Sturgeon, M. A. Cox, B. A. Hartig, G. K. Benedix, *et al.*, "The Dingle Dell meteorite: A Halloween treat from the Main Belt," *Meteoritics & Planetary Science*, vol. 53, no. 10, pp. 2212–2227, DOI: `10.1111/maps.13142`. eprint: `https://onlinelibrary.wiley.com/doi/pdf/10.1111/maps.13142`. [Online]. Available: `https://onlinelibrary.wiley.com/doi/abs/10.1111/maps.13142`.

[143] gPhoto Contributors, *gPhoto Home*, Jul. 2017. [Online]. Available: `http://gphoto.org`.

[144] Nikon Inc., *How many pictures has my camera taken? How many will it take?* Jul. 2017. [Online]. Available: `https://www.nikonimgsupport.com/ni/NI_article?lang=en_US&articleNo=000003332`.

[145] J. L. West, "Polymer-Dispersed Liquid Crystals," in *Liquid-Crystalline Polymers*, ch. 32, pp. 475–495. DOI: `10.1021/bk-1990-0435.ch032`. eprint: `http://pubs.acs.org/doi/pdf/10.1021/bk-1990-0435.ch032`. [Online]. Available: `http://pubs.acs.org/doi/abs/10.1021/bk-1990-0435.ch032`.

[146] H. Craighead, J. Cheng, and S. Hackwood, "New display based on electrically induced index-matching in an inhomogeneous medium," *Applied Physics Letters*, vol. 40, no. 1, pp. 22–24, 1982.

[147] Switch Glass, *The Haze Factor – R&D Update*, Jul. 2017. [Online]. Available: `http://www.switchglass.com.au/haze-factor`.

[148] Switch Glass, *FAQs*, Jul. 2017. [Online]. Available: `http://www.switchglass.com.au/faqs`.

[149] Switch Glass, "Switchable Privacy Class Technical Information & Installation Guide," Mar. 2015. [Online]. Available: http://www.switchglass.com.au/wp-content/uploads/2016/02/Switchglass-Tech-Info-and-Install-Guide-Revised-020315.pdf.

[150] R. Hikmet and H. Kemperman, "Switchable mirrors of chiral liquid crystal gels," *Liquid crystals*, vol. 26, no. 11, pp. 1645–1653, 1999.

[151] R. Hikmet and H. Kemperman, "Electrically switchable mirrors and optical components made from liquid-crystal gels," *Nature*, vol. 392, no. 6675, pp. 476–479, 1998.

[152] L. Li and D. Yang, *Single layer multi-state ultra-fast cholesteric liquid crystal device and the fabrication methods thereof*, US Patent 6,674,504, Jan. 2004. [Online]. Available: https://www.google.com/patents/US6674504.

[153] Kent Optronics Inc., *Switchable Mirror / Switchable Glass*, Jul. 2017. [Online]. Available: http://www.kentoptronics.com/mirror.html.

[154] STMicroelectronics, "Push-pull Four Channel Driver with Diodes," Jul. 2003. [Online]. Available: http://www.st.com/content/ccc/resource/technical/document/datasheet/04/ac/22/f9/20/5d/43/a1/CD00000059.pdf/files/CD00000059.pdf/jcr:content/translations/en.CD00000059.pdf.

# Chapter 6

# Conclusions and Future Work

The primary objective of this work was to develop a more cost effective, high performance, autonomous fireball observatory with a long service interval to expand the Desert Fireball Network to cover one million km$^2$ in order to regularly recover planetary samples of known origin for the advancement of Solar System science.

The expansion of previous fireball camera networks was hampered by the high upfront and ongoing observatory costs as well as maintenance requirements. One factor contributing to the high upfront costs was the need for a separate timing subsystem for determining a fireball's time of arrival. This is required for the calculation of an accurate heliocentric pre-atmospheric entry orbit due to the Earth's constant orbital motion and rotation. A new timing technique was developed that embeds timecodes constructed from de Bruijn sequences into the long exposure images. The technique embeds absolute timing (time of arrival) along with relative timing (for velocity determination) directly into the image which has two main benefits. Fireball observatories can be made less complex and more cost effective as the need for a separate absolute timing subsystem (such as the photomultiplier tubes used by previous observatories) is eliminated. In addition, the data produced is more compatible with automated reduction techniques as records from multiple sensors do not need to be aligned. The time encoding technique was implemented with an electro-optic liquid crystal shutter which is

precisely controlled by a microcontroller and synchronised with GNSS time and has a fast enough response time to allow timing precision of better than one millisecond. This solid state approach using liquid crystal shutters is also much less expensive than the conventional mechanical rotating or switching shutters which must be manufactured and assembled with great precision.

In addition to the cost reductions enabled by the new timing technique, a number of other design aspects have allowed the DFN's new digital fireball observatories to be significantly more cost effective than previous designs while retaining high imaging performance. The use of off-the-shelf consumer parts for the main components including the camera, lens and embedded PC lowers costs and makes it possible to take advantage of the fast development pace of consumer products for future upgrades. Computer aided design and efficient manufacturing processes have also helped keep production costs low, and design for assembly, installation and maintenance has made it possible to build, deploy and maintain the network with a small team. The resulting design has similar spatial precision ($\approx$1 arcminute) and better timing precision ($<$1 ms) compared to previous successful fireball observatory designs (such as those used by the European Fireball Network and the DFN in its initial phase), but the upfront per observatory cost was reduced by a factor of about ten. Power usage, installation time, size and weight were also significantly reduced, and the service interval was significantly extended to allow deployment to remote unpopulated locations. The success of the observatory design has allowed the DFN to expand to cover over 2.5 million km$^2$ of good meteorite searching terrain across the Australian Outback (2.5 times the initial goal for the digital expansion).

The observatory design was refined to produce a second iteration with a nearly identical observational capability but a number of improvements to other areas including service interval, modularity and ease of manufacture. The aim of the improvements is to make the system more suitable for deployment and maintenance by overseas collaborators (which has already started with the distribution of more than 20 observatories). The service interval has been extended to $\approx$20 months between drive changes and the modularity of the internal subsystems has been significantly improved to simplify maintenance. The flexibility of the design was also demonstrated with the creation of a narrow field of view satellite

observatory.

The de Bruijn time encoding technique was further developed for other motion tracking applications which require high spatial and temporal precision photographic observations. A number of different configurations for differing scenarios were described, and a proof of concept implementation operating at 36 megapixels and 1000 Hz was demonstrated. As a part of this work alternate sequence encodings were explored, one of which was deployed to the DFN observatories resulting in better observations with less fireball velocity scatter.

The result of the work described in this thesis is a reliable continental scale fireball camera network covering more than a third of Australia, which is large enough to observe several meteorite dropping fireballs per year. The new digital network has recovered two meteorites with orbits (Murrili and Dingle Dell), observed more than a dozen additional meteorite dropping fireballs and generated a dataset of more than 1000 bright fireballs with orbits (the largest dataset of this kind ever collected). As a regular source of planetary samples with known origins, in the form of pre-atmospheric entry orbits, the DFN now provides a fresh opportunity to examine the formation and evolution of the Solar System.

## 6.1 Contributions

This work has made a substantive original contribution to the field of planetary science by enabling the digital expansion of the DFN. This contribution can be split up into four main components.

De Bruijn timecodes provide a new way of encoding both the relative and absolute timing of fireball events into long exposure fireball images. This eliminates the need for a separate timing subsystem, and can substantially reduce the cost of a fireball camera observatory, especially when combined with the use of a solid state optical modulator such as a liquid crystal shutter instead of a mechanical shutter.

The careful design of the DFN's digital fireball observatories with a focus on ease of manufacture, assembly, installation and maintenance in addition to high quality observations has allowed the DFN to exceed its initial coverage goal and expand to cover over one third of Australia. This makes it the world's biggest fireball camera network and is of sufficient size to observe several meteorite dropping fireballs per year. The design aspects that can be attributed to this work are the mechanical design, electronic design, firmware development as well as the manufacture and assembly process development; some small contributions have also been made to the observatory software and data processing pipeline.

The extension of the de Bruijn time encoding technique to other applications has demonstrated that it can capture trajectory data at a higher spatial and temporal precision than traditional approaches which are limited by the data bandwidth involved. Encoding techniques explored as part of this work have been applied to the camera network implementation and yielded improvements to fireball observations.

A significant contribution has also been made to the construction, deployment and maintenance of the DFN. This has enabled the recovery of the Murrili and Dingle Dell meteorites, observation of more than a dozen other meteorite producing fireballs, collection of a dataset of more than 1000 bright fireballs with orbits, and will result in the recovery of more meteorites with orbits in the future.

## 6.2 Future Work

The latest iteration of the fireball observatory hardware satisfies all of the design requirements for a reliable high performance yet cost effective fireball observatory; few significant changes to the design are anticipated in the near term. In the longer term, it is possible that advances in the field of high resolution digital video may warrant the exploration of a digital video based high spatial and temporal precision all-sky fireball observatory. The DFN is well positioned to make this transition if required, as many of the design aspects would be transferable.

Future improvements to the DFN will focus on small refinements to the operation of the observatories through software updates and the inclusion of addition sensors within the network to provide observations which are complementary to the photographic data. Currently the most difficult parts of meteorite recovery are mass determination, dark flight modelling (due to the uncertainty in the atmospheric wind models) and finding the meteorite within the search area. Additional sensors under consideration include high temporal resolution radiometers to produce detailed fireball lightcurves and microbarometers to record the infrasound signatures of fireball events. These types of records will provide additional data that may be useful for mass or density determination to help constrain the search area. Improving wind estimations in the stratosphere is difficult, but there may be ways to assess the accuracy of the modelling which could help inform search and recovery decisions even if fall position estimates cannot be improved. The relatively featureless terrain of the Australian Outback presents a tempting opportunity to partially automate the search for meteorites using unmanned aerial vehicles in concert with computer vision algorithms.

# Appendices

# Appendix A

# Submillisecond fireball timing using de Bruijn timecodes

Robert M. Howie[1], Jonathan Paxman[1], Philip A. Bland[2], Martin C. Towner[2], Eleanor K. Sansom[2], and Hadrein A. R. Devillepoix[2]

[1]Department of Mechanical Engineering, Curtin University, Perth, Australia
[2]Department of Applied Geology, Curtin University, Perth, Australia

*This article is published in Meteoritics & Planetary Science (available at DOI: 10.1111/maps.12878),* 

The published version of "Submillisecond fireball timing using de Bruijn timecodes" is not included in the open access version of this thesis.

**JOHN WILEY AND SONS LICENSE TERMS AND CONDITIONS**

Nov 21, 2018

This Agreement between Robert Howie ("You") and John Wiley and Sons ("John Wiley and Sons") consists of your license details and the terms and conditions provided by John Wiley and Sons and Copyright Clearance Center.

| | |
|---|---|
| License Number | 4473500436126 |
| License date | Nov 21, 2018 |
| Licensed Content Publisher | John Wiley and Sons |
| Licensed Content Publication | Meteoritics & Planetary Science |
| Licensed Content Title | Submillisecond fireball timing using de Bruijn timecodes |
| Licensed Content Author | Robert M. Howie, Jonathan Paxman, Philip A. Bland, et al |
| Licensed Content Date | May 16, 2017 |
| Licensed Content Volume | 52 |
| Licensed Content Issue | 8 |
| Licensed Content Pages | 14 |
| Type of use | Dissertation/Thesis |
| Requestor type | Author of this Wiley article |
| Format | Electronic |
| Portion | Full article |
| Will you be translating? | No |
| Title of your thesis / dissertation | Augmentation and Optimisation of the Australian Desert Fireball Network to Enable New Planetary Science |
| Expected completion date | Dec 2018 |
| Expected size (number of pages) | 1 |
| Requestor Location | Robert Howie<br>GPO Box U1987<br><br>Perth, WA 6845<br>Australia<br>Attn: Robert Howie |
| Publisher Tax ID | EU826007151 |
| Total | 0.00 AUD |
| Terms and Conditions | |

## TERMS AND CONDITIONS

This copyrighted material is owned by or exclusively licensed to John Wiley & Sons, Inc. or one of its group companies (each a"Wiley Company") or handled on behalf of a society with which a Wiley Company has exclusive publishing rights in relation to a particular work (collectively "WILEY"). By clicking "accept" in connection with completing this licensing transaction, you agree that the following terms and conditions apply to this transaction (along with the billing and payment terms and conditions established by the Copyright Clearance Center Inc., ("CCC's Billing and Payment terms and conditions"), at the time that you opened your RightsLink account (these are available at any time at http://myaccount.copyright.com).

### Terms and Conditions

- The materials you have requested permission to reproduce or reuse (the "Wiley Materials") are protected by copyright.

- You are hereby granted a personal, non-exclusive, non-sub licensable (on a stand-alone basis), non-transferable, worldwide, limited license to reproduce the Wiley Materials for the purpose specified in the licensing process. This license, **and any CONTENT (PDF or image file) purchased as part of your order,** is for a one-time use only and limited to any maximum distribution number specified in the license. The first instance of republication or reuse granted by this license must be completed within two years of the date of the grant of this license (although copies prepared before the end date may be distributed thereafter). The Wiley Materials shall not be used in any other manner or for any other purpose, beyond what is granted in the license. Permission is granted subject to an appropriate acknowledgement given to the author, title of the material/book/journal and the publisher. You shall also duplicate the copyright notice that appears in the Wiley publication in your use of the Wiley Material. Permission is also granted on the understanding that nowhere in the text is a previously published source acknowledged for all or part of this Wiley Material. Any third party content is expressly excluded from this permission.

- With respect to the Wiley Materials, all rights are reserved. Except as expressly granted by the terms of the license, no part of the Wiley Materials may be copied, modified, adapted (except for minor reformatting required by the new Publication), translated, reproduced, transferred or distributed, in any form or by any means, and no derivative works may be made based on the Wiley Materials without the prior permission of the respective copyright owner.**For STM Signatory Publishers clearing permission under the terms of the STM Permissions Guidelines only, the terms of the license are extended to include subsequent editions and for editions in other languages, provided such editions are for the work as a whole in situ and does not involve the separate exploitation of the permitted figures or extracts,** You may not alter, remove or suppress in any manner any copyright, trademark or other notices displayed by the Wiley Materials. You may not license, rent, sell, loan, lease, pledge, offer as security, transfer or assign the Wiley Materials on a stand-alone basis, or any of the rights granted to you hereunder to any other person.

- The Wiley Materials and all of the intellectual property rights therein shall at all times remain the exclusive property of John Wiley & Sons Inc, the Wiley Companies, or their respective licensors, and your interest therein is only that of having possession of and the right to reproduce the Wiley Materials pursuant to Section 2 herein during the continuance of this Agreement. You agree that you own no right, title or interest in or to the Wiley Materials or any of the intellectual property rights therein. You shall have no rights hereunder other than the license as provided for above in Section 2. No right, license or interest to any trademark, trade name, service mark or other branding ("Marks") of WILEY or its licensors is granted hereunder, and you agree that you shall not assert any such right, license or interest with respect thereto

- NEITHER WILEY NOR ITS LICENSORS MAKES ANY WARRANTY OR REPRESENTATION OF ANY KIND TO YOU OR ANY THIRD PARTY, EXPRESS, IMPLIED OR STATUTORY, WITH RESPECT TO THE MATERIALS OR THE ACCURACY OF ANY INFORMATION CONTAINED IN THE MATERIALS, INCLUDING, WITHOUT LIMITATION, ANY IMPLIED WARRANTY OF MERCHANTABILITY, ACCURACY, SATISFACTORY QUALITY, FITNESS FOR A PARTICULAR PURPOSE, USABILITY, INTEGRATION OR NON-INFRINGEMENT AND ALL SUCH WARRANTIES ARE HEREBY EXCLUDED BY WILEY AND ITS LICENSORS AND WAIVED BY YOU.

- WILEY shall have the right to terminate this Agreement immediately upon breach of this Agreement by you.

- You shall indemnify, defend and hold harmless WILEY, its Licensors and their respective directors, officers, agents and employees, from and against any actual or threatened claims, demands, causes of action or proceedings arising from any breach of this Agreement by you.

- IN NO EVENT SHALL WILEY OR ITS LICENSORS BE LIABLE TO YOU OR ANY OTHER PARTY OR ANY OTHER PERSON OR ENTITY FOR ANY SPECIAL, CONSEQUENTIAL, INCIDENTAL, INDIRECT, EXEMPLARY OR PUNITIVE DAMAGES, HOWEVER CAUSED, ARISING OUT OF OR IN CONNECTION WITH THE DOWNLOADING, PROVISIONING, VIEWING OR USE OF THE MATERIALS REGARDLESS OF THE FORM OF ACTION, WHETHER FOR BREACH OF CONTRACT, BREACH OF WARRANTY, TORT, NEGLIGENCE, INFRINGEMENT OR OTHERWISE (INCLUDING, WITHOUT LIMITATION, DAMAGES BASED ON LOSS OF PROFITS, DATA, FILES, USE, BUSINESS OPPORTUNITY OR CLAIMS OF THIRD PARTIES), AND WHETHER OR NOT THE PARTY HAS BEEN ADVISED OF THE POSSIBILITY OF SUCH DAMAGES. THIS LIMITATION SHALL APPLY NOTWITHSTANDING ANY FAILURE OF ESSENTIAL PURPOSE OF ANY LIMITED REMEDY PROVIDED HEREIN.

- Should any provision of this Agreement be held by a court of competent jurisdiction to be illegal, invalid, or unenforceable, that provision shall be deemed amended to achieve as nearly as possible the same economic effect as the original provision, and the legality, validity and enforceability of the remaining provisions of this Agreement shall not be affected or impaired thereby.

- The failure of either party to enforce any term or condition of this Agreement shall not constitute a waiver of either party's right to enforce each and every term and condition of this Agreement. No breach under this agreement shall be deemed waived or excused by either party unless such waiver or consent is in writing signed by the party granting such waiver or consent. The waiver by or consent of a party to a breach of any provision of this Agreement shall not operate or be construed as a waiver of or consent to any other or subsequent breach by such other party.

- This Agreement may not be assigned (including by operation of law or otherwise) by you without WILEY's prior written consent.

- Any fee required for this permission shall be non-refundable after thirty (30) days from receipt by the CCC.

- These terms and conditions together with CCC's Billing and Payment terms and conditions (which are incorporated herein) form the entire agreement between you and WILEY concerning this licensing transaction and (in the absence of fraud) supersedes all prior agreements and representations of the parties, oral or written. This Agreement may not be amended except in writing signed by both parties. This Agreement shall be binding upon and inure to the benefit of the parties' successors, legal representatives, and authorized assigns.

- In the event of any conflict between your obligations established by these terms and conditions and those established by CCC's Billing and Payment terms and conditions, these terms and conditions shall prevail.

- WILEY expressly reserves all rights not specifically granted in the combination of (i) the license details provided by you and accepted in the course of this licensing transaction, (ii) these terms and conditions and (iii) CCC's Billing and Payment terms and conditions.

- This Agreement will be void if the Type of Use, Format, Circulation, or Requestor Type was misrepresented during the licensing process.

- This Agreement shall be governed by and construed in accordance with the laws of the State of New York, USA, without regards to such state's conflict of law rules. Any legal action, suit or proceeding arising out of or relating to these Terms and Conditions or the breach thereof shall be instituted in a court of competent jurisdiction in New York County in the State of New York in the United States of America and each party hereby consents and submits to the personal jurisdiction of such court, waives any objection to venue in such court and consents to service of process by registered or certified mail, return receipt requested, at the last known address of such party.

**WILEY OPEN ACCESS TERMS AND CONDITIONS**

Wiley Publishes Open Access Articles in fully Open Access Journals and in Subscription journals offering Online Open. Although most of the fully Open Access journals publish open access articles under the terms of the Creative Commons Attribution (CC BY) License only, the subscription journals and a few of the Open Access Journals offer a choice of Creative Commons Licenses. The license type is clearly identified on the article.

**The Creative Commons Attribution License**

The Creative Commons Attribution License (CC-BY) allows users to copy, distribute and transmit an article, adapt the article and make commercial use of the article. The CC-BY license permits commercial and non-

**Creative Commons Attribution Non-Commercial License**

The Creative Commons Attribution Non-Commercial (CC-BY-NC)License permits use, distribution and reproduction in any medium, provided the original work is properly cited and is not used for commercial purposes.(see below)

**Creative Commons Attribution-Non-Commercial-NoDerivs License**

The Creative Commons Attribution Non-Commercial-NoDerivs License (CC-BY-NC-ND) permits use, distribution and reproduction in any medium, provided the original work is properly cited, is not used for commercial purposes and no modifications or adaptations are made. (see below)

**Use by commercial "for-profit" organizations**

Use of Wiley Open Access articles for commercial, promotional, or marketing purposes requires further explicit permission from Wiley and will be subject to a fee.

Further details can be found on Wiley Online Library
http://olabout.wiley.com/WileyCDA/Section/id-410895.html

**Other Terms and Conditions:**

**v1.10 Last updated September 2015**

# Appendix B

# How to build a continental scale fireball camera network

Robert M. Howie[1], Jonathan Paxman[1], Philip A. Bland[2], Martin C. Towner[2], Martin Cupak[2], Eleanor K. Sansom[2], and Hadrien A. R. Devillepoix[2]

[1]Department of Mechanical Engineering, Curtin University, Perth, Australia
[2]Department of Applied Geology, Curtin University, Perth, Australia

*This article is published in Experimental Astronomy (available at DOI: 10.1007/s10686-017-9532-7),* © *Springer Science+Business Media Dordrecht 2017.*

*Experimental Astronomy, How to build a continental scale fireball camera network, Volume 43, 2017, pp 237–266, Robert M. Howie, Jonathan Paxman, Philip A. Bland, Martin C. Towner, Eleanor K. Sansom, and Hadrien A. R. Devillepoix,* © *Springer Science+Business Media Dordrecht 2017 with permission of Springer*

The published version of "How to build a continental scale fireball camera network" is not included in the open access version of this thesis.

## SPRINGER NATURE LICENSE
## TERMS AND CONDITIONS

Nov 21, 2018

This Agreement between Robert Howie ("You") and Springer Nature ("Springer Nature") consists of your license details and the terms and conditions provided by Springer Nature and Copyright Clearance Center.

| | |
|---|---|
| License Number | 4473500253047 |
| License date | Nov 21, 2018 |
| Licensed Content Publisher | Springer Nature |
| Licensed Content Publication | Experimental Astronomy |
| Licensed Content Title | How to build a continental scale fireball camera network |
| Licensed Content Author | Robert M. Howie, Jonathan Paxman, Philip A. Bland et al |
| Licensed Content Date | Jan 1, 2017 |
| Licensed Content Volume | 43 |
| Licensed Content Issue | 3 |
| Type of Use | Thesis/Dissertation |
| Requestor type | academic/university or research institute |
| Format | electronic |
| Portion | full article/chapter |
| Will you be translating? | no |
| Circulation/distribution | >50,000 |
| Author of this Springer Nature content | yes |
| Title | Augmentation and Optimisation of the Australian Desert Fireball Network to Enable New Planetary Science |
| Institution name | Curtin University |
| Expected presentation date | Dec 2018 |
| Requestor Location | Robert Howie<br>GPO Box U1987<br><br>Perth, WA 6845<br>Australia<br>Attn: Robert Howie |
| Billing Type | Invoice |
| Billing Address | Robert Howie<br>GPO Box U1987<br><br>Perth, Australia 6845<br>Attn: Robert Howie |
| Total | 0.00 AUD |
| Terms and Conditions | |

### Springer Nature Terms and Conditions for RightsLink Permissions

**Springer Nature Customer Service Centre GmbH (the Licensor)** hereby grants you a non-exclusive, world-wide licence to reproduce the material and for the purpose and requirements specified in the attached copy of your order form, and for no other use, subject to the conditions below:

1. The Licensor warrants that it has, to the best of its knowledge, the rights to license reuse of this material. However, you should ensure that the material you are requesting is original to the Licensor

and does not carry the copyright of another entity (as credited in the published version).

If the credit line on any part of the material you have requested indicates that it was reprinted or adapted with permission from another source, then you should also seek permission from that source to reuse the material.

2. Where **print only** permission has been granted for a fee, separate permission must be obtained for any additional electronic re-use.

3. Permission granted **free of charge** for material in print is also usually granted for any electronic version of that work, provided that the material is incidental to your work as a whole and that the electronic version is essentially equivalent to, or substitutes for, the print version.

4. A licence for 'post on a website' is valid for 12 months from the licence date. This licence does not cover use of full text articles on websites.

5. Where **'reuse in a dissertation/thesis'** has been selected the following terms apply: Print rights of the final author's accepted manuscript (for clarity, NOT the published version) for up to 100 copies, electronic rights for use only on a personal website or institutional repository as defined by the Sherpa guideline (www.sherpa.ac.uk/romeo/).

6. Permission granted for books and journals is granted for the lifetime of the first edition and does not apply to second and subsequent editions (except where the first edition permission was granted free of charge or for signatories to the STM Permissions Guidelines http://www.stm-assoc.org/copyright-legal-affairs/permissions/permissions-guidelines/), and does not apply for editions in other languages unless additional translation rights have been granted separately in the licence.

7. Rights for additional components such as custom editions and derivatives require additional permission and may be subject to an additional fee. Please apply to Journalpermissions@springernature.com/bookpermissions@springernature.com for these rights.

8. The Licensor's permission must be acknowledged next to the licensed material in print. In electronic form, this acknowledgement must be visible at the same time as the figures/tables/illustrations or abstract, and must be hyperlinked to the journal/book's homepage. Our required acknowledgement format is in the Appendix below.

9. Use of the material for incidental promotional use, minor editing privileges (this does not include cropping, adapting, omitting material or any other changes that affect the meaning, intention or moral rights of the author) and copies for the disabled are permitted under this licence.

10. Minor adaptations of single figures (changes of format, colour and style) do not require the Licensor's approval. However, the adaptation should be credited as shown in Appendix below.

## Appendix — Acknowledgements:

**For Journal Content:**
Reprinted by permission from [**the Licensor**]: [**Journal Publisher** (e.g. Nature/Springer/Palgrave)] [**JOURNAL NAME**] [**REFERENCE CITATION** (Article name, Author(s) Name), [**COPYRIGHT**] (year of publication)

For **Advance Online Publication papers:**
Reprinted by permission from [**the Licensor**]: [**Journal Publisher** (e.g. Nature/Springer/Palgrave)] [**JOURNAL NAME**] [**REFERENCE CITATION** (Article name, Author(s) Name), [**COPYRIGHT**] (year of publication), advance online publication, day month year (doi: 10.1038/sj.[JOURNAL ACRONYM].)

**For Adaptations/Translations:**
Adapted/Translated by permission from [**the Licensor**]: [**Journal Publisher** (e.g. Nature/Springer/Palgrave)] [**JOURNAL NAME**] [**REFERENCE CITATION** (Article name, Author(s) Name), [**COPYRIGHT**] (year of publication)

**Note: For any republication from the British Journal of Cancer, the following credit line style applies:**

Reprinted/adapted/translated by permission from [**the Licensor**]: on behalf of Cancer Research UK: : [**Journal Publisher** (e.g. Nature/Springer/Palgrave)] [**JOURNAL**

**NAME**] [**REFERENCE CITATION** (Article name, Author(s) Name), [**COPYRIGHT]** (year of publication)

For **Advance Online Publication** papers:
Reprinted by permission from The [**the Licensor**]: on behalf of Cancer Research UK: [**Journal Publisher** (e.g. Nature/Springer/Palgrave)] [**JOURNAL NAME**] [**REFERENCE CITATION** (Article name, Author(s) Name), [**COPYRIGHT**] (year of publication), advance online publication, day month year (doi: 10.1038/sj. [JOURNAL ACRONYM])

**For Book content:**
Reprinted/adapted by permission from [**the Licensor**]: [**Book Publisher** (e.g. Palgrave Macmillan, Springer etc) [**Book Title**] by [**Book author**(s)] [**COPYRIGHT**] (year of publication)

**Other Conditions**:

Version 1.1

# Appendix C

# First Author Conference Papers

# C.1 Advanced Digital Fireball Observatories: Enabling the Expansion of the Desert Fireball Network

Robert M. Howie[1], Jonathan Paxman[1], Philip A. Bland[2], Martin C. Towner[2], Martin Cupak[2] and Eleanor K. Sansom[2]

[1]Department of Mechanical Engineering, Curtin University, Perth, Australia
[2]Department of Applied Geology, Curtin University, Perth, Australia

*This conference abstract was presented at the XXXIst URSI General Assembly and Scientific Symposium (URSIGASS 2014) in Beijing, China.*  General Assembly and Scientific Symposium (URSI GASS), 2014 XXXIth URSI, *October 2014.*

# Advanced Digital Fireball Observatories: enabling the expansion of the Desert Fireball Network

***Robert M. Howie****[*1], ***Jonathan Paxman***[1], ***Phil A. Bland***[2], ***Martin C. Towner***[2], ***Martin Cupák***[2], ***and Eleanor K. Sansom***[2]

[1]Department of Mechanical Engineering, Curtin Univeristy, GPO Box U1987, Perth WA 6845, Australia
robert.howie@postgrad.curtin.edu.au, j.paxman@curtin.edu.au
[2]Department of Applied Geology, Curtin Univeristy, GPO Box U1987, Perth WA 6845, Australia
p.bland@curtin.edu.au, m.towner@curtin.edu.au, eleanor.sansom@postgrad.curtin.edu.au

## Abstract

The Desert Fireball Network (DFN) is an Australian Research Council project designed to track fireballs over approximately one third of Australia. Meteorites with a known orbit, detected and recovered through fireball networks such as the DFN provide information about the formation and history of the Solar System. The requirements and design of an Advanced Digital Fireball Observatory (ADFO) are presented alongside the design challenges and results of field testing. The deployment of over 60 ADFOs will allow the construction of a flexible continental scale planetary science installation producing high quality all-sky data for multiple uses.

## 1. Introduction

Meteorites provide insight into the history and formation of the Solar System, but the value of chance finds is limited due to the meteorite's unknown origin. Weathering and terrestrial contamination can also interfere with geochemical analysis, further limiting the usefulness of chance finds. Sample return missions such as Stardust [1] can provide uncontaminated samples with a known origin. However, space missions are extremely complex and costly. Meteor camera networks provide an alternative method of obtaining meteorites with a known origin, and with minimal contamination and weathering as a result of relatively quick collection.

Estimating meteorite fall positions with sufficient accuracy to enable recovery is particularly challenging, requiring accurate estimates of velocity, position and mass during bright flight, coupled with dark flight modelling taking atmospheric conditions into account. Pre atmospheric orbit calculation only requires the bright flight path and an initial velocity, but the entry mass is required for long term backward orbital calculations and fall location estimation. Meteoroid mass can be determined by the deceleration (the dynamic method [2]) or the luminosity profile (the photometric method) during bright flight. In order to calculate the deceleration with enough precision to accurately estimate the mass, the spatial *and* temporal data of the trajectory need to be highly accurate. The absolute timing data is not required to determine the deceleration and therefore mass, but it is required to determine the pre-atmospheric entry orbit, since the Earth's orientation, and therefore the orientation of the observing camera, is changing with time. The requirement for high precision on the relative timing of the bright flight trajectory is more stringent than the requirement on the absolute timing because estimating the mass accurately is vital to calculating the fall position. An imprecise or inaccurate mass estimate will make meteorite recovery unlikely.

The proof-of-concept phase of the Desert Fireball Network (DFN) commenced in 2002 with the installation of the first prototype film observatory. The trial progressed, and a network of four cameras was operating by 2007. The network comprised four film desert fireball observatories using all-sky fisheye lenses to take night long exposures onto large format sheet film. Rotating mechanical shutters were used to chop the meteor trail into a series of short segments to determine the velocity of the meteor. The film observatories used a photomultiplier tube to obtain a light curve for each meteorite, which was used to calculate fragmentation events and derive absolute timing information. The trial network resulted in two successful meteorite recoveries [3] [4], proving the viability of a meteor camera network based in the Australian Outback. The observatories used numerous custom components and moving parts in the magazine and film handling system, mechanical shutter, retractable sun shade and lens covers leading to high manufacturing and maintenance costs. Operational costs were high due to the price of developing large format film and the satellite data connections. Recent developments in digital imaging technology have pushed image resolution and low light sensitivity to the point where digital systems are now highly suited to applications in fireball camera networks at a fraction of the cost of film based solutions. This advance presented the opportunity to design a more flexible and cost effective meteor observatory in the Advanced Digital Fireball Observatory (ADFO). Reductions in the manufacture, installation and operational costs are significant because they facilitate a much larger network for the same overall cost, resulting in an increased rate of fireball detection and meteorite recovery.

## 2. Requirements

The objective when designing the new digital fireball observatories was to develop a system to record the bright flight trajectory (path and timing data) with sufficient precision for meteorite recovery and which was capable of operating autonomously in remote areas, specifically the Australian Outback. The requirements driven by this task can be broken up

into imaging and operational requirements. The imaging requirements are informed by the practicalities of searching for meteorites on foot. The imaging system must cover nearly the entire night sky and provide sufficient precision to narrow the width of the search area such that searching with a small group of people on foot for one or two weeks has a high likelihood of locating a present meteorite. The precision of the optical system depends on observatory spacing, lens characteristics, image sensor resolution and shutter frequency. The camera spacing must be at least 100 kilometres to make installation and maintenance practical; shorter spacing would result in increased setup and ongoing costs for similar area coverage.

The operational requirements are derived from the remoteness of the areas appropriate for meteor observatory installations. The ideal location has minimal light pollution to enable the detection of faint meteors, and the ideal terrain is flat and light in colour with minimal vegetation in order to maximise the likelihood of a successful search for meteorites on the ground. The Australian Outback and the Nullarbor Plain in particular fit these requirements, but their remoteness presents operational challenges. The inaccessibility and distances between cameras make maintenance trips a costly and time consuming exercise; the observatories need be capable of operating for at least a year between service intervals. Mobile data coverage is rare in these regions, and downloading all captured images over a such a connection is cost prohibitive, so the observatories also need to be able to store up to a year's worth of images locally for download or collection during annual maintenance visits. The power usage of the system also has to be low enough such that it can be powered year round by a small solar photovoltaic (PV) installation. The harsh conditions of the Outback mean that the system must be able to withstand very hot weather (up to ≈50°C), rapid temperature changes, high wind speeds (gusts in excess of 100 km/hr), dust storms, rainfall and condensation.

The expansion of the DFN aims to cover in excess of two million square kilometres. In order to achieve this goal, the initial cost and operating expenses of the fireball observatories need to be as low as possible per square kilometre of coverage whilst still satisfying the other requirements. In order to keep the per system cost low, the manufacturing and assembly time and costs also need to be minimised. Installation must be simple and fast to enable the deployment of such a large network. An installation trip to the Outback usually involves a journey of at least 2000 kilometres including significant distances off-road; the observatories need to be durable enough to be transported to the installation sites and set up without suffering damage.

## 3. Design

The imaging system of the observatory is its primary focus, so this part of the design took precedence over the other aspects. The choices made for the imaging system influenced nearly all other parts of the design. In order to keep costs as low as possible, off the shelf components were used wherever possible, including the imaging components. Two different options were tested: a Digital Single Lens Reflex (DSLR) camera with a full frame (36 x 24 mm) sensor and a mirrorless camera with an APS-C sized (24 x 16 mm) sensor. Cameras with smaller sensors were not considered due to their poor low light performance; scientific and astronomical cameras were briefly considered but excluded due to their high cost. The short sensor to lens mount flange distance on mirrorless cameras allows a wider selection lenses, but the full frame option was selected due to better low light noise performance from the larger sensor and lens apertures available: specifically, the 36 Megapixel Nikon D800E DSLR and the Samyang 8mm f/3.5 fisheye lens with removable hood. This combination crops off a small portion of the sky at the top and bottom of the image, but the loss is acceptable, and the larger image circle results in a higher angular resolution across the area that is visible. The D800E is suited for use in an autonomous observatories because it can be easily controlled from a computer using gphoto2 [5].

A mechanical rotating shutter was quickly eliminated in order to create a reliable and easy to manufacture design. The moving parts and tight tolerances required would have significantly increased the cost of manufacture over a solid state option. Designing a mechanical rotating shutter to work with a DSLR would be difficult as there is no space between the camera and lens, but the design could be used with a mirrorless camera's shorter flange distance. Three different types of electro-optical shutters were tested: Liquid Crystal (LC), Polymer Dispersed Liquid Crystal (PDLC) film and metal hydride switchable mirrors. PDLC film is not a suitable modulator because it functions by dispersing light in its closed state resulting in low contrast images for our application. LC shutters were selected due to their low cost, high contrast ratio between their open and closed states, low switching times and proven reliability. The only drawback to the LC shutters is their low transmittance in the open state (≈38%[6]). Metal hydride switchable mirrors offer a solution to this problem, but they are much more expensive and have unproven reliability; these are currently being tested as a drop in replacement for the LC shutters at a later stage.

The LC shutter is driven with a square alternating current waveform produced by an H-bridge controlled with an Atmel Atmega32u4 microcontroller. This microcontroller was selected for its USB communication functionality and its ready availability on the Freetronics LeoStick development and breakout board. The LUFA library is used for USB and bootloader support [7]. This enables remote updates to the microcontroller firmware to be flashed over the USB connection. The LC shutter is used to chop the meteor trails in the still image at 10 Hz allowing the entry velocity and deceleration of the meteor to be calculated with sufficient precision for fall position estimation. The microcontroller uses a GPS module to ensure timing accuracy. A video camera is used in conjunction with the LC shutter to obtain the arrival time and to track the brightness without interruption. The Watec WAT-902H2 ULTIMATE video camera was selected due to its exceptional

low light sensitivity, and is paired with a Fujinon all-sky fisheye lens.

A small form factor computer was required to control the camera, download and store images, interact with the microcontroller, manage the observatory and provide a communication link over an Ethernet, Wi-Fi, mobile data or satellite connection. The primary requirements on the computer were small size, low power consumption, a miniPCIe port, and enough processing power to be able to monitor a video stream for events. The Advantech MIO-5250 met these requirements and was selected after some initial testing and benchmarking. The two options for image storage were to filter and retain only the images containing meteors or to keep all images. The decision was made to keep all images to create a high resolution all sky dataset captured from multiple locations for astronomical, meteorological and other scientific uses. Each observatory is equipped with two four terabyte 3.5 inch NAS Dard Disk Drives (HDD) and one 512 gigabyte Solid State Drive (SSD). The SSD is used for image processing before archive onto the HDDs. The LeoStick, shutter driving hardware, and camera triggering hardware are integrated on a custom Printed Circuit Board (PCB) that also contains the power management electronics, distributes the power for the observatory and serves as an interconnect between the various systems.

The observatory's housing is an off the shelf IP65 general purpose enclosure which is water-jet cut to accommodate the observatory's connectors, ports and mounting patterns. The internal components are mounted on a removable laser cut steel plate. The lenses are sealed into custom Aluminium flanges turned on a CNC lathe, and the flanges mount on the top of the box using rubber gaskets. The enclosure is shaded by a laser cut sun shade that significantly reduces the internal temperature of the observatory during the day. The mechanical design was a significant portion of the design effort, but was accelerated through Computer Aided Design (CAD) and Computer Aided Manufacturing (CAM).

A major factor in the design was ease of installation and maintenance. The small size and weight allows observatories to be swapped easily in the field on annual maintenance trips and then serviced in the lab. The storage capabilities of the observatories coincide with the one year service interval dictated by the expected DSLR shutter lifetime. Swapping the observatories does not require specialist skills, and they are small enough to mail, so the exchange can be carried out by site owners via mail. The installation procedure for the new digital observatories is significantly faster and require much less equipment than the procedure for the trial film observatories.

## 4. Design Challenges

The remoteness of installation sites had a large impact on the design process. The system has to be reliable enough to operate for approximately one year without intervention; the observatory also needed to be able to recover from most faults. The most likely failure scenarios are network interruption or failure, power interruption, computer lockups and component failure. Off the shelf consumer components such as the USB mobile data modems are not designed to run for several months without interruption; substantial design effort was required to ensure all parts of the system could be power cycled if required. Reliability and a fault tolerant design is important when the observatories are installed more than 1000 kilometres from the nearest large city.

The main challenge in implementing the concept design was to minimise the manufacturing and assembly time. Manufacturing time and cost was decreased by eliminating nearly all manufacturing steps performed by hand. CAM was used extensively to produces the components that could not be bought off the shelf. The laser cutting, water-jet cutting, and flange profiles are dictated by design files generated directly from the 3D CAD model. Changes can be made to the CAD model and prototype components can be delivered within days; CAD/CAM techniques significantly reduced the development time of the new fireball observatory and the per system cost. Assembly time was minimised by using pluggable spring cage connectors on the PCB that acts as an interconnect. This significantly lessened the assembly time of the observatory as the wiring is a sizeable portion of the assembly process. The PCB uses mostly Surface Mount Devices (SMD) to allow faster production and possible mass production in the future. The internals of the pre-SMD ADFO are shown in Figure 1. The observatory stand was constructed from interlocking laser cut steel plates fastened with metal wedges. This solution resulted in a low cost support that could be quickly and easily installed as shown in Figure 2 with only two people; observatory installation only takes a few hours including the stand and PV installation.

## 5. Results

The current design is the result of multiple revisions of the original concept design, and has proven itself capable of withstanding the hot Australian summer, strong winds, and torrential rain. The systems and components have proven that they are capable of operating in the required conditions. The shutter lifetime of the Nikon D800Es had proven to be long enough that the observatories can be expected to run for the maximum expected service interval of one year with one test camera taking over 300,000 exposures before needing a shutter replacement. The latest test observatories were installed in October 2013 and have successfully detected and captured numerous meteors. These will continue to run as the software functionality is upgraded. The current design is not expected to significantly change from this point, but small incremental upgrades may be made for future production runs.

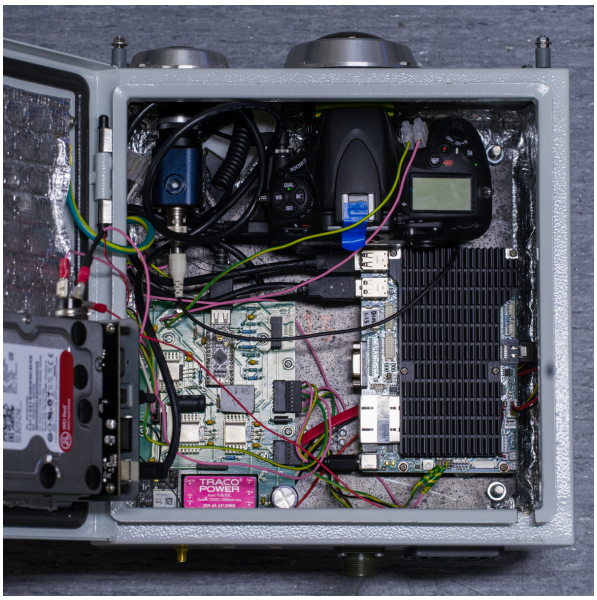


Figure 1: ADFO internals

Figure 2: ADFO installation

The ADFO is cost effective and fast to manufacture, assemble and install. Over thirty Advanced Digital Fireball Observatories have been manufactured so far; final assembly will be completed on an as needed basis as installation of the network takes place over the next year. At least another thirty ADFOs will be manufactured at a later date to turn the DFN into a continental scale planetary science installation covering in excess of 2 million square kilometres and producing data for multiple uses.

## 6. Acknowledgments

This research was supported by the Australian Research Council through the Australian Laureate Fellowships scheme and receives institutional support from Curtin University.

## 7. References

1. D. Brownlee, P. Tsou, J. Aléon, C. M. O. Alexander, T. Araki, S. Bajt *et al.*, ``Comet 81P/Wild 2 Under a Microscope,'' *Science*, vol. 314, no. 5806, pp. 1711--1716, 2006.

2. E. K. Sansom, P. A. Bland, J. Paxman, and M. C. Towner, ``Characterising Fireballs for Mass Determination: Steps Toward Automating the Australian Desert Fireball Network,'' in *General Assembly and Scientific Symposium, 2014 XXXIth URSI*. IEEE, submitted for publication.

3. P. A. Bland, P. Spurný, M. C. Towner, A. W. R. Bevan, A. T. Singleton, W. F. Bottke *et al.*, ``An Anomalous Basaltic Meteorite from the Innermost Main Belt,'' *Science*, vol. 325, no. 5947, pp. 1525--1527, 2009. [Online]. Available: http://www.sciencemag.org/content/325/5947/1525.abstract

4. P. Spurny, P. Bland, J. Borovicka, M. Towner, L. Shrbeny, A. Bevan *et al.*, ``The Mason Gully meteorite fall in SW Australia: Fireball trajectory, luminosity, dynamics, orbit and impact position from photographic records,'' *LPI Contributions*, vol. 1667, p. 6369, 2012.

5. S. Fritzinger, M. Zynel, J. Erdfelt, W. Almesberger, O. W. Saastad, V. Kaplan *et al.*, ``gPhoto - gPhoto Home,'' Jan. 2014. [Online]. Available: http://gphoto.org

6. LC-Tec, ``X-FOS(G2)/X-FOS(G2)-AR product specifications,'' Sep. 2013. [Online]. Available: http://www.lc-tec.com/UserFiles/Products/FOS_Specifications/X-FOSG2_X-FOSG2-AR_specifications_1309.pdf

7. D. Camera, ``Four Walled Cubicle - LUFA (formerly MyUSB),'' Sep. 2013. [Online]. Available: http://www.fourwalledcubicle.com/LUFA.php

## C.2 Development of the Automated Digital Fireball Observatory for the Desert Fireball Network

Robert M. Howie[1], Jonathan Paxman[1], Philip A. Bland[2], Martin C. Towner[2], Martin Cupak[2] and Eleanor K. Sansom[2]

[1]Department of Mechanical Engineering, Curtin University, Perth, Australia
[2]Department of Applied Geology, Curtin University, Perth, Australia

*This conference abstract was presented at the 14th Australian Space Research Conference (ASRC 2014) in Adelaide, Australia.*

**14th Australian Space Research Conference**

**Title:**

# Development of the Automated Digital Fireball Observatory for the Desert Fireball Network

**Authors:**

R. M. Howie[1], J. P. Paxman[1], P. A. Bland[2], M. C. Towner[2], M. Cupák[2], E. K. Sansom[2]

[1]Department of Mechanical Engineering, Curtin University
[2]Department of Applied Geology, Curtin University

## Abstract

Meteorites provide key data about the formation and evolution of the Solar System, but the value of chance finds is limited due to unknown sample origin. Meteor camera networks collect photographic trajectory information on visible meteors, enabling meteorite collection and pre-atmospheric entry orbital calculations. The Desert Fireball Network (DFN) is a continental scale meteor camera installation currently consisting of 15 Autonomous Digital Fireball Observatories (ADFOs); the final network will cover approximately one third of Australia with seventy stations.

Recent advances in consumer digital imaging technology have enabled the development of the ADFO using off the shelf components, reducing the per observatory cost to a level that permits large scale installation. After testing numerous mid to high end DSLR and mirrorless cameras, the Nikon D800E was selected for its 36MP resolution, good low light sensitivity and Linux support. The system uses a Samyang 8mm f/3.5 fish-eye lens for all sky coverage. The lens is fitted with a liquid crystal shutter to chop the thirty second exposures taken throughout the night capturing meteoroid velocity and deceleration and allowing computation of the fall distribution and pre-atmospheric entry mass. The absolute arrival time is recorded by an all sky video camera operating alongside the still camera.

The observatory is controlled by an off the shelf embedded PC linked to a custom printed circuit board and powered by a small 160W solar photovoltaic system. Eight terabytes of hard disk storage allow the observatory to retain all captured raw images for other scientific objectives until download during annual service visits.

Significant design effort was expended ensuring reliable autonomous operation in the remote Australian Outback and minimising manufacturing time and cost. The first ADFO's have proven the viability of the design and have been operating successfully since deployment in November 2013.

# C.3 Precise Fireball Trajectories Using Liquid Crystal Shutters and de Bruijn Sequences

Robert M. Howie[1], Eleanor K. Sansom[2], Philip A. Bland[2], Jonathan Paxman[1] and Martin C. Towner[2]

[1]Department of Mechanical Engineering, Curtin University, Perth, Australia
[2]Department of Applied Geology, Curtin University, Perth, Australia

*This conference abstract was presented at the 46th Lunar and Planetary Science Conference (LPSC 2015) in Houston, USA.*

**PRECISE FIREBALL TRAJECTORIES USING LIQUID CRYSTAL SHUTTERS AND DE BRUIJN SEQUENCES.** Robert M. Howie[1], Eleanor K. Sansom[2], Philip A. Bland[2], Jonathan Paxman[1] and Martin C. Towner[2], [1]Dept. of Mechanical Engineering, Curtin University, GPO Box U1987, Perth, WA 6845, Australia, robert.howie@curtin.edu.au [2]Dept. Applied Geology, Curtin University.

**Introduction:** Meteor camera networks have been used since the late fifties to characterise meteoroid orbits and calculate meteorite fall positions [1]. Previous designs used large format sheet film cameras to capture images of a meteoroid's luminous trajectory during ablation. Advances in digital imaging technology have enabled the transition from large format photographic film based systems to systems based on digital still cameras like the Desert Fireball Network (DFN) [2].

Previous stills based meteor cameras used rotating or oscillating mechanical shutters to chop or periodically interrupt the light recorded on the film plane [3],[4]. This breaks the streak on the long exposure image into short segments or dashes; the timing of which is precisely known and allows the determination of the meteor velocity after triangulation.

Exposure times can range from a few seconds to one night, so networks using long exposure images with periodic shutters for velocity determination still require a method of establishing absolute timing along a fireball path in order to determine a trajectory. Prior designs used various approaches including a combination of fixed and guided cameras [5] or photomultiplier tubes to log meteor luminosity [4], [6]. Video based systems such as [7],[8],[9] do not require an additional periodic shutter due to the high rate of image capture, nor do they require external hardware to provide absolute timing, but the resolution of video meteor cameras is poor compared to stills based systems leading to larger errors in fall position estimation.

This abstract presents a technique for encoding absolute trajectory timing with relative timing without additional hardware using a liquid crystal shutter modulated according to a de Bruijn sequence. This allows the development of high resolution, smaller, less expensive and simpler meteor cameras than previously possible.

**Meteor Velocity:** The tight tolerances and bulk of mechanical shutter assemblies used to interrupt light transmission for velocity determination significantly increase system complexity, size, cost and manufacturing time. These factors need to be minimised whilst maintaining imaging performance in order to maximise network coverage area to enable the observation and recovery of as many meteorites as possible.

The proliferation of consumer liquid crystal technology in displays and more recently active 3D display shutter glasses has made inexpensive liquid crystal (LC) shutters readily available. These shutters provide a solid-state alternative to mechanical periodic shutters, significantly simplifying the system. They do, however, have limited light transmittance in their open state, approximately 36% for those in use on the DFN. Testing has shown that the LC shutters are a suitable replacement for mechanical shutters as long as the light loss in open state transmittance is acceptable. They are a good fit with digital image sensors where the contamination from dust and dirt is of higher concern than in film based systems. The LC shutters on DFN cameras operate at a rate of 10 Hz providing 20 luminous trajectory data points per second.

**Absolute Trajectory Timing:** The DFN stations use coded operation of the LC shutter to determine the absolute timing for the start and end of the luminous trajectory. The time is encoded by modulating the LC shutter according to a de Bruijn sequence or cycle. A de Bruijn sequence is the shortest cyclic sequence containing all possible subsequence for a given alphabet size and subsequence length making it the optimal encoding for this sort of problem [10]. For example, the de Bruijn sequence generated using the prefer high method for an alphabet size of two and a subsequence length of three is '00011101'. As long as three consecutive elements in the cyclic sequence are known, it is possible to determine exactly where in the sequence the subsequence of three elements is. The LC shutter runs according to a de Bruijn sequence at a rate of ten elements per second throughout the 25 second exposure. Currently, the sequence parameters are 10 elements per second, a subsequence length of nine and an alphabet size of two, but this can be modified remotely for the network connected systems. The sequence is long enough that it doesn't repeat itself during the 25 second exposure. At least nine elements or dashes must be visible in the fireball's luminous trajectory for the start time of the trajectory to be determined. In practice, it is preferred to have more elements visible to validate the position in the sequence. Validated timing is available for all meteors clearly visible for one second or longer.

**Sequence Encoding:** The de Bruijn sequence is encoded using pulse width or dash length. A '1' is represented by leaving the shutter open longer which results in a longer dash and a '0' corresponds to a

shorter open time and therefore a shorter dash in the image.

The advantage of this approach compared to previous techniques is that the absolute trajectory and relative timing data are collected together on the same sensor without any additional hardware. The LC shutter is required to chop the meteor trail for velocity data; modulating it according to a de Bruijn sequence provides the absolute timing without requiring the integration, synchronisation and calibration of additional sensor subsystems. This simplification allows the production of much smaller, lighter, lower power and more economical meteor cameras than previously possible.

**Timing precision:** A microcontroller ensures the exposure start time and the LC shutter waveforms are synchronised with UTC via a GPS module. This module is accurate to within a few tens of nanoseconds. The shutter opens regularly every 0.1 s and closes either 0.02 s later for a short '0' dash or 0.06 s later for a long '1' dash. This system therefore enables sub-millisecond, absolute timing resolution during fireball entry. This level of precision allows reliable velocities to be calculated. The deceleration of a meteoroid is essential for determining its mass during bright flight with such a simple system, and subsequently any potential fall locations. Although only relative timing is required for meteorite fall predictions, the absolute start time of the luminous trajectory is required for accurate determination of pre-atmospheric entry due to the spin of the Earth. The sub-millisecond precision offered by the DFN cameras is well in excess of the requirements for calculating meaningful orbits.

**Example meteor:** A meteor was captured over South Australia by three DFN camera systems on 26 September 2014 at 16:42:2.80 UTC. Figure 1 shows the dashes in the fireball trail from the de Bruijn shutter sequence. Decoded timings are from the start of the exposure and some examples are given in the inset. The beginning of the de Bruijn sequence used is shown at the bottom, with the inset section highlighted. The altitude and azimuth of the start and end points of the fireball dashes are determined on each of the images and after calibration, triangulation software determines their absolute latitude, longitude and height. This fireball entered the atmosphere at 135.620° E, 28.529° S, with a height of 75.93 ± 0.15 km. Its entry velocity was 16.6 ± 1.3 km/s and its very shallow angle (~9° from the horizontal) meant that although the total duration was 6.68 s, it only penetrated 15.4 km into the atmosphere, ending with a velocity of 15.2 ± 1.3 km/s. At the end of the fireball's bright flight (135.51° E, 27.77° S) the angle to the horizontal had reduced to ~7°. Orbital parameters were also obtained for this event using the absolute entry time decoded from the sequence.

**Summary:** The combination of a liquid crystal shutter modulated by a de Bruijn sequence and synchronised via GPS makes it possible to record absolute trajectory timing data within a long exposure image without additional hardware. This enabled the development of a smaller, simpler and more economical meteor observatories than previously possible. The implementation allows the calculation of fireball trajectories with very precise timing data coupled with the high spatial resolution of 36 megapixel image sensors. The low per system cost and ease of manufacture of the automated observatories has driven rapid growth of the DFN to 30 stations covering ~1.5 million km$^2$. We are currently developing a simple 'kit' system, based on this technology, that will allow colleagues and interested amateurs to make high resolution fireball observations at low cost, see http://www.fireballsinthesky.com.au for details.

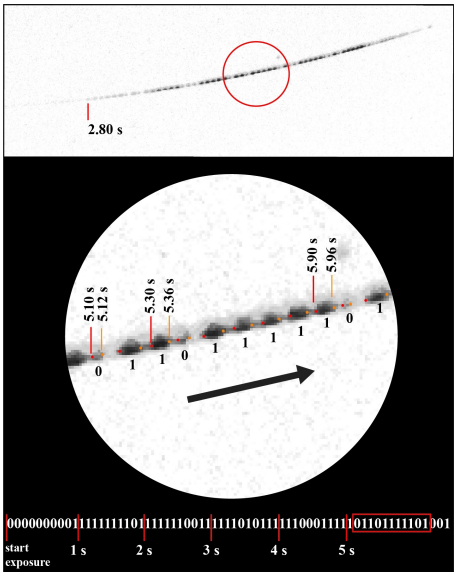


*Figure 1: Trajectory with decoded de Bruijn sequence*

**References:** [1] Ceplecha, Z. (1961) *BAC* 12, 21. [2] Bland P. A. et al. (2012) *AJES*, 59, 177-187. [3] Ceplecha, Z. et al. (1959) *BAC* 10, 147. [4] Halliday I. et al. (1978) *JRASC* 72, 15-39. [5] Ceplecha, Z. et al. (1959) *BAC* 10, 204. [6] Spurny P. et al. (2001) *Meteroids 2001*, ESA-SP 495, 135-140. [7] Olech J. et al. (2006) *IMC XXIV*, 1, 53-62. [8] Andreic, Z. and Segon, D. (2010) *IMC XXVII*, 1, 16-23. [9] Jenniskens P. et al. (2011) *Icarus*, 216, 1, 40-61. [10] de Bruijn, N. G. and Erdos, P. (1946) *KNAW*, 49, 758-764.

# C.4 How to Turn a DSLR into a High End Fireball Observatory

Robert M. Howie[1], Jonathan Paxman[1], Philip A. Bland[2], Martin C. Towner[2], Eleanor K. Sansom[2] and Monty J. Galloway[2]

[1]Department of Mechanical Engineering, Curtin University, Perth, Australia
[2]Department of Applied Geology, Curtin University, Perth, Australia

*This conference abstract was presented at the 78th Annual Meeting of the Meteoritical Society (MetSoc 2015) in Berkeley, USA.*

**HOW TO TURN A DSLR INTO A HIGH END FIREBALL OBSERVATORY**

R. M. Howie[1], J. Paxman[1], P. A. Bland[2], M. C. Towner[2], E. K. Sansom[2] and M. J. Galloway[2]. [1]Dept. of Mechanical Engineering, Curtin University, GPO Box U1987, Perth, WA 6845, Australia. E-mail: robert.howie@postgrad.curtin.edu.au [2]Dept. Applied Geology, Curtin University.

Fireball camera networks enable the recovery of meteorites with orbital data and minimal terrestrial contamination. The scientific value of the physical and chemical analysis of each meteorite is increased due to the context provided by the orbital data, providing more information about the formation and composition of the Solar System than more contaminated chance finds without orbits. Camera networks photograph fireballs during their luminous flight as they travel through the atmosphere and the trajectories are reconstructed via triangulation using images from multiple geographically distinct stations.

We have developed a novel automated digital fireball observatory with a number of advantages over previous systems allowing the rapid deployment of the Desert Fireball Network (DFN) currently covering more than 1.5 million km$^2$ of the Australian Outback. Our new observatory uses a 36MP consumer DSLR camera, off the shelf components where possible and a liquid crystal (LC) shutter instead of a mechanical shutter resulting in greatly reduced cost, complexity, assembly time, size and power consumption.

The LC shutter is used to break the fireball trail into dashes for velocity calculation, after triangulation, as previous designs have done with mechanical shutters. However, the flexibility of the LC shutter implementation allows the fireball's arrival time to be encoded by modulating the dash length according to a De Bruijn Sequence [1] synchronised with GPS time.

An automated data processing pipeline is required to handle the huge amount of data produced by the DFN. Plausible events are parameterised producing a path and light curve for each image [2]. Light curves are then matched to the precisely timed De Bruijn sequence to find the absolute timing for the dash endpoints with millisecond precision. These points are triangulated for orbital calculations and mass estimation using the dynamic method [3] to produce a fall distribution for recovery.

The integration of the trajectory timing into the primary imaging system eliminates the need for a separate fireball detector subsystem (e.g. a photomultiplier); this novel technique, combined with the careful attention to manufacturing and assembly considerations during the design phase, has enabled the new DFN digital fireball observatories to be smaller, more power efficient and significantly more cost effective than previous designs. The observatories contain an SSD equipped x86 multi-core embedded computer for data processing, a hard disk drive up to 10TB for approximately one year of image storage, Ethernet, Wi-Fi or mobile data connectivity and only take a few hours to install and configure. The observatory, minus the camera, costs roughly the same as an entry level full-frame DSLR.

DFN observatories and the data pipeline are available for colleagues interested in establishing partner networks. Contact fireballs@curtin.edu.au for more information.

**References:** [1] De Bruijn N. G. and Erdos P. 1946. *Koninklijke Nederlandse Akademie v. Wetenschappen* 49:758–764. [2] Galloway M. J. et al. 2015 *(this conference)*. [3] Sansom E. K. et al. 2015. *(this conference)*.

# C.5 Deploy Your Own Desert Fireball Network Observatory

Robert M. Howie[1], Jonathan Paxman[1], Philip A. Bland[2] and Martin C. Towner[2]

[1]Department of Mechanical Engineering, Curtin University, Perth, Australia
[2]Department of Applied Geology, Curtin University, Perth, Australia

*This conference abstract was presented at the 15th Australian Space Research Conference (ASRC 2015) in Canberra, Australia, and won "Runner-up Best Postgraduate Student Presentation - Oral".*

# Deploy Your Own Desert Fireball Network Observatory

Robert M. Howie[1], Jonathan Paxman[1], Philip A. Bland[2], and Martin C. Towner[2]

[1] *Department of Mechanical Engineering, Curtin University, Perth, Australia*
[2] *Department of Applied Geology, Curtin University, Perth, Australia*

The Desert Fireball Network (DFN) currently consists of 32 stations located in The Australian Outback covering over one million square kilometres and was deployed in less than two years. This rapid deployment was enabled by the small and cost effective fireball observatory presented at ASRC 2014. We have designed an even smaller and more inexpensive fireball observatory that other researchers and interested amateurs can easily deploy in a couple of hours in order to become part of the DFN or deploy their own partner network.

The new observatory still contains a full-frame DSLR, all-sky lens, embedded PC, hard drive, and GPS synchronised LC shutter for fireball timing but is designed for mains powered sites that can be attended more regularly (twice per year). The cost of the observatory, minus the camera, is comparable to an entry level full-frame DSLR, and it can be installed by one or two people in a couple of hours.

We are constructing 50 of the new low cost observatories to be distributed to domestic and international collaborators. We will present a brief overview of the new systems, details on the techniques enabling further size and cost reductions and information for prospective collaborators.

# Appendix D

# Provisional Patent: Spatial tracking of a moving object

## Explanatory Note

A provisional patent application was filed to protect the time encoding technique developed for the fireball observatories.

The text of this provisional patent application was prepared under contract by Neal Schutte of Patenteur Pty Ltd. (Balcatta, Australia, http://www.patenteur.com/) based on documentation primarily written by Robert Howie encompassing the work of Robert Howie, Phil Bland, Martin Towner and Jonathan Paxman (an early version of chapter 2). The drawings were created by Robert Howie.

The inventors and applicants of this provisional patent application are Robert Howie, Phil Bland, Martin Towner and Jonathan Paxman.

The filing receipt is included (redacted where necessary) followed by the application material.

Australian Government
IP Australia

Thank you. Your submission was successful. The official receipt for this transaction is available to be viewed for up to 6 months within your eServices History.

## Official Receipt

PO Box 200 Woden ACT 2606 AUSTRALIA Tel: 1300 65 1010 ABN: 38 113 072 755

This is your official receipt. We recommend that you print this page and retain for your records.

Saving this page in a Portable Document Format (PDF) is another useful way of retaining this information for your records. More information on PDFs

Note: Amounts shown include GST where applicable. Under Division 81 of *A New TAX System (Goods and Services Tax) ACT 1999,* GST is not payable on the purchase of any statutory items from IP Australia.

| | |
|---|---|
| IP Australia batch reference | SPBI 0000859068 |
| Submitted by | SMIT1 |
| Customer number | IBR5355311012 |
| Your cart reference | |
| Date/Time submitted | 26/02/2016 07:35 PM |
| Bank reference | 137134 |
| Payment Identifier | 0000000000617577 |
| Amount paid (AU) | $110.00 |
| Card type | [redacted] |
| Card holder's name | Neal Schutte |
| Card expiry | [redacted] |
| Card number | [redacted] |

## List of Service Requests

| IP RIGHT NUMBER | APPLICANT NAME | SERVICE REQUEST TYPE | YOUR REFERENCE | PHYSICAL MEDIA | FEE | ACTION |
|---|---|---|---|---|---|---|
| 2016900714 | Robert Michael HOWIE,Philip Alan BLAND,Martin Colin TOWNER,Jonathan Patrick PAXMAN | Patents New Application (Provisional) | | No | $110.00 | View |

Total Fee (AU): $110.00

Australian Government
IP Australia

Official Receipt

PO Box 200 Woden ACT 2606 AUSTRALIA Tel: 1300 65 1010 ABN: 38 113 072 755

This is your official receipt. We recommend that you print this page and retain for your records.

Saving this page in a Portable Document Format (PDF) is another useful way of retaining this information for your records. More information on PDFs

Note: Amounts shown include GST where applicable. Under Division 81 of *A New TAX System (Goods and Services Tax) ACT 1999,* GST is not payable on the purchase of any statutory items from IP Australia.

| | |
|---|---|
| Service Request type | Patents New Application (Provisional) |
| Application number | 2016900714 |
| IP Australia batch reference | SPBI 0000859068 |
| Submitted by | Patenteur Pty Ltd |
| Customer number | IBR5355311012 |
| Your reference | AU_Howie_P |
| Date/time submitted | 26/02/2016 07:35 PM |
| Amount paid (AU) | $110.00 |
| Physical media | No |

## Service Requests

| SERVICE REQUEST TYPE | PHYSICAL MEDIA | FEE |
|---|---|---|
| Patents New Application (Provisional) | No | $110.00 |

Total Fee (AU): $110.00

## Attachments

| SERVICE REQUEST/APPLICATION NUMBER | TYPE | FILE NAME | SIZE |
|---|---|---|---|
| 2016900714 | Description | Spatial tracking of a moving object Final.pdf | 635KB |

The attachments above have been submitted with this application.

# SPATIAL TRACKING OF A MOVING OBJECT

## TECHNICAL FIELD

**[0001]** This invention relates to a method and an associated system for spatial tracking of a moving object.

## BACKGROUND ART

**[0002]** The following discussion of the background art is intended to facilitate an understanding of the present invention only. The discussion is not an acknowledgement or admission that any of the material referred to is or was part of the common general knowledge as at the priority date of the application.

**[0003]** Various forms of spatial tracking of moving objects exist. One particular field of application of such movement tracking, is in the field of extraterrestrial geology, particularly involving the study of meteorites.

**[0004]** Meteorites can provide insight into the history and formation of the Solar System. However, the value of chance finds is limited by the unknown origin of meteorites discovered in such a manner. In addition, weathering and terrestrial contamination can also interfere with geochemical analysis, which further limits the usefulness of such chance finds.

**[0005]** Space missions can provide for the return of meteoroid samples that are uncontaminated and with a known origin. However, space missions are extremely complex and

costly. At present, a more viable alternative method is via meteor camera networks for locating and subsequently obtaining meteorites with a known origin, as well as with minimal contamination and weathering if such samples can be retrieved without delay.

**[0006]** Estimating meteorite fall positions with sufficient accuracy to enable recovery is particularly challenging. Such methods require accurate estimates of velocity, position and mass during so-called bright flight into the planet's atmosphere. This technique is generally combined with dark flight modelling to take atmospheric conditions into account to accurately locate meteoroids.

**[0007]** Pre-atmospheric orbit calculation only requires the bright flight path and an initial velocity. However, the entry mass for a meteoroid object is also required for long-term backward orbital calculations as well as fall location estimation. Deceleration during bright flight can provide meteoroid mass, where accurate spatial and temporal data of the trajectory is required in order to calculate the deceleration with enough precision to accurately estimate the mass.

**[0008]** Absolute temporal or timing data is not required to determine the deceleration, and therefore mass, but it is required to determine the pre-atmospheric entry orbit. This is due to the fact that the Earth's orientation, and therefore the orientation of the observing camera, changes with time.

**[0009]** An imprecise or inaccurate mass estimate of the moving object will make meteorite recovery unlikely. As a result, the requirement for high precision on the relative timing of the bright flight trajectory is more important than absolute timing requirement, as estimating the mass accurately is vital to calculating the fall position of the meteoroid.

**[0010]** Since 2002, the Desert Fireball Network (DFN) project has been in operation in the Australian Outback with the installation of four prototype film desert fireball observatories. These observatories rely on all-sky fisheye lenses to take night long exposures onto large format sheet film. Rotating mechanical shutters were used to segment or split the meteor trail into a series of short segments whereby the velocity of the meteor can be determined.

**[0011]** These DFN film observatories used a photomultiplier tube to obtain a light curve for each meteorite. This light curve was then used to calculate fragmentation events and derive absolute timing information. The DFN trial network resulted in two successful meteorite recoveries, which proved the viability of the use and efficacy of such a meteor camera network in the Australian Outback.

**[0012]** Numerous custom components and moving parts were used in the DFN observatories, including in the film magazine and film handling system, a mechanical shutter, and retractable sun shade and lens covers. These custom components resulted in high manufacturing and maintenance costs. In addition, high operational costs resulted due to the price of developing large format film and satellite data connections.

**[0013]** The present invention seeks to propose possible solutions, at least in part, in amelioration of the shortcomings in the art of spatial tracking of moving objects, such as meteors and meteorites.

**SUMMARY OF THE INVENTION**

**[0014]** It is to be appreciated that reference herein to an 'object' refers to anything that is visible or tangible and is relatively stable in form. In one example of this disclosure, reference will be made to such an 'object' including a meteoroid, but the skilled addressee will appreciate that this disclosure is not limited to such an example.

**[0015]** According to a first aspect of the invention there is provided a system for spatial tracking of a moving object, said system comprising:

a timing module configured to provide temporal data;

an image capturing device configured to operatively capture an image of a trajectory of such moving object, an exposure time of said image configured relative to the movement of the object;

an exposure modulator configured to modulate said exposure over time; and

a controller arranged in signal communication with the global positioning module, the timing module, the image capturing device and the exposure modulator, said controller configured to (i) operatively receive the temporal data, (ii) to control the image capturing device to capture the image, and (iii) to control the exposure modulator during such image

capturing in order to embed a particular sequence encoding indicative of the temporal data within the trajectory of the moving object in the captured image.

**[0016]** In one example, the system may include a positioning module configured to provide spatial positioning data, said positioning module arranged in signal communication with the controller and operatively providing such spatial positioning data to the controller.

**[0017]** In one example, the spatial positioning data may include orientation data.

**[0018]** In one example, the controller may be configured to embed the spatial positioning data within the captured image.

**[0019]** In one example, the controller may include a processor.

**[0020]** In one example, the positioning module may comprise a data entry within a register accessible by the processor, said data entry indicative of a position of the image capturing device.

**[0021]** Alternatively, or in addition, the positioning module may include a global navigation satellite system (GNNS), or the like, etc.

**[0022]** In one example, the captured image may comprise the positioning module where said image is able to provide the spatial positioning data, e.g. an orientation of stars in the night sky, etc.

**[0023]** In one example, the timing module may comprise an oscillator of the processor configured to provide the temporal data.

**[0024]** Alternatively, or in addition, the timing module may comprise a discrete electronic oscillator configured to produce a periodic, oscillating electronic signal indicative of the temporal data.

**[0025]** In one example, the timing module may comprise a global navigation satellite system (GNNS) module.

**[0026]** Typically, the system may include a global navigation satellite system (GNNS) module which comprises both the timing module and the positioning module.

**[0027]** Preferably, the image capturing device may comprise a digital camera.

**[0028]** Typically, the exposure time of the image may be configured relative to the movement of the object by having such exposure time of sufficient length relative to the velocity of the object to capture a desired trajectory length.

**[0029]** Typically, the exposure modulator may be configured to modulate the exposure by periodically obstructing light comprising the image into the image capturing device.

**[0030]** In one example, the exposure modulator may be configured to modulate the exposure by periodically lighting the object.

**[0031]** Preferably, the exposure modulator may comprise a liquid crystal optical shutter. Alternatively, the exposure modulator may comprise a switchable mirror device.

**[0032]** In one example, the exposure modulator may comprise part of an optical sensor of the image capturing device.

**[0033]** Typically, the processor executes a particular set of instructions in order to perform the functions assigned to the controller.

**[0034]** In one example, the particular sequence encoding may comprise a De Bruijn sequence encoding.

**[0035]** In one example, the system may include a non-transitory electronic storage means for storing the encoded captured images.

**[0036]** According to a second aspect of the invention there is provided a method for spatial tracking of a moving object, said method comprising the steps of:

providing spatial positioning data;

providing temporal data;

capturing an image of a trajectory of the moving object, an exposure time of said image configured relative to the movement of the object; and

modulating said exposure over time during the step of image capturing in order to embed a particular sequence

encoding indicative of the temporal data within the trajectory of the moving object in the captured image.

**[0037]** In one example, the method may include the step of providing spatial positioning data.

**[0038]** Typically, the step of providing spatial positioning data may be performed by means of a positioning module.

**[0039]** In one example, the method may include a step of embedding the spatial positioning data within the captured image.

**[0040]** In one example, the step of capturing the image may comprise providing the spatial positioning data where said image is able to provide the spatial positioning data, e.g. an orientation of stars in the night sky, etc.

**[0041]** In one example, the step of providing temporal data may be performed by means of a timing module.

**[0042]** In one example, the step of capturing an image may be performed by means of an image capturing device.

**[0043]** In one example, the step of modulating said exposure time may be performed by means of an exposure modulator.

**[0044]** Preferably, the image capturing device may comprise a digital camera.

**[0045]** Typically, the exposure time of the image may be configured relative to the movement of the object by having

such exposure time of sufficient length relative to the velocity of the object to capture a desired trajectory length.

**[0046]** Typically, the exposure modulator may be configured to modulate the exposure by periodically obstructing light comprising the image into the image capturing device.

**[0047]** Alternatively, the exposure modulator may be configured to modulate the exposure by periodically lighting the object.

**[0048]** Preferably, the exposure modulator may comprise a liquid crystal optical shutter. Alternatively, the exposure modulator may comprise a switchable mirror device.

**[0049]** In one example, the exposure modulator may comprise electronic exposure modulation on a sensor of the image capturing device.

**[0050]** In one example, the particular sequence encoding may comprise a De Bruijn sequence encoding.

**[0051]** In other examples, the particular sequence encoding may comprise any pseudo-random sequence encoding.

## BRIEF DESCRIPTION OF THE DRAWINGS

**[0052]** Further features of the present invention are more fully described in the following description of several non-limiting embodiments thereof. This description is included

solely for the purposes of exemplifying the present invention. It should not be understood as a restriction on the broad summary, disclosure or description of the invention as set out above. The description will be made with reference to the accompanying drawings in which:

**Figure 1** is a diagrammatic representation of an example of a system for spatial tracking of a moving object;

**Figure 2** is a diagrammatic representation of an additional example of a system for spatial tracking of a moving object;

**Figure 3** is diagrammatic representation of a further example of a system for spatial tracking of a moving object wherein the object is illuminated by means of a modulated light source;

**Figure 4** is a diagrammatic representation of method steps of a typical method for spatial tracking of a moving object, in accordance with this disclosure;

**Figure 5** shows an example of a pseudocode algorithm for a De Bruijn sequence encoding;

**Figure 6a and 6b** are representations of examples of an image of a meteorite across a night sky where the fireball trajectory of such meteorite shows a particular sequence encoding indicative of the spatial positioning and temporal data;

**Figure 7** is a diagrammatic representation of another example of a system for spatial tracking of a moving object, in accordance with this disclosure; and

**Figure 8** is a diagrammatic representation of a yet further example of a system for spatial tracking of a moving object, wherein the exposure modulator forms part of the image capturing device, in accordance with this disclosure.

**[0053]** In the figures, incorporated to illustrate features of an example embodiment or embodiments, like reference numerals are used to identify like parts throughout the figures.

**DETAILED DESCRIPTION OF EMBODIMENTS**

**[0054]** The following modes, given by way of example only, are described in order to provide a more precise understanding of the subject matter of a preferred embodiment or embodiments.

**[0055]** With reference now to Figure 1 of the drawings, there is shown a block diagram of representative parts or components comprising a system 10 for spatial tracking of a moving object 8.

**[0056]** In general, the system 10 comprises a positioning module 12, a timing module 14, an image capturing device 16, an exposure modulator 20 and a controller 22.

**[0057]** In a preferred example, the controller 22 includes a processor, such as a microprocessor, a programmable logic controller, a digital signal processor, a microcontroller,

and/or the like, as will be appreciated by the skilled addressee. Typically, the processor 22 executes a particular set of instructions in order to perform the functions assigned to the controller.

**[0058]** In one example, the system 10 includes a non-transitory electromagnetic storage means 24 for storing captured images and/or the particular set of instructions.

**[0059]** Typically, the positioning module 12 is configured to provide spatial positioning data. In one example, the spatial positioning data may include orientation data. In one example, the positioning module 12 may comprise a data entry within a register accessible by the processor 22, wherein this data entry is indicative of a global position of the image capturing device 16. Alternatively, or in addition, the positioning module 12 may include a global navigation satellite system (GNNS) module.

**[0060]** However, it is to be appreciated that the system 10 is not reliant on the spatial positioning data and/or positioning module 12 and examples may exist where the system 10 does not include such components and/or aspects. For example, in one embodiment, the captured image may effectively comprise the positioning module where said image is able to provide the spatial positioning data, e.g. an orientation of stars in the night sky, an image of a scene including a landmark with known spatial positioning, etc.

**[0061]** The system 10 also generally includes a timing module 14 configured to provide temporal data. It is to be appreciated that the temporal data may include absolute or

relative temporal data. In one example, the timing module 14 comprises an oscillator of the processor 22 configured to provide the temporal data. Alternatively, or in addition, the timing module 14 may also comprise a discrete electronic oscillator configured to produce a periodic, oscillating electronic signal indicative of the temporal data. For example, one embodiment may feature a global navigation satellite system (GNNS) module that provides both spatial positioning and temporal data.

**[0062]** The system 10 further typically includes an image capturing device 16 which is configured to operatively capture an image of a trajectory 18 of the moving object 8. Preferably, the image capturing device 16 includes a digital camera.

**[0063]** It is to be appreciated that an exposure time of said image is typically configured relative to the movement of the object 8. In other words, the exposure time of the image is configured relative to the movement of the object 8 by having such exposure time of sufficient length relative to the velocity of the object 8 to capture a desired trajectory length.

**[0064]** The system 10 further generally comprises an exposure modulator 20 which is configured to modulate the exposure over time of the image. Typically, the exposure modulator is configured to modulate the exposure over time by periodically obstructing light comprising the image passing into the image capturing device 16; however other configurations are possible, as described below. Preferably, the exposure modulator 20 comprises a liquid crystal optical shutter. In

further examples, the exposure modulator 20 may comprise electronic modulation of a sensor of the digital camera 16, a switchable mirror device, or the like.

**[0065]** Within the system 10, the controller 22 is generally arranged in signal communication with the global positioning module 12, the timing module 14, the image capturing device 16 and the exposure modulator 20, as shown.

**[0066]** The controller 22 is generally configured to operatively receive the spatial positioning and temporal data from the positioning and timing modules 12 and 14, respectively. In addition, the controller 22 is also configured to control the image capturing device 16 to capture the image.

**[0067]** Importantly, the controller 22 is further configured to control the exposure modulator 20 during the image capturing in order to embed a particular sequence encoding indicative of the temporal data within the trajectory 18 of the moving object 8 in the captured image. The controller 22 may also be configured to embed the spatial positioning data within the captured image.

**[0068]** In a preferred example, the particular sequence encoding comprises a De Bruijn sequence encoding. It is to be appreciated that a De Bruijn sequence is generally a sequence that includes every sub-sequence exactly once for a given sub-sequence length. As will be appreciated by the skilled addressee, this type of sequence is also known as a full length cycle sequence.

**[0069]** In one example, the sequence encoding defines the way the De Bruijn sequence is used to modulate the exposure modulator 20, e.g. the electro-optic shutter. In one example, a state of the exposure modulator 20 is generally binary in nature, such that the state varies between 'open' and 'closed'. In such a manner, the sequence encoding alters the state of the shutter over time according to the elements of the sequence. However, it is to be appreciated that other examples may feature varying an opacity of the exposure modulator to allow non-binary encoding.

**[0070]** Similarly, other types of encoding may also include pulse width modulation, pulse frequency modulation, opacity modulation, colour modulation, and/or the like. In addition to binary-based encoding, it is to be appreciated that various other bases for sequence encoding are possible depending on the configurations of the exposure modulator, i.e. colour-based, opacity-based, etc. Although these various sequence bases and encoding techniques are not described in any detail, the skilled addressee will appreciate that such sequence bases and encoding techniques can easily be adapted for use by the system 10.

**[0071]** For example, a conceptually simple encoding technique is a counter sequence with each digit encoded as a different shutter opacity. An alternate encoding with a character reserved to the start of each sub-sequence could be used. However, a preferred solution is a sequence that includes every sub-sequence exactly once for a given sub-sequence length, i.e. the De Bruijn sequence. It is, however, to be appreciated that any suitable pseudo-random sequence can be used, as appropriate.

**[0072]** A repeatable method of generating De Bruijn sequences is required to implement the encoding on the captured trajectory 18, along with subsequent decoding of the captured and encoded image. One example is to construct a De Bruijn sequence according to a 'prefer high' method, which is a generalisation of a conventional 'prefer one' method for binary alphabets. Such a construction starts with *n* zeros. Then the highest number in the alphabet *(k—1)* is inserted unless this would produce an *n-tuple* already present in the sequence. In this case, the next highest element is tried and the process continues until the sequence is complete. An implementation of an example of such an algorithm in pseudocode is shown in Figure 5.

**[0073]** Figure 2 shows a further example of a system 10 for spatial tracking of a moving object 8. In this example, the system 10 comprises a positioning module 12 in the form of a global navigation satellite system (GNSS) antenna and module, arranged in communication with the controller 22.

**[0074]** In this example, the controller 22 is in the form of a microcontroller which also includes the timing module 14 for providing the temporal data. Further included is storage and camera control means 22.1, which is in turn under control by the microcontroller 22.

**[0075]** The system 10 includes the image capturing device in the form of a digital camera 16, typically fitted with a suitable lens 17 for the desired application. In-between the lens 17 and the camera 16 is the exposure modulator 20 in the

form of a liquid crystal shutter driven by means of a shutter driver 19 under control of the microcontroller 22.

**[0076]** A yet further example of the system 10 is shown in Figure 3. In this example, the controller 22 comprises the storage means 24, which includes an internal data register with a data entry indicative of a global position of the image capturing device 16. This data entry is typically made when the system 10 is installed by an operator as part of a stationery installation, for example, or the like. Alternatively, this example also finds particular application where the captured image is able to provide the spatial positioning data, as described above.

**[0077]** However, this example of the system 10 includes a modulated light source 21 instead of the exposure modulator 20, as shown. The modulated light source 21 provides similar functionality as the exposure modulator, as it illuminates the moving object 8 so that a trajectory 18 thereof is captured by the camera 16. Such an example finds particular application in low-light conditions, for example, which lacks sufficient object illumination for the use of the exposure modulator 20.

**[0078]** As above, the modulated light source 21 is capable of modulating the exposure over time during the image capturing by the camera 16 in order to embed a particular sequence encoding indicative of the spatial positioning and temporal data within the trajectory 18 of the moving object 8 in the captured image.

**[0079]** In a yet further example (shown in Figure 8), the system 10 includes some manner or means of electronic exposure modulation 20 as part of the image capturing device's 16 optical sensor itself. It is to be appreciated that, in such an example, the exposure modulator 20 generally forms part of the image capturing device 16, whilst providing the typical functionality as described herein.

**[0080]** As shown, this example typically includes a controller and driver 23 for the electronic exposure modulation circuitry, with the other components similar as those described elsewhere herein.

**[0081]** Figure 7 provides a yet further brief diagrammatic example of the system 10, as described above, showing a digital camera comprising the image capturing device 16.

**[0082]** The current invention further provides for an associated method 30 for spatial tracking of the moving object 8. In general, the method 30 comprises the steps of providing spatial positioning data, providing temporal data capturing an image of the trajectory 18 of the moving object 8 (with an exposure time of the image configured relative to the movement of the object, as before), and modulating said exposure time during the step of image capturing in order to embed a particular sequence encoding indicative of the spatial positioning and temporal data within the trajectory of the moving object in the captured image.

**[0083]** Typically, as described above, the step of providing spatial positioning data is performed by means of the positioning module 12. Similarly, the step of providing

temporal data is performed by means of the timing module 14. Typically, the step of capturing the image is performed by means of the image capturing device 16. The step of modulating the exposure time is typically performed by means of the exposure modulator 20.

**[0084]** Figure 4 shows an example of a practical implementation of the method 30. In this example, the exposure modulator 20 and image capturing device, i.e. camera, 16 are started, as shown by method step 32, in anticipation of the object 8 moving into the camera's field-of-view.

**[0085]** The object 8 then moves into the camera's field-of-view as an event, indicated by method step 34. The sequence encoding is embedded into the captured trajectory as part of the captured image by means of the exposure modulator 20, as shown by method step 36, and the image is subsequently stored in storage means 24, indicated by method step 38.

**[0086]** When analysing the captured images, the event of the object passing through the camera's field-of-view can now be detected, as shown by method step 40. The captured images with the encoded sequences embedded as part of the captured trajectory can then be decoded to extract the spatial and temporal data of the object originally embedded therein, as indicated by method step 42. Finally, processing of the extracted data can be done, as per requirements, indicated by method step 44.

**[0087]** As mentioned above, the system 10 and associated method 30 find particular application in the field of

meteoroid tracking, i.e. the object 8 is a meteoroid. Figure 6a shows an example of a meteorite across a night sky where a resulting fireball is encoded by means of a De Bruijn sequence encoded as shutter opacity, where ‘0’ equals closed and ‘1’ equals open. Similarly, Figure 6b shows an example of a meteorite across a night sky where the fireball is encoded by means of a De Bruijn sequence decoded as pulse width, where a ‘0’ equals a short pulse length and ‘1’ equals a longer pulse length. However, as mentioned above, various other encoding techniques and encoding bases are possible and within the scope of the current disclosure.

**[0088]** Applicants find it particularly advantageous that the present invention allows an off-the-shelf digital camera to be turned into a sensitive fireball observatory without the need for additional sensors. The invention also significantly simplifies data reduction, using a technique of timecodes constructed from De Bruijn sequences to record the entry time in the fireball trail image using a liquid crystal shutter with no moving parts. This approach enables a much smaller, lower power and more cost effective meteor camera than previously possible.

**[0089]** In addition, the flexibility of the microcontroller driven LC shutter makes it possible to encode absolute timing data (arrival time) by slightly varying the pattern used for relative timing data (velocity) according to a time code but with a constantly changing sequence that does not repeat during the exposure and offers much higher timing precision. The image of the meteor trail has a part of this timecode recorded into it as the image of the fireball moves across

the frame while LC shutter is operating during the long exposure.

**[0090]** The part of the timecode visible in the meteor trail corresponds with the time within the long exposure that the fireball appeared, and this allows the precise calculation of the meteor's atmospheric entry time. The recording of the relative and absolute timing data is inherent in the image and does not require the integration of data from multiple subsystems simplifying the data processing problem.

**[0091]** As such, the combination of a liquid crystal shutter modulated by a de Bruijn sequence and synchronised via GNNS makes it possible to record absolute trajectory timing data within a long exposure image without additional hardware.

**[0092]** Although the present invention has been described with reference to the field of meteoroid tracking, various other applications exist. For example, the invention may be applied to the field of man-made projectile tracking, e.g. rockets, missiles, re-entry vehicles, etc. or high-speed data acquisition, particle image velocimetry, star tracking for spacecraft attitude determination, and/or the like. As such, as described above, an ‘object’ may include any manner of object which is tangible and is relatively stable in form.

**[0093]** Optional embodiments of the present invention may also be said to broadly consist in the parts, elements and features referred to or indicated herein, individually or collectively, in any or all combinations of two or more of

the parts, elements or features, and wherein specific integers are mentioned herein which have known equivalents in the art to which the invention relates, such known equivalents are deemed to be incorporated herein as if individually set forth.

**[0094]** It is to be appreciated that reference to "one example" or "an example" of the invention is not made in an exclusive sense. Accordingly, one example may exemplify certain aspects of the invention, whilst other aspects are exemplified in a different example. These examples are intended to assist the skilled person in performing the invention and are not intended to limit the overall scope of the invention in any way unless the context clearly indicates otherwise.

**[0095]** It is to be understood that the terminology employed above is for the purpose of description and should not be regarded as limiting. The described embodiment is intended to be illustrative of the invention, without limiting the scope thereof. The invention is capable of being practised with various modifications and additions as will readily occur to those skilled in the art.

**[0096]** Various substantially and specifically practical and useful exemplary embodiments of the claimed subject matter are described herein, textually and/or graphically, including the best mode, if any, known to the inventors for carrying out the claimed subject matter. Variations (e.g. modifications and/or enhancements) of one or more embodiments described herein might become apparent to those of ordinary skill in the art upon reading this application.

**[0097]** The inventor(s) expects skilled artisans to employ such variations as appropriate, and the inventor(s) intends for the claimed subject matter to be practiced other than as specifically described herein. Accordingly, as permitted by law, the claimed subject matter includes and covers all equivalents of the claimed subject matter and all improvements to the claimed subject matter. Moreover, every combination of the above described elements, activities, and all possible variations thereof are encompassed by the claimed subject matter unless otherwise clearly indicated herein, clearly and specifically disclaimed, or otherwise clearly contradicted by context.

**[0098]** The use of any and all examples, or exemplary language (e.g., "such as") provided herein, is intended merely to better illuminate one or more embodiments and does not pose a limitation on the scope of any claimed subject matter unless otherwise stated. No language in the specification should be construed as indicating any non-claimed subject matter as essential to the practice of the claimed subject matter.

**[0099]** The use of words that indicate orientation or direction of travel is not to be considered limiting. Thus, words such as "front", "back", "rear", "side", "up", down", "upper", "lower", "top", "bottom", "forwards", "backwards", "towards", "distal", "proximal", "in", "out" and synonyms, antonyms and derivatives thereof have been selected for convenience only, unless the context indicates otherwise. The inventor(s) envisage that various exemplary embodiments of the claimed subject matter can be supplied in any particular

orientation and the claimed subject matter is intended to include such orientations.

**[00100]** The use of the terms "a", "an", "said", "the", and/or similar referents in the context of describing various embodiments (especially in the context of the claimed subject matter) are to be construed to cover both the singular and the plural, unless otherwise indicated herein or clearly contradicted by context. The terms "comprising," "having," "including," and "containing" are to be construed as open-ended terms (i.e., meaning "including, but not limited to,") unless otherwise noted.

**[00101]** Moreover, when any number or range is described herein, unless clearly stated otherwise, that number or range is approximate. Recitation of ranges of values herein are merely intended to serve as a shorthand method of referring individually to each separate value falling within the range, unless otherwise indicated herein, and each separate value and each separate sub-range defined by such separate values is incorporated into the specification as if it were individually recited herein. For example, if a range of 1 to 10 is described, that range includes all values there between, such as for example, 1.1, 2.5, 3.335, 5, 6.179, 8.9999, etc., and includes all sub-ranges there between, such as for example, 1 to 3.65, 2.8 to 8.14, 1.93 to 9, etc.

**[00102]** Accordingly, every portion (e.g., title, field, background, summary, description, abstract, drawing figure, etc.) of this application, other than the claims themselves, is to be regarded as illustrative in nature, and not as restrictive; and the scope of subject matter protected by any

patent that issues based on this application is defined only by the claims of that patent.

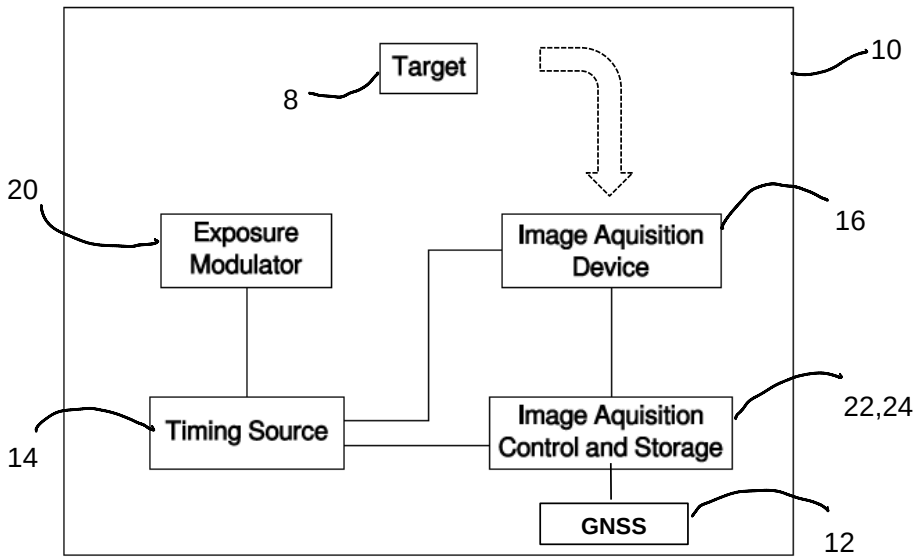


Figure 1.

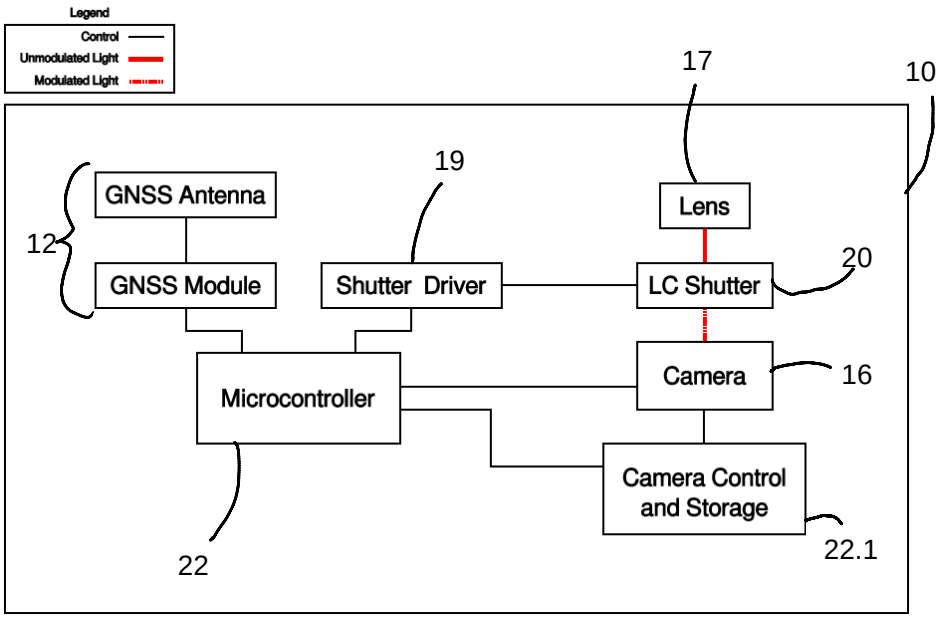


Figure 2.

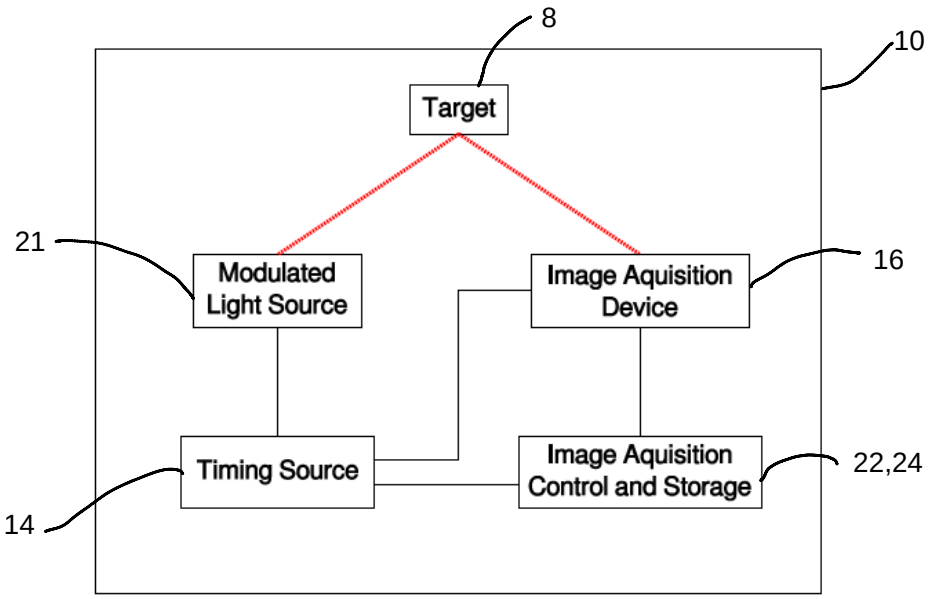


**Figure 3.**

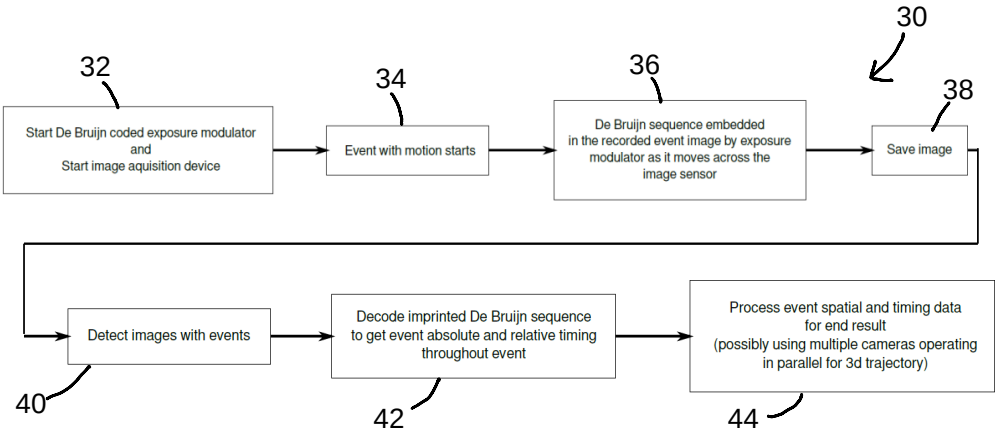


**Figure 4.**

```
algorithm prefer high De Bruijn sequence generation:
  set n to sequence length
  set k to alphabet size
  make empty list sequence
  for n times:
     append 0 to sequence
  while length of sequence is less than or equal to k^n:
     set i to k-1
     set element added to false
     while element added is false:
        set test n-tuple to last n-1 elements of sequence concatenated with i
        if s does not contain test n-tuple:
           append i to sequence
           set element added to true
        else:
           decrement i by 1
  return sequence
```

**Figure 5.**

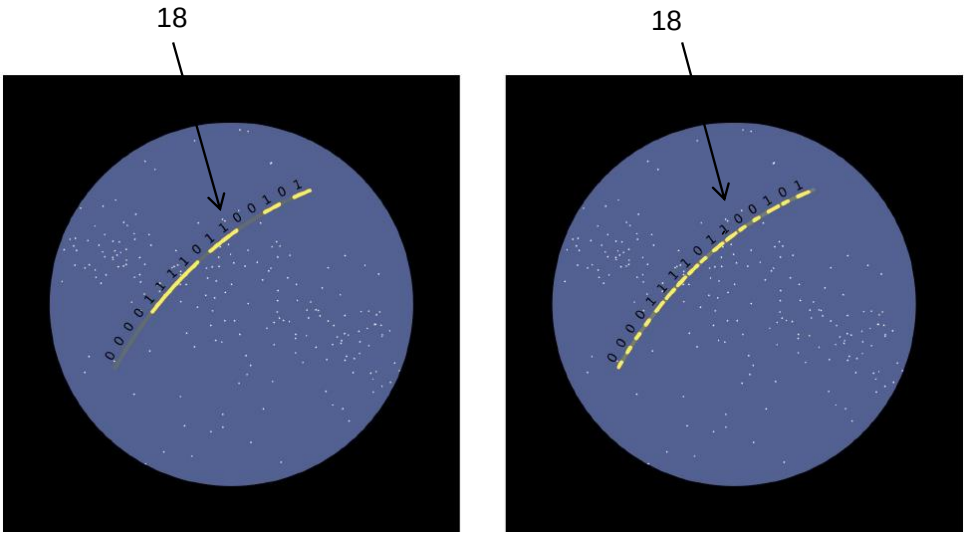


**Figure 6a & 6b.**

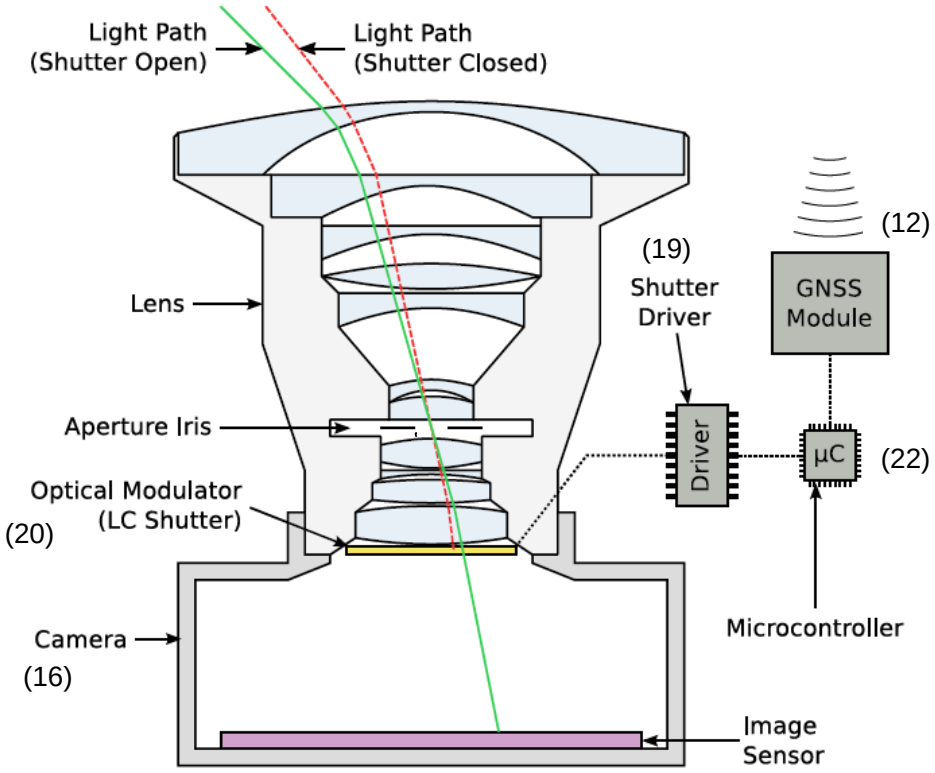
Light Path
(Shutter Open)
Light Path
(Shutter Closed)
Lens
Aperture Iris
Optical Modulator
(LC Shutter)
(20)
Camera
(16)
(19)
Shutter
Driver
Driver
GNSS
Module
(12)
µC
(22)
Microcontroller
Image
Sensor

**Figure 7.**

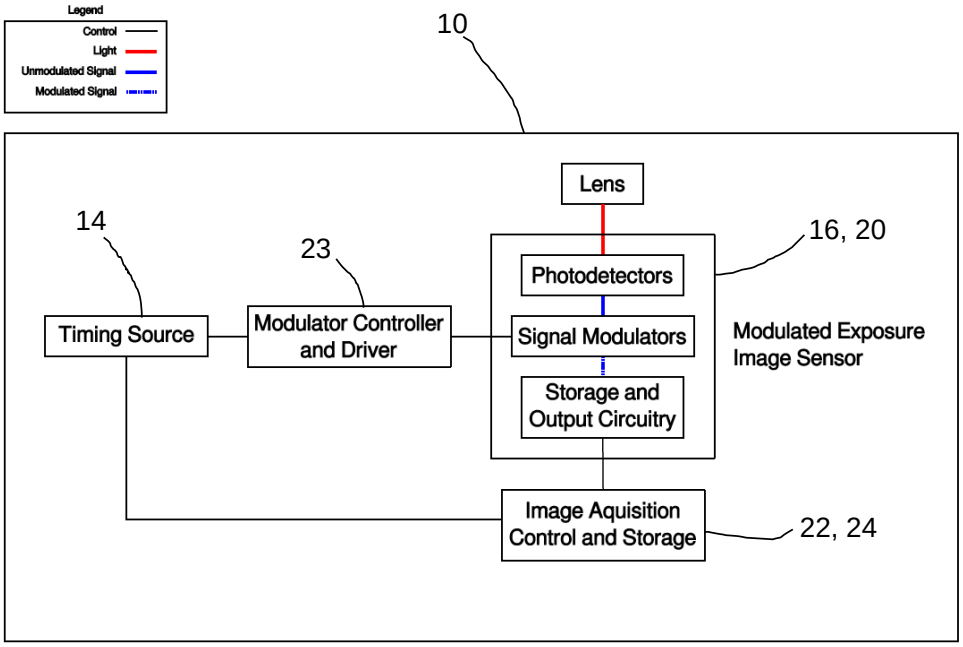
Legend
Control
Light
Unmodulated Signal
Modulated Signal
10
Lens
14
23
16, 20
Photodetectors
Timing Source
Modulator Controller and Driver
Signal Modulators
Modulated Exposure Image Sensor
Storage and Output Circuitry
Image Aquisition Control and Storage
22, 24

**Figure 8.**

# Bibliography


[1] Meteoritical Society, *Meteoritical Bulletin*, 2017. [Online]. Available: `https://www.lpi.usra.edu/meteor` (visited on 11/21/2016).

[2] R. W. Oloff, *Apollo by the Numbers: A Statistical Reference, NASA SP-2000-4029*. NASA, 2000, ISBN: 0-16-050631-X.

[3] A. P. Vinogradov, "Preliminary data on lunar ground brought to Earth by automatic probe" Luna-16"," in *Lunar and Planetary Science Conference Proceedings*, vol. 2, 1971, p. 1.

[4] A. Vinogradov, "Preliminary data on lunar soil collected by the Luna 20 unmanned spacecraft," *Geochimica et Cosmochimica Acta*, vol. 37, no. 4, pp. 721–729, 1973.

[5] V. Barsukov, "Preliminary data for the regolith core brought to earth by the automatic lunar station Luna 24," in *Lunar and Planetary Science Conference Proceedings*, vol. 8, 1977, pp. 3303–3318.

[6] D. Brownlee, P. Tsou, J. Aléon, C. M. Alexander, T. Araki, S. Bajt, G. A. Baratta, R. Bastien, P. Bland, P. Bleuet, *et al.*, "Comet 81P/Wild 2 under a microscope," *science*, vol. 314, no. 5806, pp. 1711–1716, 2006.

[7] D. Burnett, B. Barraclough, R. Bennett, M. Neugebauer, L. Oldham, C. Sasaki, D. Sevilla, N. Smith, E. Stansbery, D. Sweetnam, *et al.*, "The Genesis Discovery Mission: return of solar matter to Earth," *Space Science Reviews*, vol. 105, no. 3-4, pp. 509–534, 2003.

[8] K. McKeegan, A. Kallio, V. Heber, G. Jarzebinski, P. Mao, C. Coath, T. Kunihiro, R. Wiens, J. Nordholt, R. Moses, *et al.*, "The oxygen isotopic composition of the Sun inferred from captured solar wind," *Science*, vol. 332, no. 6037, pp. 1528–1532, 2011.

[9] T. Nakamura, T. Noguchi, M. Tanaka, M. E. Zolensky, M. Kimura, A. Tsuchiyama, A. Nakato, T. Ogami, H. Ishida, M. Uesugi, *et al.*, "Itokawa dust particles: a direct link between S-type asteroids and ordinary chondrites," *Science*, vol. 333, no. 6046, pp. 1113–1116, 2011.

[10] H. Y. McSween, D. W. Mittlefehldt, A. W. Beck, R. G. Mayne, and T. J. McCoy, "HED Meteorites and Their Relationship to the Geology of Vesta and the Dawn Mission," *Space Science Reviews*, vol. 163, no. 1, pp. 141–174, Dec. 2011, ISSN: 1572-9672. DOI: 10.1007/s11214-010-9637-z. [Online]. Available: https://doi.org/10.1007/s11214-010-9637-z.

[11] T. B. McCord, J. B. Adams, and T. V. Johnson, "Asteroid Vesta: Spectral reflectivity and compositional implications," *Science*, vol. 168, no. 3938, pp. 1445–1447, 1970.

[12] M. Meier, "Meteoriteorbits. info-Tracking All Known Meteorites with Photographic Orbits," in *Lunar and Planetary Science Conference*, vol. 48, 2017.

[13] A. E. Rubin and J. N. Grossman, "Meteorite and meteoroid: New comprehensive definitions," *Meteoritics & Planetary Science*, vol. 45, no. 1, pp. 114–122, 2010.

[14] E. Milley, R. Hawkes, and J. Ehrman, "Meteor luminosity simulation through laser ablation of meteorites," *Monthly Notices of the Royal Astronomical Society: Letters*, vol. 382, no. 1, pp. L67–L71, 2007.

[15] Z. Ceplecha, J. Borovička, W. G. Elford, D. O. ReVelle, R. L. Hawkes, V. Porubčan, and M. Šimek, "Meteor phenomena and bodies," *Space Science Reviews*, vol. 84, no. 3-4, pp. 327–471, 1998.

[16] J. Borovička, P. Koten, P. Spurný, J. Boček, and R. Štork, "A survey of meteor spectra and orbits: evidence for three populations of Na-free meteoroids," *Icarus*, vol. 174, no. 1, pp. 15–30, 2005.

[17] M. J. Belton, *Mitigation of hazardous comets and asteroids*. Cambridge University Press, 2004.

[18] International Meteor Organization, "Glossary," Aug. 2017. [Online]. Available: http://www.imo.net/resources/glossary.

[19] Z. Ceplecha and J. Rajchl, "Programme of fireball photography in Czechoslovakia," *Bulletin of the Astronomical Institutes of Czechoslovakia*, vol. 16, p. 15, 1965.

[20] R. E. McCrosky and J. H. Boeschenstein, "The Prairie Meteorite Network," *Optical Engineering*, vol. 3, no. 4, pp. 304 127–304127–, 1965.

[21] I. Halliday, A. Blackwell, and A. Griffin, "The Innisfree meteorite and the Canadian camera network," *Journal of the Royal Astronomical Society of Canada*, vol. 72, pp. 15–39, 1978.

[22] P. Spurný, J. Borovička, and L. Shrbený, "Automation of the Czech part of the European fireball network: equipment, methods and first results," *Proceedings of the International Astronomical Union*, vol. 2, no. S236, pp. 121–130, 2006.

[23] P. Spurný, "Instrumentally documented meteorite falls: two recent cases and statistics from all falls," *Proceedings of the International Astronomical Union*, vol. 10, no. S318, pp. 69–79, 2015.

[24] R. M. Howie, J. Paxman, P. A. Bland, M. C. Towner, M. Cupak, E. K. Sansom, and H. A. R. Devillepoix, "How to build a continental scale fireball camera network," *Experimental Astronomy*, vol. 43, no. 3, pp. 237–266, 2017. DOI: 10.1007/s10686-017-9532-7. [Online]. Available: https://doi.org/10.1007%2Fs10686-017-9532-7.

[25] B. Ivanov, G. Neukum, W. Bottke, and W. Hartmann, "The comparison of size-frequency distributions of impact craters and asteroids and the planetary cratering rate," *Asteroids III*, vol. 1, pp. 89–101, 2002.

[26] P. Bland and N. Artemieva, "Efficient disruption of small asteroids by Earth's atmosphere," *Nature*, vol. 424, no. 6946, p. 288, 2003.

[27] M. Zolensky, P. Bland, P. Brown, and I. Halliday, "Flux of extraterrestrial materials," *Meteorites and the early solar system II*, pp. 869–888, 2006.

[28] H. Dietzel, G. Eichhorn, H. Fechtig, E. Grun, H.-J. Hoffmann, and J. Kissel, "The HEOS 2 and HELIOS micrometeoroid experiments," *Journal of Physics E: Scientific Instruments*, vol. 6, no. 3, p. 209, 1973.

[29] J. Rendtel, "Review of amateur meteor research," *Planetary and Space Science*, 2017.

[30] P. Jenniskens, Q. Nénon, P. Gural, J. Albers, B. Haberman, B. Johnson, D. Holman, R. Morales, B. Grigsby, D. Samuels, *et al.*, "CAMS confirmation of previously reported meteor showers," *Icarus*, vol. 266, pp. 355–370, 2016.

[31] P. Bland, P. Spurný, A. Bevan, K. Howard, M. Towner, G. Benedix, R. Greenwood, L. Shrbený, I. Franchi, G. Deacon, *et al.*, "The Australian Desert Fireball Network: a new era for planetary science," *Australian Journal of Earth Sciences*, vol. 59, no. 2, pp. 177–187, 2012.

[32] P. A. Bland, "The desert fireball network," *Astronomy & Geophysics*, vol. 45, no. 5, pp. 5–20, 2004.

[33] P. Spurný, P. Bland, J. Borovička, M. Towner, L. Shrbený, A. W. Bevan, and D. Vaughan, "The Mason Gully meteorite fall in SW Australia: Fireball trajectory, luminosity, dynamics, orbit and impact position from photographic records (abstract 6369)," in *Proceedings, Asteroids, Comets, Meteors 2012*, 2012.

[34] P. A. Bland, P. Spurný, M. C. Towner, A. W. Bevan, A. T. Singleton, W. F. Bottke, R. C. Greenwood, S. R. Chesley, L. Shrbený, J. Borovička, Z. Ceplecha, T. P. McClafferty, V. David, G. K. Benedix, G. Deacon, K. T. Howard, I. A. Franchi, and R. M. Hough, "An anomalous basaltic meteorite from the innermost main belt," *Science*, vol. 325, no. 5947, pp. 1525–1527, 2009.

[35] P. Spurný, J. Oberst, and D. Heinlein, "Photographic observations of Neuschwanstein, a second meteorite from the orbit of the Příbram chondrite," *Nature*, vol. 423, no. 6936, pp. 151–153, 2003.

[36] P. Spurný, J. Haloda, J. Borovička, L. Shrbený, and P. Halodová, "Reanalysis of the Benešov bolide and recovery of polymict breccia meteorites–old mystery solved after 20 years," *Astronomy & Astrophysics*, vol. 570, A39, 2014.

[37] I. Halliday, A. T. Blackwell, and A. A. Griffin, "The typical meteorite event, based on photographic records of 44 fireballs," *Meteoritics*, vol. 24, no. 2, pp. 65–72, 1989.

[38] P. Spurný, P. A. Bland, L. Shrbený, J. Borovička, Z. Ceplecha, A. Singelton, A. W. Bevan, D. Vaughan, M. C. Towner, T. P. McClafferty, *et al.*, "The Bunburra Rockhole meteorite fall in SW Australia: fireball trajectory, luminosity, dynamics, orbit, and impact position from photographic

and photoelectric records," *Meteoritics & Planetary Science*, vol. 47, no. 2, pp. 163–185, 2012.

[39] P. S. Gural, "Algorithms and software for meteor detection," *Earth, Moon, and Planets*, vol. 102, no. 1-4, pp. 269–275, 2008.

[40] Z. Ceplecha, "Geometric, dynamic, orbital and photometric data on meteoroids from photographic fireball networks," *Bulletin of the Astronomical Institutes of Czechoslovakia*, vol. 38, pp. 222–234, 1987.

[41] J. Trigo-Rodríguez, A. Castro-Tirado, J. Llorca, J. Fabregat, V. Martínez, V. Reglero, M. Jelínek, P. Kubánek, T. Mateo, and A. de Ugarte Postigo, "The development of the Spanish Fireball Network using a new all-sky CCD system," in *Modern Meteor Science An Interdisciplinary View*, Springer, 2005, pp. 553–567.

[42] J. Borovička, "The comparison of two methods of determining meteor trajectories from photographs," *Bulletin of the Astronomical Institutes of Czechoslovakia*, vol. 41, pp. 391–396, 1990.

[43] P. S. Gural, "A new method of meteor trajectory determination applied to multiple unsynchronized video cameras," *Meteoritics & Planetary Science*, vol. 47, no. 9, pp. 1405–1418, 2012.

[44] A. Egal, P. Gural, J. Vaubaillon, F. Colas, and W. Thuillot, "The challenge associated with the robust computation of meteor velocities from video and photographic records," *Icarus*, vol. 294, pp. 43–57, 2017.

[45] E. K. Sansom, T. Jansen-Sturgeon, M. G. Rutten, H. A. Devillepoix, P. A. Bland, R. M. Howie, M. A. Cox, M. C. Towner, M. Cupák, and B. A. Hartig, "3D Meteoroid Trajectories," *Icarus*, vol. 321, pp. 388–406, 2019, ISSN: 0019-1035. DOI: 10.1016/j.icarus.2018.09.026.

[46] E. K. Sansom, M. G. Rutten, and P. A. Bland, "Analyzing Meteoroid Flights Using Particle Filters," *The Astronomical Journal*, vol. 153, no. 2, p. 87, 2017. [Online]. Available: http://stacks.iop.org/1538-3881/153/i=2/a=87.

[47] E. Sansom, T. Jansen-Sturgeon, M. Rutten, P. Bland, H. Devillepoix, M. Towner, M. Cupak, R. Howie, M. Cox, J. Desayes, J. Paxman, and B. Hartig, "Modelling fireball network data in three dimensions," in *Proceedings, Asteroids, Comets, Meteors 2017*, 2017.

[48] E. Sansom, P. Bland, M. Rutten, J. Paxman, and M. Towner, "Filtering Meteoroid Flights Using Multiple Unscented Kalman Filters," *The Astronomical Journal*, vol. 152, no. 5, p. 148, 2016.

[49] M. Fries and J. Fries, "Doppler weather radar as a meteorite recovery tool," *Meteoritics & Planetary Science*, vol. 45, no. 9, pp. 1476–1487, 2010.

[50] J. Hoppe, "Die physikalischen Vorgänge beim Eindringen meteoritischer Körper in die Erdatmosphäre," *Astronomische Nachrichten*, vol. 262, no. 10, pp. 169–198, 1937.

[51] F. L. Whipple, "Photographic meteor studies, I," *Proceedings of the American Philosophical Society*, pp. 499–548, 1938.

[52] J. G. Hills and M. P. Goda, "The fragmentation of small asteroids in the atmosphere," *The Astronomical Journal*, vol. 105, pp. 1114–1144, 1993.

[53] Z. Ceplecha, P. Spurný, J. Borovička, and J. Keclikova, "Atmospheric fragmentation of meteoriods," *Astronomy and Astrophysics*, vol. 279, pp. 615–626, 1993.

[54] Z. Ceplecha and D. O. Revelle, "Fragmentation model of meteoroid motion, mass loss, and radiation in the atmosphere," *Meteoritics & Planetary Science*, vol. 40, no. 1, pp. 35–54, 2005.

[55] E. Öpik, *Atomic collisions and radiation of meteors*. Astronomical Observatory of Harvard College, 1933.

[56] E. Öpik, "Meteor radiation, ionization and atomic luminous efficiency," in *Proceedings of the Royal Society of London A: Mathematical, Physical and Engineering Sciences*, The Royal Society, vol. 230, 1955, pp. 463–501.

[57] E. Öpik, "Tables of meteor luminosities," *Irish Astronomical Journal*, vol. 6, p. 3, 1963.

[58] P. Spurný, J. Borovička, J. Kac, P. Kalenda, J. Atanackov, G. Kladnik, D. Heinlein, and T. Grau, "Analysis of instrumental observations of the Jesenice meteorite fall on April 9, 2009," *Meteoritics & Planetary Science*, vol. 45, no. 8, pp. 1392–1407, 2010.

[59] J. Borovička, J. Tóth, A. Igaz, P. Spurný, P. Kalenda, J. Haloda, J. Svoreň, L. Kornoš, E. Silber, P. Brown, *et al.*, "The Košice meteorite fall: Atmospheric trajectory, fragmentation, and orbit," *Meteoritics & Planetary Science*, vol. 48, no. 10, pp. 1757–1779, 2013.

[60] E. K. Sansom, P. Bland, J. Paxman, and M. Towner, "A novel approach to fireball modeling: The observable and the calculated," *Meteoritics & Planetary Science*, vol. 50, no. 8, pp. 1423–1435, 2015, ISSN: 1945-5100. DOI: 10.1111/maps.12478. [Online]. Available: http://dx.doi.org/10.1111/maps.12478.

[61] P. Jenniskens, M. D. Fries, Q.-Z. Yin, M. Zolensky, A. N. Krot, S. A. Sandford, D. Sears, R. Beauford, D. S. Ebel, J. M. Friedrich, *et al.*, "Radar-enabled recovery of the Sutter's Mill meteorite, a carbonaceous chondrite regolith breccia," *Science*, vol. 338, no. 6114, pp. 1583–1587, 2012.

[62] H. Devillepoix, P. Bland, M. Towner, E. Sansom, R. Howie, M. Cupak, G. Benedix, T. Jansen-Sturgeon, B. Hartig, M. Cox, and J. Paxman, "Fall and Recovery of the Dingle Dell Metorite," in *80th Annual Meeting of the Meteoritical Society 2017*, 2017. [Online]. Available: https://www.hou.usra.edu/meetings/metsoc2017/pdf/6211.pdf.

[63] P. Brown, D. Pack, W. Edwards, D. ReVelle, B. Yoo, R. Spalding, and E. Tagliaferri, "The orbit, atmospheric dynamics, and initial mass of the Park Forest meteorite," *Meteoritics & Planetary Science*, vol. 39, no. 11, pp. 1781–1796, 2004.

[64] A. T. Jull, "Terrestrial ages of meteorites," in *Accretion of extraterrestrial matter throughout Earth's history*, Springer, 2001, pp. 241–266.

[65] V. Dmitriev, V. Lupovka, and M. Gritsevich, "Orbit determination based on meteor observations using numerical integration of equations of motion," *Planetary and Space Science*, vol. 117, pp. 223–235, 2015.

[66] D. L. Clark and P. A. Wiegert, "A numerical comparison with the Ceplecha analytical meteoroid orbit determination method," *Meteoritics & Planetary Science*, vol. 46, no. 8, pp. 1217–1225, 2011.

[67] S. Hughes, *Catchers of the Light: The Forgotten Lives of the Men and Women Who First Photographed the Heavens*. Stefan Hughes, 2012, ISBN: 9781620509616. [Online]. Available: https://books.google.com.au/books?id=iZk5OOf7fVYC.

[68] V. Fedynsky, *Meteors*. The Minerva Group, Inc., 2002.

[69] E. C. Pickering, "Spectrum of a Meteor," *Astronomische Nachrichten*, vol. 145, no. 4-5, pp. 77–80, 1898.

[70] L. G. Jacchia and F. L. Whipple, "The Harvard photographic meteor programme," *Vistas in Astronomy*, vol. 2, pp. 982–994, 1956.

[71] Z. Ceplecha, "Statistical Observations of Meteors 1951.," *Bulletin of the Astronomical Institutes of Czechoslovakia*, vol. 3, p. 53, 1952.

[72] Z. Ceplecha, "Multiple fall of Přibram meteorites photographed. 1. Double-station photographs of the fireball and their relations to the found meteorites," *Bulletin of the Astronomical Institutes of Czechoslovakia*, vol. 12, p. 21, 1961.

[73] R. McCrosky, A. Posen, G. Schwartz, and C.-Y. Shao, "Lost City meteorite—Its recovery and a comparison with other fireballs," *Journal of Geophysical Research*, vol. 76, no. 17, pp. 4090–4108, 1971.

[74] J. Oberst, S. Molau, D. Heinlein, C. Gritzner, M. Schindler, P. Spurný, Z. Ceplecha, J. Rendtel, and H. Betlem, "The "European Fireball Network": current status and future prospects," *Meteoritics & Planetary Science*, vol. 33, no. 1, pp. 49–56, 1998.

[75] A. Bischoff, J.-A. Barrat, K. Bauer, C. Burkhardt, H. Busemann, S. Ebert, M. Gonsior, J. Hakenmüller, J. Haloda, D. Harries, *et al.*, "The Stubenberg meteorite—An LL6 chondrite fragmental breccia recovered soon after precise prediction of the strewn field," *Meteoritics & Planetary Science*, 2017.

[76] J. Borovička, P. Spurný, and P. Brown, "Small near-Earth asteroids as a source of meteorites," *et al., Asteroids IV, Univ. of Arizona, Tucson*, pp. 257–280, 2015.

[77] P. Spurný, J. Borovička, J. Haloda, L. Shrbený, and D. Heinlein, "Two Very Precisely Instrumentally Documented Meteorite Falls: Žďar nad Sázavou and Stubenberg–Prediction and Reality," *LPI Contributions*, vol. 1921, 2016.

[78] P. Spurný, J. Borovička, G. Baumgarten, H. Haack, D. Heinlein, and A. Sørensen, "Atmospheric trajectory and heliocentric orbit of the Ejby meteorite fall in Denmark on February 6, 2016," *Planetary and Space Science*, 2016.

[79] M. Towner, P. Bland, P. Spurný, G. Benedix, K. Dyl, R. Greenwood, J. Gibson, I. Franchi, L. Shrbený, A. Bevan, *et al.*, "Mason Gully: The second meteorite recovered by the Desert Fireball Network," vol. 74, 2011, p. 5124.

[80] J. M. Trigo-Rodríguez, J. Llorca, J. M. M. Gil, I. Williams, A. J. C. Tirado, J. L. O. Moreno, J. A. Azcárate, J. Zamorano, V. Lanchares, J. A. Docobo, *et al.*, "The impact of neos and their fragments recorded from the ground: ongoing research lines of the spanish fireball network," in *1st IAA Planetary Defense Conference: 27-30 April 2009, Granada, Spain*, 2009.

[81] J. M. Trigo-Rodríguez, J. Borovička, P. Spurný, J. L. Ortiz, J. A. Docobo, A. J. CASTRO-TIRADO, and J. Llorca, "The Villalbeto de la Peña meteorite fall: II. Determination of atmospheric trajectory and orbit," *Meteoritics & Planetary Science*, vol. 41, no. 4, pp. 505–517, 2006.

[82] J. M. Trigo-Rodríguez, J. Borovička, J. Llorca, J. M. Madiedo, J. Zamorano, and J. Izquierdo, "Puerto Lápice eucrite fall: Strewn field, physical description, probable fireball trajectory, and orbit," *Meteoritics & Planetary Science*, vol. 44, no. 2, pp. 175–186, 2009.

[83] E. Blanch, J. M. Trigo-Rodríguez, J. Madiedo, E. Lyytinen, M. Moreno-Ibáñez, M. Gritsevich, and D. Altadill, "Detection of nocturnal and daylight bolides from Ebre Observatory in the framework of the SPMN fireball network," in *Assessment and Mitigation of Asteroid Impact Hazards*, Springer, 2017, pp. 185–197.

[84] F. Colas, B. Zanda, S. Bouley, J. Vaubaillon, P. Vernazza, J. Gattacceca, C. Marmo, Y. Audureau, M. K. Kwon, L. Maquet, *et al.*, "The FRIPON and Vigie-Ciel networks," in *Proceedings of the International Meteor Conference, Giron, France, 18-21 September 2014*, vol. 1, 2014, pp. 34–38.

[85] F. Colas, B. Zanda, J. Vaubaillon, S. Bouley, C. Marmo, Y. Audureau, M. K. Kwon, J.-L. Rault, S. Caminade, P. Vernazza, *et al.*, "French fireball network FRIPON," in *International Meteor Conference Mistelbach, Austria*, 2015, pp. 37–40.

[86] J.-L. Rault, F. Colas, and J. Vaubaillon, "Radio set-up design for the FRIPON project," in *Proceedings of the International Meteor Conference, Giron, France, 18-21 September 2014*, vol. 1, 2014, pp. 185–186.

[87] FRIPON, *Radio network*, Sep. 2017. [Online]. Available: `https://www.fripon.org/spip.php?article42`.

[88] T. Watson, "France launches massive meteor-spotting network: tracking space rocks that reach earth will give insight into the early Solar System," *Nature*, vol. 534, no. 7607, pp. 304–306, 2016.

[89] M. Gritsevich, E. Lyytinen, J. Moilanen, T. Kohout, V. Dmitriev, V. Lupovka, S. Midtskogen, N. Kruglikov, A. Ischenko, G. Yakovlev, V. Grokhovsky, J. Haloda, P. Halodova, J. Peltoniem, A. Aikkila, A. Taavitsainen, J. Lauanne, M. Pekkola, P. Kokko, P. Lahtinen, and M. Larionov, "First meteorite recovery based on observations by the Finnish Fireball Network," in *Proceedings of the International Meteor Conference, Giron, France*, 2014, pp. 162–169.

[90] A. Olech, P. Zoladek, M. Wisniewski, Krasnowski M., M. Kwinta, T. Fajfer, K. Fietkiewicz, D. Dorosz, L. Kowalski, J. Olejnik, K. Mularczyk, and K. Zloczewski, "Polish Fireball Network," in *Proceedings of the International Meteor Conference, 24th IMC, Oostmalle, Belgium, 2005*, L. Bastiaens, J. Verbert, and V. C. J.-M. Wislez, Eds., Aug. 2006, pp. 53–62.

[91] M. Wiśniewski, P. Żołądek, A. Olech, Z. Tyminski, M. Maciejewski, K. Fietkiewicz, R. Rudawska, M. Gozdalski, M. Gawroński, T. Suchodolski, *et al.*, "Current status of Polish Fireball Network," *Planetary and Space Science*, 2017.

[92] R. Weryk, P. Brown, A. Domokos, W. Edwards, Z. Krzeminski, S. Nudds, and D. Welch, "The Southern Ontario all-sky meteor camera network," *Earth, Moon, and Planets*, vol. 102, no. 1-4, pp. 241–246, 2008.

[93] P. Brown, R. Weryk, S. Kohut, W. Edwards, and Z. Krzeminski, "Development of an all-sky video meteor network in Southern Ontario, Canada The ASGARD System," *WGN, Journal of the International Meteor Organization*, vol. 38, pp. 25–30, 2010.

[94] W. J. Cooke and D. E. Moser, "The status of the NASA all sky fireball network," in *Proceedings of the International Meteor Conference, 30th IMC, Sibiu, Romania, 2011*, 2012, pp. 9–12.

[95] NASA Meteoroid Environment Office, *NASA All Sky Fireball Network*, Sep. 2017. [Online]. Available: `https://www.nasa.gov/offices/meo/outreach/all_sky_fireball_network_detail.html`.

[96] G. Kokhirova, P. Babadzhanov, and U. K. Khamroev, "Tajikistan fireball network and results of photographic observations," *Solar System Research*, vol. 49, no. 4, pp. 275–283, 2015.

[97] P. Jenniskens, P. Gural, L. Dynneson, B. Grigsby, K. Newman, M. Borden, M. Koop, and D. Holman, "CAMS: Cameras for Allsky Meteor Surveillance to establish minor meteor showers," *Icarus*, vol. 216, no. 1, pp. 40–61, 2011, ISSN: 0019-1035. DOI: 10.1016/j.icarus.2011.08.012. [Online]. Available: http://www.sciencedirect.com/science/article/pii/S0019103511003290.

[98] P. Jenniskens, A. E. Rubin, Q.-Z. Yin, D. W. Sears, S. A. Sandford, M. E. Zolensky, A. N. Krot, L. Blair, D. Kane, J. Utas, *et al.*, "Fall, recovery, and characterization of the Novato L6 chondrite breccia," *Meteoritics & Planetary Science*, vol. 49, no. 8, pp. 1388–1425, 2014.

[99] P. Jenniskens, *CAMS: Participate*, Sep. 2017. [Online]. Available: http://cams.seti.org/easyCAMS.html.

[100] R. Weryk, M. Campbell-Brown, P. Wiegert, P. Brown, Z. Krzeminski, and R. Musci, "The Canadian automated meteor observatory (CAMO): system overview," *Icarus*, vol. 225, no. 1, pp. 614–622, 2013.

[101] A. Bevan and R. Binns, "Meteorites from the Nullarbor Region, Western Australia: I. A review of past recoveries and a procedure for naming new finds," *Meteoritics*, vol. 24, no. 3, pp. 127–133, 1989.

[102] M. C. Towner, P. A. Bland, P. Spurný, G. K. Benedix, K. Dyl, A. W. R. Bevan, and D. Vaughan, "Towards a Digital Desert Fireball Network for Meteorite Recovery," vol. 75, Sep. 2012, p. 5123.

[103] I. Halliday, "Photographic Fireball Networks," in *Evolutionary and physical properties of meteoroids: the proceedings of the International Astronomical Union's colloquium # 13, held at the State University of New York, Albany, N.Y., on June 14-17, 1971*, ser. NASA Special Publications, C. Hemenway, P. Millman, A. Cook, and I. A. Union, Eds., Scientific, Technical Information Office, National Aeronautics, and Space Administration; [for sale by the Supt. of Docs., U.S. Govt. Print. Off.], 1973.

[104] Z. Ceplecha, "Photographic Geminids 1955," *Bulletin of the Astronomical Institutes of Czechoslovakia*, vol. 8, p. 51, 1957.

[105] C. Flye-Sainte Marie, "Solution to problem number 48," *L'Intermédiaire des Mathématiciens*, vol. 1, pp. 107–110, 1894.

[106] N. G. de Bruijn and P. Erdős, "A combinatorial problem," *Koninklijke Nederlandse Akademie v. Wetenschappen*, vol. 49, no. 49, pp. 758–764, 1946.

[107] K. A. Dyl, G. K. Benedix, P. A. Bland, J. M. Friedrich, P. Spurný, M. C. Towner, M. C. O'Keefe, K. Howard, R. Greenwood, R. J. Macke, *et al.*, "Characterization of Mason Gully (H5): The second recovered fall from the Desert Fireball Network," *Meteoritics & Planetary Science*, vol. 51, no. 3, pp. 596–613, 2016.

[108] Z. Ceplecha, J. Rajchl, and L. Sehnal, "Complete data on bright meteor 15761," *Bulletin of the Astronomical Institutes of Czechoslovakia*, vol. 10, p. 204, 1959.

[109] P. Spurný, "Photographic monitoring of fireballs in Central Europe," in *Optical Science, Engineering and Instrumentation'97*, International Society for Optics and Photonics, 1997, pp. 144–155.

[110] Z. Andreic and D. Segon, "The first year of Croatian Meteor Network," in *Proceedings of the International Meteor Conference, 27th IMC, Sachticka, Slovakia, 2008*, vol. 1, 2010, pp. 16–23.

[111] LC-Tec, *Fast Optical Shutter Series*. Jan. 2013. [Online]. Available: `http://www.lc-tec.se/products/fast-optical-shutters/`.

[112] N. G. de Bruijn, "Acknowledgement of priority to C. Flye Sainte-Marie on the counting of circular arrangements of 2n zeros and ones that show each n-letter word exactly once," 1975.

[113] S. Kak, "An interesting combinatoric sutra," *Indian Journal of History of Science*, vol. 35, pp. 123–127, 2000.

[114] S. K. Stein, *Mathematics: The Man-Made Universe (Dover Books on Mathematics)*. Dover Publications, 1994, ISBN: 0486404501.

[115] T. van Aardenne-Ehrenfest and N. G. de Bruijn, "Circuits and trees in oriented linear graphs," *Simon Stevin: Wis-en Natuurkundig Tijdschrift*, vol. 28, p. 203, 1951.

[116] H. Fredricksen, "A survey of full length nonlinear shift register cycle algorithms," *SIAM review*, vol. 24, no. 2, pp. 195–221, 1982.

[117] C. J. Mitchell, T. Etzion, and K. G. Paterson, "A method for constructing decodable de Bruijn sequences," *Information Theory, IEEE Transactions on*, vol. 42, no. 5, pp. 1472–1478, 1996.

[118] P. E. Compeau, P. A. Pevzner, and G. Tesler, "How to apply de Bruijn graphs to genome assembly," *Nature biotechnology*, vol. 29, no. 11, pp. 987–991, 2011.

[119] R. W. Hamming, "Error detecting and error correcting codes," *Bell System technical journal*, vol. 29, no. 2, pp. 147–160, 1950.

[120] V. I. Levenshtein, "Binary codes capable of correcting deletions, insertions, and reversals," in *Soviet physics doklady*, vol. 10, 1966, pp. 707–710.

[121] P. A. Bland, M. C. Towner, E. K. Sansom, H. A. R. Devillepoix, R. M. Howie, J. P. Paxman, M. Cupak, G. K. Benedix, M. A. Cox, T. Jansen-Sturgeon, D. Stuart, and D. Strangway, "Fall and Recovery of the Murrili Meteorite, and an Update on the Desert Fireball Network (abstract #6265)," *Meteoritics & Planetary Science*, vol. 51, no. S1, A144–A692, 2016, ISSN: 1945-5100. DOI: 10.1111/maps.12704. [Online]. Available: http://dx.doi.org/10.1111/maps.12704.

[122] M. Gritsevich and D. Koschny, "Constraining the luminous efficiency of meteors," *Icarus*, vol. 212, no. 2, pp. 877–884, 2011.

[123] M. Yoshikawa, A. Fujiwara, and J. Kawaguchi, "Hayabusa and its adventure around the tiny asteroid Itokawa," *Highlights of Astronomy*, vol. 14, pp. 323–324, 2007.

[124] J. M. Trigo-Rodriguez, E. Lyytinen, M. Gritsevich, M. Moreno-Ibáñez, W. F. Bottke, I. Williams, V. Lupovka, V. Dmitriev, T. Kohout, and V. Grokhovsky, "Orbit and dynamic origin of the recently recovered Annama's H5 chondrite," *Monthly Notices of the Royal Astronomical Society*, vol. 449, no. 2, pp. 2119–2127, 2015.

[125] Meteoritical Society, "Creston," vol. 104, 2015. [Online]. Available: http://www.lpi.usra.edu/meteor/metbull.php?code=62546 (visited on 11/21/2016).

[126] Z. Ceplecha, J. Rajchl, and L. Sehnal, "New Czechoslovak meteorite "Luhy"," *Bulletin of the Astronomical Institutes of Czechoslovakia*, vol. 10, p. 147, 1959.

[127] I. Halliday, A. A. Griffin, and A. T. Blackwell, "Detailed data for 259 fireballs from the Canadian camera network and inferences concerning the influx of large meteoroids," *Meteoritics & Planetary Science*, vol. 31, no. 2, pp. 185–217, 1996.

[128] I. Halliday, "Geminid fireballs and the peculiar asteroid 3200 Phaethon," *Icarus*, vol. 76, no. 2, pp. 279–294, 1988.

[129] M. Campbell-Brown and A. Hildebrand, "A New Analysis of Data from the Meteorite Observation and Recovery Project," in *Bulletin of the American Astronomical Society*, vol. 36, 2004, p. 1142.

[130] J. Borovička, P. Spurný, D. Šegon, Ž. Andreić, J. Kac, K. Korlević, J. Atanackov, G. Kladnik, H. Mucke, D. Vida, *et al.*, "The instrumentally recorded fall of the Križevci meteorite, Croatia, February 4, 2011," *Meteoritics & Planetary Science*, vol. 50, no. 7, pp. 1244–1259, 2015.

[131] J. Toth, L. Kornos, R. Piffl, J. Koukal, S. Gajdos, M. Popek, I. Majchrovic, M. Zima, J. Vilagi, D. Kalmancok, *et al.*, "Slovak Video Meteor Network-status and results: Lyrids 2009, Geminids 2010, Quadrantids 2011," in *Proceedings of the International Meteor Conference, 30th IMC, Sibiu, Romania, 2011*, 2012, pp. 82–84.

[132] P. Brown, P. McCausland, M. Fries, E. Silber, W. Edwards, D. Wong, R. Weryk, J. Fries, and Z. Krzeminski, "The fall of the Grimsby meteorite—I: Fireball dynamics and orbit from radar, video, and infrasound records," *Meteoritics & Planetary Science*, vol. 46, no. 3, pp. 339–363, 2011.

[133] R. M. Howie, J. Paxman, P. A. Bland, M. C. Towner, E. K. Sansom, and H. A. R. Devillepoix, "Submillisecond fireball timing using de Bruijn timecodes," *Meteoritics & Planetary Science*, vol. 52, no. 8, pp. 1669–1682, 2017, ISSN: 1945-5100. DOI: 10.1111/maps.12878. [Online]. Available: http://dx.doi.org/10.1111/maps.12878.

[134] G. Wetherill and D. ReVelle, "Which fireballs are meteorites? A study of the Prairie Network photographic meteor data," *Icarus*, vol. 48, no. 2, pp. 308–328, 1981.

[135] P. Brown, V. Marchenko, D. E. Moser, R. Weryk, and W. Cooke, "Meteorites from meteor showers: A case study of the Taurids," *Meteoritics & Planetary Science*, vol. 48, no. 2, pp. 270–288, 2013.

[136] Y. Hitomi, J. Gu, M. Gupta, T. Mitsunaga, and S. K. Nayar, "Video from a single coded exposure photograph using a learned over-complete dictionary," in *Computer Vision (ICCV), 2011 IEEE International Conference on*, IEEE, 2011, pp. 287–294.

[137] F. C. Bettonvil, "Remote and automatic small-scale observatories: experience with an all-sky fireball patrol camera," in *SPIE Astronomical Telescopes+ Instrumentation*, International Society for Optics and Photonics, 2014, 91473U–91473U.

[138] F. Rigaud, I. Jegouzo, J. Gaudemard, and J. Vaubaillon, "Control and protection of outdoor embedded camera for astronomy," in *SPIE Astronomical Telescopes+ Instrumentation*, International Society for Optics and Photonics, 2012, 84462S–84462S.

[139] R. Raskar, A. Agrawal, and J. Tumblin, "Coded Exposure Photography: Motion Deblurring Using Fluttered Shutter," *ACM Trans. Graph.*, vol. 25, no. 3, pp. 795–804, Jul. 2006, ISSN: 0730-0301. DOI: 10.1145/1141911.1141957. [Online]. Available: http://doi.acm.org/10.1145/1141911.1141957.

[140] P. Llull, X. Liao, X. Yuan, J. Yang, D. Kittle, L. Carin, G. Sapiro, and D. J. Brady, "Coded aperture compressive temporal imaging," *Optics express*, vol. 21, no. 9, pp. 10 526–10 545, 2013.

[141] H. A. Devillepoix, E. K. Sansom, P. A. Bland, M. C. Towner, M. Cupák, R. M. Howie, T. Jansen-Sturgeon, M. A. Cox, B. A. Hartig, G. K. Benedix, *et al.*, "The Dingle Dell meteorite: A Halloween treat from the Main Belt," *Meteoritics & Planetary Science*, vol. 53, no. 10, pp. 2212–2227, DOI: 10.1111/maps.13142. eprint: https://onlinelibrary.wiley.com/doi/pdf/10.1111/maps.13142. [Online]. Available: https://onlinelibrary.wiley.com/doi/abs/10.1111/maps.13142.

[142] Meteoritical Society, *Dingle Dell*, 2017. [Online]. Available: http://www.lpi.usra.edu/meteor/metbull.php?code=62546 (visited on 11/21/2016).

[143] gPhoto Contributors, *gPhoto Home*, Jul. 2017. [Online]. Available: http://gphoto.org.

[144] Nikon Inc., *How many pictures has my camera taken? How many will it take?* Jul. 2017. [Online]. Available: https://www.nikonimgsupport.com/ni/NI_article?lang=en_US&articleNo=000003332.

[145] J. L. West, "Polymer-Dispersed Liquid Crystals," in *Liquid-Crystalline Polymers*, ch. 32, pp. 475–495. DOI: 10.1021/bk-1990-0435.ch032. eprint: http://pubs.acs.org/doi/pdf/10.1021/bk-1990-0435.ch032. [Online]. Available: http://pubs.acs.org/doi/abs/10.1021/bk-1990-0435.ch032.

[146] H. Craighead, J. Cheng, and S. Hackwood, "New display based on electrically induced index-matching in an inhomogeneous medium," *Applied Physics Letters*, vol. 40, no. 1, pp. 22–24, 1982.

[147] Switch Glass, *The Haze Factor – R&D Update*, Jul. 2017. [Online]. Available: http://www.switchglass.com.au/haze-factor.

[148] Switch Glass, *FAQs*, Jul. 2017. [Online]. Available: http://www.switchglass.com.au/faqs.

[149] Switch Glass, "Switchable Privacy Class Technical Information & Installation Guide," Mar. 2015. [Online]. Available: http://www.switchglass.com.au/wp-content/uploads/2016/02/Switchglass-Tech-Info-and-Install-Guide-Revised-020315.pdf.

[150] R. Hikmet and H. Kemperman, "Switchable mirrors of chiral liquid crystal gels," *Liquid crystals*, vol. 26, no. 11, pp. 1645–1653, 1999.

[151] R. Hikmet and H. Kemperman, "Electrically switchable mirrors and optical components made from liquid-crystal gels," *Nature*, vol. 392, no. 6675, pp. 476–479, 1998.

[152] L. Li and D. Yang, *Single layer multi-state ultra-fast cholesteric liquid crystal device and the fabrication methods thereof*, US Patent 6,674,504, Jan. 2004. [Online]. Available: https://www.google.com/patents/US6674504.

[153] Kent Optronics Inc., *Switchable Mirror / Switchable Glass*, Jul. 2017. [Online]. Available: http://www.kentoptronics.com/mirror.html.

[154] STMicroelectronics, "Push-pull Four Channel Driver with Diodes," Jul. 2003. [Online]. Available: http://www.st.com/content/ccc/resource/technical/document/datasheet/04/ac/22/f9/20/5d/43/a1/CD00000059.pdf/files/CD00000059.pdf/jcr:content/translations/en.CD00000059.pdf.

Every reasonable effort has been made to acknowledge the owners of copyright material. I would be pleased to hear from any copyright owner who has been omitted or incorrectly acknowledged.